

**Transition from classical methods to new strategies: Mechanistic evaluation of inhibitors
against *Mycobacterium tuberculosis* shikimate kinase**

by

Ngolui René Fuanta

A dissertation submitted to the Graduate Faculty of
Auburn University
in partial fulfillment of the
requirements for the Degree of
Doctor of Philosophy

Auburn, Alabama
August 4, 2018

Keywords: Kinetics, spectrometry, tuberculosis, spectrofluorimetry, dissociation constants

Copyright 2018 by Ngolui René Fuanta.

Approved by

Douglas Goodwin, Chair, Associate Professor, Chemistry and Biochemistry
Holly Ellis, Professor, Chemistry and Biochemistry
Chris Easley, Professor, Chemistry and Biochemistry
Steve Mansoorabadi, Assistant Professor, Chemistry and Biochemistry
Angela Calderón, Associate Professor, Drug Discovery and Development

Abstract

Tuberculosis (TB) still stands as one of the leading causes of mortality resulting from an infectious agent. In part, this stems from the emergence of multidrug and extensive drug-resistant strains of tubercle bacilli, demonstrating the pressing need for the development of novel anti tubercular agents. Interestingly, the shikimate pathway, found in plants, bacteria, fungi and algae, is essential for the survival of *Mycobacterium tuberculosis*. This pathway produces precursors to aromatic amino acids and other aromatic cellular metabolites. Fortunately, it has no mammalian analogue. This makes the enzymes of this pathway suitable targets for the development of novel anti-microbial agents. The research presented in this dissertation focuses on *Mycobacterium tuberculosis* shikimate kinase (*MtSK*). Our objectives were to develop LC-MS-based screening and characterization of potential anti tubercular agents – natural, synthetic or semi synthetic, develop fluorescence methods for rapid mechanistic evaluation of *MtSK* inhibitors and strategies for screening out promiscuous inhibitors. Using mass spectrometry, we characterized a group of marine derived compounds, manzamine alkaloids. These inhibitors showed mixed-noncompetitive mode of inhibition, with time-dependent and slow-binding components. Of this group, one, 6-cyclohexamidomanzamine A, a derivative of the parent manzamine A scaffold, showed slow, tight-binding kinetics with an inhibition constant in the nanomolar range. Another marine-derived inhibitor we characterized was ilimaquinone, which showed irreversible inhibition evident from formation of a covalent adducts with primarily serines and threonines, and to a lesser extent lysines and tyrosines. It is worth noting that due to

the nonspecific nature of this inhibitor, as it has shown to modify other proteins (not only *MtSK*), further exploitation of this molecule as a potential antibacterial, antiviral, or anticancer agent should be approached with great care. With respect to developing rapid screening tools, we have generated a panel of *MtSK* variants with intrinsic fluorescent properties. Substitutions were made on the lid domain, V116W, the adenine binding domain, N151W, and the shikimate binding domain, E54W. These variants show differential responses to substrates and inhibitors. Interestingly, we noted that the binding of one of the substrates, shikimate produced changes in fluorescence in only one of the variants, supporting previously reported data that substrate binding induces conformational changes. Using these, we evaluated the inhibition kinetics of previously characterized inhibitor, so-called Compound 1. Our data supported a mixed-type mode of inhibition, with a slow, reversible component. Competition experiments indicated Compound 1 binds at or near the shikimate binding site, evident from spectral shifts in E54W in the presence of the inhibitor. Together, we have shown that the 6-cyclohexamido derivative of manzamine A is a potent inhibitor of *MtSK*, and this may be an indication of potential success in later drug discovery stages. The use of ilimaquinone for further drug screening and discovery purposes is at the discretion of the investigator. Our combinatorial approach to weeding out nonspecific inhibitors together with our panel of variants would increase turnover in the early drug screening stages and prevent wastage of long hours on fruitless drug investigations. Lastly, our panel of variants shows great potential for further development into high throughput screen platforms and possibly as sensors.

Acknowledgments

I dedicate this piece to my amazing parents Mr. and Mrs. Ngolui Stephen. Your encouragements and prayers have seen me through life, I stand tall because I stand on your shoulders. You are the very best a son could ever ask for. I love you.

I want to give special thanks to my advisor Dr. Goodwin Douglas aka Good Doc for his tremendous support and insight into my graduate school career. You pushed and supported me when all experiments seem to give up on me and still you pointed me to the light at the end of the tunnel. It is a rare privilege and an inexplicable experience to have been under your supervision. You truly stand out.

My sincere thanks to my committee members; Holly Ellis for her helpful and comforting words through the trials of graduate school, Chris Easley for impacting your total knowledge of fluorimetry and analytical thinking unto me, and Steven Mansoorabadi aka Dr. Man, you made me feel like I was an expert in enzyme mechanisms and arrow pushing. Thank you for all the random visits you let me pay to your offices. I salute you.

Many thanks to Dr. Angela Calderón for her continuous support and encouragements even when nothing seemed to work. Your positive attitude and outlook for better results and ground breaking findings didn't go without recognition. Thank you for the experience.

I also want to thank former and current members of our group; Drs. Elizabeth Ndontsa (aka Prof), Haijun Duan (aka Diesel), Olive Njuma (aka Miss Olive/Lab machine/proximal

tryptophan). I won't and can't leave out Dr. Johayra aka PI/PIC (Partner In Crime) for walking me through the intricacies of this research project. Hui Xu (aka Cong Cong), Jessica Krewall, Tarfi Azis, Rejaul Islam, Callie Jackson. Undergrads; Ethan McCurdy, Gobind Gill, Lauren Barr, Teddy Childers, Olivia Snider, Theresa Simermeyer, Michael Skinner, Daniel Zieman, Patrick Sarhmann and Kirclin McWhorter.

With deep gratitude, I extend sincere appreciations to Mr. and Mrs. Soweh. Thank you for opening your home for me and for supporting all the way. You are truly an invaluable part of my achievement and I cannot thank you enough. Uncle Jonathan Tingume, Raymond Tingume, Daniel Weafua, my siblings - Marcellen Nian (aka capitaine), Alain Ngolui, Cpt. Serge Nsanyui, Emile Ngolui and Edmond Ngolui. Your support and guide throughout childhood days and even now has been impeccable. I would choose you again if asked for a second time.

To all who have graced my life over the years. I say special thank you. To the friends I made in graduate school; Diana Forbes, Shamim Iqbal, Thankhoe Rantso, Mansour Alturki, Ibtisam Ibtisam, Katie Stanford, Claire Graham. Thank you for being a part of my experience and for sharing your story with me. You are boldly inscribed in my heart.

Special thanks to the ladies of the chemistry office. Carol Nixon (retired), Lynn Walker (retired), Lavvorn Howard. You all have been inspirational to me throughout my stay here. You ladies rock! To Mark and Susie, you showed me great love and I am greatly indebted.

Many a thank you to Auburn University, department of Chemistry and Biochemistry for accepting and believing in me. That a 'crude' microbiologist could survive the storms of chemistry.

All in all, from the beginning to the end, THANKS go unto He who sits far above the heavens.
For the Lord is good and His mercies endure forever. Gloria in excelsis!

Table of Contents

Chapter 1	1
Literature review	1
1.1 Overview of tuberculosis (TB) pathology	1
1.2 Kinases: Phosphorylation of small molecules to proteins	2
1.2.1 Protein kinases.....	4
1.2.2 Kinase groups and folds	7
1.2.3 Nucleoside monophosphate (NMP) kinases	16
1.2.3.1. Shikimate kinase	20
1.3 Shikimate pathway.....	23
1.4 Natural products and drug discovery	26
1.4.1 By total synthesis	26
1.4.2 By modification of existing scaffolds	27
1.4.3 By immunoconjugation.....	28
1.4.4 Total synthesis of unmodified natural products	29
1.5 Marine natural products in the drug discovery pipeline	30
1.5.1 FDA-approved marine pharmaceuticals.....	30
1.5.2 Marine pharmaceuticals in clinical pipeline.....	32

1.5.2.1 Compounds in Phase III trials e.g. Eribulin and soblidotin.....	32
1.5.2.2 Examples of compounds in Phase II trials: DMXBA	33
1.5.2.3 Examples of compounds in Phase I trials: Hemiasterlin	33
1.6 Enzyme inhibition.....	34
1.6.1 Rapid reversible inhibition.....	34
1.6.1.1 Competitive inhibition.....	36
1.6.1.2 Uncompetitive inhibition.....	36
1.6.1.3 Noncompetitive inhibition.....	37
1.6.2 Slow-onset inhibition	38
1.6.2.2 Advantages of inhibitors with slow off rate constants	42
1.6.4 Irreversible inhibition.....	43
1.6.4.1 Affinity labels.....	45
1.6.4.2 Mechanism-based inactivators	45
1.6.5 Nonspecific inhibition.....	46
1.6.5.1 PAINS (Pan-Assay INterference compoundS)	48
1.8 Kinase inhibitors	50
1.8.1 Type 1 inhibitors	50
1.8.2 Type 2 inhibitors	51
1.8.3 Allosteric inhibitors.....	51
1.8.4 Covalent inhibitors	51
1.9. LC-MS methodology	56
1.9.1.1 Top-down approach.....	56

1.9.1.2 Bottom-up approach	58
1.10.3 Fluorescence quenching	63
1.10.4 Fluorescence anisotropy	64
1.10.5 Resonance Energy transfer	65
1.10.6 Time-gated fluorescence – Homogenous time-resolved fluorescence (HTRF)	66
1.10.7 Fluorescence lifetime (FLA)	67
Chapter 2	68
2.1 Abstract	68
2.2 Introduction	69
2.3 Materials	73
2.4 Methods	74
2.4.1 <i>MtSK</i> inhibitor screening by LC-MS	74
2.4.2 LC-MS analysis	74
2.4.3 Kinetics of inhibition of manzamine alkaloids	75
2.4.4 Slow, tight-binding inhibition of <i>MtSK</i> activity	78
2.4.5 Jump dilution experiments.	80
2.4.6 Computational Methods	81
2.5 Results and discussion	82
2.6 Conclusion	96
Chapter 3	98
3.1 Abstract	98
3.2 Introduction	99

3.3 Materials.....	101
3.4 Methods.....	102
3.4.1 Ilimaquinone acquisition and isolation.....	102
3.4.2 LC-MS based time-dependent inhibition assay.....	102
3.4.3 Inhibition of other enzymes by IQ: Activity assays for <i>MtKatG</i> , PK, and LDH	104
3.4.4 Dilution experiments	104
3.4.5 Intact protein analysis by mass spectrometry	105
3.4.6 Nano liquid chromatography – tandem mass spectrometry (nLC-MS/MS) analysis of <i>MtSK</i> tryptic peptides.	105
3.4.7 Prediction of covalently bound ilimaquinone binding poses	106
Results and Discussion.....	108
Conclusion.....	132
Chapter 4.....	134
4.1 Abstract	134
4.2 Introduction	135
4.3 Materials.....	138
4.4 Methods.....	139
4.4.1 Mutagenesis.....	139
4.4.2 <i>MtSK</i> Expression and Purification	140
4.4.3 ESI-LC-MS Analysis of Intact <i>MtSK</i>	141
4.4.4 Evaluation of <i>MtSK</i> Activity.....	142
4.4.5 Fluorimetric measurements	143

4.5 Results	144
4.6 Discussion and Conclusions.....	170
Chapter 5	174
Summary	174
Appendix 1	183
Appendix 2.....	187

List of figures

Figure 1.1: Mechanisms of phosphoryl transfer observed in kinases	4
Figure 1.2: Typical representation of protein kinases using protein kinase A.....	7
Figure 1.3: Structure of human adenylate kinase 1 in complex with AP5A (bis(adenosine)-5'- tetraphosphate) and malonate.	17
Figure 1.4: Sequence alignment of nine NMPs highlighting residues with >70% conservation. 19	
Figure 1.5: Alignment of selected kinases showing the structural similarity on the nucleotide binding domain and the P-loop.	20
Figure 1.7: Structure of <i>MtSK</i> in complex with ADP and shikimate.	22
Figure 1.8: The shikimate pathway.....	25
Figure 1.9: Structure of tetracycline and its derivative eravacycline.....	27
Figure 1.10: Structure of Vancomycin.....	28
Figure 1.11: Structure of brentuximab vedotin.....	29
Figure 1.12: Structure of Artemisinin and derivatives artemether and arteether.....	30
Figure 1.13: Structure of eribulin mesylate	32
Figure 1.14: Structure of DMXB	33
Figure 1.15: Structure of Hemiasterlin	34
Figure 1.16. Schematic representation of common rapid reversible mechanisms.....	35
Figure 1.17: Structure of ibuprofen	36
Figure 1.18: Structure of ciglitazone	37

Figure 1.19: Structure of Etoposide	38
Figure 1.20: Mechanisms of slow binding inhibition	39
Figure 1.21: Images of Compound 14 and control with <i>MtSK</i> by transmission electron microscopy	47
Figure 1.22: <i>MtSK</i> inhibitors	55
Figure 1.23: Schematic illustration of the differences between top-down and bottom-up mass spectrometry-based proteomics approaches.	59
Figure 1.24: Jablonski diagram.....	61
Figure 1.25: A schematic diagram showing measurement of fluorescence anisotropy.....	65
Figure 2.1: Kinetic model for the mixed-type inhibition of <i>MtSK</i> reaction with shikimate (SA) and ATP by manzamine compounds.	77
Figure 2.2: Non-linear least-squares analyses of rapid reversible inhibition by manzamine A ...	83
Figure 2.3: Non-linear least-squares analyses of rapid reversible inhibition by 6-cyclohexamido- manzamine A	84
Figure 2.8: Effect of compound 6 on <i>MtSK</i> activity	85
Figure 2.9. Effect of inhibitor concentration and preincubation time on the activity of <i>MtSK</i>	88
Figure 2.10. Effect of inhibitor concentration and preincubation time on the activity of <i>MtSK</i> ..	89
Figure 2.11. Recovery of <i>MtSK</i> activity following dilution of <i>MtSK</i> -inhibitor complexes.....	91
Figure 2.12: Two docked poses of compound 6 are shown in the <i>MtSK</i> crystal structure, PDB code 2DFT	93
Figure 3.1. Structure of ilimaquinone (IQ).	100
Figure 3.2. Effect of IQ preincubation on <i>MtSK</i> activity	109
Figure 3.3. Time-dependent loss of <i>MtSK</i> activity in the presence of IQ	109
Figure 3.4. Recovery of activity following dilution of IQ-inhibited <i>MtSK</i>	110

Figure 3.5. Intensities of deconvoluted <i>MtSK</i> MS spectra vs. preincubation time with IQ.....	112
Figure 3.6. Deconvoluted ESI-MS spectra for <i>MtSK</i> incubated with IQ	114
Figure 3.7. Intensities of deconvoluted <i>MtSK</i> MS spectra vs. preincubation time with IQ.....	115
Figure 3.8. Deconvoluted ESI-MS spectra for <i>MtSK</i> incubated with 10 μ M IQ	116
Figure 3.9. Deconvoluted ESI-MS spectra for <i>MtSK</i> incubated with 10 μ M IQ	117
Figure 3.10. Spectrophotometric evaluation of IQ inhibition on LDH, PK, HRP and <i>MtKatG</i> . 119	
Figure 3.11. Deconvoluted ESI-MS spectra for PK incubated with 100 μ M IQ.....	120
Figure 3.12. Deconvoluted ESI-MS spectra for PK incubated with 100 μ M IQ.....	121
Figure 3.13. Deconvoluted ESI-MS spectra for LDH incubated with 100 μ M IQ.....	122
Figure 3.14. Identification of Ser44, Thr111, and Ser77 IQ-adducted peptides by nano-LC-ESI MS/MS analysis	125
Figure 3.15. Sites of <i>MtSK</i> adduction by ilimaquinone.....	126
Figure 3.16. Effect of IQ on preincubated <i>MtSK</i> -ATP complex.....	127
Figure 3.17. Proposed mechanism for <i>MtSK</i> modification by ilimaquinone	128
Figure 3.18. IQ models bonded to S77/T111 superimposed onto the <i>MtSK</i> crystal structure with ATP and Mg ²⁺ (PDB 2IYW)	129
Figure 3.19. IQ binding models based on <i>MtSK</i> (PDB 2IYY).....	130
Figure 3.20. Surface representation of <i>MtSK</i>	131
Figure 4.1: Sequence alignment of shikimate kinases.....	146
Figure 4.2: Deconvoluted ESI-LC-MS spectra of purified <i>MtSK</i> proteins	146
Figure 4.3: Evaluating enzyme activity using coupled-assay.....	149
Figure 4.4: ATP-dependent fluorimetric titrations	152
Figure 4.5: Shikimate-dependent fluorimetric titrations	153

Figure 4.6: Changes in fluorescence anisotropy of Trp-bearing <i>MtSK</i> variants in response to shikimate and ATP.....	155
Figure 4.7: Overlay of shikimate kinase structures of the free enzyme and a ternary complex with ADP and shikimate	156
Figure 4.8: Structure of Compound 1	156
Figure 4.9: <i>MtSK</i> inhibition by Compound 1.....	158
Figure 4.10: Jump dilution experiments with Compound 1.....	159
Figure 4.11: Investigating covalent adducts formation between <i>MtSK</i> and Compound 1.....	160
Figure 4.13: Effect of Compound 1 on Trp fluorescence.....	163
Figure 4.14: Compound 1 vs shikimate competitive assays.....	164
Figure 4.15: Compound 1 vs ATP competitive assays.....	165
Figure 4.16: Structure of mantATP.....	166
Figure 4.17: MantATP-dependent resonance energy transfer.....	167
Figure 4.18: Resonance energy transfer.....	168
Figure 4.19: Compound 1 vs mantATP.....	169
Appendix 1.....	183
Figure 2.1: Non-linear least-squares analyses of rapid reversible inhibition by 8-hydroxymanzamine A.....	185
Figure 2.2: Non-linear least-squares analyses of rapid reversible inhibition by manzamine E.....	186
Figure 2.3: Non-linear least-squares analyses of rapid reversible inhibition by manzamine F.....	187
Figure 2.4: Non-linear least-squares analyses of rapid reversible inhibition by deoxymanzamine X.....	189

Appendix 2.....	187
Figure 4.1: Sequence alignment for some shikimate kinases.....	188

List of Abbreviations

ADC	Antibody-drug conjugate
AK	Adenylate kinase
AMP	Ampicillin
CAM	Chloramphenicol
CMPK	Cytidine monophosphate kinase
DAHP	3-deoxy-D-arabino-heptulosnate 7-phosphate
DHQ	3-Dehydroquinone
DMSO	Dimethyl sulfoxide
DMXB	3-(2,4-dimethoxybenzylidene)-anabaseine
EIC	Extracted ion chromatogram
EMA	European agency for the evaluation of medicinal products
ESI	Electrospray ionization
FLA	Fluorescence lifetime
FTICR	Fourier-transform ion-cyclotron resonance
GSK	Glycogen Synthase Kinase
HCD	High-energy collisional dissociation
IL	Interleukin
IPTG	Isopropyl- β -d-thiogalactopyranoside

LC-MS	Liquid chromatography-mass spectrometry
LDH	Lactate dehydrogenase
MantATP	2'/3'-O-(N-Methyl-anthraniloyl)-adenosine-5'-triphosphate
MDR	Multi drug-resistant
MIC	Minimum inhibitory concentration
<i>Mtb</i>	<i>Mycobacterium tuberculosis</i>
<i>MtKatG</i>	<i>Mycobacterium tuberculosis</i> catalase-peroxidase
<i>MtSK</i>	<i>Mycobacterium tuberculosis</i> shikimate kinase
nLC-MS	Nanoliquid chromatography-mass spectrometry
NMP	Nucleoside monophosphate
PAINS	Pan-assay interference compounds
PEP	Phosphoenol pyruvate
PK	Pyruvate kinase
PMSF	Phenylmethylsulfonyl fluoride
PTM	Posttranslational modification
QTOF	Quadrupole Time-of-flight
RET	Resonance energy transfer
S3P	Shikimate-3-phosphate
SK	Shikimate kinase
TB	Tuberculosis
TRET	Time-resolved energy transfer
TIC	Total ion chromatogram

UMP Uridylate monophosphate

XDR Extensively drug-resistant

Chapter 1

Literature review

1.1 Overview of tuberculosis (TB) pathology

Mycobacterium tuberculosis (*M. tuberculosis*) is a prolific pathogen and the etiologic agent of the respiratory tract infection, tuberculosis. There are several species of *Mycobacterium*, like *M. leprae* that infect humans and other mammals, but *M. tuberculosis* is the major species infecting humans (1). TB is a growing public health problem. About one-third of the world's population is currently infected, and TB stands as the leading killer of people co-infected with HIV (Human Immunodeficiency Virus) (2). Transmission of the bacillus is by inhalation of droplet nuclei (about 1-5 microns in diameter) when a host coughs, sneezes, shouts or sings. These bacilli are ingested by macrophages and neutrophils which are attracted to the site of infection by chemotaxis. Despite the release of ready-to-use host defense components like antimicrobial peptides, reactive oxygen species and hydrolytic enzymes in the intracellular granules, the immune cells, unfortunately, fail to eliminate the bacilli and in turn serve as a suitable niche for their subsequent growth and survival and propagation within the host (3–6). Viable bacilli are spread in blood and lymphatic circulation, provoking a systemic immune response via antigen processing. The bacteria can override this systemic immune response hence moving from a latent TB infection to active TB disease (7).

Current TB treatment protocols are carried out using first- and/or second-line antitubercular agents. First-line drugs are isoniazid, rifampin, pyrazinamide, ethambutol and streptomycin. Second-line drugs include fluoroquinolones like ofloxacin, levofloxacin, moxifloxacin, and ciprofloxacin. The aminoglycosides kanamycin, amikacin and capreomycin also fall in this category (8) as do the less effective antitubercular agents ethionamide, cycloserine, and P-aminosalicylic acid (9). There has been an increase in the prevalence of resistance to these drugs. Multidrug-resistant (MDR) *M. tuberculosis*, which are strains resistant to at least isoniazid (INH) and rifampin (RIF), require the use of second-line anti-tubercular agents (10). Extensively drug-resistant (XDR) strains are resistant to INH, RIF and one or more of the second-line drugs (11). Bedaquiline fumarate, the most recent anti tubercular agent in over five decades is also used as part of combination therapy in MDR-TB, in the absence of an effective treatment (12).

The overwhelming increase in drug-resistant strains and the near absence of novel FDA-approved antitubercular agents has widened the search for antibacterials. Ubiquitous enzymes like kinases, though typically targeted by anti-cancer agents are now becoming preferred candidates for targeting infectious diseases.

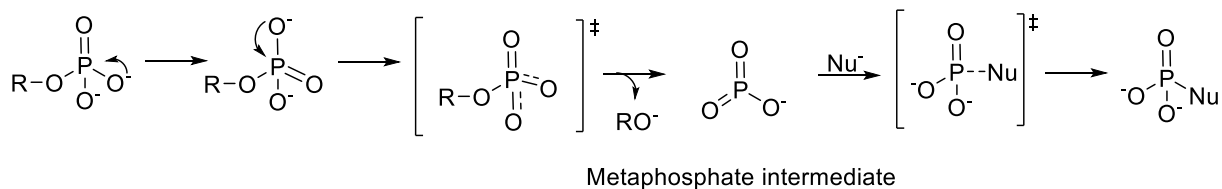
1.2 Kinases: Phosphorylation of small molecules to proteins

Kinases catalyze phosphoryl transfer reactions. The large majority of metabolic pathways have at least one kinase step. Most commonly, ATP is the phosphoryl donor, and as is described below, the range of phosphoryl acceptors is about as broad as the structures represented in biology (13–19). This section briefly explores the structural and functional properties of this diverse and ubiquitous group of enzymes. This serves to place the enzyme of focus for this

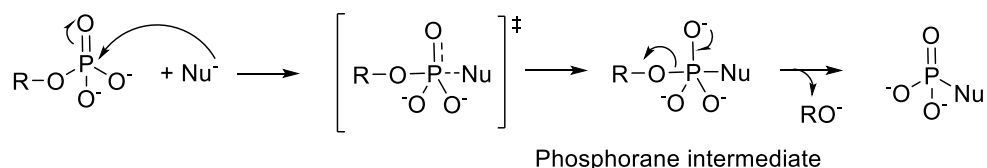
research, shikimate kinase, into its broader context. Here, a brief overview of the structural diversity of enzymes that use ATP as a transferase substrate is provided. Although the research of this dissertation is centered on a particular nucleoside monophosphate (NMP) kinase which uses a non-protein, small-molecule phosphoryl acceptor, it is important to recognize that the principles and progress described in this research are eminently transferrable to other kinases. As such, the research detailed in subsequent passages is likely to have application to other diseases (e.g., cancer). For example, a better understanding of their interaction(s) with nucleotide substrates could prove useful in the screening of ATP competitive inhibitors, one of which will be discussed in a subsequent chapter of this dissertation.

Generally, the phosphoryl transfer reactions of kinases can be divided into three broad types of mechanisms. The dissociative mechanism (**Figure 1.1A**) involves the initial cleavage of the donor O – P bond, resulting in the formation of a trigonal metaphosphate intermediate. This is followed by nucleophilic attack by the acceptor. In the associative mechanism (**Figure 1.1B**), the nucleophile attacks the donor prior to the formation of a phosphorane intermediate with subsequent release of the leaving group. The concerted mechanism (**Figure 1.1C**) is an S_N2 reaction which proceeds by the formation of a pentavalent transition state (16–18). Not only is there a variety of mechanisms of phosphoryl transfer amongst kinases, there exist a large number of different families and folds.

A) Dissociative



B) Associative



C) Concerted

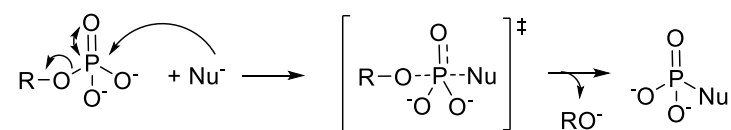


Figure 1.1: Mechanisms of phosphoryl transfer observed in kinases (20). Mechanism A proceeds through a trigonal phosphate intermediate, post P-O bond cleavage. This precedes a nucleophilic attack. In B, a nucleophilic attack occurs prior to the formation of a pentavalent phosphorane intermediate. This precedes the release of the leaving group. C proceeds via a single transition state with simultaneous bond formation and cleavage.

1.2.1 Protein kinases

Protein kinases are simply those whose phosphoryl acceptor substrate is a protein, and the phosphorylation event invariably alters the activity/function of that protein. They are implicated in many disease states including cancers and many continue to be investigated for their potential as drugable targets (21,22). They play essential roles in virtually every cell signal transduction mechanism as well as many other cellular processes (23,24).

Though there exist a plethora of kinase-centered regulatory mechanisms, protein kinases are categorized into two large groups – phosphorylating serine/threonine or tyrosine residues on target proteins. Both groups possess similar three dimensional structures with a catalytically active aspartate residue and a glycine-rich phosphate-binding (P-) loop in the catalytic center (25). The N- and C-terminal lobes of the domains are connected by a linker and the latter is predominantly α -helical and includes the activation region (**Figure 1.2**). The activation region is located between a highly conserved Asp-Phe-Gly (DFG) motif and a less conserved Ala-Pro-Glu (APE) motif (26,27). In its active conformation, the kinase's C helix stacks against the N-terminal lobe and the aspartate residue of the DFG motif chelates a Mg^{2+} ion, positioning the ATP for catalysis. In the inactive conformation, an electrostatic interaction between the aspartate residue and the divalent metal ion is disrupted and the phenylalanine residue of the DFG motif turns toward the ATP moiety.

The ATP-binding pocket is highly conserved. Within this region, specific hydrogen bonds are formed between the adenine ring's N1 and N6 and the peptide backbone of the hinge region. Lining this region are nonpolar aliphatic groups providing van der Waals interactions with the purine. Also, there is a hydrogen bonding interaction between O2' and O3' of the ribose sugar and a glutamate side chain and another main chain glutamate carbonyl oxygen, respectively. The triphosphate is oriented out of the ATP binding pocket to facilitate the transfer of γ -phosphate. A conserved glutamate in the C helix and a lysine residue on the β -sheet aid in positioning the α - and β -phosphate groups of the ATP molecule. The divalent magnesium ion ensures proper orientation of ATP for catalysis by mediating the interactions between the α - and γ -phosphate groups and aspartate (of the DFG motif) and asparagine. A second magnesium ion

interacts with the aspartate of the DFG motif and the β - and γ -phosphates to further stabilize the substrate.

The conformationally flexible activation region in protein kinases plays an essential role in substrate binding. In inactive kinases this structure is partially disordered. Transition to the active conformation is triggered in most kinases by phosphorylation. The active conformation differs from the inactive conformation by the high structural flexibility in the activation region, which attains a more rigid conformation in inactive forms. Some protein kinases have additional secondary structures in the activation regions (28,29) that promote catalysis. In addition, they possess a catalytically essential aspartate residue that deprotonates the hydroxyl group of the substrate during catalysis. In Ser/Thr kinases, a neighboring lysine stabilizes the negative charge that develops after the hydroxyl group of the substrate is deprotonated during catalysis. In tyrosine kinases, a nearby arginine residue performs the analogous function. Here the spacing of the electrostatically stabilizing cation accommodates the larger tyrosine residue of the substrate.

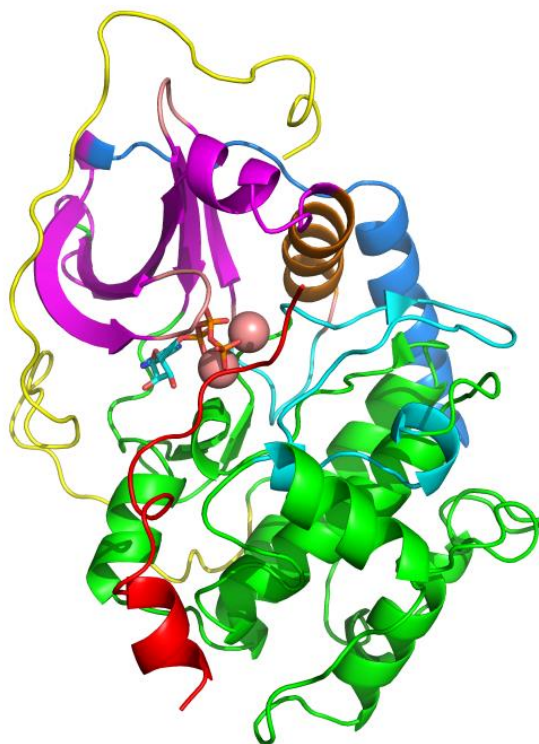
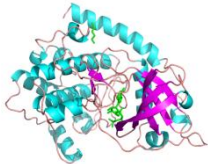
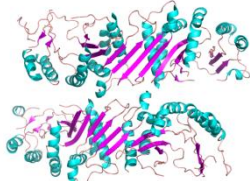
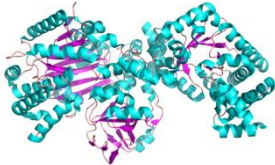
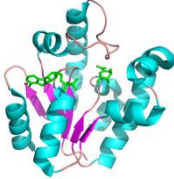


Figure 1.2: Typical representation of protein kinases using protein kinase A (PDB:1ATP)(30), showing its N-terminal lobe (purple), C-terminal lobe (green), C helix (brown), activation segment (cyan), C-terminal extension (yellow), interacting protein (red) and a linker (blue) (31).

1.2.2 Kinase groups and folds

This section covers the different kinase families. It includes a brief structural description of typical members and their interaction with ATP. Included in **Table 1.1** are selected members of each family. As stated previously, structural information and interactions with substrate(s) or other proteins can be essential in defining key mechanistic steps and in the development of throughput screens for drug discovery.

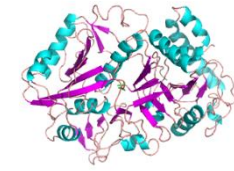
Table 1.1. Overview of kinase groups and families. Adapted from (57).

Group	Family and members	Example	Structure
Group 1: Protein S/T-Y kinase/ atypical protein kinase/ lipid kinase/ ATP-grasp	Protein S/T-Y kinase/ atypical protein kinase	CAMP-dependent protein kinase	PDB: 1CDK (32) 
	Lipid kinase	Phosphatidylinositol-4-phosphate 5-kinase	PDB: 2GK9 (33) 
	ATP-grasp	Pyruvate phosphate dikinase	PDB: 1KBL (34) 
Group 2: Rossmann-like	P-loop kinases	Shikimate kinase	PDB: 2IYQ (35) 

Phosphoenolpyruvate
carboxykinase

Phosphoenolpyruvate
carboxykinase

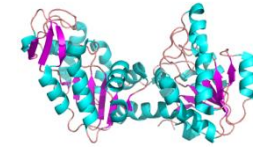
PDB: 1AYL (36)



Phosphoglycerate kinase

Phosphoglycerate kinase

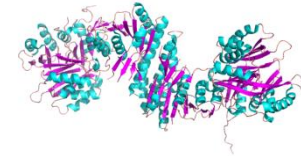
PDB: 4DG5 (37)



Aspartokinase

Aspartate kinase

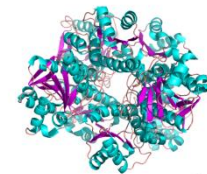
PDB: 3L76 (38)



Phosphofructokinase-like

Phosphofructokinase

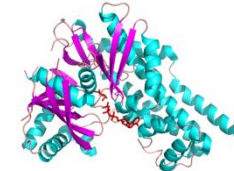
PDB: 1MTO (39)



Ribokinase-like

Glucokinase

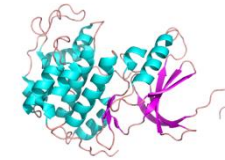
PDB: 3FGU (40)



Thiamin pyrophosphokinase

Thiamin pyrophosphokinase

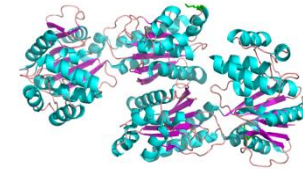
PDB: 1LG3 (41)



Glycerate kinase

Glycerate kinase

PDB: 2B8N (42)

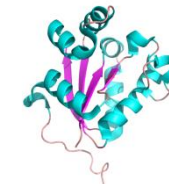


Group 3: Ferredoxin-like fold kinase

Nucleoside-diphosphate kinase

Nucleoside-diphosphate kinase

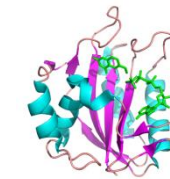
PDB: 1PAE (43)



HPPK (7, 8-Dihydro-6-hydroxymethylpterin-pyrophosphokinase)

Pyrophosphokinase

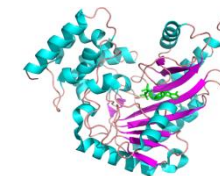
PDB: 1HQ2 (44)



Guanidino kinases

Arginine kinase

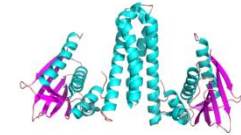
PDB: 1SD0 (45)



Histidine kinase

Histidine protein kinase

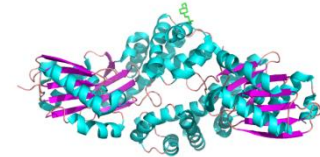
PDB: 4U7N (46)



Group 4: Ribonuclease H-like

Hexokinase

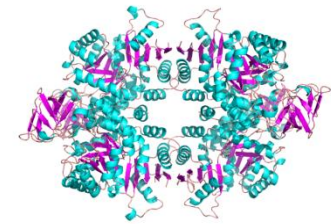
PDB: 2E2N (47)



Group 5: TIM β/α -barrel kinase

Pyruvate kinase

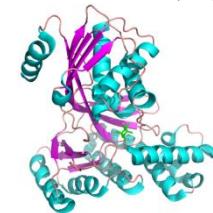
PDB: 1PKL (48)



Group 6: GHMP kinase

Galactokinase

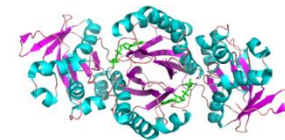
PDB: 1PIE (49)



Group 7: AIR synthetase-like

Thiamine-monophosphate kinase

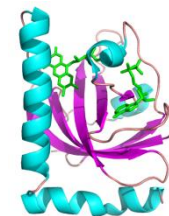
PDB: 5CC8 (50)



Group 8: Riboflavin kinase

Riboflavin kinase

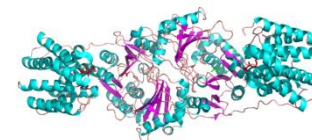
PDB: 1P4M (51)



Group 9: Dihydroxyacetone kinase

Dihydroxyacetone kinase

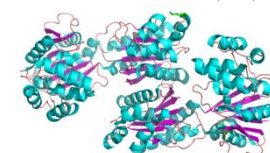
PDB: 1UN9 (52)



Group 10: Putative glycerate kinase

Glycerate kinase

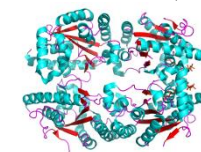
PDB: 2B8N (42)



Group 11: Polyphosphate kinase

Polyphosphate kinase 2

PDB: 5LL0 (53)

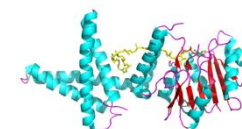


Group 12: Integral membrane kinases

Dolichol kinase

Dolichol monophosphate
mannose synthase

PDB: 5MM1 (54)



Undecaprenol kinase

Undecaprenol kinase

Group 1 kinase fold is composed of three families; protein serine/threonine-tyrosine kinase-like, the lipid kinase and the ATP-grasp family. The active sites of members of this family are sandwiched between the two α + β domains which comprise the enzyme structure. In all three families, ATP binds at the β -sheet of the $\alpha\beta\beta$ core of their C-terminal domain (55).

The Rossmann-like group (group 2) contains eight families: ribokinase-like, phosphoenolpyruvate carboxykinase, aspartokinase, P-loop kinases, phosphoglycerate kinase, glycerate kinase, thiamin pyrophosphokinase, and phosphofructokinase-like. A common feature in this family is the presence of three layers $\alpha/\beta/\alpha$ in the nucleotide-binding domain. The central β -sheet is primarily parallel with a change in direction of strand order in the middle of the sheet (56). Within families, the strands and strand order in the β -sheet may differ. Here, the extreme diversity of substrate specificity is accounted for by the vast range of additional domains that can accommodate phosphoryl-acceptor substrate binding. Members of this group also share similar nucleotide binding patterns. The nucleotide binds at the C-terminal ends of the β -strands with the phosphates at the N-terminal of either one or more α -helices.

Enzymes in ferredoxin-like group, as the name suggests, contain a nucleotide binding domain core very similar to the ferredoxin fold. This group is composed of four families: nucleoside diphosphate kinase (NDP), 7, 8-dihydro-6-hydroxymethylpterin-pyrophosphokinase (HPPK), guanidino kinase and histidine kinase. One interesting feature in the ferredoxin fold/ α - β plait fold/ α + β sandwich is the $\beta\alpha\beta\beta\alpha\beta$ unit with the four strands of anti-parallel β -sheet ordered as 2-3-1-4. There are two helices on one side of the sheet. Each family in this group possesses different nucleotide binding modes, protein-substrate interactions, substrate orientation and location relative to a ferredoxin-like core (57).

Group four, the ribonuclease H-like fold contains the ASKHA (acetate and sugar kinase/hsc70/actin) superfamily. The ribonuclease H-like fold is made of three layers, $\alpha/\beta/\alpha$ and five strands of β -sheets of order 3-2-1-4-5. The binding of nucleotides and divalent metal ion coordination are enhanced by interactions of ATP with many different conserved motifs within ASKHA superfamily (58). These motifs include the adenosine motif that interacts with α -phosphoryl and ribosyl groups of ATP, the phosphate motif 1 that interacts with the magnesium cation and phosphate 2 motif interacts with β - and γ -phosphoryl groups of ATP. Their mechanism is thought to be via acid-base catalysis. In the case of hexokinase, an aspartate residue serves as a base, deprotonating the 6-hydroxyl group of glucose (59,60).

Group five is made of enzymes with a characteristic TIM β/α - closed barrel made of eight fold repeats of $\beta\alpha$. In this group, the inner layer of the barrel is made of eight β -strands of order 12345678, encircled by eight α -helices (e.g. pyruvate kinase). Within this group, the active site is located at the C-terminal end of parallel β -strands. Pyruvate kinase's nucleotide binding involves hydrogen bonding interactions with two arginines, an asparagine, lysine residues, and metal cations. The adenine moiety is held in place by histidine, proline and tyrosine residues. In pyruvate kinase, each γ -phosphoryl oxygen atom is coordinated to a different inorganic cofactor. Pyruvate kinase phosphotransfer is said to be in-line and direct, aided by a series of conserved residues possibly responsible for acid-base catalysis (61)

Group six is composed of the GHMP kinase superfamily which was named after its original four members galactokinase, homoserine kinase, mevalonate kinase, and phosphomevalonate kinase (58). The group's fold is made of two $\alpha+\beta$ domains that sandwich the active site. The N-terminal domain contains the nucleotide-binding site and binding is assisted by

a novel conserved PXXXGSSAA P-loop motif, and the magnesium ion is coordinated by a glutamate residue.

Members of group seven are thiamine-phosphate kinase and selenide, water dikinase, which are homologous to the group's prototype AIR synthetase (PurM) (62). This prototype, AIR synthetase has two α/β domains. Its N-terminal domain is composed of six strands of β -sheets with four helices on one side. At the C-terminal end, there are six strands of β -sheets, sided by seven α -helices. AIR synthetase exists as a dimer, and its active site is located between the two subunits (62). Nucleotide binding occurs at the N-terminal end while the opposite C-terminal binds the second substrate (63).

Groups 8-12 comprise of some unsolved structures and other enzymes that have been reclassified. Group 8 contains riboflavin kinase, previously classified as group 10. Group 9 (dihydroxyacetone kinase) previously classified as group 17, contains glycerone kinase. Putative glycerate kinase, previously classified as group 16, now holds group 10 with glycerate kinase as a group member. Polyphosphate kinase is now group 11 (then group 9). Group 12 (integral membrane kinases) previously classified as group 8, contains dolichol kinase and undecaprenol kinase.

Together, understanding the structural dynamics and diversity of these enzyme families and their interaction with the ubiquitous nucleotide substrate offers potential insight, especially in the development of new therapeutics with low cross reactivity with host metabolism.

1.2.3 Nucleoside monophosphate (NMP) kinases

Within the Rossmann-like group, and listed among the members of P-loop kinases are the nucleoside monophosphate (NMP) kinases. The NMP kinases include enzymes like adenylate kinase, guanylate kinase, shikimate kinase, etc. As originally discovered and described, the NMP kinases catalyze the reversible transfer of the γ phosphoryl group from a nucleoside triphosphate (NTP), usually ATP, to the phosphoryl group on a nucleoside monophosphate, resulting in the formation of two nucleoside diphosphates. These enzymes are essential in nucleotide salvage and *de novo* biosynthetic pathways (64–68). Based on substrate specificity, the NMP kinase family is divided into four subgroups; adenylate kinases (AK), uridylylate-cytidylylate kinases (UMP-CMPK), guanylate kinases and thymidylylate kinases. Nevertheless, all four subgroups share a common three-domain structure. The main regions for phosphoryl donor binding and recognition (including the highly conserved phosphate binding P-loop) are the lid domain, and the NMP-binding domain (69,70). As with protein kinases, members of this group are conformationally flexible (71), most notably, the closure of the lid domain over the active site upon substrate binding. All of these structures are evident in the canonical representative of the NMP kinases, AK: the core (residues 1 – 28 [including the Walker A motif or P-loop], 60 – 119, 158 - 206), the lid domain (residues 120 - 157) and the NMP domain (residues 30 - 59) (71,72) (**Figure 1.3**). AK catalyzes reversible phosphoryl transfer from ATP to AMP and functions to regulate the balance of ATP, ADP, and AMP concentration in cells and organelles (73).

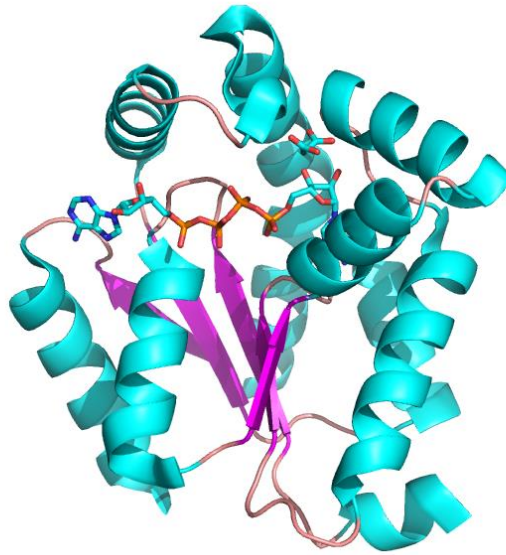


Figure 1.3: Structure of human adenylate kinase 1 (PDB: 2C95) (74) in complex with AP5A (bis(adenosine)-5'-tetrphosphate) and malonate.

Substrate-free AK exists in an 'open' conformation. Upon substrate binding, the enzyme adopts its 'closed' conformation wherein the lid domain closes over the bound substrates and facilitates that phosphoryl transfer event. The result of the phosphoryl transfer is two ADP molecules which are released upon reopening of the lid domain (75,76). To date, there are nine isozymes of AK (AK1 - AK9) numbered in order of their discovery (72,73,77). AKs use a wide range of phosphate donors (63, 64, 65).

Human AKs (AK1, AK4, AK5, AK7, AK8) and UMP-CMPK families can catalyze the conversion of any (d)NDP to its corresponding (d)NTP. These enzymes can phosphorylate both TDP and UDP with GTP as phosphate donor. Some AKs specifically bind (d)NDPs or (d)NMPs,

owing to the fact that their active sites can better accommodate specific (d)NMPs or in the case of (d)NDPs the proximity to the γ -phosphoryl group of the donor ensures its transfer (80).

More recently, several kinases whose phosphoryl acceptor substrates are not nucleoside monophosphates (e.g., gluconate kinase, pantothenate kinase, and shikimate kinase) have been shown to share substantial structural similarity with classical NMP kinases like AK. Consequently, these are also considered members of NMP kinase family. Interestingly, shikimate kinase shows great structural similarity to other NMPS especially in the P-loop, nucleotide binding and lid domains (**Figure 1.4**). Within NMPs, there is high sequence similarity in the P-loop sequence $X_hX_hX_hGXXGKG/ST$, where X represents any amino acid and X_h is any hydrophobic residue (**Figure 1.5**) (81). In contrast to many of the classical NMP kinases like AK, some kinases like pantothenate, gluconate, shikimate kinase, etc. possess distinct specificity for their phosphoryl donor; ATP is their only substrate to serve in this capacity.

```

shikimate      1
cytidylate    1
Adenylate     1
Adenylate     1
Guanylate     1
Pantothenate  1 MTFYLQFDRSQWAALRDSVPMTLTEDEIAQLKGINEDLSLEEVAEIYLPLSRLLNFYISSNLR
Gluconate     1
UMP-CMP       1
Thymidylate   1

                                P-loop
shikimate      1          MAPKAVLVGLFPGSGKSTIGRRLLAKALRVGLLDTDVAIEQR-----
cytidylate    1          MTDIVVAIDGPAAGTGSVSVSRGLARELGARYLDTGAMYRMMTLAVLRAGID
Adenylate     1          MRLILLGPPGAGKGTQAQRLVEKYGIPQLSTGDMLEAAVQAGTEV---
Adenylate     1          MRVLLGPPGAGKGTQAVKLAEKLGIPQISTGELFRNIEEGTKL---
Guanylate     1          MAGPRPVVLSGPGAGKSTLLKLLFQEHSSIFGFSVSHTRNRPGEED---
Pantothenate  65 QAVLEQFLGTNGQRIPIYIISIAGSVAVGKSTTARVLLQALLSRWPEHRRVELITTDGFLHPNQVL
Gluconate     1          MSVHPSPKPSPPIVVMGVCAGKTTVAAAALSQRLGVPFMEADTLHFQAN-----
UMP-CMP       1          MMEKSKPNVVFVLGGFSGKGTQCANIVRDFGWVHLSAGDLLRQEQSGSKD---
Thymidylate   1          MDSRGGGIGHWISFEGIDVGVKTTQASRLAEWL--VQHGRDALLVRE-PGGTAL---

shikimate      41 -----TGRSIADIFAT-----DGEQEFRRIEEDVVRaalADHDGVLSLGGGAVTSPGVRA
cytidylate    52 PADAAAIGESVWVQMLSDHdryFLGGEDVSSeirTEEVtQAVSAVSAIPAVRVLVDLQRQMA
Adenylate     46 -----GKRAKAVMD-----AGELVSDAIVNAIvaERIDQADcANGFiLDG-YPRtLVQ
Adenylate     46 -----GVEAKRYLD-----AGDLVPSDLTnELVDDrLNNPDAANGFiLDG-YPRsVEQ
Guanylate     50 -----GKDYFVTR-----EMMQRDIAAGDFIEHAEfSGNLYGTSKEAVRAVQAMNR
Pantothenate  129 KERGLMkkkGfPESyDMHRLVkfVSDLkSGVpNVTAPVYshLIYdVIEpGDKtVAQpDILILEG
Gluconate     49 -----VTkMAAG-----KPLDDDRRfPwLRRVGRWlADHPGGGViSCSAL
UMP-CMP       53 -----GEMiATMIK-----NGEiVPSiVtVKLLkNAIDANQgkn-FLVdG-fPRNEEN
Thymidylate   52 -----GEALRHMiLHDVEIHDAWAEfLLFAAARAEltVtVIRPALAAGRwViSDRfTDSsIA

shikimate      91 ALAGHTVVYLEISAAEGVR-----RTGGNTVRPLLAGPD-----RAEKYRALMA
cytidylate    116 EGRGSVVVEGRDIGTVVLPDAPV--KIFLTASpETRARRRNDQNVASG-----SADdyDRVLA
Adenylate     93 ADAVESMLSDRGLTLDAV-----IELVDDRALVGRIGKRAEEAKAAGLPVRKDDNPAVFE
Adenylate     93 AKALHEMLERRGTDIDAV-----LEFRVSEEVLLERLkGRG-----RADtDDVIL
Guanylate     97 ICVLDVLDLQGVRSIKKTDLCPIY--IFVQPPSLDVLEQRlRLRN-----TETEESLA
Pantothenate  193 LNVLQSGMDYPHDPHHVfVSDfVDFSIYVDAPeELLQTwYINrFLkFREG----AFTDPDSYfH
Gluconate     89 ARRYRDTLREncPQVAFLH-----LSGSAEliGRRLAARS-----DHfMP
UMP-CMP       99 NNSWEENMKD-FVDTKFV-----LFFDCPEEVMTQRLLkRGESSG-----RSDDNiESiK
Thymidylate   109 YQVFGRGLPwGpVDQVNR-----WiSRGERPDMtVWLDGQP-----LTARGDDRLE

shikimate      135 KRAPLYRRVATMRVDTNRRN-----PGAVVRHILSRlQVfSPSEAA
cytidylate    172 EVRRRDHLDSTRAVSPLYVAQDAMIvDTSkMAEAeVIAHlMDLVkQRSGAVW
Adenylate     149 ERLKEYYKkTSPLIGYYAK--GKLRGVDGMADIDAVTRQIEVVLtATTQqVGGQAAS
Adenylate     139 NRMKVYRDETAPLLEYR-----DQLkTVDAVG-TMDEVFARALRALGK
Guanylate     147 KRLAAARTDMESSEKPEGLFD-----LVIINDDLKAYATLkQALSEEIKKAQGTGHA
Pantothenate  253 NYAKLSKEAVNTATSLWKEINWLNlKQNIlPTrERASLiMTKSANHAVEQVRLRK
Gluconate     129 ATLLRSQldTLEPLGDdERG-----VTVDiDGVGGDvDSiVEAPfLAsG
UMP-CMP       148 KRfNTfNVQTKLViDHYNkF--DKVKIIPANrDVNEVYNDVENlFKSMGF
Thymidylate   155 QREAAyFDRVQEGYAWLWAREPNRIYrVPANQPAEAVSDAIKeALIRWpDLERkGESp

```

Figure 1.4: Sequence alignment (82) of nine NMPs highlighting residues with >70% conservation. Alignment includes sequences of *MtSK*, cytidylate kinase from *M. leprae*, human AK, *M. tuberculosis* AK, mouse guanylate kinase, pantothenate kinase from *Salmonella enterica*, UMP-CMP kinase from *Dictyostelium discoideum*, and thymidylate kinase from *Sulfobacillus acidophilus*. Only the P-loop sequence (XXXGXXGXXGK/ST) showed >70% sequence conservation.

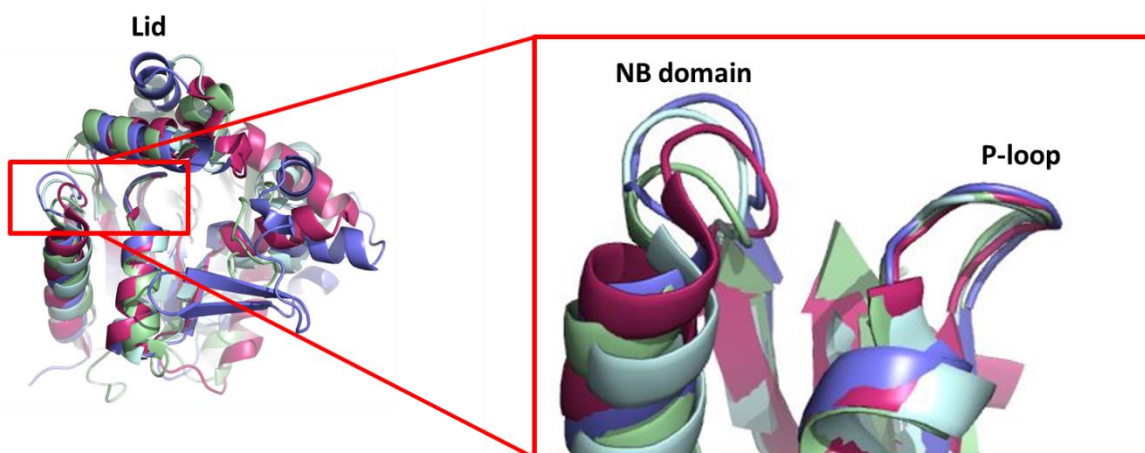


Figure 1.5: Alignment of selected kinases showing the structural similarity on the nucleotide binding domain and the P-loop. Structure in red represents mouse guanylate kinase (PDB: 1LVG) (83). In pale cyan is *Mycobacterium tuberculosis* shikimate kinase (*MtSK*) (PDB: 1WE2) (84). Human adenylate kinase expressed in *E. coli* is shown in pale green (PDB: 2C95) (74) while cytidine monophosphate kinase (CMP) from *E. coli* is represented in purple (PDB: 1CKE) (85).

1.2.3.1. Shikimate kinase

As mentioned above, shikimate kinase (SK) has a nucleoside monophosphate (NMP) kinase fold. It catalyzes the stereospecific transfer of the γ -phosphoryl group of ATP to the C3 hydroxyl of shikimate. To date, coordinates for over 20 structures of shikimate kinase (*MtSK*) have been deposited in the Protein Data Bank (PDB), including several with bound substrates,

products, and/or substrate analogs (35,86–92). The core of the SK structure is an α/β mononucleotide binding fold (i.e., five parallel β -stands flanked by α -helices) (**Figure 1.6**) as is observed in AK and other NMP kinases (90,93,94,95). On this foundation, the three other components which comprise the typical structure of an NMP kinase are also evident: 1) the nucleotide-binding (NB) domain which contains a P-loop (residues 9-17,) (94), adenine binding (AB) loop (residues 148-155), and an α_6 helix (residues 104-110) (93), 2) the conformationally dynamic lid domain (residues 112-124) (95), and 3) the equivalent of an NMP (i.e., phosphoryl acceptor) binding domain. Here, the core NMP binding domain (residues 32-61) is augmented by additional residues which together comprise the extended substrate binding (ESB) domain (residues 32-93) (96) (**Figure 1.7**).

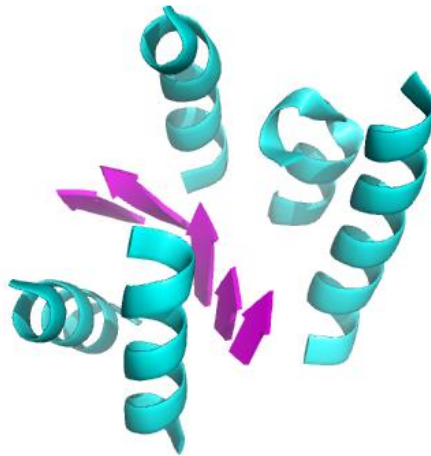


Figure 1.6: Structure of shikimate kinase from *Mycobacterium tuberculosis* showing five central parallel β -sheets flanked by α -helices. PDB: 1WE2 (84).

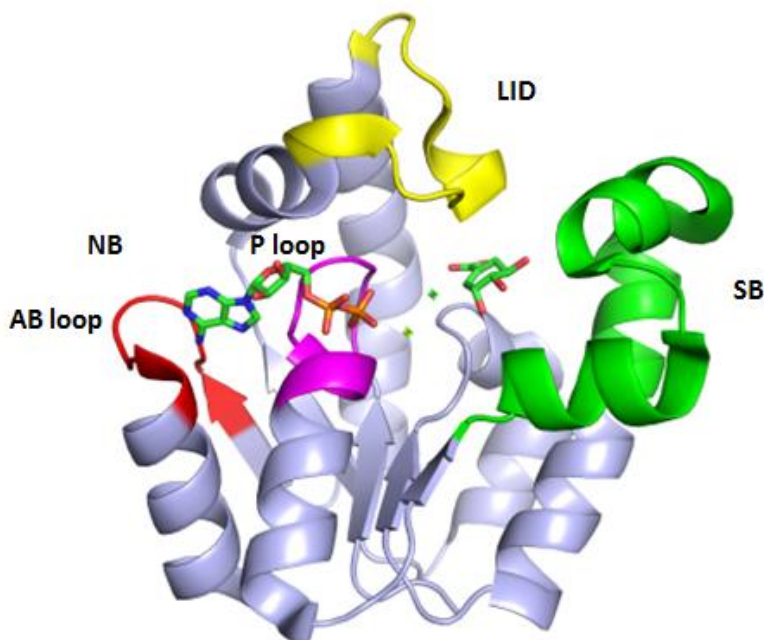


Figure 1.7: Structure of *MtSK* in complex with ADP and shikimate. Yellow (lid domain), green (shikimate binding domain), red (Adenine binding loop), purple (P-loop). Coordinates are from Protein Data Bank (PDB) accession number 1WE2 (90).

Using fluorescence spectroscopy (91), circular dichroism (93), crystallography (87,89–92,96–98), and molecular dynamics simulations (86), key interactions in *MtSK* catalysis have been identified. The shikimate binding pocket is highly conserved with respect to charged residues Arg 136, Arg 58, Glu 61, Asp 34 and Lys 15 as well as two phenylalanines (Phe 49 and Phe 57), a consecutive series of three glycines (Gly 79, Gly 80, and Gly 81) and Pro 118. Interactions with Asp 34 and Arg 136 are key to proper positioning of shikimate (99). Shikimate binds in an unstable conformation with two of its hydroxyl groups (C4 and C5) in an axial

orientation. This way the enzyme controls the equatorial disposition of the C3 hydroxyl group, allowing for its phosphorylation. Asp 34 stabilizes the C4 hydroxyl via hydrogen bonding (92).

1.3 Shikimate pathway

First elucidated by Davis and Sprinson and their collaborators over a half-century ago (100), the shikimate pathway is a seven-step metabolic route for the synthesis of essential aromatic compounds, including *p*-aminobenzoic acid (PABA), tocopherols (e.g., vitamin E), phyloquinones (e.g., vitamin K), folates, L-Phe, L-Tyr, L-Trp etc. The pathway generates chorismate from erythrose-4-phosphate and phosphoenol pyruvate, making a clear connection between carbohydrate metabolism and the biosynthesis of aromatic compounds.

There are seven enzymes of the shikimate pathway (**Figure 1.8**). The first committed step of the pathway is the condensation of phosphoenol pyruvate with erythrose-4-phosphate to produce 3-deoxy-D-arabino-heptulosonate-7-phosphate (DAHP) and inorganic phosphate, a reaction catalyzed by DAHP synthase. Cyclization of DAHP concomitant with elimination of phosphate generates 3-dehydroquinate (3-DHQ). The reaction is catalyzed by DHQ synthase using NAD^+ as a cofactor, however, the reaction does not result in the net reduction of NAD^+ to NADH. 3-DHQ dehydratase eliminates H_2O to generate the cyclohexenone derivative, 3-dehydroshikimate (3-DHS). DHS dehydrogenase catalyzes NADH-dependent reduction of DHQ to shikimate, and then in step five shikimate kinase catalyzes ATP-dependent phosphorylation of the shikimate C3 hydroxyl group to form shikimate-3-phosphate (S3P). A second PEP enters the pathway in the sixth step. The condensation reaction between PEP and S3P to generate 5-enolpyruvyl shikimate-3-phosphate (EPSP) is catalyzed by EPSP synthase. The final step involves the trans-1, 4 elimination of the phosphate group from EPSP by chorismate synthase to

form chorismate (101,102) which is a precursor to aromatic amino acids and other essential aromatic metabolites.

Because this pathway has no mammalian counterpart, its enzymes make attractive targets for drug development. Herbicides like RoundUp[®] (103), Zero[®], Tumbleweed[®] contain the active ingredient, glyphosate (N-phosphonomethyl glycine). It is a potent inhibitor ($K_I = 1 \mu\text{M}$) of EPSP synthase where it competes with PEP as it mimics an intermediate in the ternary EPSP-substrate complex (103,104). It is active against the apicomplexan parasite, malaria (105), highlighting the importance of the pathway enzymes as targets for antimicrobials (106).

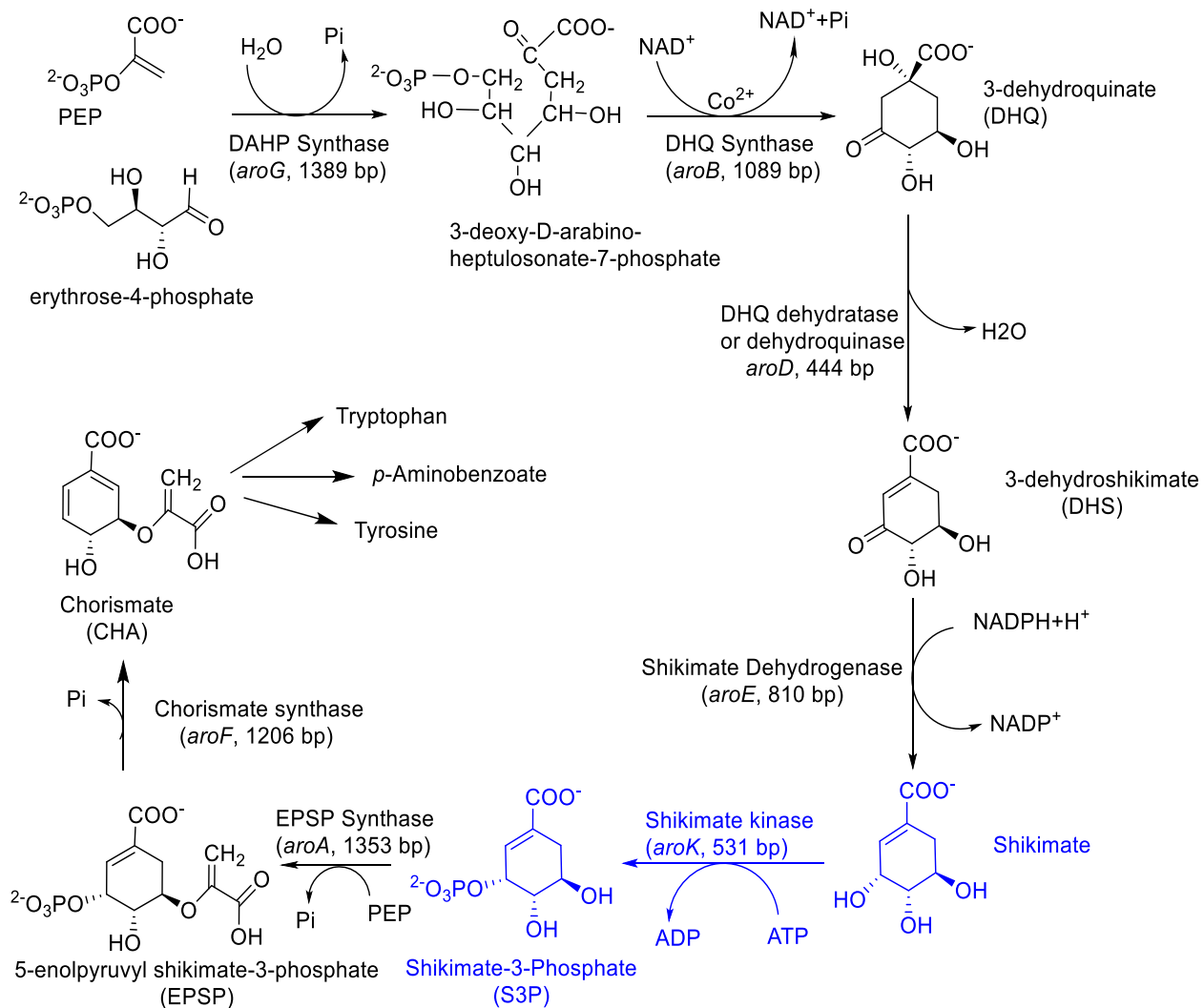


Figure 1.8: The shikimate pathway. A seven-step metabolic route producing precursors to aromatic metabolites (105,107–111). Shikimate kinase catalyzes the fifth step of this pathway, converting shikimate, a product of the dehydrogenase reaction to shikimate-3-phosphate.

1.4 Natural products and drug discovery

Natural products have garnered considerable attention in medicinal chemistry research and the work presented in subsequent chapters of this thesis explore the potential in exploiting them as antimicrobials, particularly with respect to shikimate kinase as a target. Natural products comprise a myriad of uncharacterized compounds, and as such they represent a wealth of potential leads for drug discovery (112). The surge in natural product drug discovery is associated with the advancements in isolation and purification techniques (113–115). Further, the characterization of their targets and mechanisms of action have facilitated great advancement towards the treatment of many human diseases (116,117).

Much progress had been made in the discovery and development process of natural products as a result of increased understanding and exploitation of their biosynthetic pathways (118,119). Biosynthetic, semisynthesis and total synthesis have been utilized to accelerate the drug discovery time scale. Improving the potency of natural products has been done via a variety of methods.

1.4.1 By total synthesis

Infectious diseases like tuberculosis and other lower respiratory infections remain the most communicable diseases worldwide (120). The class of antibiotics called tetracyclines have been very effective in the treatment of bacterial infections. The first representative of this family to be isolated was chlortetracycline (121,122), followed by other related analogues. The analogues were products of unmodified natural products or synthetic modifications of chlortetracycline and tetracycline (123). The complex nature of tetracycline attracted many an organic chemist, leading to the first published racemic total synthesis of tetracycline by

Woodward group (124,125) and has served as a platform for a variety of synthetic routes for many decades (126). A new candidate eravacycline (**Figure 1.9**) is claimed to override tetracycline resistance mechanisms (127). It has completed phase II trials for complicated intra-abdominal infections and is cost effective. This shows novel synthetic routes as a promising approach towards the discovery of effective drug candidates.

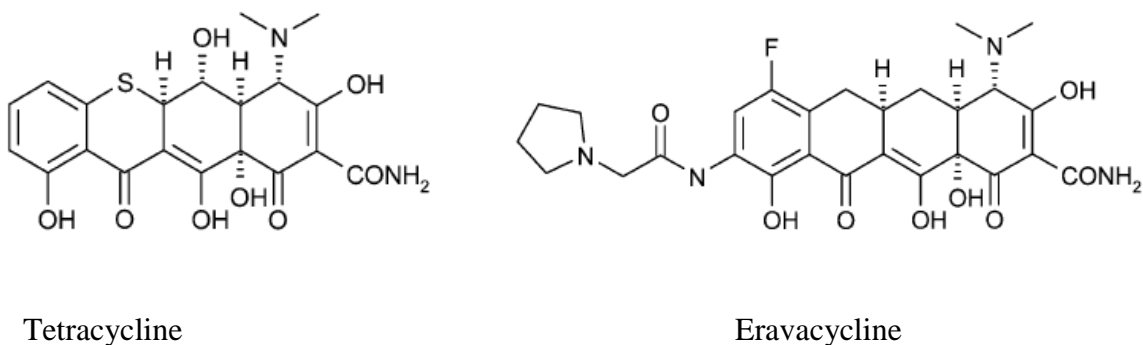


Figure 1.9: Structure of tetracycline and its derivative eravacycline

1.4.2 By modification of existing scaffolds

The glycopeptide, vancomycin (**Figure 1.10**) has been the drug of choice for the treatment of multidrug-resistant bacterial infections (128,129) for a long time. About three decades ago, vancomycin-resistant bacteria have been detected. These include vancomycin-resistant enterococci (VRE), vancomycin-intermediate susceptibility (VISA) and vancomycin-resistant *Staphylococcus aureus* (VRSA) strains (130–135).

Bacterial inhibition is by inhibition of cell wall synthesis through tight binding of the antibiotic to peptidoglycan terminus D-Ala-D-Ala. Modification of this terminus to D-Ala-D-Lac is the cause of two most common forms of vancomycin resistance, vanA and vanB (136).

Resistance was overcome by the use of total synthesis to redesign the vancomycin peptide backbone, reversing the repulsion between D-Ala-D-Lac of the resistant bacteria and the carbonyl of central substituted phenylglycine by replacing the carbonyl with a methylene or imine group. This restored affinity for drug to target (137–139).

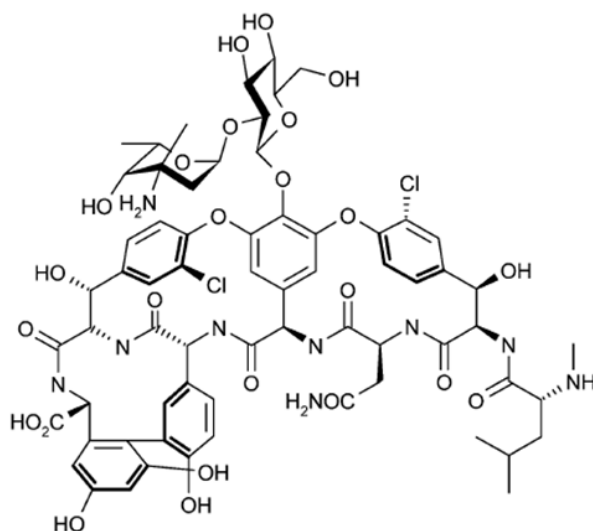


Figure 1.10: Structure of Vancomycin

1.4.3 By immunoconjugation

Natural Products constitute a rich source of potent cytotoxic agents (140). Many have served as leads towards development of anti-cancer agents. With the advent of fully humanized monoclonal antibodies (mAbs), target specificity, affinity and tolerance have been increased, improving clinical response to cancer immunotherapy. This is through the formation of an immunoconjugate or antibody-drug conjugate (ADC), by the covalently coupling the monoclonal antibody to a natural product. With this approach, the effector (natural product) toxicity and the specificity of the mAbs mediate killing of cancer cells. Once the antibody binds to cancer cell

surface antigen, the conjugate is internalized and the linked natural product is released, killing the cell. An example of such is Brentuximab vedotin (Adcetris™) (**Figure 1.11**), first isolated from the sea hare *Dolabella auricularia* (141). It was approved for the treatment of Hodgkin's and systemic anaplastic large cell lymphoma.

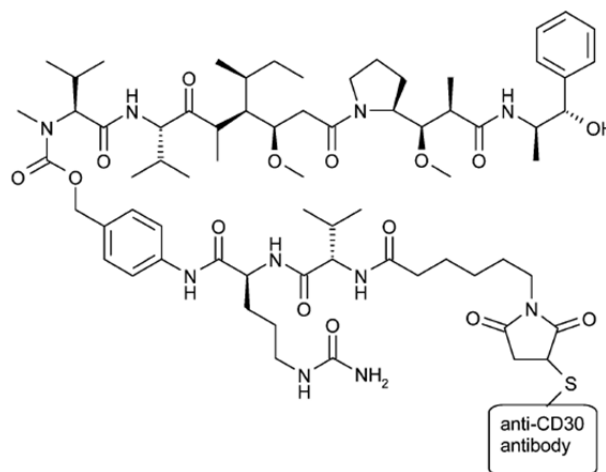


Figure 1.11: Structure of brentuximab vedotin

1.4.4 Total synthesis of unmodified natural products

About 20% of natural product-derived drugs are in this group (140). A classic example in this category is artemisinin used in the treatment malaria. Artemisinin is a sesquiterpene lactone peroxide that was originally extracted from the aerial parts of the shrub *Artemisia annua* (142). The first total synthesis of artemisinin was in 1983 (143). Though other synthetic routes have been published (144–146), the commercialization artemisinin remains costly. Its very short half-life and poor water solubility (147), motivated efforts toward semisynthesis of derivatives like artemether, arteether, and artesunate. Artemisinin and its derivatives (**Figure 1.12**) are currently

the most effective antimalarial drugs available on the market (148) and are prescribed in a combination called ‘artemisinin-based combination therapies (ACTs)’ (149).

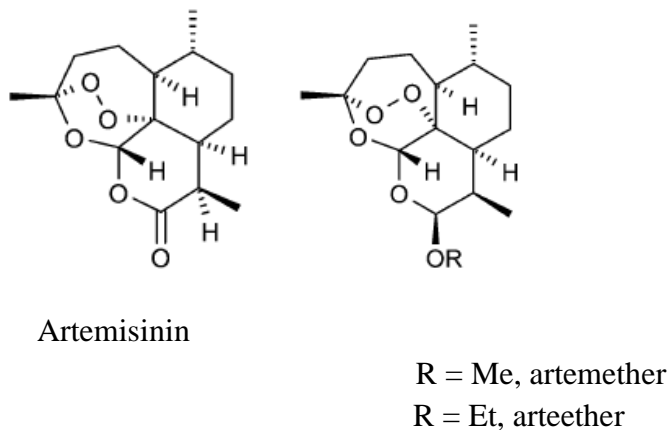


Figure 1.12: Structure of Artemisinin and derivatives artemether and arteether.

1.5 Marine natural products in the drug discovery pipeline

Marine organisms have served as a great source of marine-derived natural products that could potentially be developed into therapeutics. Though very few marine natural products have been FDA-approved so far, there is a substantial amount of marine natural products in different phases of clinical trials.

1.5.1 FDA-approved marine pharmaceuticals

Currently, cytarabine, vidarabine, and ziconotide are the three FDA-approved marine pharmaceuticals in the US Pharmacopeia. Trabectedin has also been approved by EMEA (European Agency for the Evaluation of Medicinal Products) and also completed key approval studies in the US.

The FDA-approved synthetic pyrimidine nucleoside, cytarabine (arabinosyl cytosine or Ara-C) was developed from spongothymidine isolated from the Caribbean sponge *Tethya crypta* (150). It is a specific antimetabolite of the S-phase that undergoes intracellular conversion into cytosine arabinoside triphosphate. This competitively excludes the physiologic substrate deoxycytidine triphosphate, inhibiting DNA polymerase and synthesis of new DNA. The conventional cytarabine is recommended for treatment of acute lymphocytic leukemia, acute myelocytic leukemia and meningeal leukemia (151,152) while liposomal cytarabine is recommended for treatment of lymphomatous meningitis (153).

The synthetic purine nucleoside, vidarabine or Ara-A, developed from the nucleoside spongouridine extracted from the Caribbean sponge *Tethya crypta* (150) and currently obtained from *Streptomyces antibioticus*. In cells, there is rapid conversion of Ara-A to adenine arabinoside triphosphate, inhibiting viral DNA polymerase and DNA synthesis in viruses like herpes, vaccinia and *Varicella zoster*.

The third approved drug ziconotide is a synthetic equivalent of ω -conotoxin MVIIIA, a naturally occurring 25-amino acid peptide in the venom of marine snail *Conus magnus* (154). Ziconotide functions as an analgesic, reversibly blocking N-type voltage-gated calcium channels located in the afferent nerves of the dorsal horn of the spinal cord (155,156). Ziconotide was approved by the FDA in 2004 and is currently used for the management of severe chronic pain in patients with AIDS or cancer (157,158).

Trabectin is a tetrahydroisoquinoline alkaloid extracted from the marine tunicate *Ecteinascidia turbinata* (159,160). It is the first marine anticancer agent to be approved in the European Union against soft tissue carcinoma (161) and relapsed Pt-sensitive ovarian cancer (162). The mechanism of action of trabectin is not fully understood but it forms a reversible

covalent bond with DNA minor groove (163) and interacts with a variety of nucleotide excision repairs systems (164–166).

1.5.2 Marine pharmaceuticals in clinical pipeline

1.5.2.1 Compounds in Phase III trials e.g. Eribulin and soblidotin

The polymacrolide ether, eribulin mesylate (E7389, **Figure 1.13**) Halichondrin B (HB) from marine sponges (167) has shown potent anticancer activity preclinical animal models (168). Macrocyclic ketone analogues (169) of this compound are also active and the parent/natural compound still shows potent biological and pharmacological activity (170). Though its mechanism of inhibition may be similar to those of the taxanes and vinca alkaloids, it inhibits microtubule dynamics by binding to tubulin, thus suppressing the microtubule growth phase during interphase (171,172). It exhibits potent, irreversible antimitotic effects in cancer cells leading to apoptosis (173).

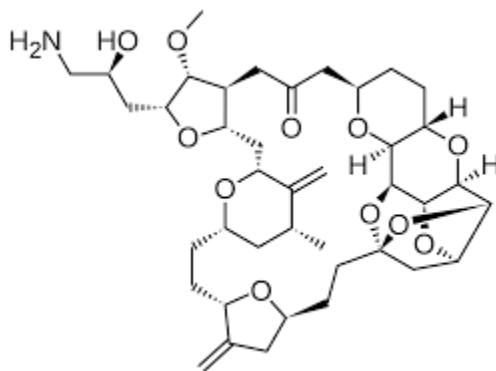


Figure 1.13: Structure of eribulin mesylate

1.5.2.2 Examples of compounds in Phase II trials: DMXBA

3-(2,4-dimethoxybenzylidene)-anabaseine (DMXB) (**Figure 1.14**) is a synthetic derivative of an anabaseine alkaloid from marine worms, and it can selectively stimulate $\alpha 7$ nicotinic acetylcholine receptors (174) expressed in CNS neurons and astrocytes and peripheral macrophages. DMXB has shown neuroprotective abilities in both *in vitro* and *in vivo* studies (175,176). In cultures of cerebral cortex neurons, it slows down the adverse effect of β -amyloid (177) and has shown anti-inflammatory activities in some animal models (178,179). Substantial cognitive improvements have been observed in healthy young males (180) and schizophrenics (181) during Phase I clinical trials. Phase II trials have shown enhanced cognitive functions in patients with schizophrenia (182).

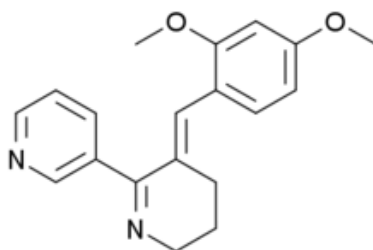


Figure 1.14: Structure of DMXB

1.5.2.3 Examples of compounds in Phase I trials: Hemiasterlin

Hemiasterlin (**Figure 1.15**) is a cytotoxic tripeptide from marine sponges (183). Analogues resulting from substitutions to the N-terminal amino acid possessed a high potency in *in vitro* systems, suitable pharmaceutical properties and were resistant to p-glycoprotein-mediated efflux (184). It binds preferentially to α -tubulin leading to apoptosis in tumor cells

(185). Associated adverse effects observed in Phase I studies include nausea, constipation, fatigue and vomiting (186).

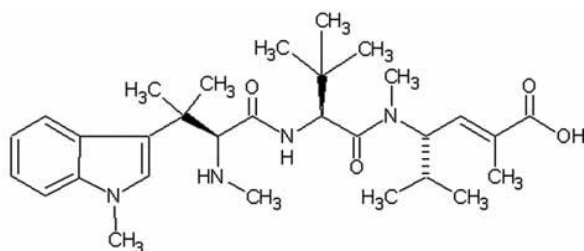


Figure 1.15: Structure of Hemiasterlin

1.6 Enzyme inhibition

There are a myriad of molecules that can bind or interact with enzymes. Molecules/compounds that bind to and decrease the activity of an enzyme are called inhibitors. This decrease in activity can ultimately result in the death of a pathogen or slow down metabolic processes at cellular and subcellular levels. Inhibitors exert their actions via a variety of mechanisms.

1.6.1 Rapid reversible inhibition

As illustrated in the general scheme below (**Figure 1.16**), the range of common rapid reversible mechanisms of inhibition (e.g., competitive, uncompetitive, etc.) can be understood to fall on a continuum depending on the extent to which the inhibitor in question prefers the free enzyme versus enzyme-substrate complex(es). Here, the former is represented by the value of the dissociation constant K_I (Equation 1), and the latter is represented by the value of the dissociation constant αK_I (Equation 2). Rapid equilibrium between free inhibitor and the corresponding enzyme-inhibitor complexes is assumed, and formation of an enzyme-inhibitor complex (EI and/or ESI) renders the enzyme inactive (i.e., unable to carry out substrate conversion to

product). The range of common, rapid-reversible inhibition mechanisms can be accounted for by a single equation (Equation 3), where each mechanism is distinguished by the value of α , from values far greater than 1 (competitive) to far less than 1 (uncompetitive) to values close to or equal to 1 (mixed or pure noncompetitive, respectively).

$$K_I = \frac{[E][I]}{[EI]} \dots\dots\dots \text{Eq. 1}$$

$$\alpha K_I = \frac{[ES][I]}{[ESI]} \dots\dots\dots \text{Eq. 2}$$

$$\frac{v_0}{[E]_T} = \frac{\frac{k_{cat}}{(1+\frac{[I]}{\alpha K_I})} [S]}{[S] + K_M \left(\frac{(1+\frac{[I]}{K_I})}{(1+\frac{[I]}{\alpha K_I})} \right)} \dots\dots\dots \text{Eq. 3}$$

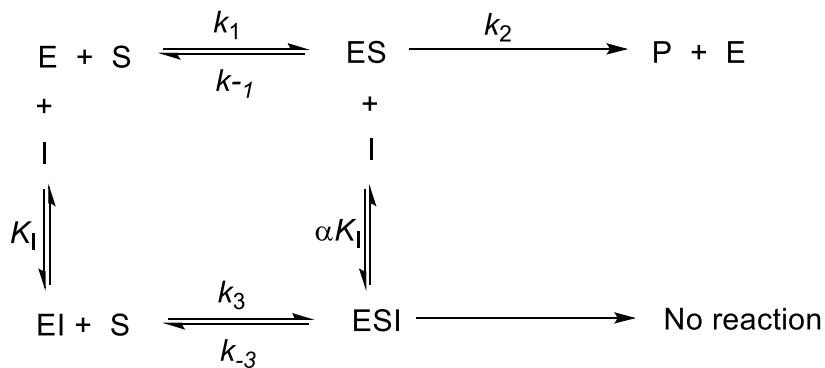


Figure 1.16. Schematic representation of common rapid reversible mechanisms.

1.6.1.1 Competitive inhibition

With competitive inhibition, enzyme association with the inhibitor and the substrate are mutually exclusive events. Most commonly this is because the inhibitor and the substrate compete for binding within the active site (i.e., binding of inhibitor and substrate are mutually exclusive). Of course, an enzyme that is unable to associate with its substrate due to an interfering inhibitor will be unable to catalyze its reaction. According to the continuum represented in **Figure 1.16** a competitive inhibitor would be one in which $\alpha \gg 1$ (i.e., $K_I \ll \alpha K_I$)

With increasing concentrations of a competitive inhibitor, the k_{cat} (i.e., the maximum catalytic output of the enzyme) remains unchanged, but the apparent K_M for substrate (i.e., the concentration of substrate necessary to reach $\frac{1}{2} k_{cat}$) increases by $1 + [I]/K_I$. Likewise, the apparent second-order rate constant for the enzyme-catalyzed reaction (i.e., k_{cat}/K_M or k_{on}) decreases by the same factor (187). An example of a competitive inhibitor is ibuprofen (**Figure 1.17**) (188).

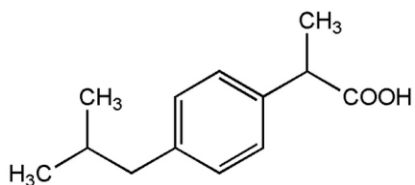


Figure 1.17: Structure of ibuprofen

1.6.1.2 Uncompetitive inhibition

On the opposite end of the continuum, an uncompetitive inhibitor is one that requires that substrate be bound to the enzyme. In other words, the inhibitor binds exclusively to the ES complex(es) but not the free enzyme (i.e., $\alpha \ll 1$). Increasing concentrations of an uncompetitive inhibitor produce decreases in both k_{cat} and K_M by the same factor, $1 + [I]/\alpha K_I$. As such, the value of k_{on} (i.e., k_{cat}/K_M) is unaffected by the concentration of an uncompetitive inhibitor. Compared to competitive, uncompetitive inhibitors are relatively rarely observed; however, one example is ciglitazone an uncompetitive inhibitor of 15-hydroxyprostaglandin dehydrogenase with respect to the prostaglandin E_2 (189).

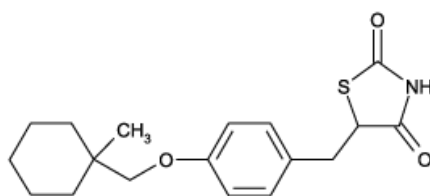


Figure 1.18: Structure of ciglitazone

1.6.1.3 Noncompetitive inhibition

A noncompetitive inhibitor binds to both the free enzyme and the enzyme-substrate complex(es). If the inhibitor binds with equal affinity to E and ES (i.e., $\alpha = 1$), the inhibitor is referred to as pure noncompetitive. Here, both k_{cat} and k_{on} will be diminished with increasing concentrations of the inhibitor by the same factor $(1 + [I]/K_I)$, and accordingly, the apparent K_M will be unaffected by the inhibitor. If the noncompetitive inhibitor displays a preference for the free enzyme (i.e., $\alpha > 1$) or the enzyme-substrate complex (i.e., $\alpha < 1$), it is referred to as a mixed-noncompetitive. In both cases k_{cat} and k_{on} are diminished by the inhibitor; the former is according to the factor $1 + [I]/\alpha K_I$, and the latter is according to $1 + [I]/K_I$. Where the inhibitor prefers the free enzyme, k_{on} will be diminished to a greater degree than k_{cat} , and *vice versa* where

the inhibitor prefers the enzyme-substrate complex (190). Inhibition of topoisomerase II by etoposide (**Figure 1.19**) is an example of noncompetitive inhibition (191). This mode of inhibition ultimately results in cell death by forming a ternary complex with DNA and topoisomerase II, preventing ligation of single-stranded DNA (192). This forms the basis for a cancer chemotherapeutic approach.

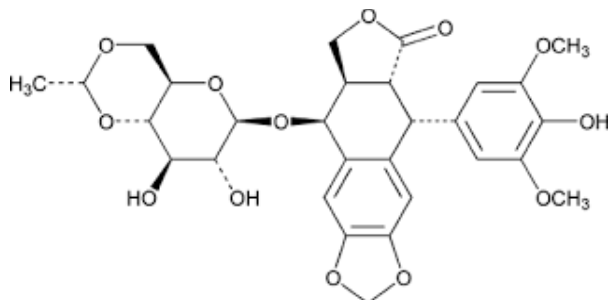


Figure 1.19: Structure of Etoposide

1.6.2 Slow-onset inhibition

In contrast to the rapid reversible inhibition mechanisms described above, where on the time-scale of the typical steady-state experiment, inhibition is essentially instantaneous and constant, this form, though typically non-covalent and reversible, is slow with respect to onset. As a result, the extent of inhibition increases with the time of enzyme exposure to the inhibitor (i.e., time-dependent inhibition is observed) (190).

There are common ways to monitor time-dependent inhibition. One is to monitor the effect of pre-incubation time on the activity of the enzyme which results afterward. A single-exponential decrease in activity (equation 4) is typically observed, and the effect of inhibitor concentration on k_{obs} can be evaluated to make inferences regarding the steps involved in the inhibition mechanism and estimate their rate constants. Alternatively, the ability of an inhibitor

to decrease enzyme activity over the course of an assay can be evaluated. Here, burst-exponential behavior is observed (equation 5). The value of k_{obs} captures that rate at which the enzyme transitions from full activity (v_i) to the activity once equilibrium between enzyme and inhibitor has been established (v_s). Here as well the effect of inhibitor concentration on k_{obs} can be evaluated to help elucidate the steps involved the onset of inhibition and the rate constants that govern those steps.

$$v_s = v_i e^{(-k_{obs}t)} \dots \dots \dots \text{Eq.4}$$

$$[P] = v_s t + \frac{v_i - v_s}{k_{obs}} [1 - e^{(-k_{obs}t)}] + c \dots \dots \dots \text{Eq.5}$$

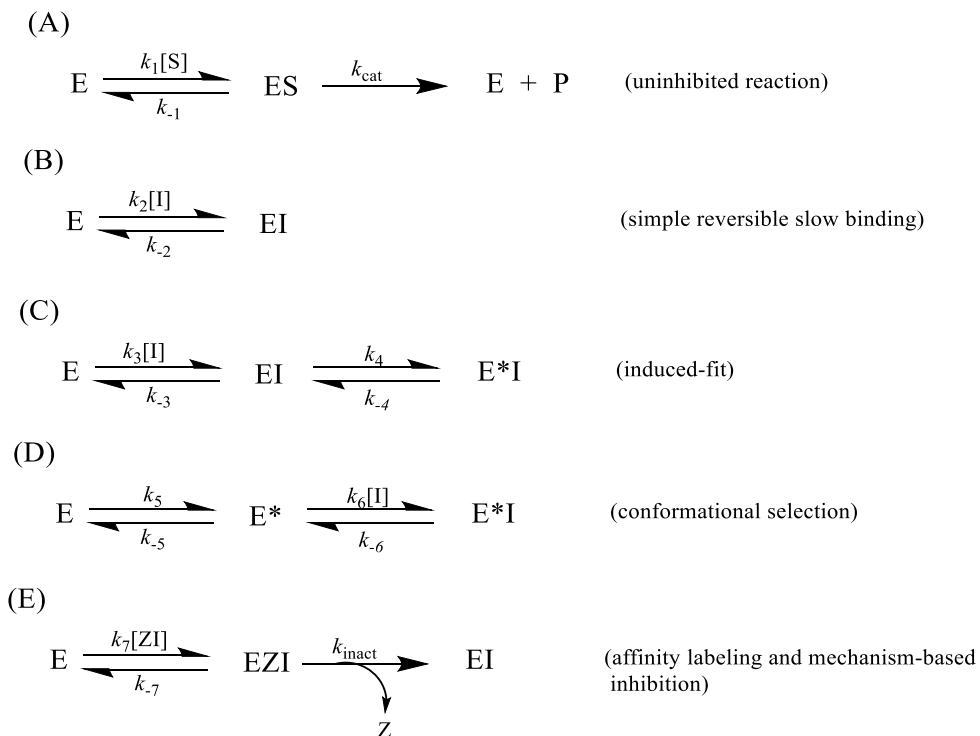


Figure 1.20: Mechanisms of slow binding inhibition. A represents uninhibited reaction, B represents a simple reversible slow binding mechanism, C is an induced-fit mechanism, D represents conformational selection and E, mechanism-based inhibition and affinity labeling.

Over years of enzyme inhibition analyses, several mechanisms which produce slow-onset inhibition have been uncovered. The most common of these are summarized in **Figure 1.20**. These are presented in the context of a simple Michaelis-Menten enzyme mechanism (**Figure 1.20 A**) where the rate constants governing enzyme association with substrate and dissociation of the ES complex to free enzyme and substrate are represented k_1 and k_{-1} , respectively. Simple, slow-binding inhibition involves a single-step reversible association between enzyme and inhibitor (**Figure 1.20 B**), and in this way it resembles the rapid-reversible mechanisms discussed above. The distinction is that, k_2 and k_{-2} , the respective association and dissociation rate constants for the inhibitor are much smaller, leading to a slow onset of inhibition. Alternatively, slow onset can be rationalized by relatively slow conformational changes that occur after (induced-fit, **Figure 1.20 C**) or before (conformational selection, **Figure 1.20 D**) association of the inhibitor with the enzyme. Finally, initial association of an inhibitor with an enzyme may be followed by formation of an irreversible (often covalent) complex, as is the case with affinity labels and mechanism-based inactivation of enzymes.

1.6.2.1 Slow binding

For an inhibitor which conforms to a simple slow-binding mechanism (**Figure 1.20 B**), increasing its concentration results in a linear increase in k_{obs} , (rate of formation of EI complex) an apparent first-order rate constant corresponding to the onset of inhibition measured either by a preincubation experiment (i.e., application of equation 4) or by the burst-exponential onset of inhibition during the reaction of an enzyme with its substrates (i.e., application of equation 5). The preincubation experiments establish an equilibrium between enzyme and inhibitor before the reaction is initiated. Thus, there is an initial encounter between the enzyme and inhibitor and the K_I is usually low. In the burst exponential inhibitory experiments, the enzyme encounters both

inhibitor and substrate(s) within the progress of the reaction. Here, the resulting inhibition constants are usually higher than in the preincubation experiments. The slope of k_{obs} vs inhibitor concentration returns k_2 the second-order rate constant for the slow onset of inhibition. Extrapolation to the y-axis (i.e., $[I] = 0$) allows for the estimation of k_{-2} , the first-order rate constant for dissociation of the EI complex. Of course, K_I can be determined from k_{-2}/k_2 .

When an inhibitor conforms to an induced fit mechanism (**Figure 1.20 C**), the dependence of k_{obs} on inhibitor concentration is not linear, but hyperbolic. An initial rapid-equilibrium association of enzyme and inhibitor is captured by activity when $E + I$ preincubation time = 0, or by initial rates of enzyme activity in the presence of inhibitor. The exponential increase in inhibition with time (i.e., k_{obs}) is a function of the slow conversion of the initial EI complex to EI^* and back (i.e., k_4 and k_{-4} , respectively). Here, the asymptote of the hyperbolic function (k_{obs} vs $[I]$) corresponds to the sum of k_4 and k_{-4} , and the extrapolated k_{obs} when $[I] = 0$ (i.e., the y-intercept) corresponds to k_3 . Thus, the amplitude of the hyperbolic response gives k_4 , and interestingly, the K_I (i.e., k_3/k_3) for the initial encounter complex is determined by the concentration of inhibitor that returns 1/2 the change in amplitude.

With slow, tight binders (for example **Figure 1.20C**) which typically follow a multi-step mechanism, k_{obs} is defined as;

$$k_{obs} = k_{-4} + \frac{k_4 [I]}{K_I^{app} + [I]} \dots \dots \dots \text{Eq. 6}$$

And K_I^* , which corresponds to the ratio of the rate constants that account for the formation and dissociation of EI^* ;

$$K_I^* = \frac{K_I}{1 + \frac{k_4}{k_{-4}}} \dots \dots \dots \text{Eq. 7}$$

However, the use of integrated rate equations is not applicable to every mechanism, and is also applied with underlying assumptions; $[S] \approx [S]_t$ and $[I] \approx [I]_t$, implying $[S]_t, [I]_t \gg [E]_t$. For example, if $[E]_T \approx [I]_T$, then the inhibitor's K_I will be extremely low, then a slow-tight binding mechanism is operating.

1.6.2.2 Advantages of inhibitors with slow off rate constants

In some clinical cases, the potency of a drug is dependent on its pharmacodynamics which correlates to its dissociation half-life or the duration of inhibition. The half-life and the apparent k_1 are critical factors in determining dosing concentrations and intervals in *in vivo* studies. Inhibitors with significantly lower off-rates (e.g., k_4 in **Figure 1.20 C**) display longer half-lives and considerable clinical advantage over rapid reversible inhibitors. Inhibitors with these mechanistic/kinetic features can effectively halt enzyme activity for a considerable length of time, even indefinitely in cases of irreversible inhibition. Here the return of activity is dependent upon the transcription/translation of new enzyme.

1.6.3 Tight binding inhibition

In evaluating mechanism of inhibitors as they encounter the enzyme, the concentration of bound inhibitor to that of the free is very low. The concentration of free inhibitor can essentially be assumed constant. As such, in determining dissociation constants, $[I]$ can be treated as constant, allowing the use of hyperbolic functions to determine K_I or K_D . However, with tight-binding inhibitors or when $K_I < [E]$, this assumption no longer valid. This can be addressed by the use of the Morrison's quadratic function (193,194) presented below. No assumptions are made with respect to the changes in the concentration of free enzyme or other components.

$$\frac{v_i}{v_o} = 1 - \frac{([E]_T + [I]_T + K_I^{app}) - \sqrt{([E]_T + [I]_T + K_I^{app})^2 - 4[E]_T[I]_T}}{2[E]_T} \dots \text{Eq.8}$$

v_i and v_o (initial velocities with and without inhibitor respectively) are experimentally determined at known values of total inhibitor concentration, $[I]_T$, while K_I^{app} and $[E]_T$ are allowed can be set as constants.

1.6.3.1 Clinical advantages of tight binders

Their low K_I and longer half-lives make them better inhibitors *in vivo*. Low K_I values allow for extended or complete inhibition, associated with their slow ‘off’ rates. Their low clearance rates make them suitable candidates for *in vivo* studies. The high affinity for these inhibitors for their targets also allows for lower prescribed doses in patients, and as such, helps minimize off-target toxicity. The slow dissociation of the tightly bound binary complex ensures near or complete enzyme inactivation and slows drug clearance. These make tight binders suitable for later drug discovery stages (190).

1.6.4 Irreversible inhibition

This is a form of enzyme inactivation wherein there is a non-zero rate for inhibitor association with the enzyme, but at least one of the rate constants for inhibitor dissociation is zero. In reality, this simply an extension of slow tight binding inhibitors, but k_{-2} (**Figure 1.20 B**), k_{-4} (**Figure 1.20 C**), or k_{-6} (**Figure 1.20 D**) is zero. In these cases, the action of the inhibitor eliminates activity for the remaining lifetime of the enzyme, and a given cell must synthesize (i.e., transcribe and/or translate) more of the enzyme to restore activity.

In many ways the analyses of irreversible inhibition are the same as those for reversible slow-onset inhibition. If a variant of the slow-binding mechanism (**Figure 1.20 B**), a linear response of k_{obs} with inhibitor concentration will still be observed, the slope of which will be k_2 , but within error, the y-intercept will be zero, consistent with a $k_{-2} = 0$. Likewise, a variant of the induced fit mechanism (e.g., **Figure 1.20 E**) will also produce a hyperbolic response of k_{obs} to inhibitor concentration. The amplitude of the hyperbolic response will return the rate constant of the latter irreversible step (i.e., k_{inact}), and the concentration of inhibitor that produces $\frac{1}{2}$ the change in amplitude will correspond to K_I for the initial encounter complex. However, because EI^* is an irreversible complex, k_{obs} will extrapolate to zero at the y-intercept. In a similar manner, the v_s terms of equations 4 and 5 (depending on the type of experiment performed) will approach zero.

Also, jump dilution experiments will show no gain of enzyme activity post-dilution, if inhibitor is irreversible. Slow-tight binders will show a lag phase in product generation which is conspicuously absent in rapid reversible inhibitors. The most typical mode of irreversible inhibition is one where the inhibitor covalently modifies a residue in or near the active site of the enzyme, atypical of reversible inhibitors. This covalent modification can be detected by mass spectrometry, as the inhibitor causes increases in protein mass. This is the best way to detect irreversible inhibition. This does not require long kinetic investigations and is less prone to error, in contrast to the more popular $x, y = 0$ intercept interpretation, which may be misleading. The intercept interpretation relies on a specific set of data points and thus defining the irreversibility becomes subjective, especially if the error margin is high. Post covalent bond formation, neither dialysis nor gel filtration restores enzyme activity, contradistinctive to reversible inhibitors.

Irreversible inactivation by covalent means can be classified into two major groups; affinity labeling and mechanism-based inactivation

1.6.4.1 Affinity labels

These contain functional groups that form covalent bonds with other reactive molecules. Affinity labels contain electrophilic groups that form covalent bonds with counterpart protein nucleophiles. Some interact with specific amino acids, making them useful agents for enzyme mechanistic investigations. An example of affinity label is Tosyl-L-phenylalanine chloromethyl ketone (TPCK), a substrate analogue for chymotrypsin which covalently modifies histidine of the enzyme's catalytic triad, inactivating the enzyme.

1.6.4.2 Mechanism-based inactivators

Mechanism-based inhibitors are unreactive molecules; substrate analogues, enzyme products – that are catalytically converted by the enzyme to active species which inactivate the enzyme prior to release from the active site. These use the enzyme's catalytic mechanism to convert the inactive compound to an active inactivator (**Figure 1.20 E**).

The formation of covalent bonds with target serves as an advantage to this class of inhibitors too, decreasing the frequency of administration of the drug. In contrast to affinity labeling agents, mechanism-based inhibitors being unreactive solves the problem of non-specificity and off-target toxicity since only the enzyme catalyzing the conversion of these molecules are in turn inactivated (195).

1.6.5 Nonspecific inhibition

A stark contrast to the previously described inhibition mechanism is nonspecific inhibition where compounds exert inhibition by the formation of micelles or aggregates. Specific inhibitors act on their targets via strong and selective binding. A common observation with non-polar compounds is that they form micelles relatively easily. Interaction of a target enzyme with these micelles producing some extent of protein unfolding of the enzyme and the resulting loss of activity (196). Obviously, this cannot be considered any kind of specific or targeted inhibition. This has posed substantial problems in the high-throughput screening (HTS) of compound libraries by producing numerous false-positive “hits”(197).

The promiscuity of these inhibitors – interaction with target proteins and several mechanisms have been postulated to explain this behavior. One popular thought is that the onset of inhibition is from by forming particles of 30 – 1000 nm in diameter in solution, preventing substrate binding, hence ‘inhibition’ (196). As with slow binders, the potency of this set of inhibitors is time dependent as aggregates stick to enzymes, resulting in decrease free enzyme in solution.

Interestingly, increasing the ionic strength of the medium increases particle size, resulting in fewer amounts of aggregates and more free enzyme. Thus in a high ionic strength buffer, higher concentrations of inhibitor are required to exert the same effect, increasing the observed IC 50 values (197). Slope steepness is also a feature of aggregate-based compounds. The observed hill slopes (n) of promiscuous inhibitors is almost a factor of two that of a specific inhibitor (198).

The use of small amount of detergent like Triton X-100 has been shown to reduce aggregation of small molecules by lowering the surface tension (**Figure 1.21**). Only aggregator

based inhibitors are sensitive to the addition of detergents, decreasing the effect of inhibition (196,199).

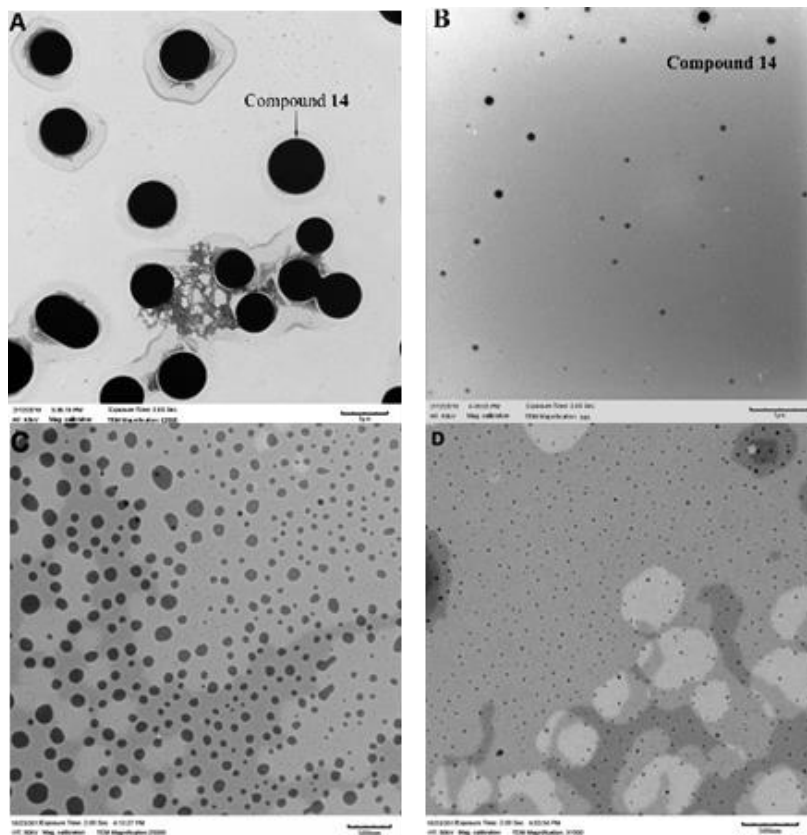


Figure 1.21: Images of Compound 14 and control with *MtSK* by transmission electron microscopy. A. Compound 14 100 μM formed aggregates with an average size of 0.7 μm (Bar = 1 μm). B. Compound 14 with 0.01% v/v Triton X-100, average size of 0.03 μm (Bar = 250 nm). C. Control at 30 μM exhibited aggregation with an average size of 100 nm (Bar=500 nm). D. Control with 0.01% v/v Triton X-100, particle size of 5 nm (Bar = 500 nm) (199; Elsevier, 2018)

1.6.5.1 PAINS (Pan-Assay INterference compounds)

Pan-assay interference compounds (so-called PAINS) are responsible for many false-positive readings in activity screens. Often these compounds have a broad reactivity that alters features likely to be common to many proteins/enzymes. Examples include redox active compounds that alter cysteine thiols, or compounds with a capacity to chelate catalytically necessary metal ions, interfering fluorescence signals from compounds or breakdown of compounds to smaller units (200–202). PAINS-type molecules are usually of low molecular weight, a fraction of larger compounds. Inhibitors/compounds likely to cause interference could either be of a synthetic or natural source (203,204). Recently a number of natural products have been reported to exhibit artificial bioactivity (204).

Identification and classification of PAINS (200,202,205) are often corroborated by other techniques like X-ray crystallography (206), NMR, dynamic light scattering (207) etc. PAINS molecules show high deflections in pulsed light as compared to non-aggregators under X-ray and dynamic light scattering. Their NMR spectra shows broadening of signals resulting for micelle formation. The wide distribution and appearance of false-positive data make PAINS identification difficult (200,205). As a result of this, characterization of such a molecule may be pursued for a considerable length of time prior to hitting a dead end, significantly slowing the drug discovery process.

Many drugs contain PAINS alerts (200,208,209) and have received much attention recently (203). Many PAINS alerts in some drugs (e.g. quinone containing) have been linked to undesirable ADMETox (Absorbance Distribution Metabolism Elimination Toxicity) properties (200). However, Drugs-PAINS are more active than Drugs-NoPAINS with 24% vs 15% activity in bioassays (210) and a good number of these drugs show a quinone PAINS alert (211,212).

Quinone drugs are one of the very promiscuous classes of drugs (200,203), a classic example being doxorubicin which has the quinone_A(370) alert, tested in over 400 assays, with about an 85% PAINS call. However, reporting PAINS molecules should not only rely on PAINS filter (213) results but also the use of orthogonal experimental assays to complement them (210).

1.7 Coupled enzyme assays and HTS

In reactions where neither analyte can be easily measured directly and in real time, a coupled-enzyme assay can be developed to evaluate activity in response to substrates, inhibitors, etc. Because such assays typically make a target enzyme's activity much easier to detect, they are often adapted for HTS efforts. The typical coupled assay uses one of the reaction products of the enzyme of interest as a substrate for a secondary enzymatic reaction, the product of which can be easily and directly measured in real time (e.g., a product with a unique chromophore with high molar absorptivity). A typical example is the lactate dehydrogenase/pyruvate kinase coupled assay where pyruvate kinase readily converts ADP to ATP and phosphoenol pyruvate to pyruvate, neither of which has a distinct unique UV-visible absorption spectrum. This is coupled to lactate dehydrogenase, another bisubstrate enzyme which catalyzes the conversion of pyruvate to lactate with a corresponding NADH oxidation to NAD⁺. The consumption of NADH is monitored at 340 nm and a decrease in absorbance signal is observed.

Coupled systems allow for probing of reactions in systems with no distinct chromophore to be applicable for HTS. For successful coupling reactions, the detected signal must be sensitive to the catalytic activity of the analyte under investigation and less sensitive to small changes in the activity of the other coupled enzymes. This is achieved by using higher concentrations of other coupled enzymes while using a lower or rate-limiting concentration of the enzyme under

investigation. As such the product formed is rapidly converted into a detectable form or the detectable analyte is rapidly converted to an undetectable form.

Another critical factor in the use of coupled enzyme systems for HTS is ensuring that the observed inhibition results from inactivation of target enzyme and not inhibition of other coupled enzyme (s). Adjusting coupling conditions, ensuring high enough concentrations of coupling enzymes can help mitigate this problem. Target specificity can also be validated by evaluating the toxicity of inhibitors to the coupling enzymes in the absence of the enzyme under investigation. The cost of purchasing coupling enzymes, substrates and co-substrates may be a considerable drawback towards the use of these systems for HTS (190).

1.8 Kinase inhibitors

Over the past decade, kinases have become the pharmaceutical industry's most targeted class of enzymes with about 30 different kinase targets in phase I clinical trials. Many kinases are targeted for treatment of different cancers. The effect of their deregulation has also been implicated in immunological, neurological, metabolic, and infectious diseases, driving interest towards the development of kinase inhibitors to treat these diseases (214).

1.8.1 Type 1 inhibitors

Many inhibitors belong to this class and they recognize the active conformation – conducive to phosphotransfer (215). The vast majority of kinase inhibitors being class 1 may be as a result of using these compounds in assays where kinases were introduced in their active conformations and many were synthesized to resemble ATP. These usually possess heterocyclic

ring system that binds to the purine binding site and extends to hydrophobic regions of the enzyme (216).

1.8.2 Type 2 inhibitors

These recognize the inactive conformation commonly referred to as DFG-out. This conformation exposes the additional hydrophobic binding site adjacent to the ATP binding region (216). FDA-approved type 2 inhibitors like imatinib, nilotinib (217) and sorafenib (218) act through this mechanism. Crystal structures of kinase-bound type 2 inhibitors show that the active site is highly mobile making it feasible for kinases to accommodate a broad range of inhibitors (215). However, this is not unique to type 2 inhibitors. PIK-39, a type 1 inhibitor, also induced this type of conformational rearrangement (219).

1.8.3 Allosteric inhibitors

As the name implies, these inhibitors bind outside the ATP-binding site. Inhibitors in this class show greater selectivity since they target sites that are unique to a particular kinase. An example in this category is CI-1040 which inhibits MEK1 and MEK2 (Dual Specificity Mitogen-Activated Protein Kinase 1 and 2) by binding to a region near to but distinct from the ATP binding site (220).

1.8.4 Covalent inhibitors

This fourth class of compounds forms an irreversible, covalent bond with the enzyme. This rare type of inhibitors typically react with an active site cysteine nucleophile (221,222), as in the cases of inhibitors targeting epidermal growth factor receptor, HKI-272 and CL-387785 (223). These inhibitors are designed by attaching an electrophile, reactive towards the rare

nucleophilic sulfur in the cysteine residue. The inhibitor undergoes a Michael addition during which it forms a covalent bond with the active site cysteine. This irreversibly blocks ATP binding, inactivating the enzyme. Some naturally existing cytotoxic compounds like hypothemycin, a resorcylic acid lactone polyketide has been shown to act using this same mechanism (224). Though a vast majority of kinases can be targeted using this approach, off-target toxicity is still of great concern.

1.8.5 *MtSK* inhibitors

Though the shikimate pathway had long been described, it is only fairly recently that significant efforts have been made towards targeting *MtSK* for the development of novel anti-tubercular agents. In this section we review the evaluation different *MtSK* inhibitors and the potencies. These were characterized by the use techniques and approaches including virtual screening or molecular dynamic simulations (225,235, 236, 237), mass spectrometry (229, 342), X-ray crystallography (236), *in vitro* and *in vivo* assays (225, 234, 236,237), etc.

Compounds **5489375** and **5311863** (**Figure 1.22**) were two in the library of 2000 compounds that showed significant inhibition of *MtSK* (225). Dose-response evaluations of **5489375** and **5311863** yielded IC_{50} values of 10 and 45 μM , respectively. Both compounds passed the PAINS filter servers, i.e. they lacked structural characteristics of typical PAINS compounds. Inhibition kinetics displayed by **5489375** suggest it is uncompetitive and noncompetitive to shikimate and ATP, respectively, with an overall K_I of 13 μM , αK_I (SA) of 8 μM and αK_I (ATP) of 11 μM .

A class of heterocyclic compounds, pyrazolones and derivatives thereof, has shown antimicrobial and anti-*MtSK* properties (226–229). Compounds **2**, **3**, and **4** (**Figure 1.22**), pyrazolone derivatives showed substantial activity against *MtSK* with EC_{50} s of 0.24, 0.07 and

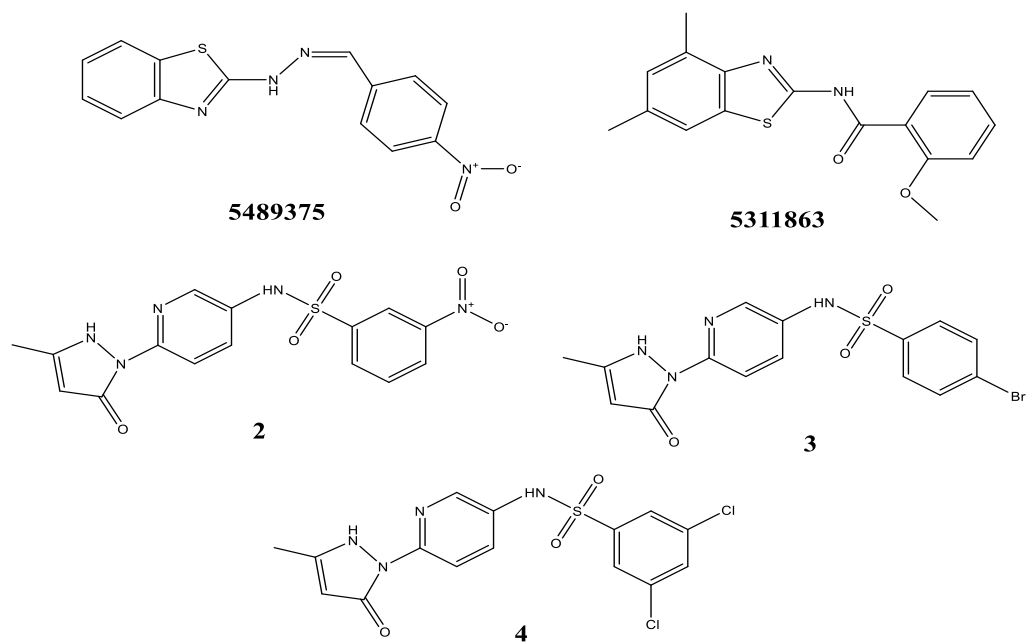
0.18 μM , respectively (230). The fatty acid, α -linoleic acid isolated from *Sutherlandia frutescens*, previously shown to be active against some bacterial, viral and fungal pathogens (231–234) demonstrated significant inhibition of *MtSK* with an IC_{50} of about $4\mu\text{g/mL}$ (235). Virtual screens of molecules with triazoles or tetrazole moieties predicted these to be potential inhibitors of *MtSK* (236).

Shikimate analogues – bicyclic derivatives (**3** and **4**), hydroxyl derivatives (**5** and **6**), 4-aminoshikimate (**7**), 3-*epi*-shikimate (**8**) and 3-aminoshikimate (**9**) (**Figure 1.22**) exhibited different levels of potency against *MtSK*, with the bicyclic derivatives being most potent (237). The conformationally restricted bicyclic analogues, **3** and **4** had K_{I} s of 60 and 45 μM , respectively. The K_{I} s for the hydroxyl derivatives were in the near millimolar range, while the amino derivatives had K_{I} s around 65 μM . The least potent was compound **8**, with an estimated K_{I} above 4 mM.

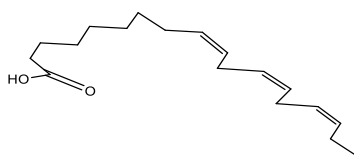
Representative inhibitors from the thiobarbiturate, naphthoquinone, thiazoleacetonitrile, chalcone and thiazolidinedione classes showed ATP-competitive inhibition (238). Of these, the thiobarbiturate, thiazoleacetonitrile and thiazolidinedione were uncompetitive with respect to shikimate with K_{I} 's of 10, 20 and 10 μM , respectively and αK_{I} 's (SA) of about 10 μM . The naphthoquinone and chalcone were non-competitive with respect to shikimate with K_{I} 's of around 10 μM and αK_{I} s (SA) of 15 and 10 μM , respectively. The thiobarbiturate inhibitor was synergistic with rifampicin, while the thiazoleacetonitrile showed some synergism with rifampicin, isoniazid and ethambutol (238).

Though this section is focused on inhibitors against *MtSK*, *in vivo* evaluations of promising inhibitors can be carried out on *Mycobacterium* species. Being a biosafety level 3 organism, screening with *M. tuberculosis* can be very challenging. However, level 1

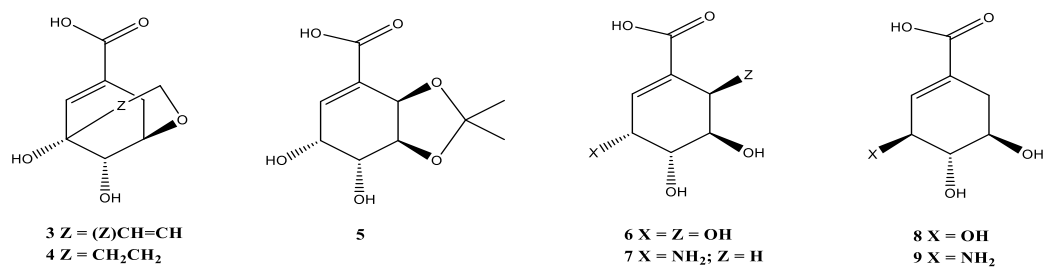
Mycobacterial species like *M. smegmatis* can be used for this purpose. *M. smegmatis* is non-pathogenic, it shares similar cell wall structures with pathogenic species and grows rapidly, forming colonies within 3-5 days. Other level 1 species which could possibly make good models for studying *M. tuberculosis* include; *M. gilvum*, *M. vanbaalenii*, *M. goodii* etc. These are rapid growing species and only require biosafety level (BSL) 1 laboratories.



Pyrazolone derivatives



alpha-linolenic acid



Shikimic acid analogues

Figure 1.22: *MtSK* inhibitors

1.9 Drug screening and LC-MS

The research presented in this dissertation relied, in large part, on mass spectrometric-based analyses used for the mechanistic evaluation and screening of potential antitubercular agents. Presented in this section are two main techniques applicable to the drug discovery pipeline, and protein analyses.

There has been a rapid increase in the use of hyphenated techniques for protein and inhibitor characterization. There has not only been a shift in paradigm from sequencing to identification in proteomics, but also a major shift in the drug screening. Though there have been significant advances made towards the discovery of new molecular entities (NMEs) for the treatment and prevention of diseases, the major causes of drug attrition have been attributed to poor efficacy and lack of safety (239). But, today, hyphenated techniques are essential in target identification, evaluating compound purity and identity, identifying lead compounds, efficacy, and control of bulk drug substance, pharmacokinetics to solve the above-stated problems. LC-MS has become a powerful drug discovery tool with varied applications of drug chemistry.

1.9.1 LC-MS methodology

Proteomics has gained much attention in this post-genomic world. Over the last couple of years, several LC-MS based methods have been developed for proteomics studies.

1.9.1.1 Top-down approach

Mass spectrometry-based proteomic studies have been typically carried out using bottom-up approach (240,241) as described above. Inferred identification of proteins from peptide fragments, may lead to loss of information regarding PTMs or variations in the peptide sequence. The top-down MS approach to solving these problems is via the introduction of the intact peptide

to the MS, measuring both intact and fragmented peptides (**Figure 1.23**). This allows for full sequence coverage, proteoform characterization, identifying specific molecular forms of the protein resulting from genetic variation, PTMs and alternative splicing (242). The ability to perform intact protein characterization has led to the widespread use of top-down MS approaches (243–248). However, the challenges in carrying out intact protein proteome-wide analyses using top-down proteomics (in areas like proteome coverage, sensitivity, and throughput) has caused employment of these techniques to lag behind the use of bottom-up methodology. But, advances in MS, separation techniques and bioinformatics have driven top-down MS towards becoming an essential tool and better alternative to peptide digest methods (249).

With the continuous use and complexity of samples analyzed, data processing must also be able to meet this increasing demand. The first tool used for intact protein identification was ProSight PTM (250,251), which was later updated to ProSight 2.0. The latter had the ability to include fixed modifications like cysteine alkylation and N-terminal modifications like N-terminal acetylation (251). ProSightPC, a desktop version contains a high-throughput mode for rapid analyses via the TRASH algorithm (252). It is also used in computing clusters for processing large amounts of top-down data (253). There are alternatives to ProSight, though with limited use (254,255). These include tools like BIG Mascot or MascotTD which use a bottom-up software of Mascot (256) but with an extended cut off mass of 110 kDa from the typical 16 kDa (254). PIITA (precursor ion independent top-down algorithm) is another alternative tool for comparing tandem mass spectra against a database (255).

1.9.1.2 Bottom-up approach

This approach involves the enzymatic digestions of proteins and subsequent analyses of the resulting peptides by tandem MS (**Figure 1.23**) (257,258). Two approaches are used for further protein identification. In one, the peptides are subjected to a direct search against a protein or genome database. The other entails performing a tandem mass spectrometric analysis (MS-MS) to obtain a mixture of peptide fragments (259). The pattern of fragmentation is indicative of the amino acid sequence. Cleavages from the N-terminus of peptide fragments are 'b' ions and those from the C-terminus are classified as 'y' ions. Based on molecular weight, sequences are selected from the database (Mascot, Pepsea, Mowse etc.) and their predicted patterns compared with those obtained from spectra. If most of the ion fragments match, it is termed a good fit. Tandem MS provides information with higher accuracy since the data is built from highly specific information. It is also essential in identifying type and site of modification (260) and can also identify proteins in a mixture (257,260,261). MS systems used for bottom-up approach include 3D and linear ion trap (262,263), quadrupole-time-of-flight (264), Orbitrap (265), Fourier-transform ion-cyclotron resonance (FTICR)-MS (266) etc.

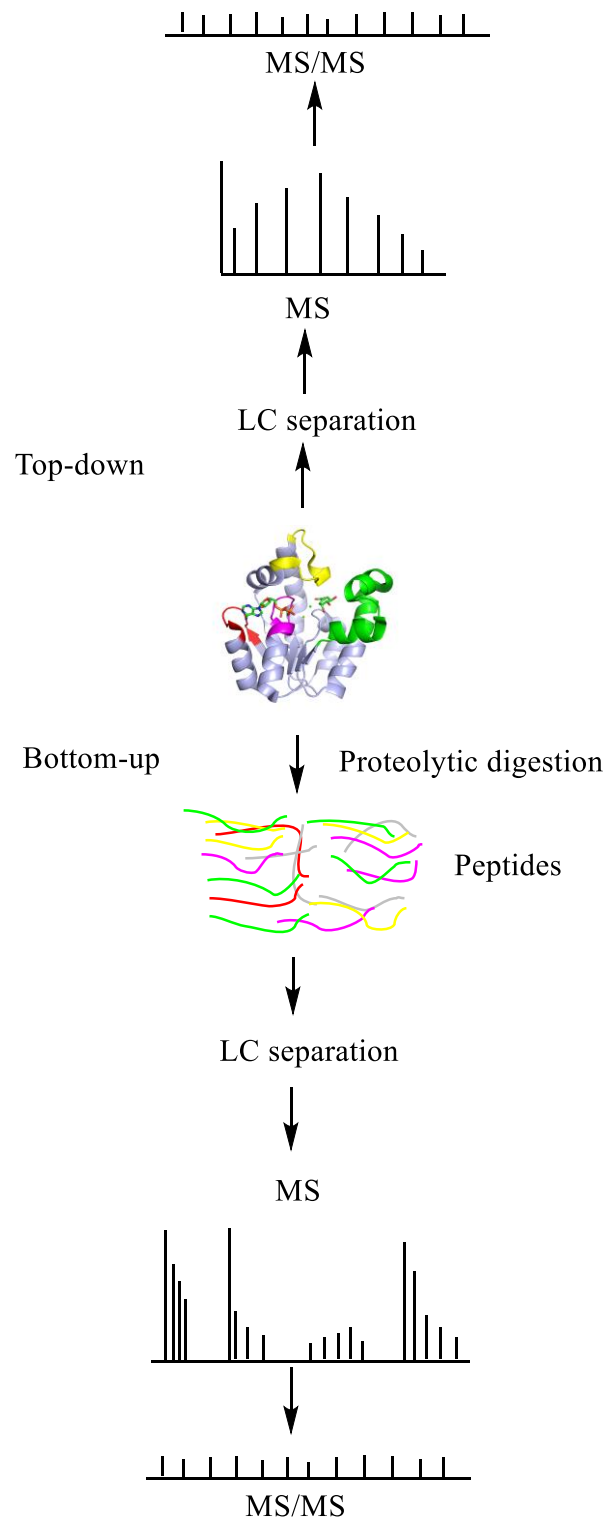


Figure 1.23: Schematic illustration of the differences between top-down and bottom-up mass spectrometry-based proteomics approaches.

1.10 Fluorescence and techniques in drug discovery and screening

The advances made towards the development of a high throughput screening (HTS) system presented in this dissertation utilize intrinsic and extrinsic fluorescence. Presented in this section are brief descriptions and applications of fluorescence approaches in drug screening.

1.10.1 Energy states of a fluorophore

The processes of absorption and fluorescence can be explained by a typical Jablonski diagram (**Figure 1.24**). A single electronic ground state with a variety of vibrational energy levels is represented by S_0 . Absorption of a photon by the fluorophore produces excitation to S_1 . Some molecules rapidly relax to lower vibrational levels in a process called internal conversion, occurring in a time frame of about 10^{-12} s or less. Fluorescence lifetimes are usually in the nanosecond range.

The return to S_0 usually occurs to a higher excitable vibrational state which rapidly attains thermal equilibrium in about 10^{-11} s. From the S_1 state, molecules can undergo spin conversion to a triplet state T_1 . From T_1 to S_0 , this emission is termed phosphorescence and it occurs at a higher wavelength. The transition from S_1 to T_1 is called intersystem crossing.

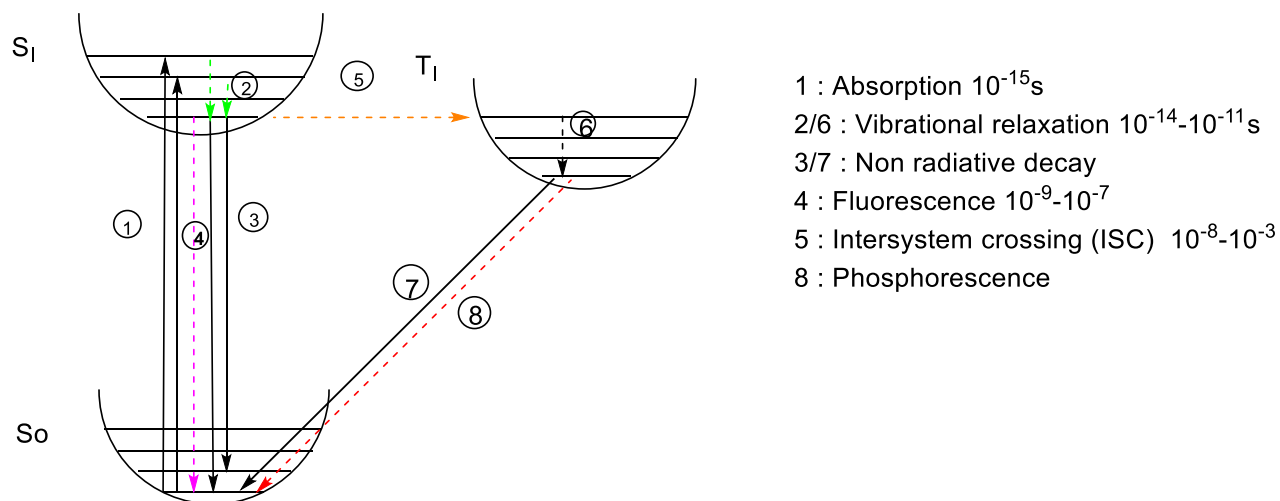


Figure 1.24: Jablonski diagram showing the excitation from ground state S_0 to an excited singlet state S_1 which may undergo vibrational relaxation or intersystem crossing to a transition state T_1 . Emission from T_1 to S_0 results in phosphorescence while emission from S_1 to S_0 is called fluorescence.

Fluorimetric measurements are usually classified into two categories – steady-state and time-resolved (267). Steady-state measurements require constant illumination of the sample with a continuous beam of light while recording the emitted spectrum using a scanning monochromator, adjusted for desired wavelengths and data correction (268). Steady-state spectra are collected under equilibrium conditions, wherein the vibrational and solvent induced relaxation of all excited species are completed and rates of excitation and emission under said illumination conditions are equal. In contrast, time-resolved fluorimetric measurements are done with a pulsed light source. The corresponding fluorescence decay data are monitored using rapid detection systems. Steady-state observations are an average of several time-resolved emissions over fluorescence decay of the sample.

1.10.2 Implications of tryptophan in protein fluorescence

Trp, Tyr and Phe are the three fluorescent amino acids found in proteins, with Trp being the most abundant and most widely used in fluorescence as a reporter of protein structure, dynamics and function (269). The latter is as a result of its comparatively higher quantum yield and sensitivity to its environment (270–272). The quantum yield of Trp can vary from 0.35 – 0.01 based on its environment (273). This change is thought to be associated with electron transfer from the peptide backbone or from surrounding residues (274–276). In addition to its sensitivity, Trp has at least two different fluorescent lifetimes (~0.5 and ~3.1 ns) (277,278) which have been shown to be inherent to its structure but independent of its excitation wavelength (279). Interestingly, a third Trp fluorescence lifetime is observed in ethanol, thought to be from interactions between hydrophobic and hydrophilic dipoles or ethanol and Trp (279).

However, interpretation of data from Trp fluorescence can be quite challenging, taken together the low photostability and its absorption/emission at UV region. Though this research makes use of natural Trp fluorescence, unnatural Trp can also be used. Significant efforts have been made to identify small unnatural fluorophores to solve this problem (280–286). Unnatural fluorophores like prodan (285) and aladan (280) have been used to overcome this. Unfortunately, they are larger in size than Trp, making them less attractive in application requiring unique fluorophore sizes and structure. Trp analogues like azatryptophan (281,282,287) have also been used to substitute for the natural Trp. Though some analogues show enhanced fluorescent properties over Trp, they all lack photostability. Recently, a new analogue 4-cyanotryptophan has been shown to solve the photostability issues (288,289). It has a reasonably higher molar extinction coefficient (~6000 M⁻¹cm⁻¹), a fluorescence lifetime of about 13.7 ns, a quantum yield

greater than 0.8 (288). These enhanced spectroscopic properties make it a suitable molecule for intrinsic fluorescence studies.

1.10.3 Fluorescence quenching

Fluorescence quenching has become a vital tool in protein research since it usually requires small sample volumes and using intrinsic fluorescence quenching information can be gathered on the location of the fluorophore (usually Trp) within the macromolecule (290–293). Quenching can either be collisional or static. In collisional quenching, fluorescence is quenched on contact with quencher. Fluorophore returns to the ground state during a diffusive encounter with a quencher. Both molecules remain chemically unaltered in the process. This can be described by the Stern-Volmer equation:

$$\frac{F_0}{F} = 1 + K[Q] = 1 + k_q \tau_0 [Q] \dots \dots \dots \text{Eq. 9}$$

Where K is the Stern-Volmer constant, k_q represents the bimolecular quenching constant, τ_0 is the unquenched lifetime, and $[Q]$ represents concentration of quencher. F_0 and F are fluorescence intensities in the absence and presence of Q , respectively. The value of K quantifies the sensitivity of fluorophore to quencher, buried or water-inaccessible fluorophores usually have lower K values. Larger K values are observed if fluorophore is water accessible or at the surface. Other than collisional quenching, some fluorophores are able to form non-fluorescent complexes with quencher molecules. This is termed static quenching since it occurs at the ground state and is independent of molecular collisions or diffusive encounter.

1.10.4 Fluorescence anisotropy

Fluorescence anisotropy has a wide range of applications in biological and chemical assays. It provides a measure of protein interactions, information on proteins molecular environment, conformational dynamics, protein-protein interactions, the environment of different fluorophores etc. (294–298). Both extrinsic and intrinsic fluorophores can be used for fluorescence anisotropy measurements. Trp anisotropy is low when fluorophore motions are rapid and high when motions are slow.

The measurements are based on wavelength selective excitation of the desired fluorophore by polarized light. The fluorophores absorb photons with vectors aligned parallel to that of fluorophore (**Figure 1.25**). In an isotropic solution, fluorophores have no unique orientation. Upon excitation only those whose transition dipoles are oriented parallel to the excitation vector are excited. The result of this selective excitation is partial emission and partial polarization. Fluorescence anisotropy (r) and polarization (P) are defined by

$$r = \frac{I_{\parallel} - I_{\perp}}{I_{\parallel} + 2I_{\perp}} \dots \dots \dots \text{Eq. 10}$$

$$P = \frac{I_{\parallel} - I_{\perp}}{I_{\parallel} + I_{\perp}} \dots \dots \dots \text{Eq. 11}$$

Where I_{\parallel} and I_{\perp} represent fluorescence intensities due to vertically and horizontally polarized emission when excited with vertically polarized light (see diagram below).

There are several factors that account for lower experimental anisotropy values than theoretically predicted. A common one is a rotational diffusion which displaces the emission dipole of the fluorophore causing a decrease in emission. In fluids most fluorophores rotate in about 50 – 100 ps, resulting in multiple rotations during a 1- 10 ns excitation lifetime and

randomly polarized emission. As a result of this fluorophores in non-viscous solutions tend to have near zero anisotropies. Rotational diffusion can be decreased if the fluorophore is attached to a macromolecule like protein (299).

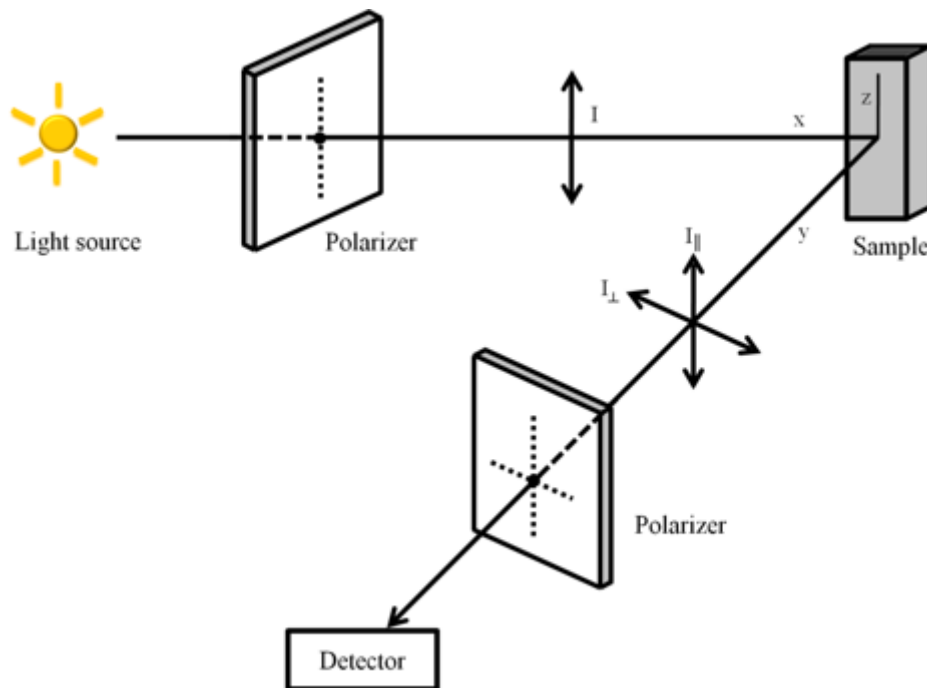


Figure 1.25: A schematic diagram showing measurement of fluorescence anisotropy

1.10.5 Resonance Energy transfer

Resonance energy transfer (RET) is unique in its ability to detect and measure spatio-molecular interactions between fluorescent molecules within a 10 – 100 Å range and is very applicable to bioassays. RET entails a non-radiative transfer of energy from an excited chromophore (donor, D) to another (acceptor, A) via intermolecular long-range dipole-dipole

coupling (300). Non-radiative energy transfer implies photons are neither emitted or absorbed, hence the name resonance energy transfer and not FRET.

For effective energy transfer over this 10 - 100 Å distance there must be a considerable overlap between the emission spectrum of the donor and the absorbance spectrum of the acceptor, and the quantum yield of D and the absorption coefficient of A should be sufficiently high. As a requirement for dipole-dipole interaction to occur, there must be a favorable orientation of the transition dipoles of D and A relative to each other or either one or both chromophores must have a certain degree of rapid rotational freedom for favorable orientation of their individual dipoles (301). The rate of energy transfer is given by

$$k_T(r) = \frac{1}{\tau_D} \left(\frac{R_0}{r}\right)^6 \dots\dots\dots \text{Eq. 12}$$

Where r represents donor-acceptor distance and τ_D represents lifetime of donor without energy transfer to acceptor. The efficiency of a single donor-acceptor transfer pair at a fixed distance is given by

$$E = \frac{R_0^6}{R_0^6 + r^6} \dots\dots\dots \text{Eq. 13}$$

The extent of transfer depends on r . for biological molecules Forster radii are in the range of 30 – 60 Å making energy transfer a useful tool for measuring distances between different protein binding sites (302).

1.10.6 Time-gated fluorescence – Homogenous time-resolved fluorescence (HTRF)

Elements, especially of the lanthanide series have long been applied as tracers for time-resolved fluorescence. Europium chelates (303) and cryptates (304) have also been applied to

immunoassays. A variety of RET assays have been developed using lanthanide complexes as donors (305,306), commonly referred to as time-resolved energy transfer (TRET). A major advantage of TRET systems is the vast difference in donor-acceptor lifetime (μs to ms) from low lifetime background components ($< 10 \text{ ns}$). Hence fluorescence is gated to received delayed signals, typically beyond 10 ns post excitation.

1.10.7 Fluorescence lifetime (FLA)

Representing molecular property of a fluorophore and its molecular environment, fluorescence lifetime has been a wide range of scientific applications (301). The sensitivity and intrinsic properties of this technique make FLA a valuable tool for HTS applications (307–309). There are two main methods generally applied for FLA; frequency and time domain data acquisition. In the frequency domain, phase shift fluorescence lifetime and the demodulated fluorescence emission are calculated with the use of sinusoidal modulated light (310,311). In time domain fluorescence, lifetimes are measured from time-dependent emission decay after the application of brief excitation pulses like time-correlated-single-photon-counting (312,313). However, the biological applications of FLA are limited since fluorescence lifetimes resulting from environmental quenching and/or solvent polarity effects are very unpredictable. So, recent advancements in assay development use additional quencher labels to monitor lifetime changes during binding (307).

Chapter 2

Slow-binding inhibition of *Mycobacterium tuberculosis* shikimate kinase by manzamine alkaloids

This chapter is recovered from a publication of the same title: Simithy, J.; Fuanta, N.R.; Alturki, M.; Hobrath, J.V.; Wahba, A.E.; Pina, I.; Rath, J.; Hamann, M.T.; DeRuiter, J.; Goodwin, D.C.; Calderón, A.I. *Biochemistry*, 2018, in press (DOI 10.1021/acs.biochem.8b00231). JS and NRF contributed equally as first authors.

2.1 Abstract

Tuberculosis (TB) possess a significant public health challenge and there is urgent need for novel potent antitubercular agents. This chapter focuses on screening and mechanistic evaluation of a small marine sponge metabolite and its derivatives against *Mycobacterium tuberculosis* (*MtSK*). However, most comparisons will be made using the scaffold manzamine A (**1**) and one of its derivatives 6-cyclohexamidomanzamine A (**6**). This small, yet promising group of compounds called manzamines that have previously shown to be active against *M. tuberculosis* were characterized as *MtSK* inhibitors: manzamine A (**1**), 8-hydroxymanzamine A (**2**), manzamine E (**3**), manzamine F (**4**), 6-deoxymanzamine X (**5**), and 6-cyclohexamidomanzamine A (**6**). Interestingly, all these compounds showed mixed-noncompetitive inhibition of *MtSK* with **6** being the most potent. They all showed time-dependence with a two-step slow binding inhibition. **1** showed typical tight binding characteristics with an apparent K_I of $\sim 30 \mu\text{M}$ and

forward (k_5) and reverse (k_6) rate constants for isomerization to a tightly-bound EI* complex of 0.18 min^{-1} and 0.08 min^{-1} , respectively. Contradistinctive to **1**, **6** showed a lower K_I for the initial encounter complex ($\sim 1.5 \text{ }\mu\text{M}$), substantially faster isomerization to EI* ($k_5 = 0.91 \text{ min}^{-1}$), and slower back conversion of EI* to EI ($k_6 = 0.04 \text{ min}^{-1}$). Thus, the overall inhibition constants, K_I^* , for **1** versus **6** were $10 \text{ }\mu\text{M}$ and $0.06 \text{ }\mu\text{M}$, respectively. Our data aligns with docking predictions of a first, favorable binding mode and a second, less tightly bound pose for **6** at *MtSK*. Our results suggest that manzamine alkaloids, **6** in particular, constitute a new scaffold from which potential drug candidates with novel mechanisms of action could be designed for the treatment of tuberculosis by targeting *MtSK*.

2.2 Introduction

Tuberculosis (TB) still stands a major health scare being and is second leading cause of mortality from a single infective agent (314). Complicated by the emergence of HIV-TB co-infection, multi-drug resistant (MDR) and extensively drug-resistant (XDR) strains of *Mycobacterium tuberculosis*, there is an urgent need for new therapeutics. In 2012, a new drug (SIRTUROTM Bedaquiline) that targets *M. tuberculosis* ATP synthase was approved by the Food and Drug Administration (FDA) exclusively for the treatment of MDR-TB (315,316). It was the first drug approved in over four decades for the treatment of TB. Unfortunately, Bedaquiline has already been associated with an increased risk of potentially fatal heart conditions, further stressing the unmet need for safer antitubercular drugs with novel targets and mechanisms of action to treat resistant forms of the disease (317,318).

Recently identified targets essential for *M. tuberculosis* survival and persistence include shikimate kinase (*MtSK*) from the shikimate pathway (319). This pathway is responsible for the

biosynthesis of aromatic compounds in microorganisms and higher plants, and gene knock-out studies have established that it is an essential enzyme and a valid target (320). *MtSK*, the fifth enzyme of the pathway, catalyzes the phosphorylation of shikimate (SA) using ATP to form shikimate-3-phosphate (S3P) and ADP (321). With no mammalian counterpart, *MtSK* makes an attractive target for the design of drugs specific to the *M. tuberculosis* pathogen with reduced risk of toxicity in the human host (99,322).

Some of the strategies for the development of new drugs for the treatment of TB include the phenotypic and target-based screening of libraries of small molecules and natural products to identify novel chemical entities, the repurposing of existing antibiotics, and the modification of existing scaffolds with known antimicrobial activities (323–325). Although optimization of existing drugs can shorten the length and reduce the cost of the drug discovery process, more efforts are being directed towards the combination of whole-cell screening followed by target-based screenings. Using this integrated approach, compounds that can penetrate the mycobacterial cell wall and also inhibit the activity of a validated target can be identified (326–328).

For millennia, natural products have played a pivotal role in the treatment and prevention of many diseases (329). Some first- and second-line anti-TB drugs (e.g., rifampicin, polypeptides, cycloserine, and aminoglycosides) are derivatives of natural products, supporting the role of natural products in generating novel chemical entities and new drug classes (326,330). In the past, more attention was directed towards plants as sources for bioactive lead compounds and antibacterials (331). However, more recently, marine organisms have come into focus as potential sources for new therapeutic agents against infectious diseases including TB (332). In particular, manzamine alkaloids, a novel structural class of compounds isolated from Indo-

Pacific marine sponges, have been reported to possess anti-inflammatory, antiparasitic, insecticidal, and antibacterial activities with potential for their development against malaria and TB (333–337).

The manzamines contain a complex polycyclic ring system coupled to a β -carboline moiety (**Figure 2**). Manzamine A, first isolated in 1986, has been followed by more than 80 manzamine and manzamine-related alkaloids obtained from more than 16 different species of marine sponges (338,339). Manzamine A, the archetype of the group, has shown promising antitubercular activity *in vitro* with an MIC value of 1.5 $\mu\text{g/mL}$ (*M. tuberculosis* strain H37Rv), an activity comparable to the first-line drug for TB treatment, rifampicin (MIC 0.5 $\mu\text{g/mL}$) (339,340).

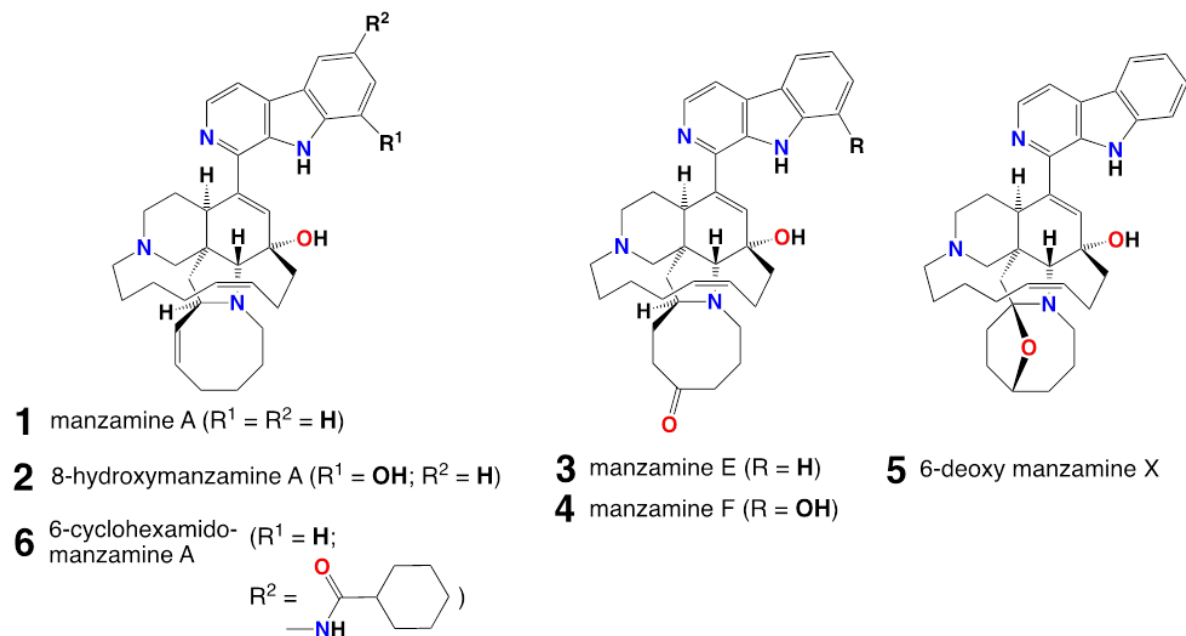


Figure 2: Structures of manzamines presented in this chapter. Manzamine A (**1**), 8-hydroxy manzamine A (**2**), manzamine E (**3**), manzamine F (**4**), 6-deoxymanzamine X (**5**), and 6-cyclohexamidomanzamine A (**6**).

Despite their promising anti-tubercular activity, the cytotoxicity of the manzamines has been a major drawback for their development into drugs. One proposed mechanism for their cytotoxicity posits the planar β -carboline moiety as a DNA intercalating agent (341). Consistent with this notion, amidation of the β -carboline ring to produce 6-cyclohexamidomanzamine A (**Figure 2**) eliminated the cytotoxicity observed for manzamine A but produced only a modest reduction in activity against *M. intracellulare* ($IC_{50} = 1.26 \mu\text{M}$) relative to manzamine A ($IC_{50} = 0.640 \mu\text{M}$) (342).

To date, mechanisms underlying the potent biological activities of these alkaloids remain unclear. In this report, we have screened a library of 26 marine-derived alkaloids against *MtSK*. From them, six inhibited *MtSK*, including manzamine A (**1**), 8-hydroxymanzamine A (**2**), manzamine E (**3**), manzamine F (**4**), 6-deoxymanzamine X (**5**), and 6-cyclohexamidomanzamine A (**6**) (**Figure 2**). Initial kinetic evaluations showed all six to be mixed non-competitive inhibitors of the enzyme, with **6** showing the lowest K_I values against all forms of *MtSK* (free enzyme, each enzyme-substrate binary complex, and the enzyme-substrate ternary complex). Further analyses revealed that each compound also showed time-dependent inhibition of *MtSK*. Only **6** showed isomerization of the initial EI complex to a more tightly-bound EI* complex. Again, **6** showed the most favorable properties as an inhibitor with the highest forward and lowest reverse rate constants for the isomerization step. Inhibitor jump-dilution experiments confirmed that **6** was the only slow, tight-binding inhibitor distinct in its potency from the other manzamines tested. Indeed, the K_I^* value obtained for **6** was at least 40-fold lower than that obtained for any of the other manzamines. Docking simulations of **6** with *MtSK* predicted two possible binding modes for this compound in the substrate binding pockets of *MtSK*. In the most favorable pose **1** obtained, the 6-cyclohexamido moiety occupied the shikimate binding site,

while in an alternative pose 2 overlapped with the co-crystallized ADP. Our results suggest that manzamine alkaloids may be viable lead compounds for the development of antimycobacterial drugs and that *MtSK* may be a fruitful target for manzamines and other compounds to exert their antitubercular activity.

2.3 Materials

Manzamine A (1), 8-hydroximanzamine A (2), manzamine E (3), manzamine F (4), and 6-deoxymanzamine X (5), were isolated from a common Indo-Pacific sponge, *Acanthostrongylophora* sp., collected from Manado, Indonesia through an optimized isolation procedure (340). 6-cyclohexamidomanzamine A (6) was synthesized by amidation of aminomanzamines (342). All compounds evaluated on this study were supplied with a minimum purity of 90% as analyzed by HPLC or ¹H-NMR. Dimethyl sulfoxide (DMSO), shikimate-3-phosphate (S3P) used for the calibration curve, the substrates adenosine-5'-triphosphate (ATP) and shikimate (SA) were purchased from Sigma-Aldrich (St. Louis, MO). All organic solvents were HPLC or LC-MS grade and were purchased from Thermo Fisher (Hanover Park, IL). All buffers and media were prepared using water purified by a Milli-Q purification system (Millipore, Billerica, MA). *MtSK* was expressed and purified following procedures described in a previous report (343). The purity of the protein after Ni²⁺ affinity chromatography was determined by SDS-PAGE and LC-ESI-MS, and aliquots were stored at -80 °C in 50 mM Tris-HCl, pH 7.4; 0.5 M NaCl.

2.4 Methods

2.4.1 *MtSK* inhibitor screening by LC-MS

The inhibitory effect of the small library of marine-derived compounds was evaluated by an end-point LC-MS enzymatic activity assay based on the quantitative measurement of the reaction product shikimate-3-phosphate (S3P) ($m/z = 253.0117 [M - H]^-$). All assays were performed at 25 °C as described previously, using 100 mM ammonium acetate, pH 7.6, 50 mM KCl and 5 mM MgCl₂ in a reaction volume of 500 µL (343). Primary screening was carried out by measuring the activity of *MtSK* in the presence of each compound (50 µM) dissolved in DMSO at saturating concentrations of the substrates ATP (1.2 mM) and SA (5 mM). Reactions were initiated by the addition of 0.2 µM of *MtSK*, for 30 seconds and quenched by the addition of 2 µL of 98% formic acid and vortexing. Negative control experiments were carried out in the same manner in the presence of DMSO. For mass spectrometric analyses, 5 µL of each reaction mixture were injected onto the HPLC system.

2.4.2 LC-MS analysis

Reversed-phase HPLC separation of the reaction mixtures was performed on an Agilent 1200 RRLC system, using a Zorbax Eclipse Plus Phenyl-hexyl (4.6 x 100 mm 3.5 µm, Agilent Technologies, Inc.) column. The mobile phase consisted of water with 0.1% (v/v) formic acid (A) and acetonitrile 100% (B) with a gradient elution as follows: 0 min, 2% B held for 4 min, to 30% B in the next 2 min. Each elution was followed by a 1 min post-elution with 2% B. The total elution-time analysis was 7 min at a flow rate of 0.4 mL/min and column temperature of 45 °C. Mass spectrometry was carried out in an Agilent (Little Falls, DE) 6520 Accurate-Mass Q-TOF under negative ionization mode using a narrow m/z range (m/z 100-300). Nitrogen was used as the nebulizing gas (25 psig) and drying gas (10 L/h, 350 °C). A capillary voltage of 3200

V was used for the ESI source, and the fragmentor voltage was set to 175 eV. For quantification of S3P, extracted ion chromatograms (EIC) of m/z 253.0117 $[M - H]^-$ were integrated using Agilent MassHunter Workstation Qualitative Analysis software (version B.02.00), and the peak area was used to evaluate enzymatic activity.

2.4.3 Kinetics of inhibition of manzamine alkaloids

Initial assessment of compounds 1 - 6 was carried out to determine the mechanism of rapid-reversible inhibition exerted by each. A range of concentrations (0 - 250 μ M in DMSO) for compounds 1 – 5 and (0- 50 μ M in DMSO) for compound 6 was evaluated to determine the effect on the linear initial rates of MtSK activity. For these experiments, there was no pre-incubation of enzyme with the manzamines (1 – 6). For each concentration of 1 – 6, five ATP concentrations varying from 0.05 to 1.2 mM were evaluated, while keeping the SA concentration constant at saturating concentrations (i.e., 5 mM SA against an apparent K_M with respect to SA of 0.53 mM). Likewise, five different concentrations of SA ranging from 0.2 to 5 mM were used for each concentration of 1 – 6, while the concentration of ATP was kept constant at a saturating concentration (i.e., 1.2 mM ATP against an apparent K_M with respect to ATP of 0.20 mM) (343). Each reaction was initiated by the addition of *MtSK* (0.2 μ M), allowed to proceed for 30 seconds, and then quenched as described above.

The initial rate data were evaluated using GraphPad Prism 5.02 software (Mountain View, CA) in two ways. In the first, all data obtained from varying SA against a constant concentration ATP were fit to one of four common models of inhibition (competitive, uncompetitive, non-competitive, and mixed-noncompetitive). The same was done for all data obtained by varying ATP against a constant concentration of SA. As described below, both data

sets were best fit by a mixed-noncompetitive model where compounds show unequal affinities for the free enzyme (E) versus the enzyme-substrate (ES) complexes. That is, the ratio of $K_{I(ES)}/K_{I(E)} \neq 1$, and in all cases reported here $K_{I(ES)}/K_{I(E)}$ values were ≥ 1 (344). In the second approach, each hyperbolic curve in a set (e.g., varied ATP, constant saturating SA, and a chosen concentration of 1 – 6) was fit individually to a Michaelis-Menten equation (1), where S represents the substrate whose concentration was varied in order to obtain an individual

$$\frac{v_o}{[E]_T} = \frac{(k_{cat})_{app} [S]}{(K_M)_{app} + [S]} \quad (1)$$

apparent k_{on} (i.e., $[k_{cat}/K_M]_{app}$) with respect to the varied substrate and an apparent k_{cat} in the presence of a given concentration of inhibitor and saturating concentrations of the second substrate. The effects of inhibitor concentration on these two parameters were then evaluated in secondary plots to make assessments regarding the mechanism of inhibition and then determine K_I 's involved.

Given the random sequential kinetic mechanism of *MtSK* catalysis, (345) we interpreted our results in the context of a cubic model (**Figure 2.1**). In this model, the term “ α ” accounts for the ratio of K_{ATP} for the free enzyme (E) versus the enzyme bound to shikimate (E-SA), and the complementary situation applies for K_{SA} . Since each binding sequence establishes a thermodynamic square, α applies to both substrates (i.e., $K_{SA} * \alpha K_{ATP} = \alpha K_{SA} * K_{ATP}$). Previous reports indicate that the value of α is close to 1.(345) The cubic model allows that the inhibitor may bind to any form of the enzyme (E, E-SA, E-ATP, and E-SA-ATP) where each form of the enzyme has its own K_I for a given inhibitor. These are, respectively, K_I , γK_I , $\gamma\beta K_I$, and $\beta\gamma K_I$.

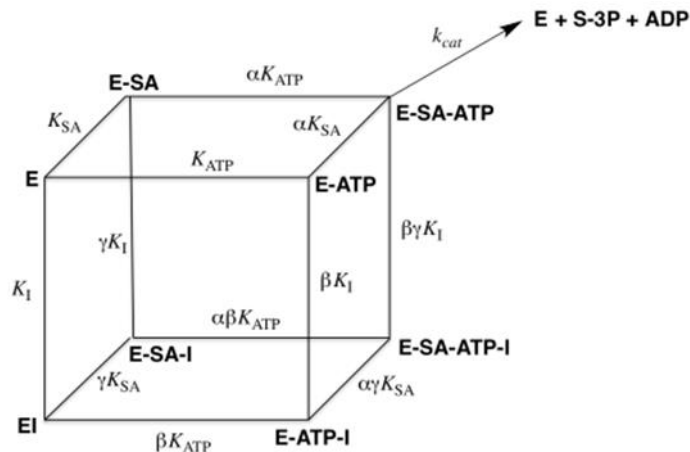


Figure 2.1: Kinetic model for the mixed-type inhibition of *MtSK* reaction with shikimate (SA) and ATP by manzamine compounds.

From fitting the mixed-noncompetitive inhibition model to experiments where ATP concentration is varied, the Prism-designated “ K_I ” corresponds to βK_I , and the Prism-designated “ αK_I ” corresponds to $\beta \gamma K_I$ (i.e., the “ α ” returned by the software corresponds to γ in the cubic model). Similarly, when SA is the varied substrate, the K_I corresponds to γK_I and the Prism-designated “ αK_I ” corresponds to $\beta \gamma K_I$ (i.e., now “ α ” refers to β in the cubic model). The dissociation constant for the inhibitor binding to the free enzyme (K_I) can be estimated by dividing βK_I (obtained from experiments where ATP was varied), β (obtained from experiments where SA was varied). The same was determined using γK_I and γ from the complementary experiments (i.e., where SA was varied, and ATP was varied, respectively). Importantly, there was good agreement between both estimations of K_I .

To ensure that the mixed-noncompetitive model was a model well supported across the data we collected, we also used an approach where each curve was individually fit to a

Michaelis-Menten equation. Briefly, a hyperbolic decrease in apparent k_{cat} with increasing inhibitor concentration was fit to obtain $\beta\gamma K_I$ (Equation 2). In principle,

$$(k_{cat})_{app} = \frac{k_{cat}}{\left(1 + \frac{[I]}{\beta\gamma K_I}\right)} \quad (2)$$

the same value should be obtained whether SA or ATP is the substrate varied to obtain the individual curves. For individual curves where SA is the varied substrate, the hyperbolic decrease in apparent k_{cat}/K_{SA} with increasing inhibitor concentration can be fit to obtain βK_I (Equation 3). Likewise, when ATP is the varied substrate, the decrease in apparent k_{cat}/K_{ATP} with increasing concentration of inhibitor can be fit to obtain γK_I (Equation 4).

$$\left(k_{cat}/K_{SA}\right)_{app} = \frac{k_{cat}}{\alpha K_{SA} \left(1 + \frac{[I]}{\beta K_I}\right)} \quad (3)$$

$$\left(k_{cat}/K_{ATP}\right)_{app} = \frac{k_{cat}}{\alpha K_{ATP} \left(1 + \frac{[I]}{\gamma K_I}\right)} \quad (4)$$

Importantly, where there was overlap in determined dissociation constants across both methods (e.g., γK_I and βK_I), there was close agreement, indicating the mixed-noncompetitive inhibition model and the equilibrium dissociation constants obtained from it provided a reasonable description of the initial encounter of *MtSK* with these two inhibitors.

2.4.4 Slow, tight-binding inhibition of *MtSK* activity

Initial kinetic experiments which included a pre-incubation of *MtSK* and a given manzamine (**1 – 6**) produced greater *MtSK* inhibition, suggesting the inhibition involved a time-

dependent mechanism. Therefore, two methods were used to characterize the slow-binding component of the inhibition. In the first, preincubation times of *MtSK* (0.2 μM) with various fixed concentrations of inhibitors (0 – 250 μM) were varied (0 – 60 min). The *MtSK* activity remaining following incubation was measured by initial rates of S3P production as described above. For the second approach, *MtSK* (2.5 nM) was used to initiate S3P formation in reactions containing both substrates and some concentration (0 – 150 μM) of 1 – 6. The progressive decrease in rate of S3P formation by *MtSK* was monitored for 20 min. All reactions were performed using the same buffer and conditions as described above. Data generated using the first approach were analyzed by Equation 5 for time-dependent inhibition:

$$v_t = v_i \exp(-k_{obs}t) \quad (5)$$

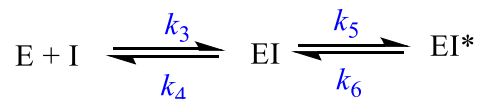
where v_t is the measured steady-state velocity after preincubation time t , and v_i represents the steady-state velocity measured at preincubation $t = 0$. k_{obs} is the apparent first-order rate constant for the loss of activity with preincubation time. Progress curves generated using the second approach were analyzed by Equation 6 for slow-binding inhibition:

$$[P] = v_s t + \left(\frac{v_i - v_s}{k_{obs}} \right) * (1 - \exp(-k_{obs}t)) \quad (6)$$

where $[P]$ represents the amount of S3P generated by *MtSK* at time t , v_i and v_s represent the initial and final steady-state rates, respectively, in the presence of inhibitors, and k_{obs} is the rate constant for the transition from the initial to final steady-state rates of *MtSK* reaction.

Scheme 1 below describes a two-step mechanism that can account for the slow binding of inhibitors. The first step involves the formation of a loose initial encounter complex (EI), and

the second step involves the slow isomerization of the enzyme to form a higher affinity complex (EI*):



Scheme 1. Two-step mechanism for slow binding inhibition

In this type of inhibition, the value of k_{obs} is a saturable function of [I] conforming to Equation 7. Therefore, plots of k_{obs} versus inhibitor concentration yield a rectangular hyperbola, where the y-intercept is nonzero and indicates the rate constant k_6 . The maximum value of k_{obs} approached as an asymptote with increasing concentration of inhibitor is equal to $k_6 + k_5$. The concentration of inhibitor yielding a half-maximal value of k_{obs} is equal to the apparent dissociation constant for the initial enzyme-inhibitor complex (K_I) and the true affinities (K_I^*) or dissociation constants of the high-affinity enzyme-inhibitor complex were calculated according to Equation 8.(346)

$$k_{obs} = k_6 + \left(\frac{k_5 [I]}{K_I^{app} + [I]} \right) \quad (7)$$

$$K_I^* = \frac{K_I}{1 + \left(\frac{k_5}{k_6} \right)} \quad (8)$$

2.4.5 Jump dilution experiments.

MtSK (20 μ M) was incubated with 1 mM of a given manzamine (**1 – 6**) for 1 h. The reaction was initiated by diluting the EI complex in 1.2 mM ATP and 5 mM SA in 100 mM ammonium acetate, 50 mM KCl and 5 mM MgCl₂, pH = 7.6 to a final enzyme concentration of 0.2 μ M. Reactions were quenched with formic acid at times ranging from 0 - 60 min. Quenched

reactions were analyzed by LC-MS as described above to quantify S3P. Concentration of S3P produced was plotted against reaction time. Data were fit to Equation 9:

$$[\text{S3P}]_t = [\text{A}]\left\{1 + \frac{1}{k_1 - k_2} [k_2 \exp(-k_1 t) - k_1 \exp(-k_2 t)]\right\} \quad (9)$$

where [A] is the total concentration of S3P generated by *MtSK* over the reaction (i.e., the amplitude) and k_1 and k_2 are the rates governing the recovery of activity from EI*. The slower of the two is taken to represent k_6 from Scheme 1.

2.4.6 Computational Methods

The *MtSK* crystal structure (PDB code 2DFT) (321) was refined by applying the Prime preparation and refinement tools of the Protein preparation wizard implemented in the Schrödinger software package (Schrödinger, LLC). After the addition of hydrogen and detection of disulfide bonds, the structure was optimized by applying default parameters of the Impref utility using the OPLS2001 force field. The maximum allowed root-mean-square deviation between the refined structure and the input crystal structure was 0.3. Ligand structures were prepared using the LigPrep utility at pH = 7.4. The Induced Fit program of the Schrödinger software applies the Glide docking method combined with Prime structural refinement tools to account for the flexibility of protein side chains within 5 Å of the ligand during docking. Three docking set-ups were used in the docking runs, defining the center of the docking grid based on the centroid position of ligands present in the *MtSK* crystal structures as follows: a. SA, b. ADP and c. the center of mass of SA and ADP. The latter site definition allowed docking into the region that included both the SA and the ATP binding site. Induced Fit settings were at default values except the size of the box enclosing the targeted site, which was set to 30 Å.

2.5 Results and discussion

For all the manzamines examined (**1** – **6**), the effects of their concentrations on the *MtSK* reaction kinetics with varying concentrations of substrates were best fit by a mixed-type inhibition model. Data obtained for **1** and **6** are shown in **Figures 2.2** and **2.3**. The data for 2-5 are shown in **Figures 2.1- 2.4** (Appendix 1). A decrease in apparent k_{cat} with increasing inhibitor concentration (observed for **1** – **6**) suggested that the mechanism of inhibition could not be exclusively competitive. However, a decrease in apparent k_{cat}/K_M (with respect to either substrate) with increasing concentrations of **1** – **6** indicated that all six compounds bound to the free enzyme. As described below, values for β and γ in all cases were ≥ 1 , indicating the preference of the inhibitors for the free enzyme. Visual inspection of double reciprocal plots (e.g., **Figure 2.8** for **6**) confirmed these conclusions.

A mixed-type mechanism of inhibition with respect to both substrates implies that the manzamine alkaloids can bind to *MtSK* forming four different complexes, but their affinities for these forms can be different. Thus, there are likely four different dissociation constants within the system: one for inhibitor interaction with the binary complex E-SA (γK_I), one for inhibitor interaction with the alternative binary complex, E-ATP (βK_I), one corresponding to the ternary complex E-SA-ATP ($\beta\gamma K_I$), and one for the interaction of the inhibitor with the free enzyme E (K_I) (**Figure 2.2**).

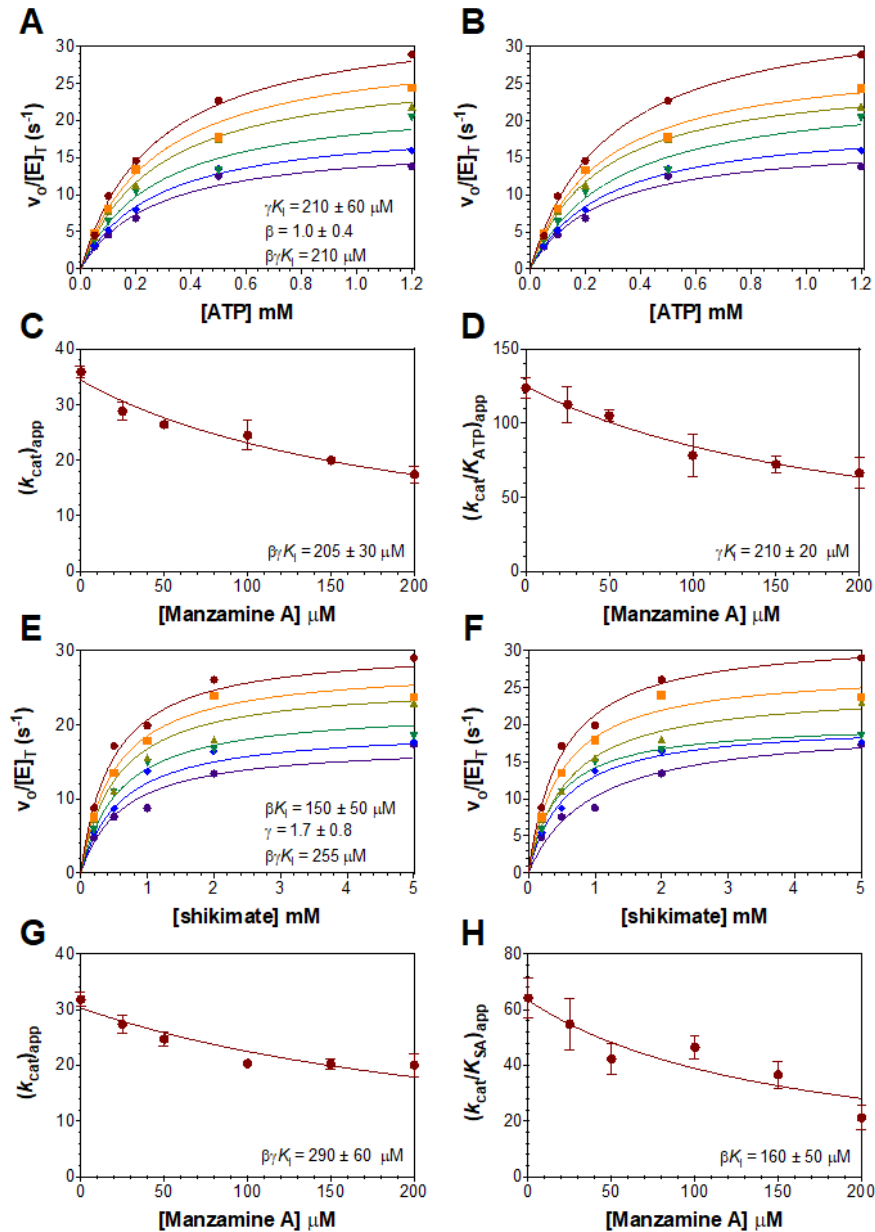


Figure 2.2: Non-linear least-squares analyses of rapid reversible inhibition by manzamine A (1). Data acquired varying [ATP] at fixed [SA] (and *vice versa*) were either fit to a global mixed-noncompetitive mechanism of inhibition or as individual Michaelis-Menten curves. Concentrations of 1 evaluated were 0 (●), 25 (■), 50 (▲), 100 (▼), 150 (◆), and 200 (●) μM .

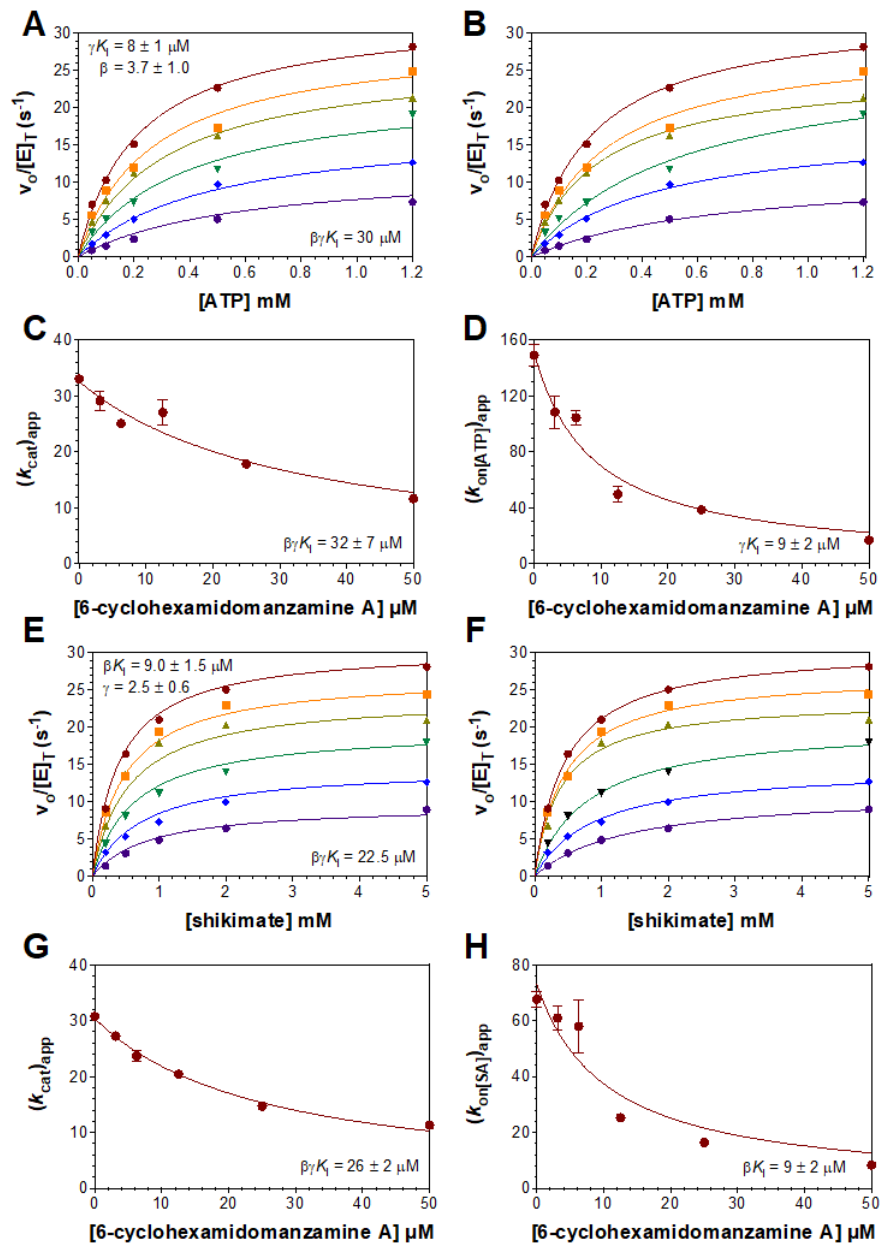


Figure 2.3: Non-linear least-squares analyses of rapid reversible inhibition by 6-cyclohexamidomanzamine A (6). Data acquired varying [ATP] at fixed [SA] (and *vice versa*) were either fit to a global mixed-noncompetitive mechanism of inhibition or as individual Michaelis-Menten curves. Concentrations of 6 evaluated were 0 (●), 3.12 (■), 6.25 (▲), 12.5 (▼), 25 (◆), and 50 (●) μM.

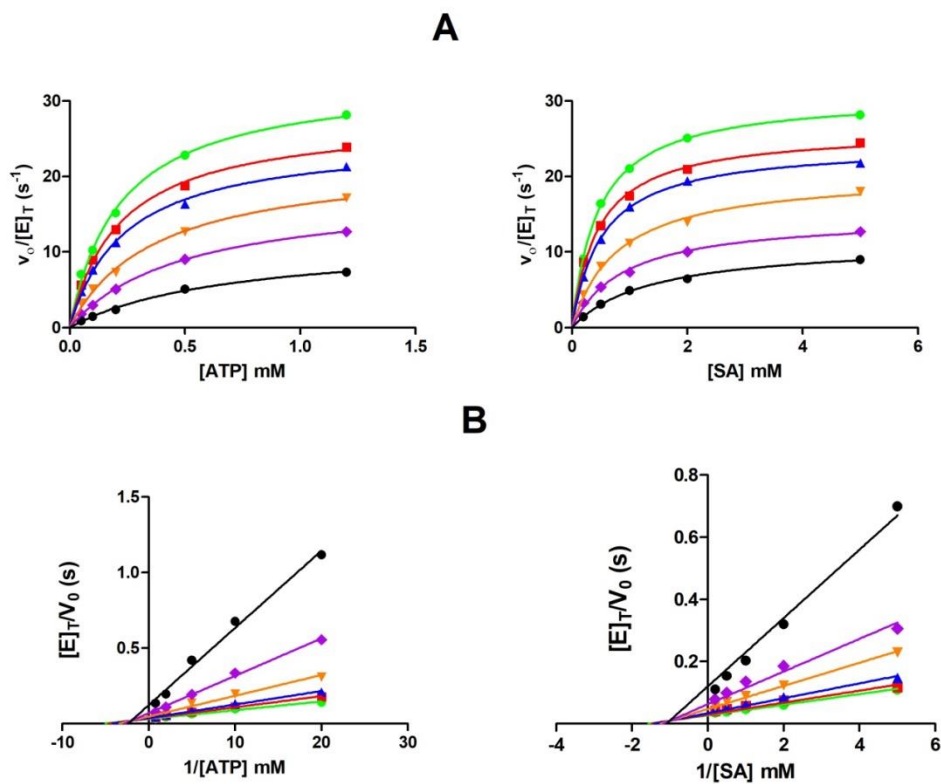


Figure 2.8: Effect of compound 6 on *MtSK* activity. The concentration of ATP was varied relative to a constant 5 mM shikimate concentration (A) or the concentration of shikimate was varied against a constant 1.2 mM ATP concentration (B) in the presence of 0 μM (\bullet), 3.12 μM (\blacksquare), 6.25 μM (\blacktriangle), 12.5 μM (\blacktriangledown), 25 μM (\blacklozenge), and 50 μM (\bullet) of compound 6.

There was good general agreement on the values of β , γ , βK_I , γK_I , and $\beta\gamma K_I$ across our methods of data analysis, and this extended to our estimates of K_I . Across all complexes, inhibition constants for **6** were 4- to 60-fold lower than those determined for the other manzamines **1** – **5** (Tables 2 and 2.1). For example, for **1**, β and γ were relatively small values (between 1 and 2), such that the range of inhibition constants observed for **1** was from ~ 140 μM for free *MtSK* (i.e., K_I) to ~ 250 μM for the ternary *MtSK*-ATP-SA complex (i.e., $\beta\gamma K_I$). Conversely, for **6**, values for β and γ were both determined to be about three. Here, the inhibition constants ranged from ~ 30 μM for the ternary complex (i.e., $\beta\gamma K_I$) down to ~ 3 μM for the free enzyme (i.e., K_I). Thus, overall, **6** is a far more potent inhibitor of *MtSK* than **1**, and with its greater preference for free *MtSK* over the *MtSK*-substrate complexes, **6** shows an apparent affinity for free *MtSK* that exceeds **1** by about 50-fold.

Table 2. Inhibition constants determined by varied [ATP], fixed [shikimate]

Compound	Inhibition Parameter ^a				
	β^b	γK_i (μM) ^c	γK_i (μM) ^d	$\beta\gamma K_i$ (μM) ^e	est K_i (μM) ^f
1	1.0 \pm 0.4	210 \pm 60	210 \pm 20	205 \pm 20	120 \pm 60
2	2 \pm 1	76 \pm 25	83 \pm 22	180 \pm 80	11 \pm 7
3	1.8 \pm 1.0	180 \pm 60	175 \pm 44	312 \pm 96	63 \pm 46
4	6.6 \pm 3.6	121 \pm 23	130 \pm 15	1100 \pm 660	40 \pm 15
5	6.6 \pm 3.7	96 \pm 18	105 \pm 24	1000 \pm 400	21 \pm 8
6	3.7 \pm 1.0	8 \pm 1	9 \pm 2	32 \pm 8	3.2 \pm 0.9

^aShikimate held constant 5.0 mM; ATP was varied (0.05 – 1.2 mM) against a series of fixed inhibitor concentrations.

^bDetermined as “ α ” from fitting to a mixed-type inhibition model.

^cDetermined as “ K_i ” from fitting to a mixed-type inhibition model.

^dDetermined from replotting of $(k_{\text{cat}}/K_{\text{ATP}})_{\text{app}}$ vs. [inhibitor].

^eDetermined from replotting of $(k_{\text{cat}})_{\text{app}}$ vs. [inhibitor].

^f K_i (i.e., dissociation constant for inhibitor binding to free *MtSK*) was estimated by dividing γK_i from mixed-type fitting (this table) by γ from mixed-type fitting (Table 2).

Table 2.1. Inhibition constants determined by varied [shikimate], fixed [ATP]

Compound	Inhibition Parameter ^a				
	γ^b	βK_i (μM) ^c	βK_i (μM) ^d	$\beta\gamma K_i$ (μM) ^e	est K_i (μM) ^f
1	1.7 ± 0.8	150 ± 50	160 ± 50	290 ± 60	151 ± 67
2	7 ± 4	31 ± 10	22 ± 9	187 ± 46	15 ± 9
3	2.9 ± 1.9	105 ± 39	139 ± 76	112 ± 20	58 ± 39
4	3 ± 1	142 ± 32	141 ± 24	442 ± 68	22 ± 13
5	4.5 ± 1.5	77 ± 15	44 ± 18	272 ± 73	12 ± 7
6	2.5 ± 0.6	9.0 ± 1.5	7.6 ± 1.7	19 ± 3	2.4 ± 0.8

^aATP held constant at 1.2 mM; shikimate was varied (0.2 – 5.0 mM) against a series of fixed inhibitor concentration.
^bDetermined as “ α ” from fitting to a mixed-type inhibition model.
^cDetermined as “ K_i ” from fitting to a mixed-type inhibition model.
^dDetermined from replotting of $(k_{\text{cat}}/K_{\text{SA}})_{\text{app}}$ vs. [inhibitor].
^eDetermined from replotting of $(k_{\text{cat}})_{\text{app}}$ vs. [inhibitor].
^f K_i (i.e., dissociation constant for inhibitor binding to free *MtSK*) was estimated by dividing βK_i from mixed-type fitting (this table) by β from mixed-type fitting (Table 1).

Pre-incubation of *MtSK* with a fixed concentration of any of the manzamines (**1** – **6**) for 60 min produced increased inhibition with time. Time-dependent inhibition is suggestive that a given inhibitor operates by either a slow-binding or irreversible mechanism of inhibition, wherein an initial EI complex undergoes a relatively slow transition (e.g., isomerization, conformational change, and/or covalent modification) to EI* (Scheme 1). Here, the rate constant k_6 is either very small or zero, respectively. In either case, determination of inhibition constants using typical rapid-equilibrium methods could result in an underestimation of the true potency of active compounds.⁽³⁴⁷⁾ In the presence of either **1** or **6**, *MtSK* activity decreased exponentially with pre-incubation time (**Figure 2.9**). Notably, there was also a decrease in *MtSK* activity at preincubation $t = 0$ with increasing concentrations of **1** and **6**. This confirmed a two-step inhibition mechanism where formation of the initial EI complex is reflected in the decrease along the y-axis with increasing inhibitor concentration, and the exponential decrease in activity

thereafter reflecting the transition to EI*.(348) Similar results were obtained with compounds 2 – 5.

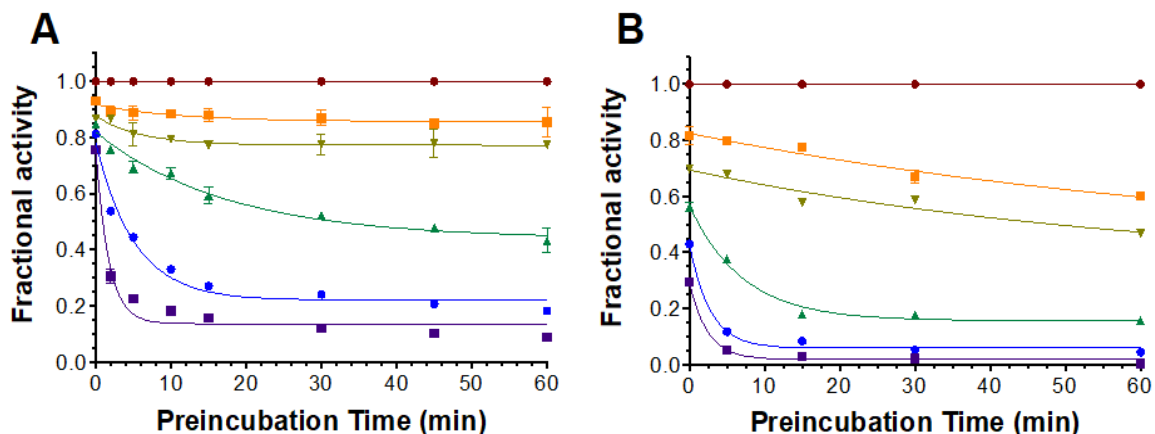


Figure 2.9: Effect of inhibitor concentration and preincubation time on the activity of *MtSK*. *MtSK* was preincubated for the times indicated with 0 μM (●), 10 μM (■), 25 μM (▼), 50 μM (▲), 100 μM (●), and 150 μM (■) of compound 1 (A), or 0 μM (●), 3.12 μM (■), 6.25 μM (▼), 12.5 μM (▲), 25 μM (●), and 50 μM (■) of compound 6 (B).

Because of the long pre-incubation times ($\geq 1\text{h}$) required for the experiments above, enzyme stability became a factor. Therefore, we instead monitored the burst-exponential decrease in rates of product formation over time in the presence increasing inhibitor concentration to determine the inhibition mechanism rate constants for **1** – **6**. Using this approach, the progress curve in the presence of **1** displayed an initial burst followed by a linear steady-state generation of product (**Figure 2.10A**), diagnostic of a slow-onset of inhibition.(349) For **6**, product formation appeared to be nearly linear but the rates were visibly reduced (**Figure**

2.10B) as compared to the uninhibited reaction, suggesting a more rapid conversion of EI to EI* than that of **1**. For **1**, k_{obs} increased hyperbolically with inhibitor concentration. From the fit of the data to equation 8, the rate constants k_5 and k_6 were estimated to be 0.18 min^{-1} and 0.08 min^{-1} , respectively, with a $^{app}K_I$ of $33 \text{ } \mu\text{M}$ (**Table 2.2**). For **6**, the data revealed an upper limit for the sum k_5 and k_6 of 0.95 min^{-1} and indicated that the $^{app}K_I$ must be $\leq 2 \text{ } \mu\text{M}$. This type of time-dependent inhibition was also observed for each of the other manzamines as well (**2 – 5**). Whereas **2** and **3** behaved in a manner similar to **1**, the time-dependence of inhibition by **4** and **5** showed weak dependence on inhibitor concentration. As such, we were unable to reach the limit set by the sum of k_5 and k_6 , and consequently, we were unable to determine $^{app}K_I$ or K_I^* for these compounds.

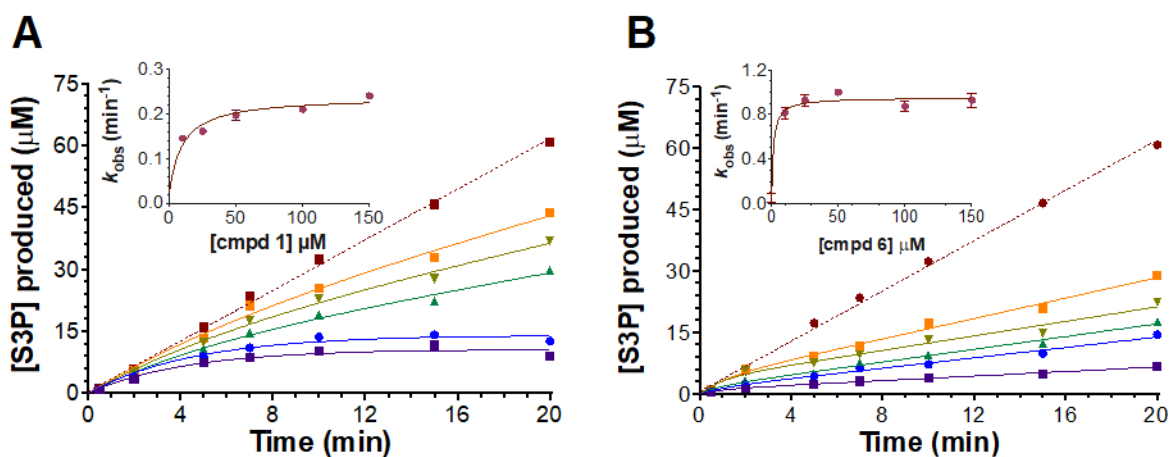


Figure 2.10: Effect of inhibitor concentration and preincubation time on the activity of *MtSK*. *MtSK* was preincubated for the times indicated with $0 \text{ } \mu\text{M}$ (●), $10 \text{ } \mu\text{M}$ (■), $25 \text{ } \mu\text{M}$ (▼), $50 \text{ } \mu\text{M}$ (▲), $100 \text{ } \mu\text{M}$ (●), and $150 \text{ } \mu\text{M}$ (■) of compound 1 (A), or $0 \text{ } \mu\text{M}$ (●), $3.12 \text{ } \mu\text{M}$ (■), $6.25 \text{ } \mu\text{M}$ (▼), $12.5 \text{ } \mu\text{M}$ (▲), $25 \text{ } \mu\text{M}$ (●), and $50 \text{ } \mu\text{M}$ (■) of compound 6 (B).

Table 2.2. Inhibition constants slow and tight-binding inhibition models.

Cmpd	^{app} K _I Mm	K _I [*] μM	k ₅ (min ⁻¹)	k ₆ (min ⁻¹)
1	33 ± 3	10 ± 2	0.18 ± 0.01	0.08 ± 0.01
2	15 ± 11	2.4 ± 0.01	0.37 ± 0.09	0.07 ± 0.1
3	55 ± 15	6.9 ± 0.9	0.09 ± 0.01	0.013 ± 0.004
4	ND ^a	ND	ND	ND
5	ND ^a	ND	ND	ND
6	1.4 ± 0.9	0.06 ± 0.03	0.91 ± 0.03	0.04 ± 0.02 ^b

^aTime-dependent inhibition evident, but k₅ could not be reached, thus, ^{app}K_I, K_I, and k₆, could not be determined.
^bDetermined from jump dilution experiments (see Fig. 6)

Analyses of intact *MtSK* by ESI-MS following its incubation with **1** or **6** did not reveal any covalent modification of the *MtSK* protein (data not shown), eliminating one major mechanism of irreversible inhibition. To determine the value of k₆ and in so doing distinguish whether the manzamines were irreversible or slow-binding inhibitors, a jump-dilution experiment was carried out for pre-formed complexes of *MtSK* with each manzamine (**1** – **6**). Upon 1:100 dilution into assay solution, recovery of activity as monitored by production of S3P was observed for *MtSK* preincubated with all six compounds (**Figure 2.11**). This confirmed that none of the manzamines act as irreversible inhibitors. Interestingly, only recovery of activity for *MtSK* reacted with **6**, was substantially delayed, and a fit of the data to a double-exponential function (Equation 10) returned 0.04 min⁻¹ as the value for the slower of the two exponentials. We interpret this as an estimate for k₆ in the inhibition mechanism of **6**. In contrast, no delay in the return of activity upon dilution was evident and only slightly diminished activity was observed where *MtSK* was reacted with **1** – **5**. This suggested that EI* more readily reverted to EI with these compounds compared to **6**. Consistent with a slow, tight-binding mechanism, the potency of **6** is enhanced by nearly 25-fold upon isomerization of the first initial enzyme-inhibitor (EI) complex to form a more stable complex (EI*) (i.e., [1 + k₅/k₆] = 23.8; Table 3). We

obtained much more modest values for **1**, **2**, or **3** (i.e., $[1 + k_5/k_6] = 3.3, 6.3, \text{ and } 7.9$, respectively; **Table 2.2**). Ultimately, K_I^* values estimated were 40-fold lower for **6** than any of the other manzamine inhibitors. Our results indicate that this resulted from a combination of a substantially lower K_I for formation of the initial EI complex with **6** as well as a more facile isomerization of the initial complex to EI*.

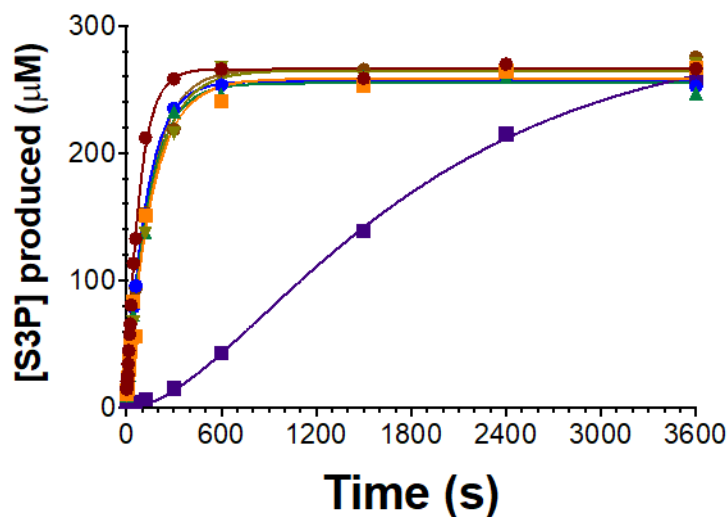


Figure 2.11: Recovery of *MtSK* activity following dilution of *MtSK*-inhibitor complexes. *MtSK* (20 μ M) was pre-incubated for 1 hour without any inhibitor (\bullet) or with 1 mM **1** (\blacksquare), **2** (\blacktriangledown), **3** (\blacktriangle), **4** (\bullet), **5** (\blacklozenge), or **6** (\blacksquare) to achieve significant target inactivation. Enzyme-inhibitor complexes were then diluted 1:100 into a reaction buffer containing 5.0 mM shikimate, 1.2 mM ATP, and 100 mM ammonium acetate, pH 7.6, to follow enzyme reactivation.

Compound **6** was docked into *MtSK* (PDB 2DFT)(321) targeting both, the shikimate and ATP binding site regions. **Figure 2.12** illustrates that this compound may be accommodated in two alternative docked poses, which differ in the position and conformation of pyridoindole-

cyclohexamide while the rest of the molecule shows close overlap. Of the two poses the binding model with more favorable contacts (pose 1) places the pyridoindole-hexamide moiety in a deeper cavity, where its cyclohexamide group occupies the shikimate binding pocket. In the alternative binding model (pose 2) the pyridoindole-hexamide moiety binds close to the surface, and the cyclohexamide group overlaps with the co-crystallized ADP. The latter pose may correspond to a weaker bound complex compared to pose 1. The most favorable binding model obtained in our docking study is pose 1, accommodated in a deep region of the *MtSK* active site (**Figure 2.12B**). This pose predicts the following interactions between compound **6** and *MtSK* (**Figure 2.12C**). Thr 115 participates in two, near optimal hydrogen bonding interactions with compound **6**, while Glu 38 forms a salt bridge with a protonated amine of the ligand. The carbonyl oxygen of compound **6** coordinates the co-crystallized Mg²⁺. The guanidinium group of Arg117 forms positive charge – aromatic stacking interactions with the pyridoindol ring system. Arg 20 is hydrogen bonding with the N of the pyridine ring. Residues involved in favorable non-polar contacts with the ligand are Pro 11, Val 35, Ile 45, Phe 49, Val 116, Pro 118, Leu 119 and Leu 132.

Docking results suggested that compound **6** may adopt two alternative poses, blocking the binding of either substrate. Of these, the pose interfering with shikimate binding may represent the more tightly bound complex. These hypotheses are consistent with the mixed-type mechanism of inhibition suggested by our kinetic analyses. The presented model may be tested in future experimental designs elucidating interactions between manzamine A derivatives and *MtSK* residues. Furthermore, the active compounds in this study have been previously evaluated for their *in vitro* antibacterial activity against *Mycobacterium tuberculosis* (R37Rv). MIC values along with cytotoxicity in mammalian cells are summarized in **Table 2.3**. It is noteworthy that

the *in vitro* activity against *M. intracellulare* of the best candidate, compound **6** (1.8 μM), is comparable to that of the second drug of treatment for TB, ciprofloxacin (1.05 μM).

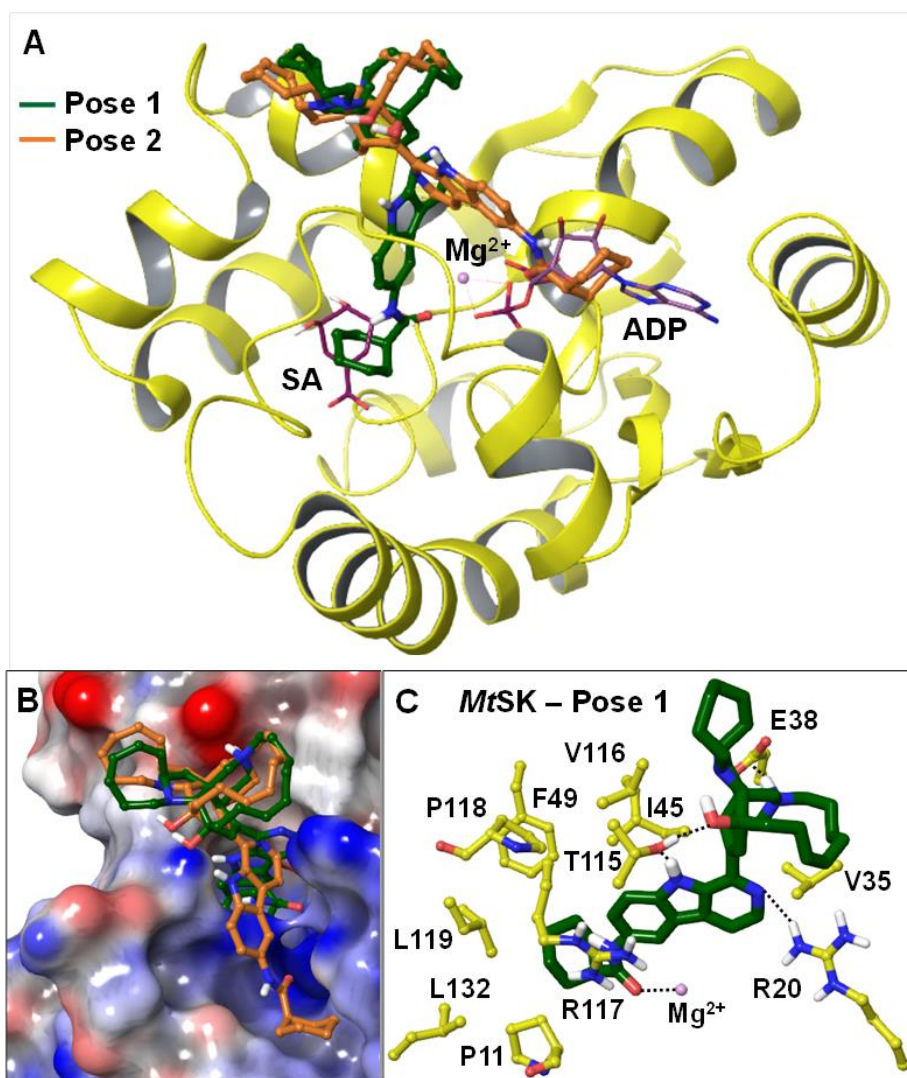


Figure 2.12: Two docked poses of compound 6 are shown in the *MtSK* crystal structure, PDB code 2DFT (panel A). The electrostatic potential surface of the *MtSK* binding site with docked poses 1 and 2 is shown in panel B, with analogous color scheme for the ligands as in A. A close-up view of docked pose 1 with *MtSK* residues closest to the ligand is displayed in panel C. All other atoms are colored by atom type.

Table 2.3. *In vitro* anti *Mycobacterial* activities and cytotoxicities of manzamines **1** and **2**.

Compound	<i>Mtb</i> (H37Rv) MIC ($\mu\text{g/mL}$)	<i>M. intracellulare</i> IC ₅₀ (μM)	Cytotoxicity (Vero) IC ₅₀ ($\mu\text{g/mL}$)
1	1.5	0.64	1.2
2	NT	1.8	NC
Rifampin	0.5	NT	NT
Ciprofloxacin	NT	1.05	NT
Doxorubicin	NT	NT	5.0

Values were obtained from the literature (23, 27, 28 and 30). MIC values for the first and second line of treatment drugs rifampin and ciprofloxacin are reported as a reference, as well the cytotoxicity of the drug doxorubicin against Vero cells. NC = no cytotoxicity up to 4.76 $\mu\text{g/mL}$. NT = not tested.

Kinetic profiling has demonstrated that several manzamines (1 – 5) inhibit *MtSK* though, only **6** follows the two-step mechanism where an initial EI complex undergoes a slow isomerization, resulting in a higher affinity EI* complex. Of the six manzamines evaluated, the 6-cyclohexamido derivative of manzamine A (**6**) was clearly the superior inhibitor of *MtSK*, a property that was evident in both steps of the inhibition mechanism. Apparent K_I values corresponding to mixed inhibition were lower for **6** than the other five manzamines regardless of the presence of either or both *MtSK* substrates. Similarly, a higher rate constant for conversion of EI to EI* (i.e., k_5) along with the largest quotient between on and off rate constants (i.e., k_5/k_6) combined to yield a slow, tight-binding inhibitor with an overall inhibition constant (K_I^*) in the 60 nM range, at least 40-fold lower than the other manzamines evaluated.

Docking simulations of compound **6** at *MtSK* predicted two binding poses that differ in the pyridoindole-cyclo-hexamide region while the rest of the ligand structure closely overlaps between the two poses (Fig. 8). The most favorable binding mode is pose 1, in which the pyridoindole-cyclo-hexamide occupies a deep lying region of the binding site. Its 6-cyclohexamide group binds favorably in the shikimate binding pocket through non-polar

contacts of the cyclohexyl group while the carbonyl is anchored through Mg^{2+} coordination. In pose 2 this moiety is accommodated less favorably in a polar, solvent exposed region near the surface. Comparison of docked poses suggests that pose 1 may correspond to a more tightly bound complex than pose 2. We hypothesize that **6** may first bind in a mode similar to pose 2, then transition to adopt the more favorable pose 1. Re-orientation of pyridoindole-cyclohexamide from a region close to the surface into a deeper site may require induced conformational changes of the structure over time. This hypothesis derived from docking predictions is a possible model consistent with the kinetic profile of **6** presented in this study. The favorable contribution of the cyclohexamide group to ligand binding also provides a possible explanation to why manzamine A (**1**) as well as **2** – **5**, all of which lack the 6-cyclohexamido- modification are inferior as *MtSK* inhibitors at all stages of the mechanism. Notably, we have previously evaluated the potential of 6-nitroharmane and ircinol A, two compounds containing the biogenetic precursors of the manzamine alkaloids, to act as inhibitors of *MtSK*,⁽³⁵⁰⁾ and no significant inhibition was observed for these compounds. These data suggest that the entire manzamine structure is required to observe inhibition, a property that is enhanced by the 6-cyclohexamido addition.

Interestingly, other observed biological activities of the manzamines point toward a synergistic function in fighting TB infection. For example, the manzamine alkaloids have been reported to inhibit the activity of glycogen synthase kinase-3 beta ($GSK-3\beta$).^(351,352) $GSK-3\beta$ is a serine/threonine protein kinase involved in the regulation of several cellular pathways including insulin signaling, glycogen synthesis, neurotrophic factor signaling, Wnt signaling, neurotransmitter signaling and microtubule dynamics.⁽³⁵³⁾ Most importantly, $GSK-3\beta$ has been implicated in mycobacterial-induced interleukin-10 (IL-10) production in human peripheral

blood monocytes.(354) IL-10 is an anti-inflammatory cytokine mainly produced by macrophages, and it plays an important role in the regulation of immune response against infectious pathogens. Despite IL-10 protective role in the host, its immunosuppressive properties have been shown to be exploited by mycobacteria to facilitate immune evasion and long-term infections in the lungs.(355,356) BCG vaccine, widely used for vaccination against *M. tuberculosis* has been reported to inhibit GSK-3 β activity resulting in increased production of IL-10, consistent with that inhibition of this protein kinase is beneficial to the host in the development of protective immunity against *M. tuberculosis*.(354) Interestingly, manzamine A and some of its analogs showed selective binding for human GSK-3 β .(340) When tested in a cell-based assay that measures GSK-3 β dependent tau phosphorylation, manzamine A significantly inhibited tau phosphorylation within cells at concentrations as low as 5 μ M with no cytotoxicity.(340)

2.6 Conclusion

Despite their structural complexity, the manzamine alkaloids in this study constitute a novel scaffold for the potential development of new leads for the treatment of tuberculosis. The time-dependent component of the inhibition exerted by these compounds on *MtSK* represents a significant clinical advantage, as a prolonged residence time of a drug on a particular target may result in an enhanced duration of the desired pharmacological effect *in vivo*.(357,358) Since manzamine A and some of its analogs can inhibit both GSK-3 β and *MtSK*, we suggest that these compounds are promising candidates for further studies leading to the development of new drug candidates specific to the *M. tuberculosis* pathogen. This is most particularly so for the 6-

cyclohexamido derivative, compound **6**, due to its inhibition profile, *in vitro* antibacterial activity, and lack of cytotoxicity.

Chapter 3

Mechanism of irreversible inactivation of *Mycobacterium tuberculosis* shikimate kinase by ilimaquinone

This chapter is recovered from a publication of the same title: Simithy, J.; **Fuanta, N.R.**; Kochanowska-Karamyan, A.; Hobrath, J.V., Hamann, M.T.; Goodwin, D.C.; Calderón, A.I. *Biochim. Biophys. Acta - Proteins and Proteomics*, 2018 5(6), 731-739. JS and NRF contributed equally as first authors.

3.1 Abstract

Ilimaquinone (IQ), a metabolite from marine sponge *Hippospongia metachromia*, has been considered as a potential therapeutic agent for many a disease due to its broad range of biological activities. In this chapter, we show an IQ-based irreversible inactivation of *Mycobacterium tuberculosis* shikimate kinase (*MtSK*) through covalent modification of the protein. This inactivation is rather slow, with an apparent second-order rate constant of about $60 \text{ M}^{-1}\text{s}^{-1}$. Following reaction with IQ, LC-MS analyses of intact *MtSK* revealed covalent modification of *MtSK* by IQ, with the concomitant loss of a methoxy group, suggesting a Michael-addition mechanism. Evaluation of trypsinated fragments of IQ-derivatized *MtSK* by MS/MS demonstrated that Ser and Thr residues were most frequently modified and to a lesser extent Lys and Tyr. In or near the *MtSK* active site, three residues of the P-loop (K15, S16, and T17) as well as S77, T111, and S44 showed evidence of IQ-dependent derivatization.

Accordingly, inclusion of ATP in IQ reactions with *MtSK* partially protected the enzyme from inactivation and limited IQ-based derivatization of K15 and S16. Additionally, molecular docking models for *MtSK*-IQ were for IQ-derivatized S77 and T111. In the latter, ATP was observed to sterically clash with the IQ moiety. Out of three other enzymes evaluated, lactate dehydrogenase was derivatized and inactivated by IQ, but pyruvate kinase and catalase-peroxidase (KatG) were unaffected. Together, these data suggest that IQ is promiscuous (though not entirely indiscriminant) in its reactivity. As such, the potential of IQ as a lead in the development of antitubercular agents directed against *MtSK* or other targets is questionable.

3.2 Introduction

Terpenylquinones comprise a class of marine natural products considered attractive scaffolds for drug design due to their ubiquity in nature and their versatile bioactivities (359). These compounds are characterized as having a bicyclic sesquiterpene skeleton coupled to a quinone moiety (360). Among them, ilimaquinone (IQ) (Fig. 1), first isolated in 1979 from the Red Sea sponge *Hippospongia metachromia* (361), has been reported to possess several biological activities of potential therapeutic value, including antiviral (362), anti-inflammatory (362), antimicrobial (363), antimalarial (364) and anti-HIV (365) properties. Most prominently, IQ has been recognized for its ability to degrade Golgi membranes into small vesicular structures (i.e., vesiculated Golgi membranes), a phenomenon which blocks cellular secretion (366–369). In addition, IQ has shown to induce the transcriptional activation of autophagic target genes in tumor cells, (370,371) and to inhibit the growth of several cancer cell lines, including multiple myeloma (372), prostate cancer (PC-3, DU145 and LNCaP), non-small cell lung cancer (A549), human osteosarcoma (MG63) and hepatocellular carcinoma cells (Hep3B) (373).

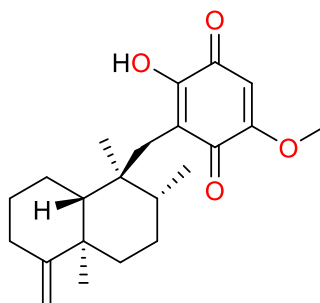


Figure 3.1: Structure of ilimaquinone (IQ).

Although IQ has proven to exert a myriad of biological activities through multiple pathways, the specific interactions of IQ with its cellular targets have not been clearly elucidated (374–376). Our interest in this compound arose from an initial observation that IQ inhibited shikimate kinase from *M. tuberculosis* (*MtSK*). The shikimate pathway is responsible for the biosynthesis of aromatic compounds in microorganisms and higher plants, and *MtSK* catalyzes the fifth step of the process. Because this pathway is absent from human metabolism, numerous investigators have suggested that small molecule inhibitors of shikimate pathway enzymes may produce new leads for the development of antibiotics to treat drug-resistant tuberculosis (106,320,377).

In this study, we investigated the mechanism of *MtSK* inhibition by IQ. Time-dependent inhibition kinetics suggested that IQ was either a slow-reversible or irreversible inhibitor of *MtSK*. Dilution of IQ-inhibited *MtSK* failed to produce an increase in *MtSK* activity, suggesting an irreversible mechanism of inhibition by IQ. In accord with this conclusion, mass spectrometry

evaluation of intact *MtSK* revealed the time-dependent loss of unmodified *MtSK* concomitant with increases in IQ-derivatized enzyme (+326.3 Da and +652.6 Da). This was consistent with covalent addition of one and two IQ units, respectively, each of which lacked the mass corresponding to a methoxy moiety. LC-ESI MS/MS analyses of *MtSK* trypsinized following its reaction with IQ indicated a range of possible targets, including several threonine and serine residues. Our data supports an irreversible mechanism through a Michael addition involving serine and threonine residues. IQ shows modest specificity to *MtSK* and does not necessarily modify any exposed Thr or Ser residues. Molecular docking studies show that target specificity can be enhanced by modification of the inhibitor

3.3 Materials

Dimethyl sulfoxide (DMSO), adenosine-5'-triphosphate (ATP), shikimate, 2,2'-azino-bis[3-ethylbenzthiazoline-6-sulfonic acid (ABTS), H₂O₂ (30%), rabbit muscle lactate dehydrogenase (LDH) and rabbit muscle pyruvate kinase (PK) were purchased from Sigma-Aldrich (St. Louis, MO). *MtSK* (378) and *M. tuberculosis* catalase-peroxidase (*MtKatG*) (379) were expressed and purified as previously described. The purity of *MtSK* and *MtKatG* were determined by SDS-PAGE and LC-ESI-MS, and aliquots were stored at -80 °C in 50 mM Tris-HCl, pH 7.4; 0.5 M NaCl for *MtSK* and 5 mM phosphate, pH 7.0, for *MtKatG*. All organic solvents were HPLC or LC-MS grade and were purchased from Thermo Fisher (Hanover Park, IL). All buffers and media were prepared using water purified by a Milli-Q purification system (Millipore, Billerica, MA).

3.4 Methods

3.4.1 Ilimaquinone acquisition and isolation.

Ilimaquinone was obtained with a minimum purity of 90% as analyzed by HPLC or H-NMR. This natural product was obtained from *Smenospongia cerebriformis*. The sponge was collected from shallow (3-21 m depth) coral reef habitat at Key Largo, Florida, on July 1 and August 7, 2005. Voucher specimens have been deposited in the Natural History Museum, London (BMNH 2007.4.23.5 [University of Mississippi voucher 05FL-020(1)]; BMNH 2007.4.23.6 [University of Mississippi voucher 0505FL-161]). The sponge was stored frozen until extracted. Six kilograms (wet weight) of the frozen sponge *S. cerebriformis* were extracted exhaustively with EtOH in a sonicator. The extracts were then combined, filtered and concentrated *in vacuo* until dry. The resulting crude extract (260 g) was subjected to vacuum-liquid chromatography with a gradient solvent system starting from hexanes through acetone to methanol, yielding 20 fractions. Nonpolar fractions (mainly 2 and 3) after purification yielded 2.5 g (0.9615% dry weight) of ilimaquinone, which was identified by comparison of ¹H NMR and ¹³C NMR data with a standard.

3.4.2 LC-MS based time-dependent inhibition assay.

The effect of ilimaquinone on the activity of *MtSK* was evaluated by an *in vitro* time-dependent inhibition assay. In this assay, *MtSK* (0.2 μM) was pre-incubated with ilimaquinone (in DMSO) at 0, 5, 10, 25, 50, 100 and 150 μM for 0 - 60 min prior to initiation of the shikimate kinase reaction assay. All assays were performed in 100 mM ammonium acetate, pH 7.6, supplemented with 50 mM KCl and 5 mM MgCl₂. All assays were performed at 25 °C in a final volume of 500 μL. Reactions were initiated by the addition of 5 mM shikimate and 1.2 mM

ATP, followed for 30 seconds and quenched by the addition of 2 μ L of 98% formic acid and vortexing. To study the effects of substrate competition during inhibition by IQ, time-dependent experiments were performed in the presence of 1.2 mM ATP, added prior to the addition of IQ, and reactions were initiated by the addition of 5mM shikimate. The amount of the product shikimate-3-phosphate (S3P) formed in each reaction was quantified using liquid chromatography-mass spectrometry. LC separation of S3P was carried out as described previously (378).

Data analyses for the time-dependent inactivation of *MtSK* were performed using least-squares non-linear regression fitting to the appropriate equation. Data were collected in duplicate and initial velocities were calculated by dividing the concentration of S3P formed in each reaction by the reaction quenching time ($V_0 = [\text{S3P}]/t_q$). The remaining enzyme activity was determined by comparing the initial velocities in control experiments (in the presence of DMSO) to the initial velocities of the enzyme in the presence of various concentrations of IQ, and plotted against the pre-incubation times. These data were fitted to the equation [1]:

$$V_t = V_i e^{(-k_{\text{obs}}*t)}$$

where V_t is the measured steady-state velocity after pre-incubation time t , V_i is the steady-state velocity when pre-incubation time is zero, and k_{obs} is the pseudo first-order constant of observed inactivation at a given inhibitor concentration (346). The k_{obs} values obtained were re-plotted as a function of ilimaquinone concentration, and the data were fit using linear regression. The resulting slope corresponded to a second-order rate constant for inactivation (k_{inact})(346). All data fitting was carried out using GraphPad Prism (version 5.02).

3.4.3 Inhibition of other enzymes by IQ: Activity assays for *MtKatG*, PK, and LDH

MtKatG, PK, and LDH were each incubated with 100 μM IQ for 1 hour at 25 $^{\circ}\text{C}$. Reactions with LDH and PK were run in 100 mM Tris, pH 7.6, supplemented with 50 mM KCl and 5 mM MgCl_2 , while reactions with *MtKatG* were run in 5 mM phosphate, pH 7.0. An aliquot was drawn after 1 hr and assayed for its activity. The catalase activity of *MtKatG* was monitored by the decrease in absorbance at 240 nm resulting from the consumption of H_2O_2 ($\epsilon_{240} = 39.4 \text{ M}^{-1} \text{ cm}^{-1}$) (380) in 100 mM phosphate, pH 7.0, as previously described (379). LDH and PK activities were monitored by decrease in NADH concentration as measured at 340 nm ($\epsilon_{340} = 6220 \text{ M}^{-1} \text{ cm}^{-1}$). Reaction conditions were as previously described (378), except for the final LDH and PK concentrations which were set at 1 μM . Interference in the PK assay from the inhibition of LDH by IQ was avoided by the exclusion of LDH from the preincubation cocktail of PK with IQ, the low concentration of IQ in the final assay (1 μM), and the very short time of exposure of LDH to IQ.

3.4.4 Dilution experiments

MtSK (20 μM) was incubated with 250 μM IQ (greater than 50-fold excess over the IC_{50} for IQ), for 1 hour. The shikimate kinase reaction was initiated by diluting the EI complex (100 fold) into 1.2 mM ATP, 5 mM shikimate in *MtSK* assay buffer (100 mM ammonium acetate, pH 7.6, supplemented with 50 mM KCl and 5 mM MgCl_2). The final concentration of enzyme following dilution was 0.2 μM . The reactions were allowed to run for times ranging from 0 - 60 min prior to quenching with formic acid. The quenched reactions were analyzed by LC-MS as previously described (378) and the concentrations of S3P produced were plotted against reaction time. In reactions where ATP was present during pre-incubation, *MtSK*-ATP complex was

formed prior to the addition of the inhibitor. Subsequent steps were the same as when *MtSK* was preincubated only with IQ. All data fitting was carried out using GraphPad Prism (version 5.02).

3.4.5 Intact protein analysis by mass spectrometry

MtKatG, LDH and PK (each at 1 μM) were incubated with 100 μM IQ at 4 °C for 30 hr; *MtSK* (1 μM) was incubated with 100, 10 and 1 μM . With the exception of *MtKatG*, all reactions were carried out in 100 mM ammonium acetate, pH 7.6, supplemented 50 mM KCl and 5 mM MgCl_2 . Reactions with *MtKatG* were performed in phosphate, pH 7.0. chromatograms and mass spectra were collected each hour and analyzed using Agilent MassHunter BioConfirm software version B.06.00.

3.4.6 Nano liquid chromatography – tandem mass spectrometry (nLC-MS/MS) analysis of *MtSK* tryptic peptides.

Post pre-incubation of *MtSK* (1 μM) and Ilimaquinone (100 μM) at 25°C for 1, excess, unbound ilimaquinone was removed by filtration using Macrosep® Advance centrifugal device prior to enzymatic digestion. Desalting was carried out following manufacturer's instructions using *MtSK* assay buffer as the wash buffer. Modified and unmodified *MtSK* were digested with trypsin at a ratio of 1:20 (w/w) trypsin/substrate overnight at 37 °C in an assay buffer consisting of 100 mM ammonium bicarbonate pH = 8. Tryptic peptides were separated using a 75 μm i.d \times 17 cm Reprosil-Pur C₁₈-AQ (3 μm ; Dr. Maisch GmbH, Germany) nano-column (packed in-house) using an EASY-nLC nano HPLC (Thermo Scientific, Bremen, Germany). The mobile phases consisted of water with 0.1% (v/v) formic acid (A) and acetonitrile with 0.1% (v/v) formic acid (B). Peptides were eluted using a gradient of 2 - 50% B in 50 min followed by 50 - 98% B in 5 min and maintained over 10 minutes at 300 nL/min. The nano-HPLC was coupled to

a Orbitrap FusionTM Tribrid mass spectrometer (Thermo Scientific, San Jose, California). Spray voltage was set at 2.3 kV and capillary temperature was set at 275 °C. The mass spectrometer was set to perform a full MS scan (350 – 1200 m/z) at 120,000 FWHM resolving power (at 200 m/z), followed by sequential HCD (higher-energy collisional dissociation) MS/MS fragmentation at normalized collision energy of 27% and 7,500 FWHM resolution. The monoisotopic precursor selector (MIPS) filter for peptides was activated. All MS/MS scans were performed in the ion trap mass analyzer (rapid scan rate) using an isolation window of 2.0 m/z . Maximum injection times of 50 ms and 80 ms were defined for MS and MS/MS scans, respectively. AGC values were set to 5×10^5 for MS and 5×10^4 for MS/MS. MS data were collected in profile mode and MS/MS data were collected in centroid mode. All acquisitions were performed under positive mode polarity. Thermo Proteome Discoverer (PD, version 2.2.0.388) was used to perform database searching against UniProt shikimate kinase *Mycobacterium tuberculosis* FASTA database. Search engine Sequest-HT implemented in Thermo Proteome Discoverer was applied for all MS raw files. The search parameters were set to 10 ppm for precursor tolerance and 0.5 Da for MS/MS fragment ions and a maximum of three missed cleavages. Custom modifiers were created for the mass of ilimaquinone minus 32 Da. ($C_{21}H_{26}O_3$) with preference for the target amino acids (S, T, Y, R and K) and each sample was searched against each modifier separately as fix custom modifications.

3.4.7 Prediction of covalently bound ilimaquinone binding poses

All computations were performed using the Small Molecule Drug Discovery Suite of the Schrödinger software package, 2016-1 release (Schrödinger, LLC). Two *MtSK* X-ray structures (PDB entry codes 2IYT and 2IYY) were prepared using the Protein Preparation Wizard suite of

tools. Hydrogens were added, protonation states assigned, and any ligands present removed. The structures were relaxed through restrained minimization within 0.3 root-mean-square-deviation (RMSD) of heavy atoms from the original crystal structures using the OPLS3 force field, further referred to as prepared crystal structures. Following preparation with LigPrep, IQ was docked into both structures in three binding site regions, in proximity of S44, S77 or T111. In order to include protein flexibility and increase sampling of ligand binding poses the Induced Fit docking method was applied with extended sampling, without constraints. Default parameters were used except for increasing the residue refinement region around the ligand to 8 Å. Out of docked poses that placed the 5-methoxy substituent of the benzoquinone ring in close proximity of the S/T modification sites two favorable docked poses were selected: one with the methoxy group near S77 and one near T111. No suitable pose could be obtained for IQ in the region of S44. Both selected poses originated from docking based on the same X-ray structure (PDB 2IYY). Side chain conformations of the following residues close to the covalent modification sites were adjusted: S77 and T111 side chains conformers were selected from the side chain rotamer library. In the complex structure with the IQ pose suitable for linking with T111, side chain conformations of R117 and T115 were also adjusted. IQ was then covalently linked to T111/S77 using modeling tools, followed by restrained energy minimization of the two complexes using Protein Preparation Wizard suite of tools with default parameters. The protein in the obtained structures was discarded and the ligand merged with the original prepared crystal structure (PDB code 2IYY), followed by the same side chain conformational adjustments described above. The ligand pose was covalently linked to either S77 or T111 and the two structures relaxed through restrained energy minimization. This cycle of extracting the ligand poses, merging with the *MtSK* structure prior to energy minimization, and restrained energy minimization of the

complexes was repeated until the energy minimized IQ poses were readily accommodated through covalent linking to S77/T111. Structural refinement of the obtained two complexes was achieved through Prime Protein-Ligand Complex Refinement of the region within 8 Å of the covalently linked IQ using default parameters. The root-mean-square deviation of the final structures with covalently bound IQ compared to the *MtSK* crystal structure used (PDB 2IYY) is 0.39 in case of IQ linked to S77 and 0.45 in case of IQ linked to T111.

3.5 Results and Discussion

Preincubation of IQ with *MtSK* revealed an exponential decrease in *MtSK* activity with time, and the pseudo-first order rate of inactivation (k_{obs}) increased linearly with IQ concentration (**Figure 3.2**). From the slope of k_{obs} dependence on IQ concentration, an apparent second-order rate constant for inactivation was estimated to be $80 \pm 10 \text{ M}^{-1}\text{s}^{-1}$. In an alternative approach, we observed that inclusion of IQ in assays of *MtSK* activity produced an exponential decrease in the rates of S3P formation following the initiation of reactions with *MtSK* (**Figure 3.3**). There was a linear increase in k_{obs} with IQ concentration. From the slope of the line, an apparent second-order rate constant was estimated as $45 \pm 10 \text{ M}^{-1}\text{s}^{-1}$ which is in reasonable agreement with preincubation studies.

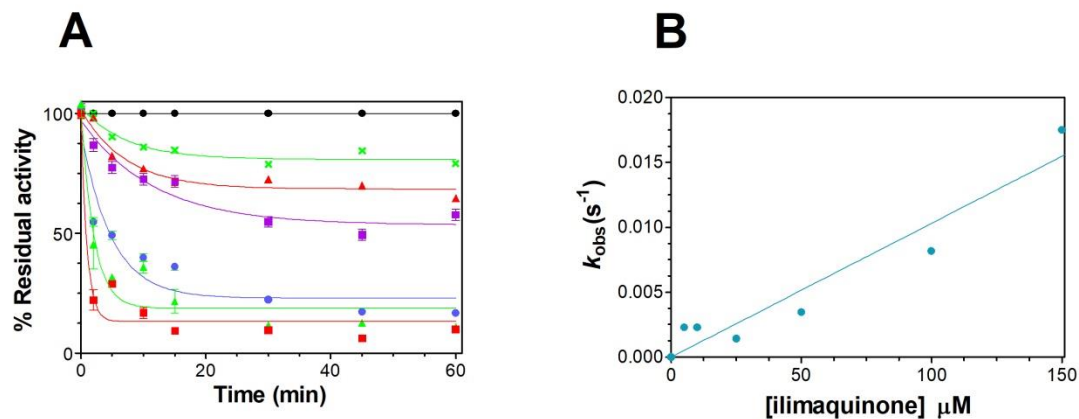


Figure 3.2: Effect of IQ preincubation on *MtSK* activity. The loss of *MtSK* activity as a function of incubation time with IQ (A) was evaluated for 0 (●), 5 (×), 10 (▲), 25 (■), 50 (●), 100 (▲), and 150 (■) μM IQ. The observed pseudo-first order rate constants (k_{obs}) are shown as a function of IQ concentration (B). The slope (k_{obs} vs [IQ]) represents the second-order rate of inactivation k_{inact} .

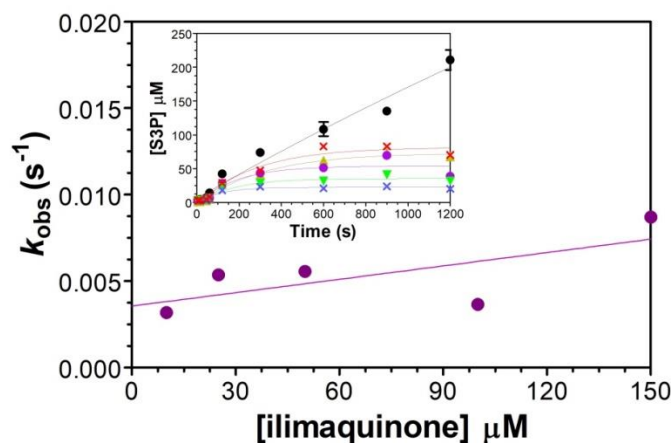


Figure 3.3: Time-dependent loss of *MtSK* activity in the presence of IQ. Production of shikimate-3-phosphate (S3P) was initiated by adding *MtSK* (0.01 μM) to solutions containing 5.0 mM shikimate, 1.2 mM ATP, as well as 0 (●), 10 (×), 25 (▲), 50 (●), 100 (▼), and 150 (×) μM IQ (inset).

The time-dependent component of *MtSK* inhibition by IQ is consistent with either a slowly reversible or irreversible inhibition mechanism. To differentiate between these two possibilities, we preincubated 20 μM *MtSK* with 250 μM IQ and then monitored S3P production following dilution of *MtSK*-IQ into an enzyme assay cocktail. A low level of activity (10%) was observed following dilution of IQ-treated *MtSK* compared to the untreated *MtSK* control (**Figure 3.4**). This was a far greater extent of inhibition than could be accounted for by the post-dilution concentration of IQ present in the assay (2.5 μM). In addition, little if any acceleration of S3P production was observed following dilution (**Figure 3.4**), indicating that the inhibition achieved by IQ during preincubation was irreversible. Taken together, these data suggest a slow, one-step irreversible inactivation of *MtSK* by IQ governed by a second-order rate constant (k_{inact}) of about $60 \text{ M}^{-1}\text{s}^{-1}$ as depicted in the following scheme:

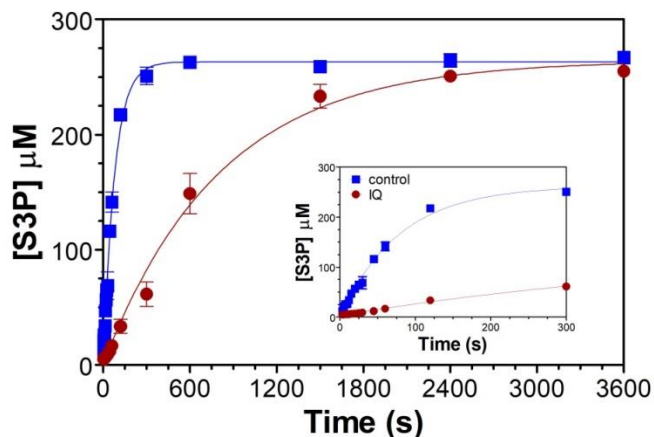
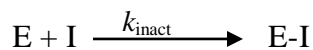


Figure 3.4. Recovery of activity following dilution of IQ-inhibited *MtSK*. *MtSK* (20 μM) was preincubated for 1 hour in the presence (●) and absence (■) of 250 μM IQ.

One of the most common mechanisms by which irreversible inhibition is achieved is through covalent enzyme modification by the inhibitor. We explored IQ-dependent covalent alteration of *MtSK* by LC-MS. LC-MS total ion chromatograms showed an elution time of 5.3 min for intact *MtSK*, and the deconvoluted ESI-MS spectra for our *MtSK* preparations revealed two species with average molecular masses of 19648.74 and 19517.57 Da. As described previously, the difference, 131.2 Da, is consistent with the post-translational removal of the N-terminal methionine [22]. Incubation of *MtSK* with IQ produced a time-dependent decrease in the intensity of the chromatographic peak at 5.3 min concomitant with the appearance of a shoulder at 5.5 min and a new peak eluting later in the chromatogram at 6.0 minutes (**Figure 3.5**). For *MtSK* incubated with IQ for 30 h, deconvoluted mass spectra collected across the chromatographic range (5.164 – 6.615 min.) showed three pairs of peaks. In each pair, the lighter and heavier masses were separated by 131 Da, and the intensity of the peak corresponding to the heavier mass was ~60% of the intensity of the peak corresponding to the lighter mass. Further, the lighter of each pair was separated from one another by increments of 326 Da, starting at 19517.73, the mass of *MtSK* lacking its N-terminal methionine. The same pattern was observed for the heavier mass of each pair, starting at 19648.97, the mass of intact, full-length *MtSK* (**Figure 3.6A**). These data suggested that *MtSK* (with or without its N-terminal Met) was covalently modified by IQ, and this could occur at more than one site on the *MtSK* intact protein.

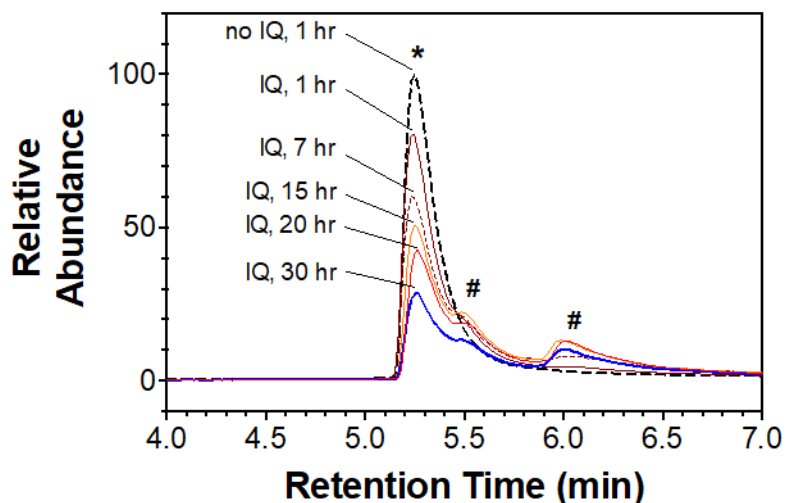


Figure 3.5: Intensities of deconvoluted *MtSK* MS spectra vs. preincubation time with IQ. *MtSK* (1.0 μM) was incubated with 100 μM IQ at 4°C for 30 hours. At the times indicated, a sample was withdrawn and evaluated by LC-MS. MS signals corresponding to unmodified *MtSK* (*, retention time = 5.3 min) diminish over time. MS signals corresponding to IQ-derivatized *MtSK* (#, retention times = 5.5 and 6.0 min) result from incubation of *MtSK* with IQ.

No IQ-*MtSK* adducts were observed at 5.25 min (5.164 – 5.438 min range) (**Figure 3.6B**). Deconvolution of the MS spectrum of the peak shoulder observed at 5.5 min (5.438 – 5.841 min.) (**Figure 3.6C**) showed nearly equal contributions of underivatized *MtSK* and *MtSK* derivatized once by IQ. Finally, the deconvoluted MS spectrum of the peak eluting at 6.0 min (5.841 – 6.615 min.) was dominated by *MtSK* derivatized twice by IQ (**Figure 3.6D**). The mass shifts, in each case 326.4 Da, precisely match the molecular mass of one IQ with an average loss of 32.2 Da, which corresponds to the loss of H-OCH₃ from IQ upon each reaction with *MtSK*.

Intensities of the deconvoluted MS spectra of *MtSK* preincubated with IQ for 30 hrs, showed a gradual loss of the mass of free enzyme - with or without its N-terminal Met (**Figure 3.7A**). Concomitantly, there was a transient increase in the intensity of the mass of singly modified *MtSK* derivative (*MtSK*-IQ), reaching a maximum at around 15 hours. Its intensity was constant over a five hour range, after which it slowly declined (**Figure 3.7B**). As shown in **Figure 3.7C**, the appearance of the doubly modified IQ-*MtSK* adduct (*MtSK*-IQ₂) was relatively slow, marked by a slow increase in intensities for both forms of *MtSK*. It reached a maximum at around 20 hrs, after which there was slow decline in peak intensities.

Reaction of *MtSK* with 10-fold lower concentrations of IQ (i.e., 10 μ M), resulted in the loss of unmodified *MtSK* (5.25 min retention peak) and an increase in derivatized species (retention time > 5.4 min). However, in both cases these were observed to a lesser extent than in reactions using 100 μ M IQ. In addition, only once-derivatized *MtSK*-IQ species were observed in deconvoluted mass spectra (**Figure 3.8**). As would be expected from IQ-dependent inactivation kinetics (see **Figure 3.2**), reaction of *MtSK* with equimolar IQ (i.e., 1 μ M) produced minimal though detectable modification of *MtSK* (**Figure 3.9**).

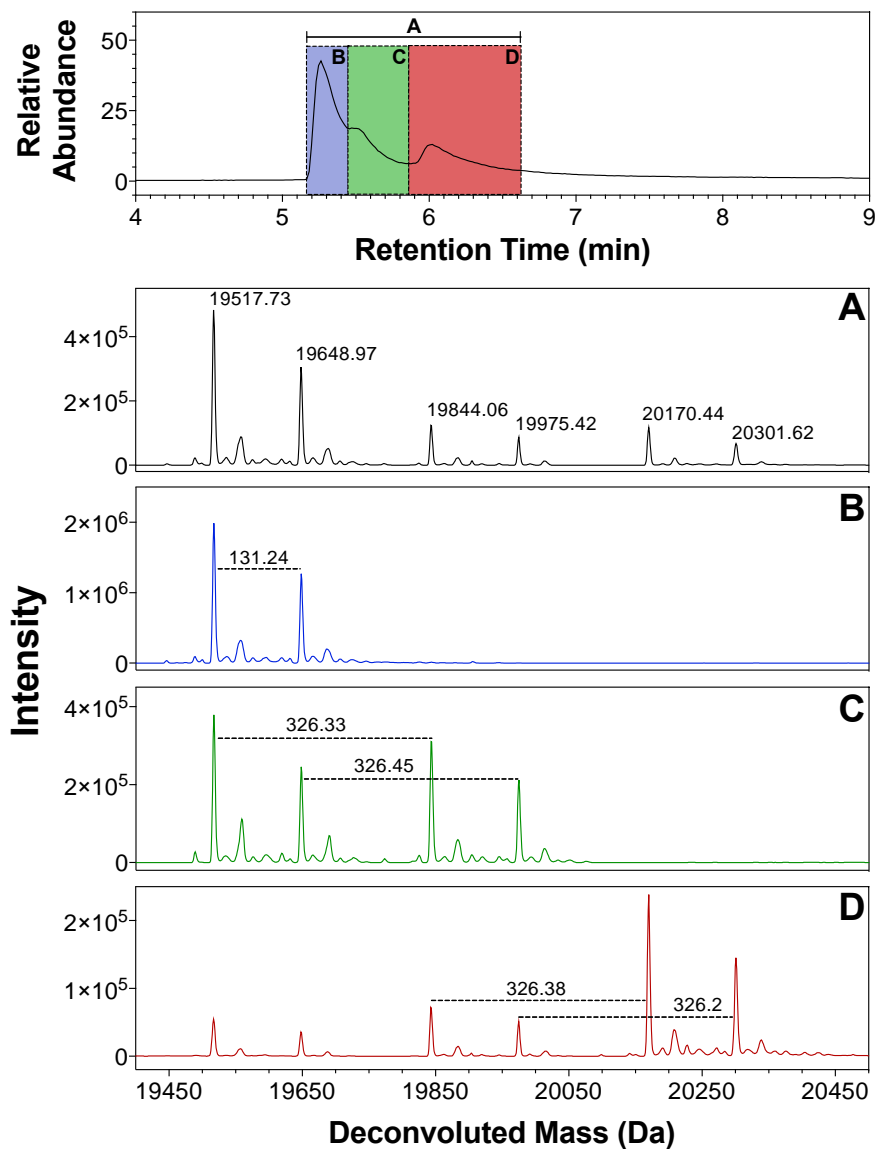


Figure 3.6: Deconvoluted ESI-MS spectra for *MtSK* incubated with IQ. The deconvoluted mass spectrum corresponding to the entire elution envelop (5.16 – 6.62 min) (A) is compared to that of the first (5.16 – 5.44 min) (B), second (5.44 – 5.84 min) (C), and third (5.84 – 6.62 min) (D) elution features of the chromatogram.

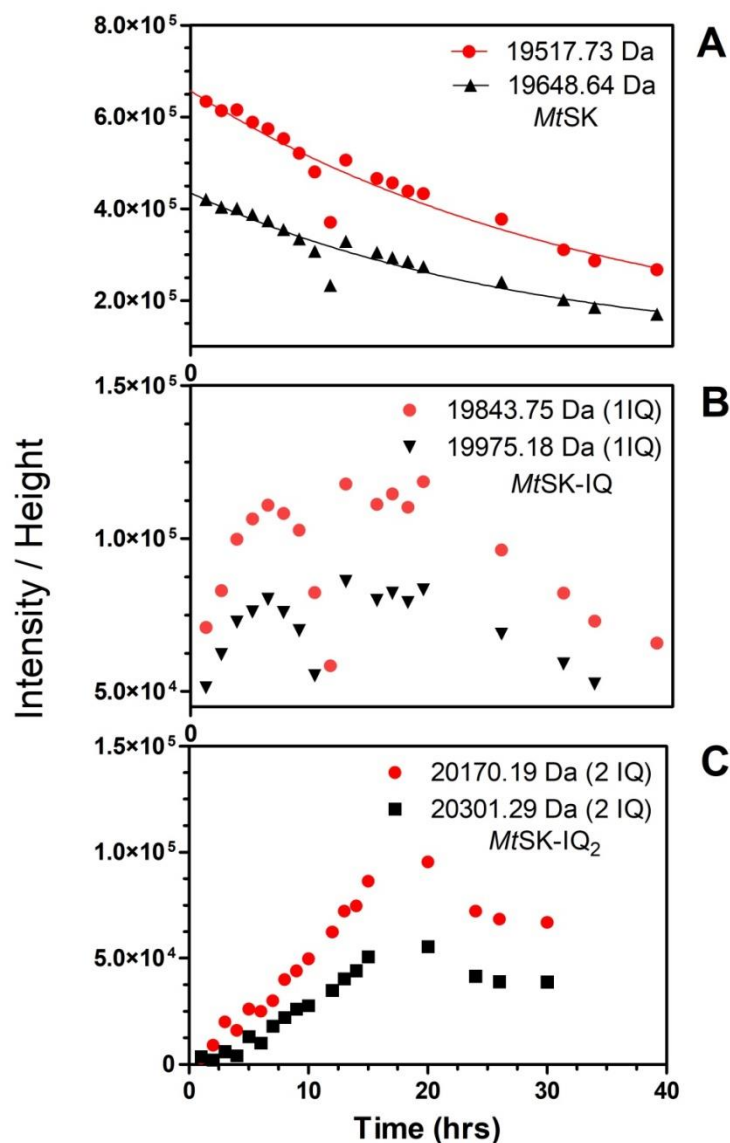


Figure 3.7: Intensities of deconvoluted *MtSK* MS spectra vs. preincubation time with IQ. With increasing preincubation time, a decrease in the intensities free *MtSK* (19648.68 and 19517.73 Da) was observed suggesting the formation of IQ-adducts (A). Increase of both forms of singly modified (*MtSK*-IQ) was observed reaching a maximum intensity at around 15 hours (B). Increase of doubly modified (*MtSK*-IQ₂) enzyme was observed reaching a maximum intensity at around 20 hours (C).

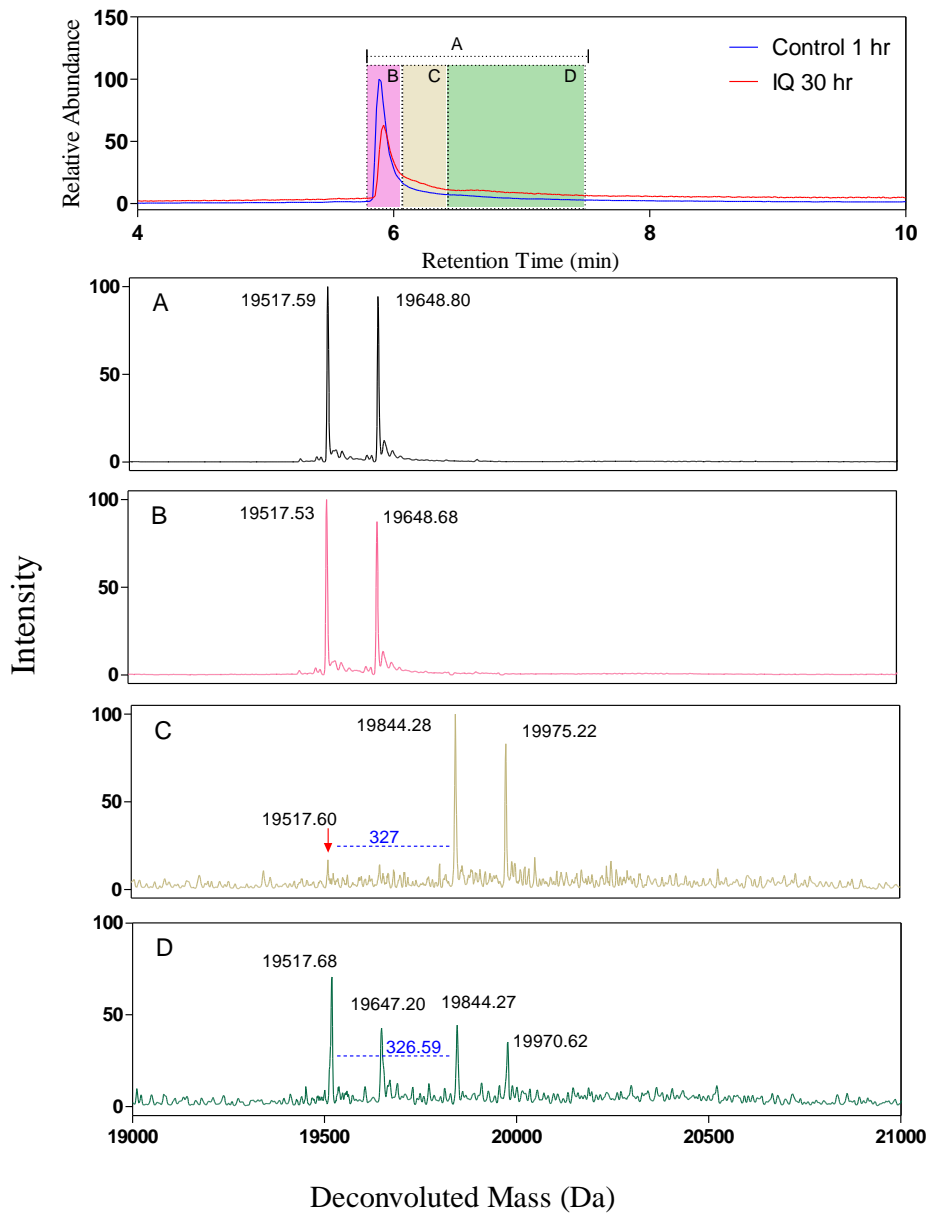


Figure 3.8: Deconvoluted ESI-MS spectra for *MtSK* incubated with 10 μ M IQ. The deconvoluted mass spectrum corresponding to the entire elution envelop (5.16 – 6.62 min) (A) is compared to that of the first (5.16 – 5.44 min) (B), second (5.44 – 5.84 min) (C), and third (5.84 – 6.62 min) (D) elution features of the chromatogram.

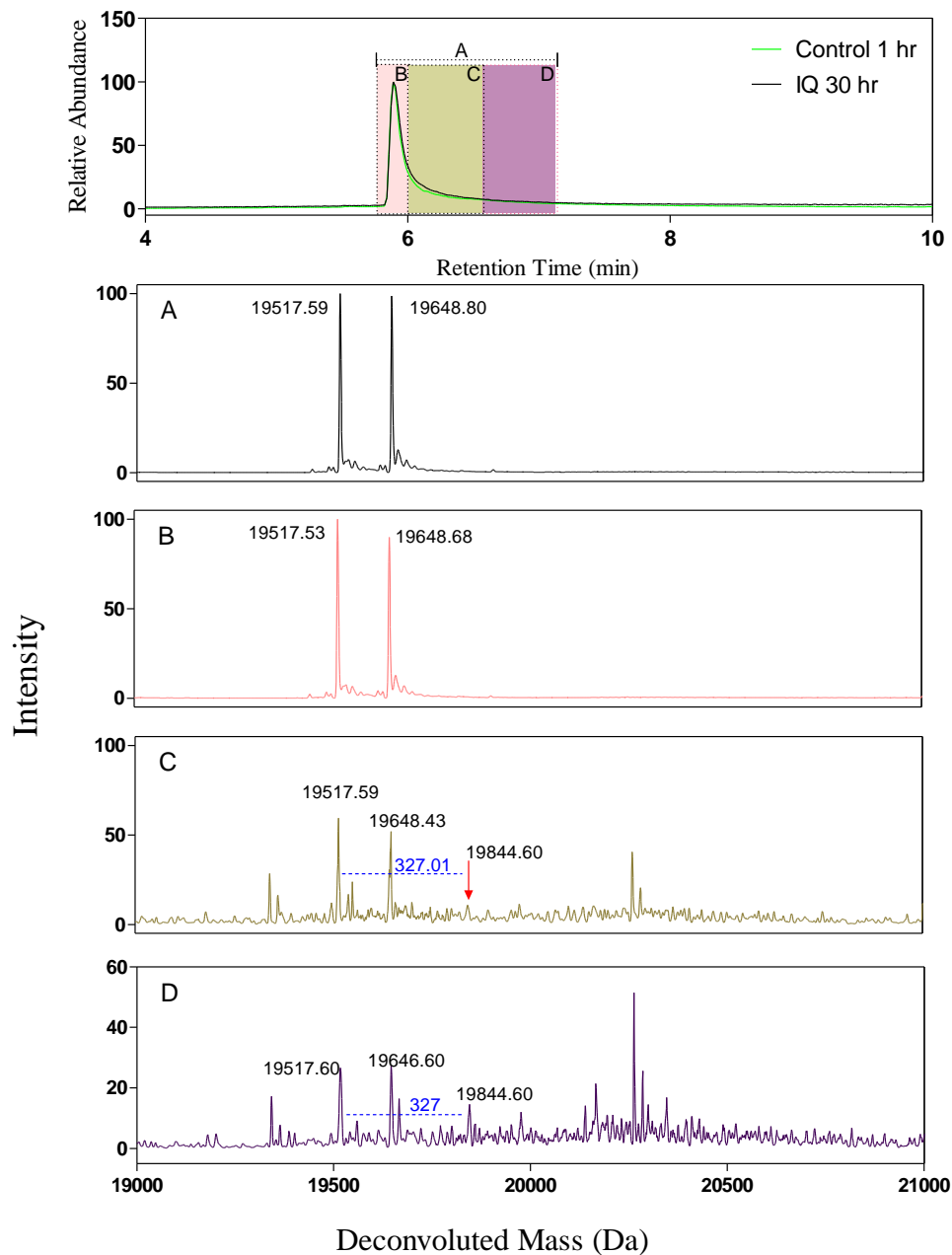


Figure 3.9: Deconvoluted ESI-MS spectra for *MtSK* incubated with 10 μ M IQ. The deconvoluted mass spectrum corresponding to the entire elution envelop (5.16 – 6.62 min) (A) is compared to that of the first (5.16 – 5.44 min) (B), second (5.44 – 5.84 min) (C), and third (5.84 – 6.62 min) (D) elution features of the chromatogram.

To evaluate the specificity of IQ for covalent alteration of *MtSK*, we investigated three other enzymes, *MtKatG*, PK, and LDH. Incubation of *MtKatG* and PK with 100 μ M IQ for 1 hour produced no discernable loss of enzyme activity relative to controls lacking IQ, but LDH lost nearly 90% of its activity under the same conditions (**Figure 3.10**). We evaluated each intact protein by LC-MS in a manner similar to *MtSK*. No change in the total ion current LC retention profile was observed for *MtKatG* and PK. Likewise, mass spectra collected across the LC range showed no evidence of covalent derivatization of these enzymes by IQ (**Figures 3.11 and 3.12**). However, in a manner very similar to *MtSK*, the total ion current LC retention profile for LDH showed a transition to species with longer retention times that became more pronounced with longer times of LDH preincubation with IQ. As shown in **Figure 3.13** mass spectral analyses revealed the appearance of LDH-IQ adducted proteins, with a mass difference of 326 Da as observed with *MtSK*. As an aside, issues such as these reveal the problems inherent in coupled assays for evaluation of inhibition kinetics and mechanism. The coupling enzymes themselves (LDH is commonly used for this purpose) can be subject to the action of candidate inhibitors.

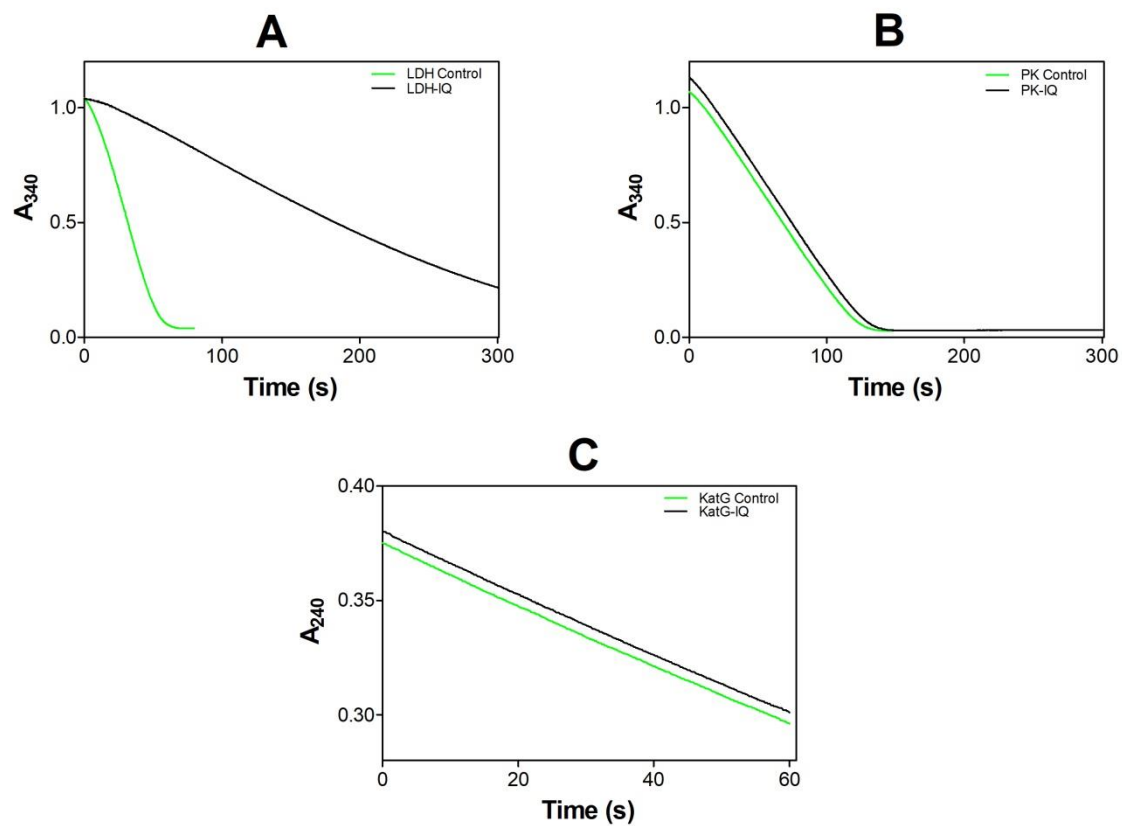


Figure 3.10: Spectrophotometric evaluation of IQ inhibition on LDH, PK, HRP and *MtKatG*.

LDH (A), PK (B) and *MtKatG* (C) were preincubated with 100 μM IQ for 1 hr at 25 $^{\circ}\text{C}$.

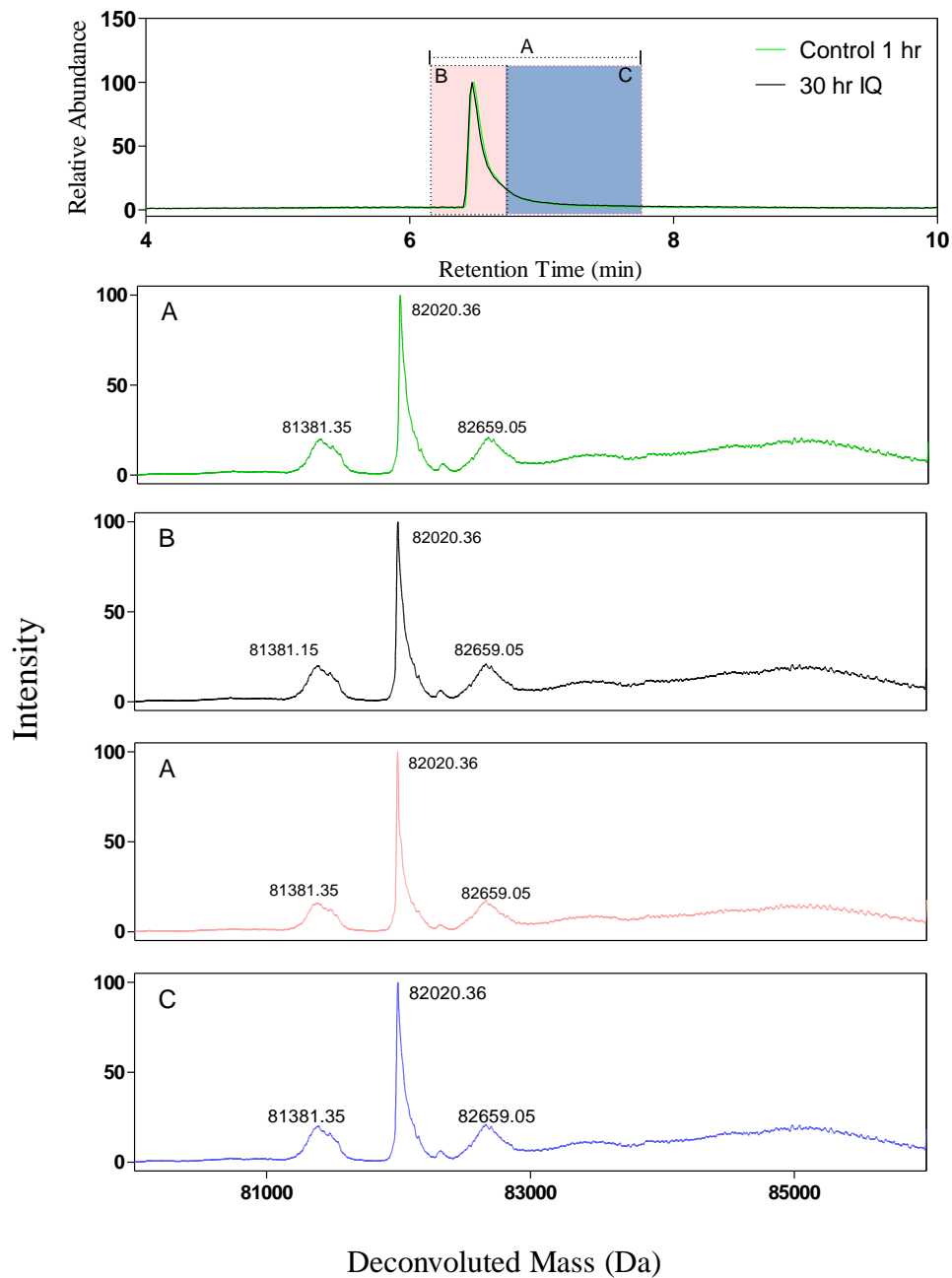


Figure 3.11: Deconvoluted ESI-MS spectra for *MtKatG* incubated with 100 μM IQ. The entire deconvoluted mass spectrum (A) of the control and sample from 6 – 6.8 min shows unmodified *MtKatG* with molecular weight of 82020 Da. No mass shifts were observed post incubation.

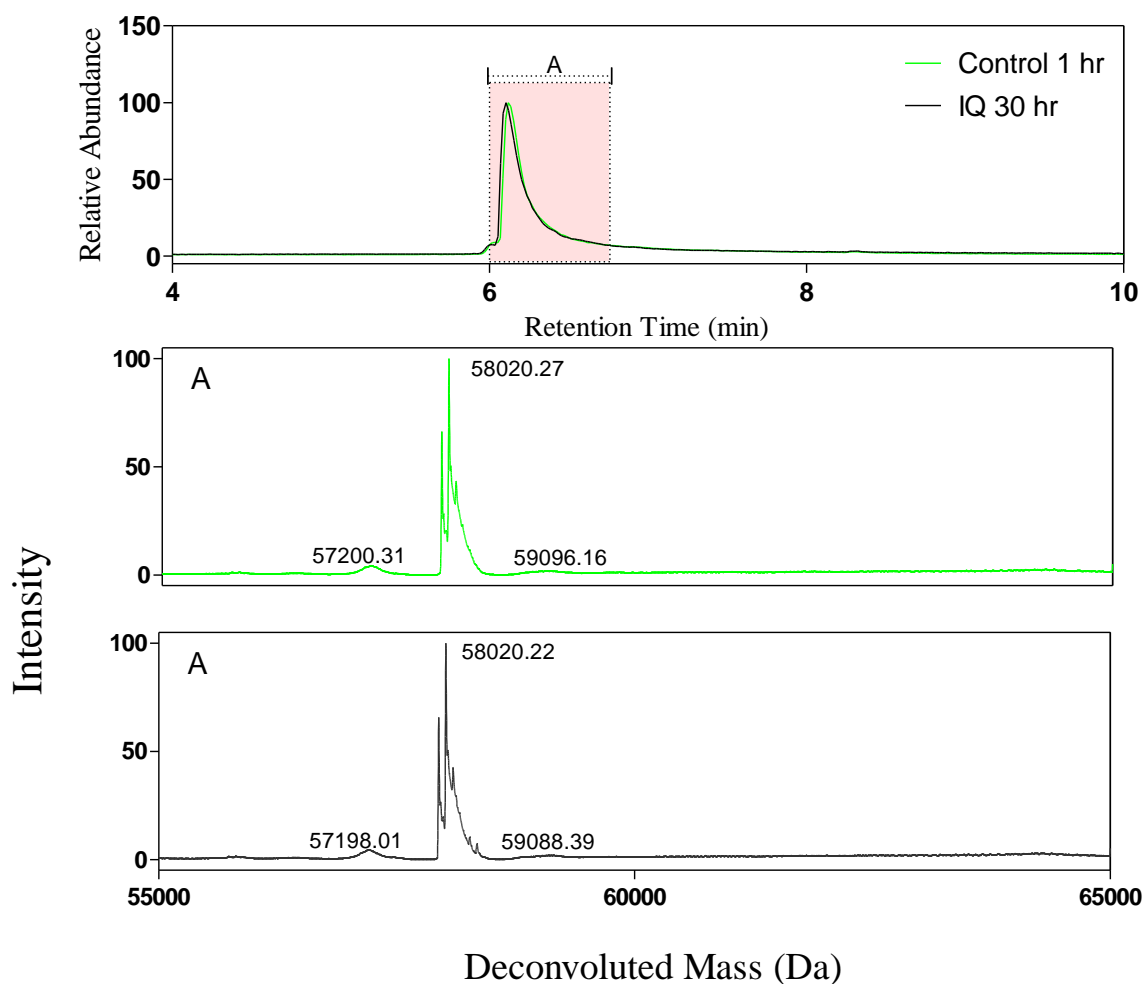


Figure 3.12: Deconvoluted ESI-MS spectra for PK incubated with 100 μ M IQ. The entire deconvoluted mass spectrum (A) of the control and sample from 6 – 6.8 min shows unmodified PK with molecular weight of 58020 Da. No mass shifts were observed post incubation.

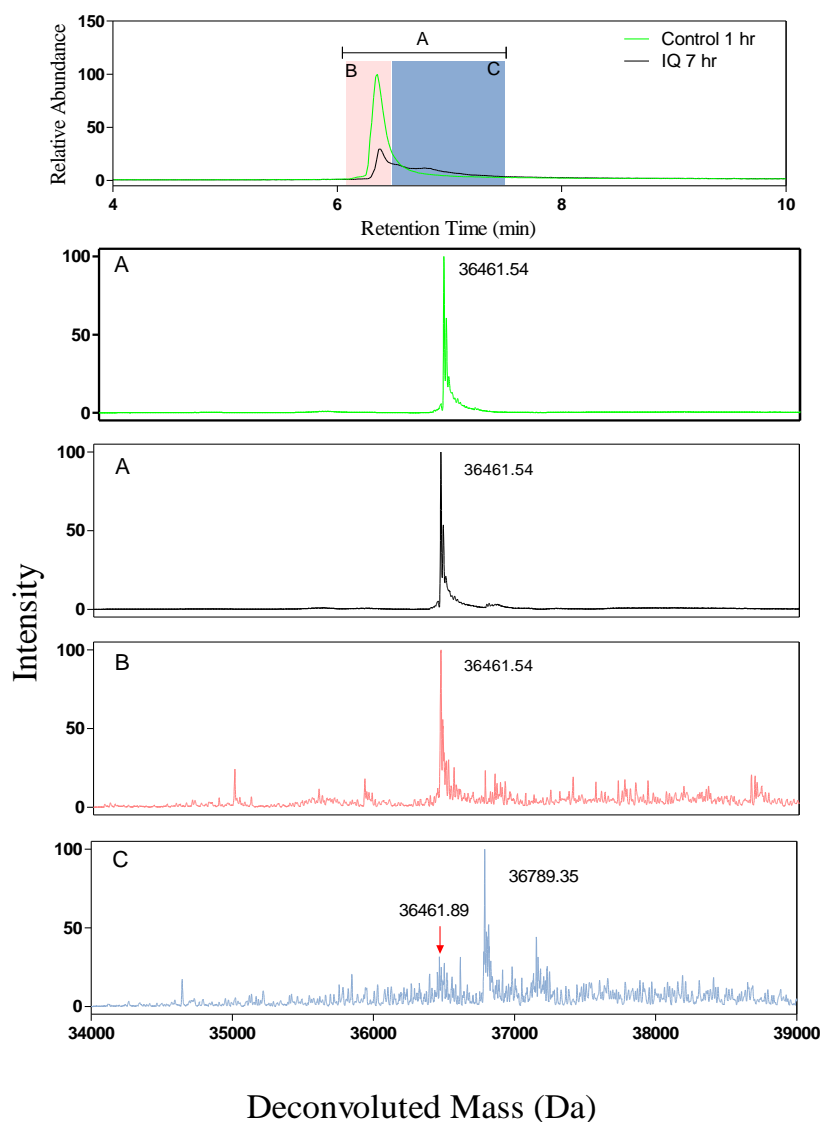


Figure 3.13: Deconvoluted ESI-MS spectra for LDH incubated with 100 μM IQ. The deconvoluted mass spectra corresponding to the entire elution envelop (6.21 – 7.51 min) of the control and sample (A) is compared to that of first (6.21 – 6.53 min) (B) and last (6.53 – 7.51 min) (C) elution features of the chromatogram. The 36461 Da peak represents the unmodified protein. Comparing panels B and C, the mass shift of 326 Da in panel C corresponds to IQ-modified LDH.

MS/MS spectra of tryptic peptides from *MtSK* reacted with IQ were searched with Sequest-HT for automated detection of modified residues. Peptides that were identified through Sequest-HT with a XCorr values above 2.0 were considered positive hits for covalent adduction. Examples of MS/MS spectra used to confirm the modification of these residues are shown in **Figure 3.14**.

Tandem MS/MS analyses showed evidence for the modification of several amino acid residues (**Figure 3.15**). Serines and threonines, and to a lesser extent, lysines and tyrosines were the most susceptible to modification by IQ. Several IQ-modified sites were remote from the enzyme's substrate binding pockets, active site, and conformationally dynamic lid domain (**Figure 3.15A**). It is possible that derivitization of one or more of these sites may account in part for IQ-dependent inactivation of *MtSK*, but one would anticipate that such would arise from a generic impact on protein structural stability.

Modification of any of these sites could easily account for the loss of *MtSK* activity caused by IQ. In order to explore this possibility further, we evaluated the effect of the ATP substrate on IQ-dependent inactivation of *MtSK*. Inclusion of a saturating concentration of ATP limited both the rate and extent of enzyme inactivation. Inclusion of ATP in time-dependent inhibition and inhibitor dilution experiments (**Figure 3.16A** and **B**, respectively) confirmed that the presence of ATP prevented (or at least delayed) a substantial proportion of *MtSK* inactivation; however, it was also clear that, as before, what IQ-inactivated *MtSK* was formed during the incubation period was irreversibly inactivated. Interestingly, trypsinization and MS/MS analyses of *MtSK* reacted with IQ in the presence of ATP indicated that ATP partially limited Lys 15 and Ser 16 derivitization, particularly when IQ concentrations were low (i.e., 1

and 10 μM). Conversely, clear protective effect of ATP could not be discerned with respect to derivatization of Ser 44, Ser 77 or Thr 111. These data suggest that modification of P-loop amino acids accounts for some but not all IQ-dependent inactivation of *MtSK*, and inactivation due to modification of these residues is prevented to some extent when ATP is also present.

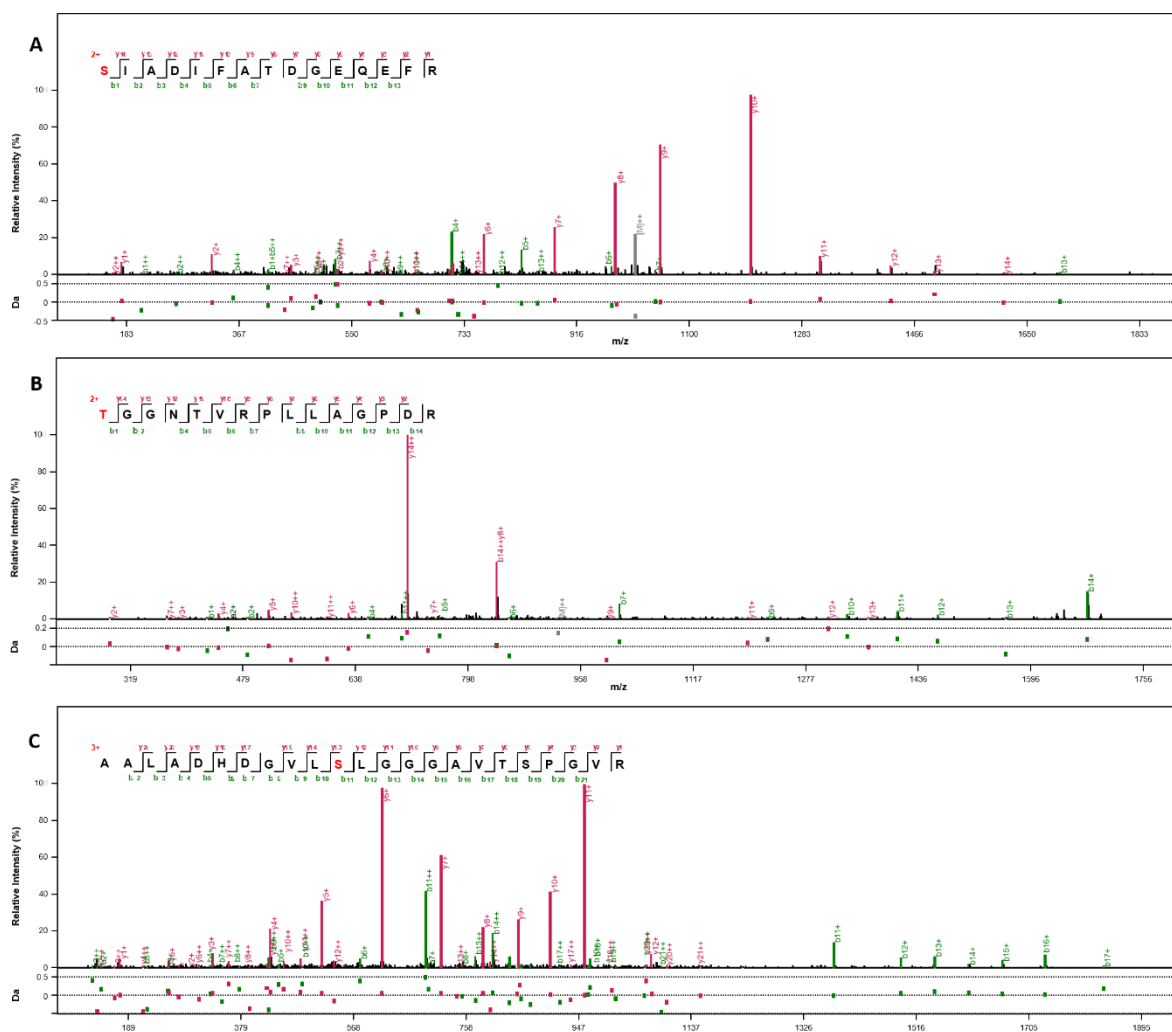


Figure 3.14: Identification of Ser44, Thr111, and Ser77 IQ-adducted peptides by nano-LC-ESI MS/MS analysis. MS/MS spectra of the peptide SIADIFATDGEQEFR $[M + 2H]^{+2}$ m/z 1012.99 (A). MS/MS spectra of the peptide TGGNTVRPLLAGPDR $[M + 2H]^{+2}$ m/z 925.56 (B). MS/MS spectra of peptide AALADHDGVLSLGGAVTSPGVR $[M + 3H]^{+3}$ m/z 816.10 Ser77 as the residue modified by IQ (C).

A

10	20	30	40	50
MAPKAVLVGL	PGSGKSTIGR	RLAKALGVGL	LDTDVAIEQR	TGRSIADIFA
60	70	80	90	100
TDGEQEFRI	EEDVVRAALA	DHDGVLSLGG	GAVTSPGVRA	ALAGHTVVYL
110	120	130	140	150
EISAAEGVRR	TGGNTVRPLL	AGPDRAEKYR	ALMAKRAPLY	RRVATMRVDT
160	170	176		
NRRNPGAVVR	HILSRLQVPS	PSEAAT		

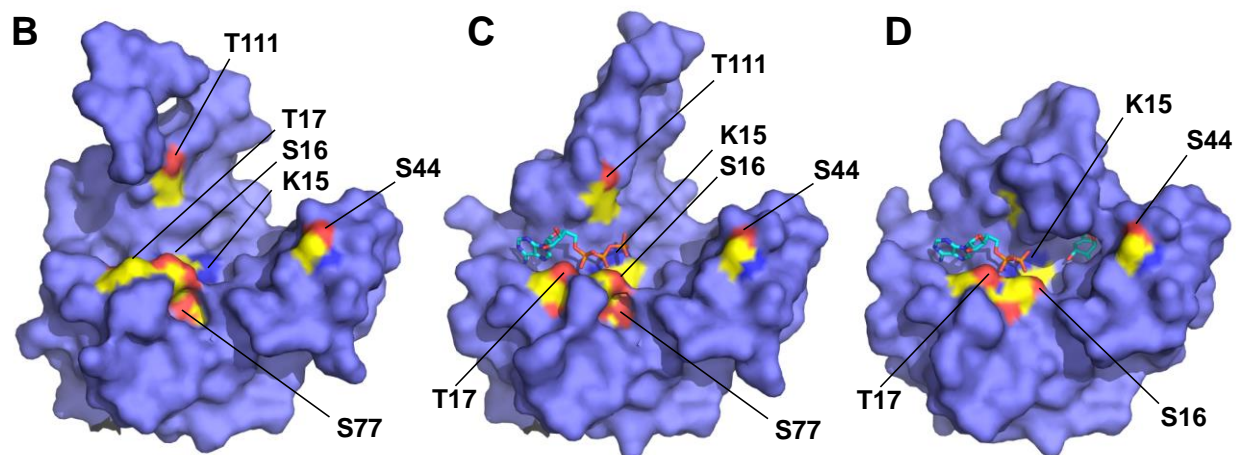


Figure 3.15: Sites of *MtSK* adduction by ilimaquinone. *MtSK* residues for which LC-ESI-MS/MS evidence for IQ-based modification was observed are highlighted in green or red, with those in close proximity to the active site highlighted in red (A). The conformational positions of IQ-derivatized active site residues K15, S16, and T17 (Walker A motif), T111 (lid domain), S77 (Walker B motif), and S44 (extended substrate binding domain) are shown in substrate-free *MtSK* (PDB 2IYT) (B), the *MtSK*-ATP complex (PDB 2IYW) (C), and the *MtSK*-ADP-shikimate ternary complex (PDB 2IYQ) (D) (96). Images were produced using PyMol (version 1.3).

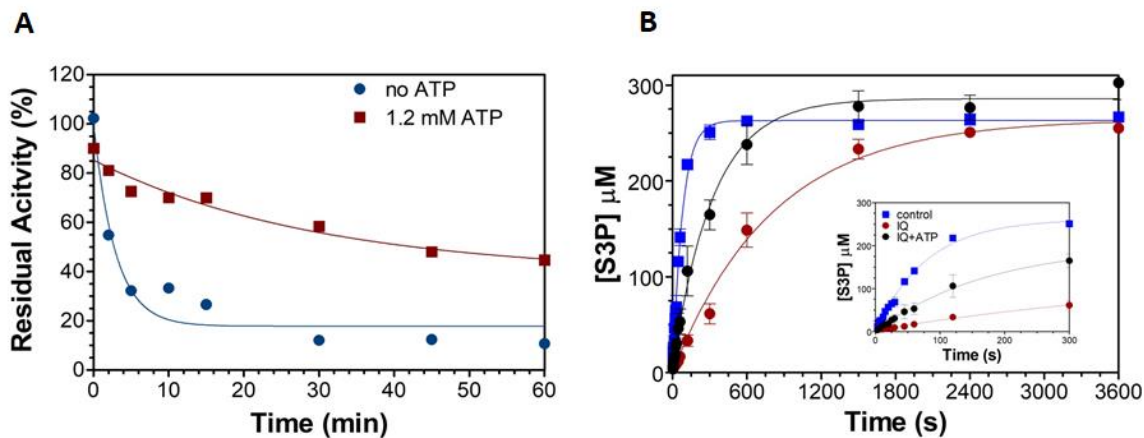


Figure 3.16: Effect of IQ on preincubated *MtSK*-ATP complex. (A) Preincubating *MtSK* (0.2 μM) with IQ (■) and with 1.2 mM ATP (●), less inhibition was observed in the preformed *MtSK*-ATP complex. (B) *MtSK* (20 μM) was preincubated for 1 hour in the absence (■) and presence (●) of IQ (250 μM) and 1.2 mM ATP (●). Reaction time ranged from 3 – 3600s. With two injections per sample, samples were withdrawn and S3P production evaluated. Inset shows reaction at early time points.

Based on the nature of the residues modified by IQ and the consistent neutral loss of 32 Da, we propose a mechanism of IQ-dependent inactivation of *MtSK* which proceeds by Michael addition (**Figure 3.17**). Here, *MtSK* Ser and Thr (and to a lesser extent, Lys and Tyr) side chains act as nucleophiles and attack the benzoquinone C5 position, generating a methoxy leaving group. Together with the intact protein analyses and time-dependent inhibition kinetics, our results suggest that IQ inhibits the *MtSK* activity irreversibly as a protein modification reagent.

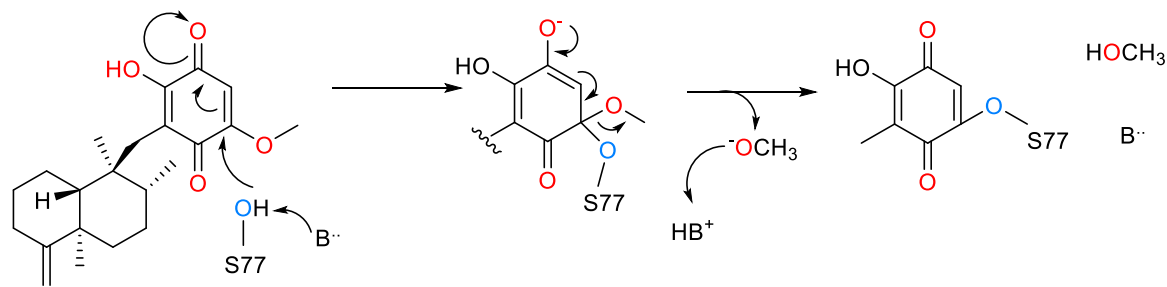


Figure 3.17: Proposed mechanism for *MtSK* modification by ilimaquinone. Ser and Thr-based nucleophiles attack the quinoid ring (C5) of ilimaquinone, resulting in the formation of an enolate ion. Due to charge stabilization, the methoxy group is eliminated. The result of this is ilimaquinone bound to protein via Ser/Thr residue, with a corresponding loss of HOCH₃ from the inhibitor, as observed by MS.

For residues where it was not as clear that ATP might interfere with derivatization by IQ (i.e., Ser 44, Ser 77, and Thr 111), we explored possible binding modes of IQ covalently linked to *MtSK* at these residues. These were predicted through docking, restrained energy minimization and complex structural refinement, as described under *Materials and Methods*. For generating binding mode hypotheses we utilized two *MtSK* crystal structures: an apo structure with open lid domain (PDB 2IYT) and a closed lid structure, co-crystallized with shikimate phosphate (PDB 2IYY) (96). The latter structure resulted in more favorable non-polar contacts with IQ in the shikimate binding site region compared to the apo structure. Therefore, our best binding models are based on the closed lid *MtSK* structure (PDB 2IYY), describing IQ covalently bound to S77 and to T111. No favourable fit could be obtained for the IQ structure in proximity of S44. The two IQ bound complexes developed based on the structure (PDB 2IYY)

were superimposed onto *MtSK* with co-crystallized ATP and Mg ion (PDB 2IYW) to compare the position of ATP to that of the predicted IQ poses (**Figure 3.18**).

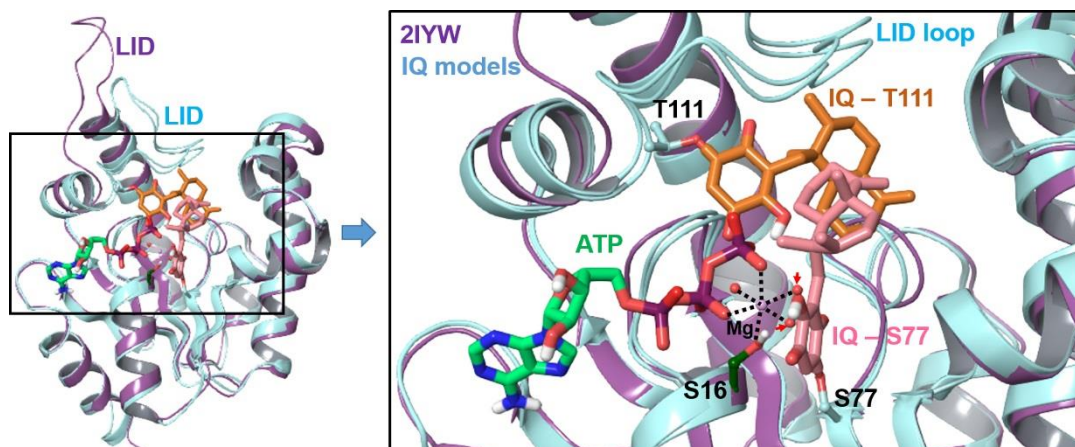


Figure 3.18: IQ models bonded to S77/T111 superimposed onto the *MtSK* crystal structure with ATP and Mg²⁺ (PDB 2IYW). The secondary structure of *MtSK* with co-crystallized ATP is colored purple, while *MtSK* with IQ models are colored light blue. Full structures are shown the left; a close-up view of the ATP/IQ binding sites is shown to the right. The Mg ion is coordinated by S16, ATP phosphate groups and three crystal waters (PDB 2IYW).

IQ covalently bound to S77 binds to a site adjacent to the ATP binding pocket. This pose would displace two crystal waters coordinating Mg²⁺ (marked with red arrows in **Figure 3.18**). However, in this pose IQ may contribute to metal coordination through a hydroxyl group that closely overlaps with one of the crystal waters. In this pose IQ does not penetrate into the ATP binding site and shows no interference with bound ATP. In the IQ pose covalently linked to

T111, the ligand partially penetrates the ATP binding pocket resulting in severe steric clashes with an ATP phosphate group restrained by Mg^{2+} coordination. As discussed below, the benzoquinone ring of IQ is sandwiched between R117 and P11 while covalently bound to T111, which interactions would prevent re-orientation of the benzoquinone ring away from the phosphate group. Therefore, this IQ binding model is not compatible with ATP binding. A close-up view of the binding site of covalently bound IQ in the two models is illustrated in **Figure 3.19**.

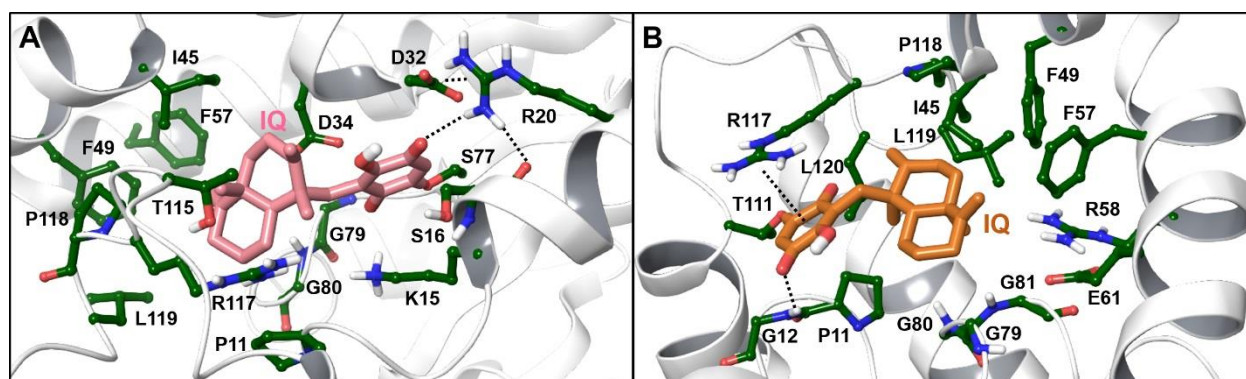


Figure 3.19: IQ binding models based on *MtSK* (PDB 2IYY) with IQ covalently linked to A. S77 and B. T111. Residues shown form the binding site of IQ. Carbon atoms of *MtSK* are colored dark green, while ligand carbons are colored pink or light brown. All other atoms are colored by atom type (as in **Figure 3.18**). Polar interactions discussed in text are indicated by dashed lines.

In both IQ binding models the hydrophobic part of the ligand is accommodated in a mainly non-polar region, partially overlapping with the shikimate binding site, where lid domain residues

form part of the IQ binding pocket. In the IQ model covalently bound to S77 the hydrophobic part of the ligand forms favourable non-polar contacts with P11, I45, F49, F57, P118, the aliphatic chain of R117 and CB atom of the D34 side chain. Its benzoquinone forms a hydrogen bond with R20. The side chain conformation of R20 is restrained through hydrogen bonding /salt bridging interactions, as shown in **Figure 3.19A**. In the IQ model covalently linked to T111 the following residues participate in non-polar contacts with the ligand: P11, I45, F49, F57, P118, L119, L120 and the aliphatic part of the R117 side chain. In this pose the benzoquinone moiety of IQ is sandwiched between P11 and R117, forming aromatic – cation interactions with the guanidinium group of R117, and a weak hydrogen bond with G12 (**Figure 3.19B**). Both IQ binding modes show excellent shape complementarity with their binding sites, as illustrated by the electrostatic potential surface of *MtSK* displayed in **Figure 3.20**.

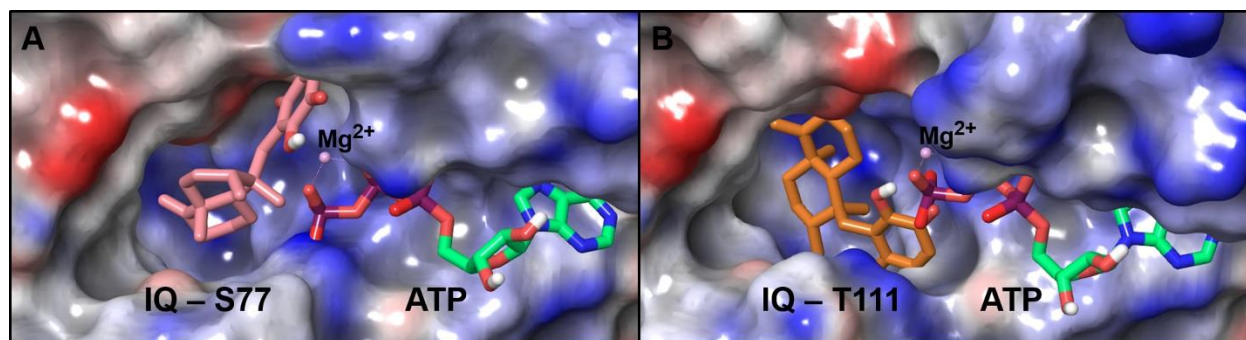


Figure 3.20: Surface representation of *MtSK* in the developed models with IQ covalently linked to A. S77 and B. T111. The electrostatic potential surfaces are displayed for both IQ binding models. ATP and the Mg ion shown are from the crystal structure with PDB code 2IYW following superposition of *MtSK* between the structures, as in **Figure 3.19**.

Although our data suggest that IQ inactivates *MtSK* by derivatizing residues in or near the active site, IQ has a clear capacity toward collateral modification of *MtSK* amino acids well removed from the enzyme's active site. Similarly, we observed IQ cross reaction with other proteins/enzymes. Out of three other enzymes evaluated, LDH activity showed a similar sensitivity to IQ, and it was derivatized by IQ. Notably, IQ neither inhibited nor derivatized two other enzymes, KatG and pyruvate kinase. This indicates that though IQ may be promiscuous in its reactivity, it is not indiscriminant as a protein modification reagent; across the four enzymes evaluated there are numerous solvent-exposed Ser, Thr, Lys and/or Tyr residues. A substantial proportion of these do not appear to be reactive with IQ. All things considered, in its present form, IQ does not exhibit stellar specificity for *MtSK*, and there is a clear capacity to cross react with unintended targets. As such, the potential of IQ as a lead in the development of antitubercular agents directed against *MtSK* or other targets is questionable.

3.6 Conclusion

IQ-based irreversible inactivation of *MtSK* is via covalent adduct formation. Covalent inhibitors have proven to be more potent than typical reversible inhibitors and highly profitable (381). Acetylsalicylic acid [aspirin], esomeprazole [Nexium], and clopidogrel [Plavix] are a few examples among many. Covalent inhibitors possess several advantages over non-covalent inhibitors including increased biochemical efficiency of target disruption, longer duration of action that outlasts the pharmacokinetics of the compound, and the potential to prevent the emergence of acquired resistance conferred by mutations (24). However, off-target modification is a major concern for drugs acting through covalent mechanisms. By virtue of its tendency to covalently derivatize Ser and Thr as well as Lys and Tyr residues and its ability to inactivate two

targets across a limited set of four enzymes, IQ has all the appearances of a non-specific or PAINS-type inhibitor. Certainly, caution is warranted in the use of IQ in drug-discovery applications. On the positive side, IQ is not indiscriminant. Across the four enzymes evaluated, a large proportion of available residues (i.e., solvent exposed Ser, Thr, Lys, and Tyr) were not modified, and two enzymes, KatG and PK, were entirely unaffected by IQ. Molecular docking studies indicate that there may be potential paths forward for modification of the IQ scaffold to increase its specificity and suitability as an *MtSK* active site-directed agent.

Chapter 4

Probing conformational dynamics and mechanistic evaluation of tuberculosis shikimate kinase inhibitors using strategic intrinsic fluorescence

4.1 Abstract

The primary function of the shikimate pathway is to produce precursors for aromatic compounds, most prominently, the aromatic amino acids. Shikimate kinase (SK) and other enzymes of the pathway are essential for viability of pathogens like *M. tuberculosis*. The absence of a mammalian counterpart makes SK and the other enzymes of the pathway attractive targets for the development of new antitubercular agents. Our aim is to develop tools to rapidly evaluate critical aspects of the mechanisms of SK catalysis and inhibition. Shikimate kinase from *M. tuberculosis* (*MtSK*) has no tryptophan residues, even though homologs from several other SKs do. Alignments of SK amino acid sequences along with evaluations of known *MtSK* structures were used to guide Trp substitution at strategic sites in the enzyme. Three viable *MtSK* variants were generated by site-directed mutagenesis. One, N151W, targeted the nucleotide binding domain, a second, E54W, targeted the shikimate-binding domain, and a third, V116W, targeted the conformationally dynamic lid domain. For all three variants, kinetic parameters with respect to ATP and shikimate were similar to the wild-type enzyme. With Compound 1, traditional enzyme inhibition suggests a noncompetitive type inhibitory mechanism. ESI-LC-MS data suggest this inhibitor forms no covalent adducts with the enzyme and dilution experiments also suggest a slow reversible mechanism is operating. K_{DS} for Compound 1 ranged from 16 to 33

μM depending on the variant evaluated. Displacement experiments indicated a preferential binding of Compound 1 at or near the shikimate binding arm. Resonance energy transfer data show differential yet unique spectral signatures in the presence and absence of Compound 1. Together, our data show that these variants can be used as tools for mechanistic investigation of inhibitors, as in the case of Compound 1 and can screen off ATP competitive inhibitors.

4.2 Introduction

The shikimate pathway is an essential route for the synthesis of aromatic cellular metabolites (382). Though present in bacteria, algae, fungi, plants, yeasts and certain apicomplexans, it has no mammalian analogue (383–385). This makes it a potential target for the development of potent antimicrobials, antiparasitics and herbicides (106,386,387).

Tuberculosis is the leading cause of death from a single infectious agent. The *aroK* gene encodes for tuberculosis shikimate kinase (*MtSK*), which is essential for the survival of the pathogen (319). Shikimate kinase (SK; EC 2.7.1.71) catalyzes the phosphorylation of shikimate using ATP as co-substrate. *MtSK* is a nucleoside monophosphate kinase with a five-stranded parallel β -sheet core (388). Structurally similar to NMPKs, it has a lid domain and a nucleotide-binding domain. The shikimate binding domain is responsible for shikimate binding (388). The P-loop (also known as the Walker A-motif) (90) forms a part of the nucleotide binding domain (94,388) while the Walker B-motif is situated between the shikimate and ATP-binding sites (90).

The random-sequential substrate binding mechanism of *MtSK* (389) is accompanied by large protein conformational changes; these are observed with both binary complexes, E-ATP and E-shikimate, as well as the ternary complex. The lid domain is essential for catalysis as it interacts with the substrates and also stabilizes the changes in charge distribution during catalysis

using the conserved basic residues Lys 15 and Arg 117 (92). Asp 32 of the Walker B-motif coordinates with the divalent magnesium cation. The Asp-Mg²⁺ interaction occurs across two water molecules. The Mg²⁺ in *MtSK* is hexacoordinated (92). When ATP is bound, the adenine moiety is positioned between Pro 155 and Arg 110. It hydrogen bonds with Arg 153 and, via a bridging water molecule contacts Ser 13. The shikimate binding pocket is made of conserved residues Asp 34, Arg 58, Gly 80 and Arg 136 (93). Arg 58 forms a hydrogen bond with Glu 54 which helps to position the guanidinium group of Arg 58 for shikimate binding.

A modified lactate dehydrogenase/pyruvate kinase coupled assay was used to obtain the steady-state kinetic parameters for *MtSK*. The reactions were monitored at 340 nm corresponding to the oxidation of NADH (390). Though this assay has wide applications, its time consuming and cumbersome nature poses many challenges due to cross reactivity of assay analytes, making it cumbersome (at best) or unworkable (at worst) for mechanistic evaluation of *MtSK* catalysis and inhibition. Though mass spectrometry offers a direct measurement of enzyme activity it is however time consuming, material and labor intensive. Several of these drawbacks may be averted by the use of intrinsic fluorophores (e.g. tryptophan) to obtain detailed information regarding protein-substrate and even protein-protein interactions. The use of intrinsic fluorescence addresses this problem as inhibitor is in direct interaction with the target enzyme, reporting on the direct interaction between enzyme and inhibitor. This approach offers a mechanistic advantage as ‘on’ and ‘off’ rate constants could be determined using rapid reaction techniques like stopped-flow fluorimetry. In addition, the strategic insertion of a fluorophore on key regions of the enzyme can report on binding events occurring at each region. This offers mechanistic information on ligand interaction with the protein and can serve as a potential mechanistic tool. For example, targeted intrinsic fluorescence can be applied in screening out

ATP competitive inhibitors, thereby reducing the amount of time invested in evaluating this class of inhibitors which may not make it to subsequent stages of the drug discovery pipeline.

Fluorescence titration can be applied to evaluate binding mechanisms and interactions between enzymes and substrates (299,300,344,391–394). This encompasses the use of steady-state, transient-state techniques to evaluate enzyme mechanisms and also interactions with substrates and inhibitors. Being sensitive to environment, most fluorophores serve as molecular probes, elucidating key mechanistic events occurring during catalysis.

This chapter explores targeted incorporation of intrinsic protein fluorescence as an alternate strategy to probe interactions between key regions of the *MtSK* enzyme and its substrates (ATP and shikimate) and inhibitors. We have generated three tryptophan-bearing *MtSK* variants to give each one intrinsic fluorescence associated with a different domain of the enzyme. Each variant also has activity similar to the wild-type enzyme. The data presented here show that fluorescence quenching can be used to monitor ATP binding. Further, although shikimate binding does not result in fluorescence quenching, changes in fluorescence anisotropy upon shikimate binding are detectable with the variant (V116W) which targets the conformationally dynamic lid domain. Also, we demonstrate here that these variants can be used to investigate inhibition mechanism as we have shown using the inhibitor known as Compound 1. They can also serve as a panel for screening out ATP-competitive inhibitors. In the case of *MtSK* this is highly advantageous because ATP-competitive inhibitors would potentially cross react with host kinases (off-target toxicity) rather than shikimate kinase. The ability of this panel of variants to screen out these kinds of inhibitors would minimize the cost of preliminary drug screens, preventing pursuit of dead ends.

4.3 Materials

Imidazole, ampicillin (AMP), chloramphenicol (CAM), and phenylmethylsulfonyl fluoride (PMSF) were purchased from Sigma (St. Louis, MO). Compound 1 [3-methoxy-4-{ [2-((2-methoxy-4-[(4-oxo-2-thioxo-1,3-thiazolidin-5-ylidene) methylphenoxy] methyl) benzyl]oxy} benzaldehyde] was obtained from SPECS. MantATP (2'/3'-O-(N-Methyl-anthraniloyl)-adenosine-5'-triphosphate) was purchased from Jena Biosciences. Isopropyl- β -D-thiogalactopyranoside (IPTG) was obtained from Fisher (Pittsburgh, PA). Benzonase nuclease was purchased from Novagen (Madison, WI). All restriction enzymes were purchased from New England Biolabs (Beverly, MA). All oligonucleotide primers were purchased from Invitrogen (Carlsbad, CA). The *E. coli* strains (BL-21-Gold [DE3] pLysS and XL-1 Blue), *Pfu* polymerase, and T4 DNA ligase were purchased from Agilent (La Jolla, CA). All restriction enzymes were purchased from New England Biolabs (Beverly, MA) and all oligonucleotide primers were purchased from Invitrogen (Carlsbad, CA). Nickel-nitrilotriacetic acid (Ni-NTA) resin was purchased from Qiagen (Valencia, CA). Desalting 10DG chromatography columns were purchased from Bio-Rad (Hercules, CA). The substrates adenosine-5'-triphosphate (ATP), shikimate, reduced nicotinamide adenine dinucleotide (NADH), phosphoenol-pyruvate (PEP) and the enzymes pyruvate kinase (PK) and lactate dehydrogenase (LDH) used in the coupled assay were purchased from Sigma-Aldrich (St. Louis, MO). Black round-bottom 96-well microtitre plates from Corning® (Corning, NY). All organic solvents were HPLC or LC-MS grade and were purchased from Thermo Fisher (Hanover Park, IL). All buffers and media were prepared using water purified by a Barnstead EasyPure II system (18.2 M Ω /cm resistivity).

4.4 Methods

4.4.1 Mutagenesis

Site-directed mutagenesis was carried out by ‘Round-the-horn’ approach (395) to the construct used for the expression of wild-type *MtSK* in pET21b vector bearing *M. tuberculosis* shikimate kinase gene. The forward primers designed for substitution N151W, (5’ GTGGACACCT**TGGCGCCGCAAC** 3’); E54W, (5’**TGGCAGGA**ATTCCGACGTATCGAGG-AGGAC 3’); V116W (5’ ACGTGGCGCCCACTGCTGGCCGGC 3’) included in bold, a site for codon replacement and underlined are silent mutations. Because of this approach, the reverse primers carried no substitutions - N151W (5’ TCGCAT**TGGTCGCGACGCGCCGGTA** 3’); E54W (5’ CCGTCGG**TGGCGAAGATGTCGGCGAT** 3’); V116 (5’ GTTGCCGCCGGTGC-GGCGCACTCCCT 3’). All primers were modified by a 5’-phosphorylation, allowing for blunt-end ligation of PCR products. PCR reactions for the generation of these variants were carried out using *Pfu* polymerase and dNTPs (deoxynucleotide triphosphates). PCR products were *Dpn* 1 digested to eliminate parent template and ligated using quick T4 DNA ligase. The ligation products were used to transform XL-1 Blue *E. coli* cells. Transformants were selected on the basis of ampicillin resistance. Selected N151W, E54W, and V116W plasmids were screened with BsaHI, EcoR1, and AflIII restriction endonucleases, respectively. Successful clones were sent for full DNA sequence analysis (Davis Sequencing, Davis CA) to verify that intended mutations were present.

4.4.2 *MtSK* Expression and Purification

MtSK expression was carried out in *E. coli* (BL-21-Gold [DE3] pLysS) using lysogenic broth supplemented with ampicillin (100 µg/mL) and chloramphenicol (0.034 mg/mL). Cells were grown at 37 °C with constant agitation (250 rpm) to mid-log phase ($OD_{600} = 0.4$) and induced by IPTG (1 mM). The cells were then grown for an additional 4 h post induction, harvested by centrifugation at 5,000 rpm for 15 min at 4 °C and stored at -80 °C until purification. Expression analysis was carried out using a trichloroacetic acid (TCA) precipitation protocol as described by Varnado et al. except that 11% acrylamide SDS-PAGE gels were used (396). A solubility test protocol was followed to determine the proper method of purification. Expression analyses revealed the presence of a protein with the anticipated molecular weight in the soluble and insoluble fractions. Consequently, protocols were developed to purify the protein from its soluble and insoluble (i.e., inclusion body) states.

For protein purification, cell pellets were resuspended in buffer A (50 mM Tris-HCl, pH 7.4; 0.5 M NaCl) in the presence of PMSF (0.1 mM). The mixture was homogenized with a dounce homogenizer and lysed by sonication using a Branson Sonifier 250 (Branson Ultrasonics Corp., Danbury, CT, USA). Sonication was carried out with an output control of 3.5 and a 30% duty cycle for 8 intervals of 42 s each with cooling on ice between each sonication. Following sonication, benzonase nuclease (250 U) was added, and the mixture was incubated for 2 h at 4 °C with gentle stirring. The cell lysate was centrifuged at 10 000 rpm for 15 min at 4 °C, the supernatant was collected and the pellets were stored at -80 °C for further purification under denaturing conditions. The supernatant was loaded onto a column with Ni-NTA resin by recirculating the solution through the column at 1 mL/min overnight. After loading, the column

was washed in succession with 50 mM Tris, pH 8.0, followed by buffer A supplemented with 2 mM, 20 mM, 50 mM, 0.1 M, 0.5 M, and 1 M imidazole. The eluted fractions were collected and analyzed by SDS-PAGE. The fraction containing the protein (0.1 M imidazole) was concentrated by ultrafiltration with a 3 kDa molecular cutoff filter (Amicon, Billerica, MA) and subjected to buffer exchange using a 10 DG size exclusion column (BioRad, Hercules, CA) equilibrated with buffer A.

The concentration of *MtSK* was measured using the Pierce BCA Protein Assay (Pierce, Rockford, IL) according to manufacturer's instructions using bovine serum albumin as a standard. Enzyme purified by denaturing conditions was employed for the results presented in this report.

4.4.3 ESI-LC-MS Analysis of Intact *MtSK*

Analyses of intact *MtSK* were performed on an Agilent (Little Falls, DE) 6520 Accurate-Mass Q-TOF mass spectrometer coupled to an Agilent 1200 RRLLC system. ESI was conducted using a capillary voltage of 4000 V. Nitrogen was used as the nebulizing gas (25 psig) and drying gas (10 L/h; 350 °C). The TOF fragmentor and skimmer were set to 180 and 65 V, respectively. Samples were injected onto a 2.1 × 100 mm; 3.5- μ m Zorbax 300SB-C18 column (Agilent Technologies, Inc.) using a flow rate of 0.4 mL/min. The mobile phase consisted of water with 0.1% (v/v) formic acid (A) and acetonitrile with 0.1% (v/v) formic acid (B) with a gradient elution as follows: 30% B at 0 min, 80% B at 3 min, and 30% B at 5 min. Each run was followed by a 1 min post run with 30% B. The total run-time analysis was 6 min and the column temperature was 27 °C. Spectra were acquired in the positive (ES⁺) ion mode, and full scan mass spectra (m/z 300–3200) were collected at a rate of 1 spectrum/sec. Mass data obtained from LC-

MS was analyzed using Agilent MassHunter Qualitative Analysis software and Agilent MassHunter BioConfirm software version B.02.00.

4.4.4 Evaluation of *MtSK* Activity

The enzymatic activity of *MtSK* was also assayed by a modified pyruvate kinase/ lactate dehydrogenase coupled-assay following procedures described by Rosado et al (344). In this assay, the generation of ADP by the *MtSK*-catalyzed reaction leads to the oxidation of NADH to NAD⁺; the decrease in NADH concentration is monitored at 340 nm ($\epsilon = 6220 \text{ M}^{-1} \text{ cm}^{-1}$). Assay mixtures (1 mL final volume) consisted of 0.1 M Tris pH 7.6, 50 mM KCl, 5 mM MgCl₂, 5 mM shikimate, 1.2 mM ATP, 1.5 mM PEP, 0.2 mM NADH, 3 U/mL pyruvate kinase and 2.5 U/mL lactate dehydrogenase. Reactions were initiated by the addition of *MtSK* (20 nM), and the change of absorption was monitored for 3 min at 340 nm. In this reaction, the oxidation of NADH is stoichiometrically equivalent to the production of ADP and S3P by *MtSK* because *MtSK* is the rate-limiting factor of the coupled reaction.

Steady-state kinetic parameters were determined from initial velocity measurements varying the concentrations of one substrate while keeping the other substrate concentration fixed as described above. Data were collected in triplicate, and the data were fitted to the Michaelis-Menten equation (eq.1) using GraphPad Prism 5.02 software (Mountain View, CA).

$$v_o = \frac{k_{cat}[S]}{\frac{k_{cat}}{k_{on}} + [S]} \dots\dots\dots \text{Eq. 1}$$

All reactions, (ATP- and shikimate-dependent) were performed at room temperature on a Shimadzu UV-1601 spectrophotometer (Columbia, MD) with a cell path length of 1.0 cm.

4.4.5 Fluorimetric measurements

Fluorescence experiments were carried out on a Varioskan® fluorimeter (Thermo Fisher Scientific, Hanover Park, IL). Samples were excited at 290 nm and emission spectra collected from 300 – 400 nm, with a 5 nm bandwidth. All samples contained 10 μM *MtSK* and reactions were carried out using 100 mM Tris, pH 7.6, 50 mM KCl, 5 mM MgCl₂. Samples were loaded in a black 96-well microtitre plate (Corning Inc., Corning, NY) to a total volume of 200 μL. The concentration range for ligands used in these experiments were; 0 – 1.5 mM, 0 – 2.5 mM, 0 – 0.2 mM, 0 – 0.2 mM, for ATP, shikimate, Compound 1 and mantATP, respectively. Collected spectra were corrected by subtracting baseline signals (buffer and substrate) from that of the reaction.

Resonance energy transfer efficiencies (E, from titrations with mantATP) by the using equation 2, where F_D is the fluorescence intensity of the donor and F_A is the fluorescence intensity in the presence of the donor and acceptor.

$$E = 1 - \frac{F_D}{F_A} \dots\dots\dots \text{Eq. 2}$$

Data were normalized (except RET efficiencies) to a scale of 0 - 1 and fitted to a quadratic function for ligand binding (Eq. 3) to obtain corresponding K_{DS}.

In the ATP/shikimate vs Compound 1 and mantATP vs Compound 1 competitive binding experiments, proteins were preincubated for 20 min with 10 μM inhibitor. After which increasing concentrations of shikimate (0 – 5 mM), ATP (0 – 1.2 mM) and mantATP (0 – 0.18 mM) were added to the samples before excitation at 290 nm.

Fluorescence anisotropy experiments were performed on a Cary Eclipse Fluorescence spectrometer (Agilent, Santa Clara, CA) using ultra-microsized cuvettes. Excitation (290 nm) and emission (340 nm) slits were set at 5 nm. All samples contained 10 μ M *MtSK* and reactions were carried out using 100 mM Tris, pH 7.6, 50 mM KCl, 5 mM MgCl₂ in a 100 μ L total volume. For titrations evaluating shikimate binding, shikimate concentrations ranged from 0.1 – 2.5 mM. For titrations evaluating ATP binding, concentrations ranged from 0.01 - 1.2 mM. All measurements were carried out in triplicate and fitted to a quadratic function for ligand binding (Eq. 3) to obtain corresponding K_{DS} .

$$Y = (E_T + S + K_D) - \frac{\sqrt{(E_T+S+K_D)^2-4(E_T*S)}}{2} \dots\dots\dots \text{Eq. 3}$$

4.5 Results

Wild-type *MtSK* has no tryptophanyl residues. This allows for the strategic or targeted incorporation of the residue into the protein by site-directed mutagenesis to impart intrinsic fluorescent properties. Amino acid sequence alignments along with the known structural features of *MtSK* were used to identify sites that would be more likely to accommodate the inclusion of the indole-bearing side chain of Trp. Within key domain structures of the enzyme, sites that showed little, if any, sequence conservation were preferred. The appearance of non-polar residues (and especially Trp) in orthologs at sites of poor conservation was also desirable as it indicated that Trp would be better accommodated at the corresponding site in *MtSK*. Target sites were identified that covered key components of the *MtSK* structure (**Figure 4.1**): L10 and N151 from the ATP-binding domain, E54 from the shikimate-binding domain, as well as V116, L119, and L120 from the lid domain. In the shikimate binding domain, though some level of sequence

conservation (**Appendix Figure 4.1**) is observed at position 54, some orthologs do possess a tryptophanyl residue at this position, suggesting that this position can accommodate this large aromatic amino acid and maintain catalytic output. Positions 10, 116 and 151 (*MtSK* numbering) showed very weak sequence conservation, with a mix of aromatic, charged, polar and non-polar amino acids. In addition, positions 119 and 120 also showed weak sequence conservation with polar uncharged, non-polar aliphatic and positively charged amino acid residues. In each of these cases, it seemed a reasonable possibility that replacement of the existing amino acid with a tryptophanyl residue would impart fluorescent properties while preserving substantial catalytic activity.

Site-directed mutagenesis procedures yielded plasmids for the expression of L10W, E54W, V116W, L119W, L120W, and N151W *MtSK*. Following mutagenesis, plasmids were sequenced and the presence of correct substitution, as well as the absence of other unintended mutations, were verified. All six variants were overexpressed in *E. coli* (BL-21-Gold [DE3] pLysS) and were subsequently evaluated for purity using ESI-LC-MS (**Figure 4.2**). Due to the poor activity of L101W, L119W and L120W they were not evaluated further. As described previously (377), deconvoluted spectra of purified wild-type *MtSK* show two species differing in mass by 131 amu. The heavier of the two species is *MtSK* bearing its N-terminal methionine, and the lighter is *MtSK* in which this residue has been cleaved. All the *MtSK* variants showed proteins with and without the N-terminal methionine with differences in masses compared to the wild-type corresponding to the replacement of the target wild-type residue with Trp (**Table 4.1**). This confirmed the results of DNA sequencing.

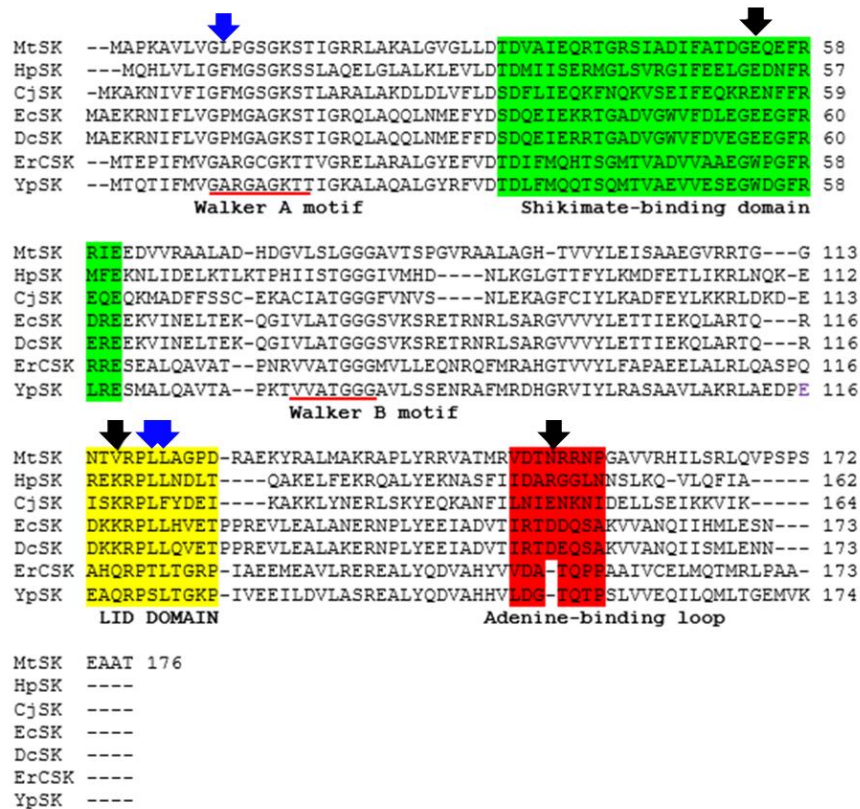


Figure 4.1: Sequence alignment of shikimate kinases from *M. tuberculosis*, *Helicobacter pylori*, *Campylobacter jejuni*, *E. coli*, *Dickeya dadantii* (formerly known as *Erwinia chrysanthemi*), *Yersinia pestis*. Regions highlighted represent the shikimate binding domain (green), the lid domain (yellow) and the nucleotide-binding domain (red). Underlined in red are the Walker A and B motifs. Arrows show positions of Trp insertion based on sequence conservation, polarity and likely interaction(s) with the substrate(s). Variants with very little, if any, activity and those with activity similar to wild-type *MtSK* are shown by blue and black arrows, respectively.

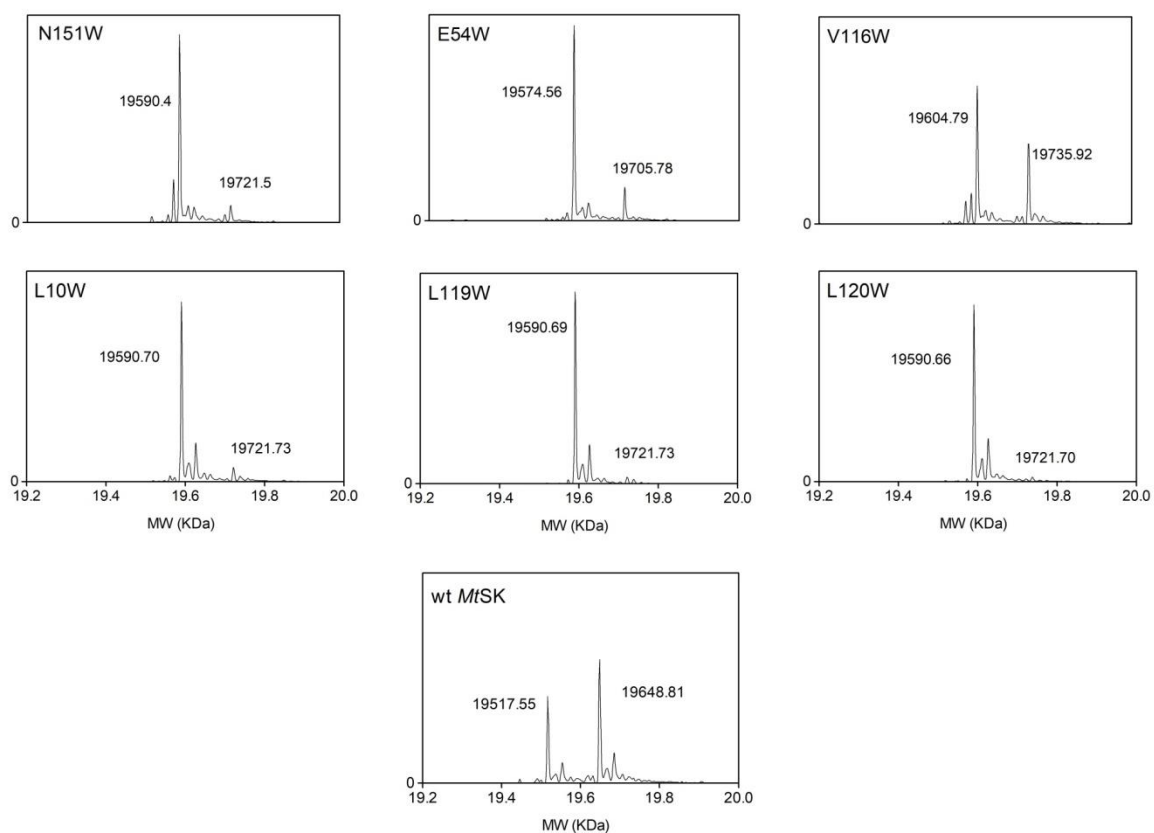


Figure 4.2: Deconvoluted ESI-LC-MS spectra of purified *MtSK* proteins. Peaks corresponding to 19590.40, 19574.56, 19604.79, 19517.55, 1959.70, 1959.69, 1959.66 Da represent protein without N-terminal methionine while species with 19721.50, 19705.78, 19735.92, 19721.73, 19721.73, 19721.70 Da possess an N-terminal methionine. Protein masses with and without N-terminal methionine are in good agreement with theoretical mass calculations for all four proteins. Samples were stored at 4°C prior to injection.

		Table 4.1 Theoretical and experimental masses (Da) for wild-type <i>MtSK</i> and variants			
		<i>MtSK</i> Protein			
		Wild-type	E54W	N151W	V116W
ESI-LC-MS	+ N-met	19468.81	19705.78	19721.50	19735.92
	No N-met	19517.55	19574.56	19590.40	19604.79
Theoretical	+ N-met	19648.59	19705.69	19720.70	19735.68
	No N-met	19517.40	19574.49	19589.51	19604.47

E54W, V116W, and N151W *MtSK* all showed activity similar to the wild-type enzyme (e.g., wild-type vs V116W in **Figure 4.3**). Indeed, with respect to k_{cat} , all three variants showed values between 35 and 50% of unmodified *MtSK*, and with respect to k_{on} corresponding to either substrate, values were between 25 and 60% of the wild-type enzyme. These data suggested that E54W, V116W, and N151W would be suitable surrogates for wild-type *MtSK* in subsequent fluorometric analyses. Significantly, each variant represented a key aspect of *MtSK* structure and catalytic mechanism. The E54W substitution targeting the shikimate-binding domain, the N151W substitution targeting the ATP-binding domain, and the V116W variant targeting the conformationally dynamic lid domain.

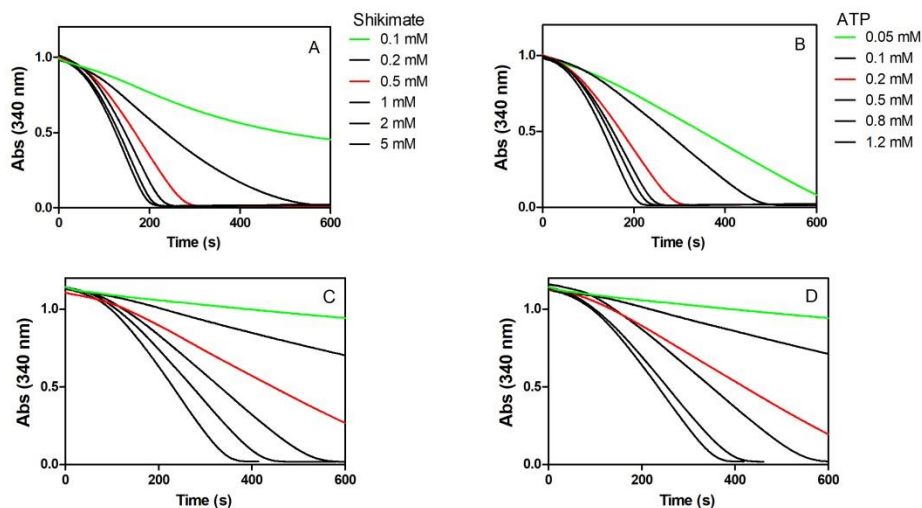


Figure 4.3: Evaluating enzyme activity using coupled-assay. Reactions were initiated by the addition of *MtSK*. Panels A and C show traces for reactions using shikimate concentrations ranging from 0.1 – 5 mM and 1.2 mM ATP for wild-type and V116W, respectively. Panels B and D show traces for reactions using ATP concentrations ranging from 0.05 – 1.2 mM and 5 mM shikimate for wild-type and V116W, respectively. All reactions were carried out at room temperature with 20 nM enzyme in 100 mM Tris, pH 7.6, 50 mM KCl, 5 mM MgCl₂. NADH oxidation resulting from the coupled activities of pyruvate kinase and lactate dehydrogenase was monitored as described in *Materials and Methods*.

Table 4.2. Kinetic parameters with respect to shikimate*

<i>MtSK</i>	Kinetic parameters		
	k_{cat} (s ⁻¹)	K_{M} (mM)	k_{on} (x 10 ⁴ M ⁻¹ s ⁻¹)
Wild-type	63 ± 1	0.51 ± 0.04	12 ± 3
E54W	24 ± 2	0.3 ± 0.2	7 ± 1
N151W	33 ± 2	0.5 ± 0.3	6.3 ± 0.2
V116W	24 ± 1	0.8 ± 0.2	3 ± 1

*All reactions contained 1.2 mM ATP

<i>MtSK</i>	Kinetic parameters		
	k_{cat} (s ⁻¹)	K_{M} (mM)	k_{on} (x 10 ⁴ M ⁻¹ s ⁻¹)
Wild-type	64 ± 2	0.17 ± 0.04	38 ± 1
E54W	24 ± 2	0.22 ± 0.02	11 ± 1
N151W	35 ± 1	0.33 ± 0.30	11 ± 3
V116W	32 ± 1	0.40 ± 0.04	9 ± 1

[#]All reactions contained 5 mM shikimate

As anticipated, each *MtSK* variant showed a UV absorption spectrum ($\lambda_{\text{max}} = 281$ nm) consistent with the presence of a Trp residue in contrast to the lack thereof in wild-type *MtSK*. Likewise, fluorescence emission spectra consistent with the presence of Trp were also observed in all three cases. Titration of each variant with increasing concentrations of ATP produced a hyperbolic decrease in fluorescence emission intensity (**Figure 4.4**). The apparent K_{D} s obtained for ATP binding to E54W (0.47 ± 0.08 mM), N151W (0.1 ± 0.03 mM), and V116W (0.32 ± 0.04 mM) were similar to the apparent K_{M} 's with respect to ATP (**Table 4.2**).

In contrast to ATP binding, the formation of enzyme-shikimate complexes for E54W and N151W showed no change in fluorescence emission spectra (**Figure 4.5**). Only modest decreases in emission intensity were observed for the lid domain variant V116W. On their own, the structural and electronic properties of shikimate seem unlikely to produce substantial fluorescence quenching. However, should shikimate binding produce conformational shifts in *MtSK* structure that would alter the environment of a Trp residue, shifts in Trp-dependent fluorescence emission would be anticipated. It is well known that the lid domain of *MtSK* (which includes V116) occupies a wide range of conformational states depending on the presence or absence of its substrates (89–91,93). In light of these facts, the modest changes in V116W fluorescence in response to shikimate raised the possibility these may be indicative of shikimate-

dependent conformational changes in the *MtSK* lid domain. To investigate this hypothesis, changes in fluorescence anisotropy on titration of V116W *MtSK* with shikimate were monitored.

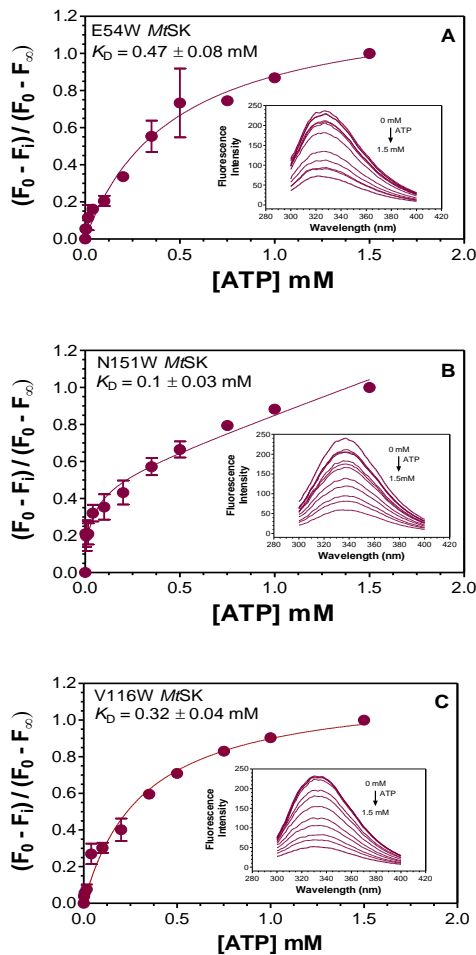


Figure 4.4: ATP-dependent fluorimetric titrations with 10 μ M E54W (A), N151W (B), and V116W (C). Insets show Trp emission spectra for the three proteins in response to increasing concentrations of ATP. All reactions were run in 100 mM Tris, pH 7.6, 50 mM KCl, 5 mM $MgCl_2$ at room temperature on black 96-well microtitreplates (Corning®). Intensities were normalized on a scale of 0 - 1. Data points represent the average of triplicate measurements, and the error bars represent the standard deviation.

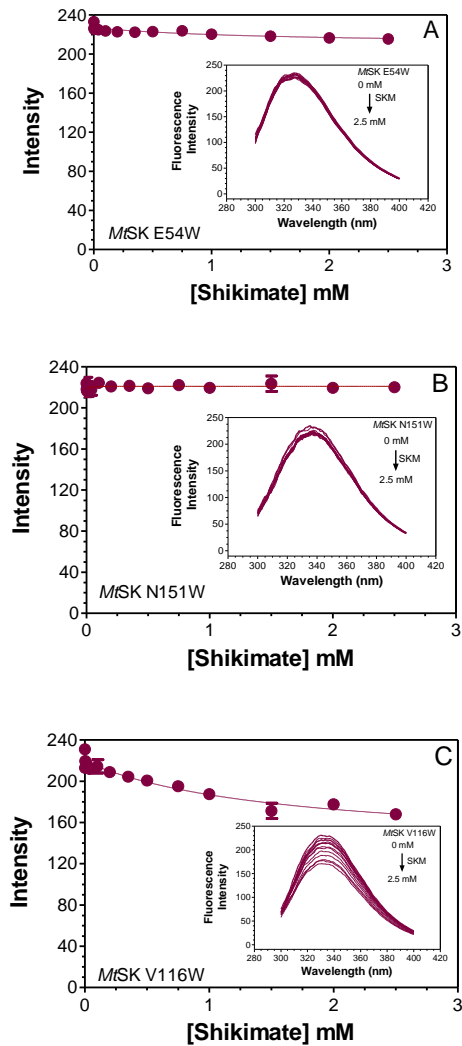


Figure 4.5: Shikimate-dependent fluorimetric titrations of 10 μ M E54W (A), N151W (B), and V116W (C). Insets show Trp emission spectra for the three proteins in response to increasing concentrations of shikimate. All reactions were run in 100 mM Tris, pH 7.6, 50 mM KCl, 5 mM MgCl_2 at room temperature on black 96-well microtitre plates (Corning®). Data points represent the average of triplicate measurements, and the error bars represent the standard deviation.

For V116W *MtSK* small but significant changes in steady-state fluorescence anisotropy were observed in response to increasing concentrations of either substrate, shikimate (**Figure 4.6A**) or ATP (**Figure 4.6B**). Neither E54W nor N151W showed any change in fluorescence anisotropy in response to shikimate (**Figure 4.6A**); N151W but not E54W showed an increase (albeit sporadic) in fluorescence anisotropy in response to ATP (**Figure 4.6 B**). The increases anisotropy of V116W in response to ATP would be consistent with the reduced mobility of the indole ring of W116 upon formation of an ES complex (397,398). Indeed, shikimate kinases (as well as other NMP kinases) are well known to undergo substantial conformational changes associated with substrate binding (**Figure 4.7**). The most dramatic of these is the closing of the enzyme's lid domain (which includes residue 116) over the substrates bound in the enzyme active site. Indeed, all indications from NMP kinase structures solved to date are that the lid domain is highly dynamic and conformationally variable in the absence of substrates, but collapses into a highly organized and closed conformation upon substrate binding.

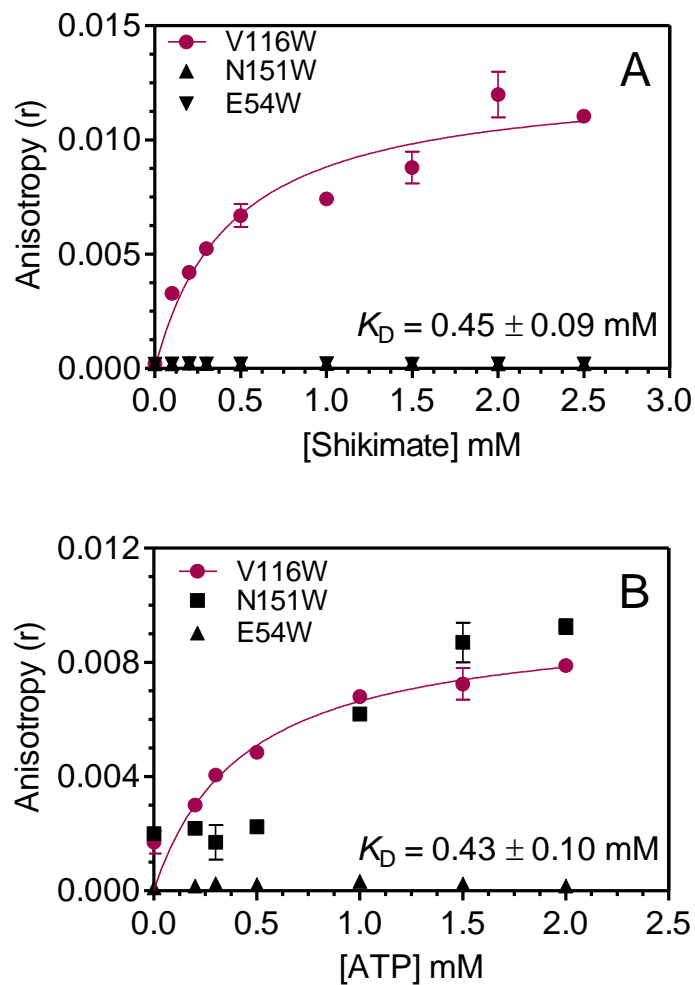


Figure 4.6: Changes in fluorescence anisotropy of Trp-bearing *MtSK* variants in response to shikimate and ATP. Titrations were carried out using 10 μ M enzyme in 100 mM Tris, pH 7.6, 50 mM KCl, and 5 mM $MgCl_2$ at room temperature. Only V116W showed consistent changes in anisotropy. Hence, only one K_D value was determined in both data sets. Error bars represent standard deviations of the mean.

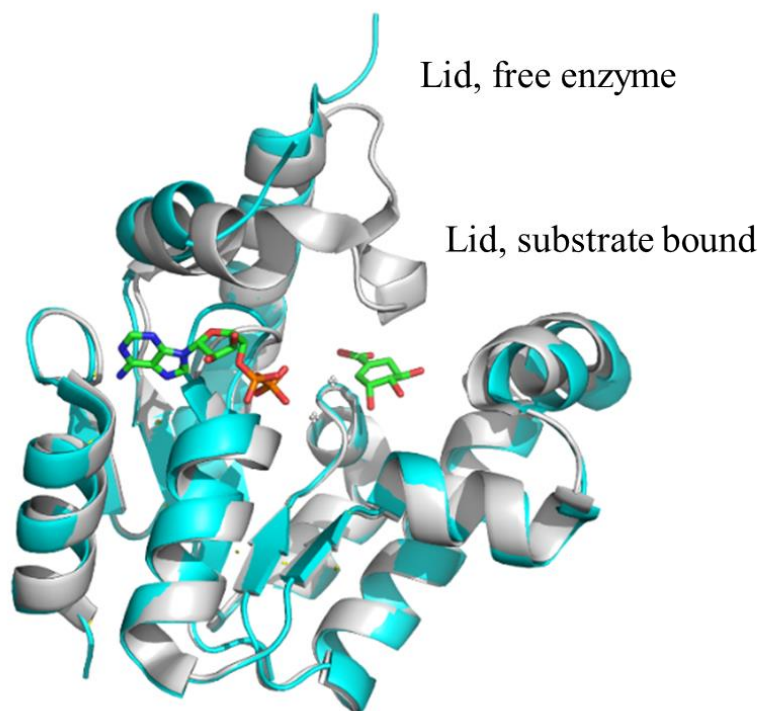


Figure 4.7: Overlay of shikimate kinase structures of the free enzyme (PDB: 2D1K, cyan)(388) and a ternary complex with ADP and shikimate (PDB: 1WE2, grey) (90). The overlay shows domain movements in both free and substrate-bound enzyme.

Having used Trp-bearing *MtSK* variants to evaluate ATP and shikimate binding by the enzyme, we sought to evaluate the interaction of *MtSK* with inhibitors, particularly the pyrazolone-based SK inhibitor known as Compound 1 (**Figure 4.8**). However, it was first necessary to evaluate inhibition by Compound 1 using the standard coupled assay for *MtSK* activity. This assay relies on the activities of, first, PK to convert SK-generated ADP to ATP, in the process converting phosphoenolpyruvate to pyruvate, and second, LDH to convert pyruvate to lactate with the concomitant oxidation of NADH to NAD⁺. Ultimately, SK activity is inferred from the decrease in concentration of NADH monitored at 340 nm.

To determine the extent to which the coupled assay could reliably report specific inhibition of *MtSK* as opposed to the collateral inhibition the enzymes of the coupled assay, we evaluated the effect of Compound 1 on PK and LDH activities. Oxidation of NADH by LDH in reactions containing PK, PEP, and ADP in the presence of Compound 1 (0 - 30 μM) was examined. Above 10 μM , significant inhibition of the coupled enzyme system was observed, setting an upper limit for Compound 1 concentration in these studies of 10 μM (data not shown).

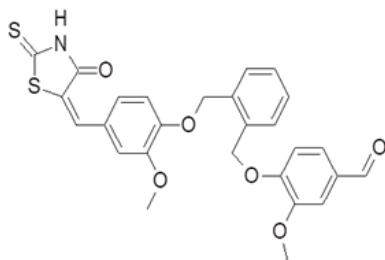


Figure 4.8: Structure of Compound 1 ([3-methoxy-4-{ [2-({2-methoxy-4-[(4-oxo-2-thioxo-1,3-thiazolidin-5-ylidene) methylphenoxy] methyl) benzyl] oxy} benzaldehyde])

Increasing concentrations of Compound 1 produced a decrease in the *MtSK* k_{cat} (**Figure 4.9**). Whether shikimate or ATP was the varied substrate, k_{cat} was reduced by about 70% in the presence of 10 μM Compound 1. Compound 1 also produced a clear decrease in k_{on} with respect to shikimate and ATP. The Compound 1-dependent decrease in both k_{cat} and k_{on} suggested a non-competitive mechanism of inhibition, consistent with previous observations for *H. pylori* shikimate kinase. However, the data were not readily fit to obtain dissociation constants (i.e., K_i values) for *MtSK*-Compound 1 complexes.

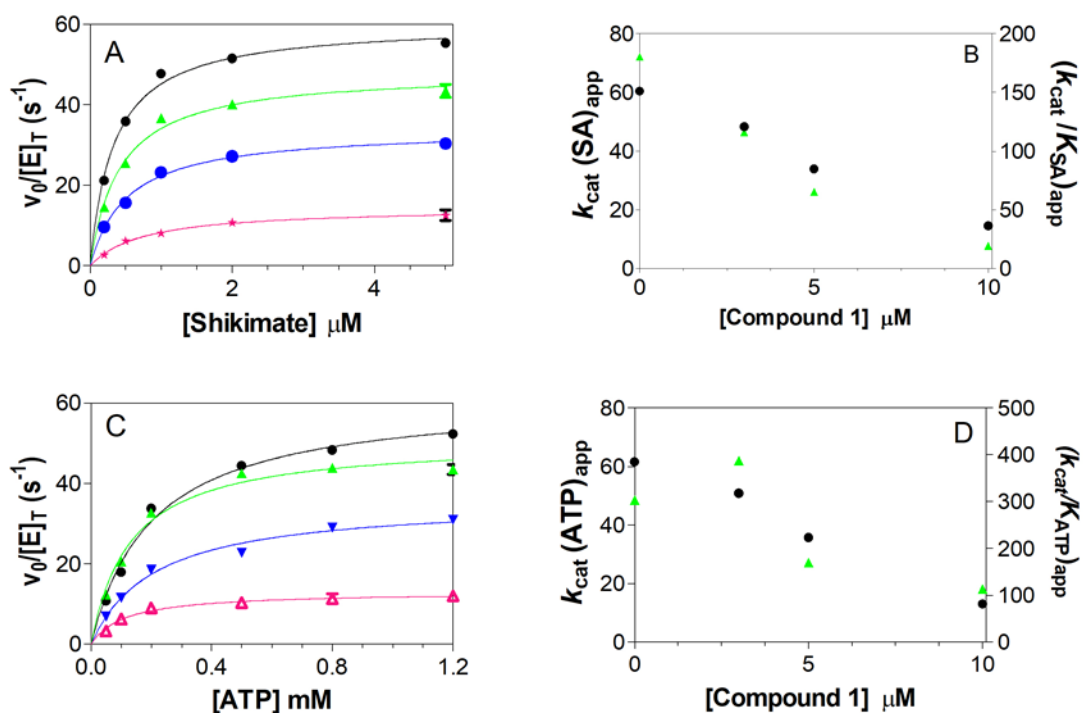


Figure 4.9: *MtSK* inhibition by Compound 1. The effect of Compound 1 on *MtSK* activity in response to shikimate (A) and ATP (C) concentration. The effects of Compound 1 on the apparent k_{cat} (●) and k_{cat}/K_S (▲) with respect to shikimate (B) and ATP (D) are also shown. All reactions contained 20 nM *MtSK* and were carried out in 100 mM Tris, pH 7.6, 50 mM KCl, 5 mM MgCl₂ at room temperature. Points represent the average of triplicate measurements, and the error bars represent the standard deviation from the mean.

Jump dilution experiments performed to evaluate reversibility of Compound 1 inhibition at final concentrations of 1 and 5 μM showed a slow but complete oxidation of NADH, when

compared to the control (**Figure 4.10**). This indicates that diluting the equilibrated EI complex in the reaction mixture results in slow, yet subsequent gain of enzymatic activity; the inhibitor may not be tightly or covalently bound to the enzyme. Upon incubation and hourly injection (for 24 hr) of the EI complex, the resulting deconvoluted chromatogram and mass spectra (**Figure 4.11**) indicate that the inhibitor is not covalently bound to the enzyme. Hence, no change in enzymes molecular weight or appearance of modified enzyme in the mass spectra or additional peaks in the chromatogram. These set precedence from which we utilized the tryptophan-bearing variants to elucidate the mechanism of action of Compound 1. Albeit to develop a high throughput screening approach for rapid mechanistic evaluate of shikimate kinase inhibitors.

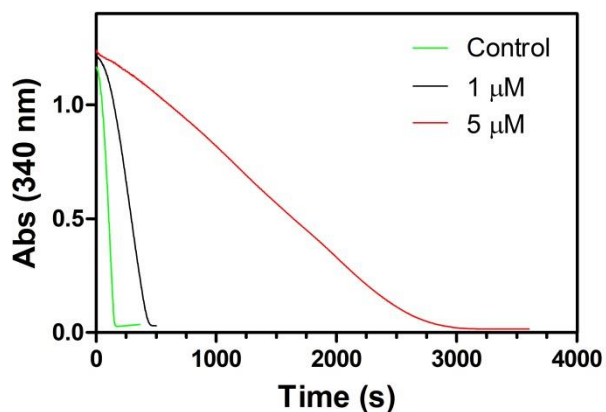


Figure 4.10: Jump dilution experiments with Compound 1. *MtSK* (5 μ M) was preincubated with 0.01 % DMSO, 100 and 500 μ M Compound 1 for 1 hr at room temperature in a 50 μ L total volume. The enzyme-inhibitor complex was then diluted 100-fold (50 nM final concentration) into a PK/LDH coupled reaction cocktail containing 5 mM shikimate and 1.2 mM ATP. Preincubations and activity assays were carried out in 100 mM Tris, pH 7.6, 50 mM KCl, and 5 mM MgCl₂. Representative traces from triplicate measurements are shown.

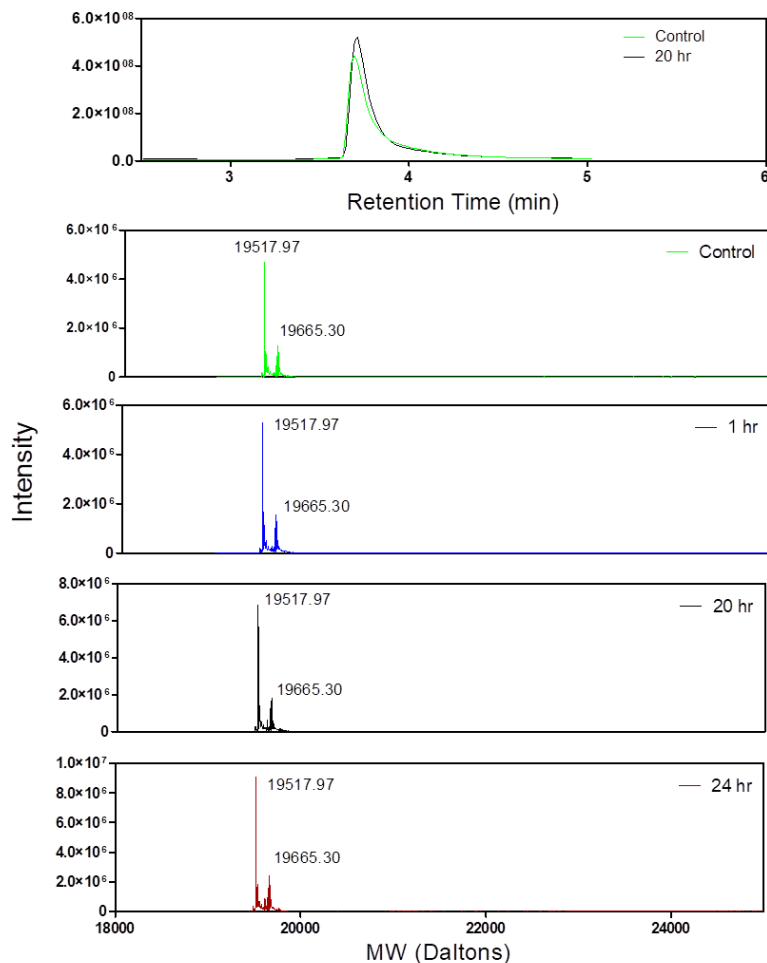


Figure 4.11: Investigating covalent adducts formation between *MtSK* and Compound 1. 1 μM *MtSK* was preincubated with 100 μM Compound 1 for 24 hr at 4°C. Samples were injected hourly into the mass analyzer. Chromatogram of samples shows no evidence of multiple peaks.

The *MtSK* Trp-bearing variants previously described, N151W (nucleotide-binding domain), E54W (shikimate-binding domain) and V116W (Lid domain) were used to evaluate binding of Compound 1 by *MtSK*. A K_I of 10 μM was previously reported for Compound 1 on *Helicobacter pylori* shikimate kinase (*HpSK*) (399). Titrating these variants with Compound 1

produced hyperbolic decreases in fluorescence emission across all three proteins (**Figure 4.13 A, C, and E**). Across the three variants K_D values for association with Compound 1 were similar, ranging by a factor of two from E54W ($16 \pm 2 \mu\text{M}$) to N151W ($33 \pm 6 \mu\text{M}$) with V116W falling in between ($26 \pm 2 \mu\text{M}$).

To further investigate the nature of Compound 1 binding, pre-formed complexes of Compound 1 with *MtSK* variants were titrated with increasing concentrations of shikimate. Differential behavior was observed with each Trp-bearing variant. The enzyme inhibitor complex for N151W showed no shift in emission spectrum λ_{max} and a relatively small decrease in emission intensity (**Figure 4.14B**). Similarly, V116W showed no shift in emission λ_{max} , but a more substantial loss of emission intensity was detected (**Figure 4.14C**). In contrast, the Compound 1-E54W binary complex showed a 15-nm red shift in emission maximum relative to the free enzyme, suggesting that the inhibitor may be altering the environment at or near W54 in the shikimate binding domain (**Figure 4.14A**). The inclusion of increasing concentrations of shikimate up to 5 mM to each E-I complex produced little if any change in fluorescence for E54W or N151W, indicating that the substrate was unable to displace Compound 1. Interestingly, the formation of the ternary complex with V116W resulted in an additional quenching of intrinsic fluorescence. Given the placement of this tryptophan in the *MtSK* lid domain and the known conformational change in this domain upon shikimate binding, it is possible that inclusion of shikimate has altered the position of W116 relative to pre-bound Compound 1.

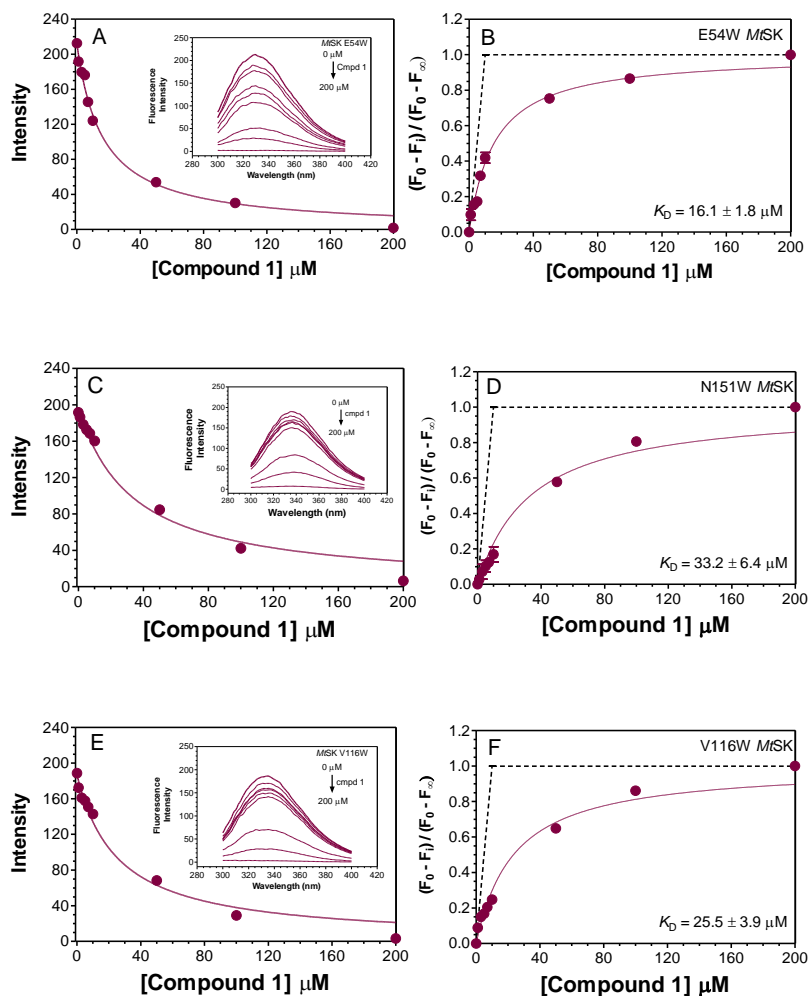


Figure 4.13: Effect of Compound 1 on Trp fluorescence. All reactions were run with 10 μM enzyme at 25°C, with Compound 1 concentrations from 0 – 200 μM . Reactions were performed in 100 mM Tris, pH 7.6, 50 mM KCl, 5 mM MgCl_2 . Error bars represent standard deviations from the mean.

Titration of the *MtSK* variant-Compound 1 binary complexes with ATP produced substantial decreases in emission intensities, indicative of the formation of a ternary complex (**Figure 4.15**). However, quenching in E54W is comparatively very weak. Still, a similar, yet unique behavior is observed in E54W; red shifting when Compound 1-bound (**Figure 4.15 A**). N151W (**Figure 4.15 B**) and V116W (**Figure 4.15 C**) showed no shifts in their emission spectra. The preformation of the V116-Compound 1 complex increases the apparent K_D for ATP by at least two fold (data not shown). Though no gain in fluorescence emission was observed in all proteins, this unique behavior in E54W suggests that the inhibitor is in close proximity to W54.

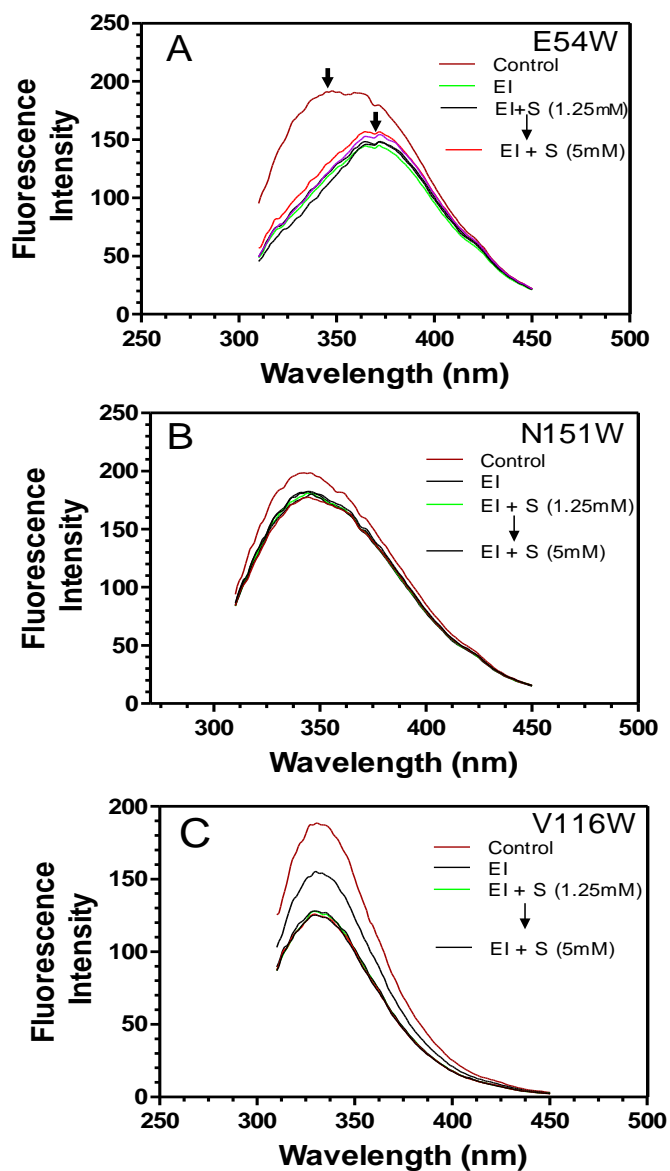


Figure 4.14: Compound 1 vs shikimate competitive assays with 10 μ M E54W (panel A), N151W (panel B), and V116W (panel C). 10 μ M Compound 1 was preincubated with proteins for 20 min after which shikimate (1.25 – 5 mM) was added to the binary complex. All reactions were performed at room temperature in 100 mM Tris, pH 7.6, 50 mM KCl, 5 mM MgCl₂. Spectra are representative of triplicate experiments.

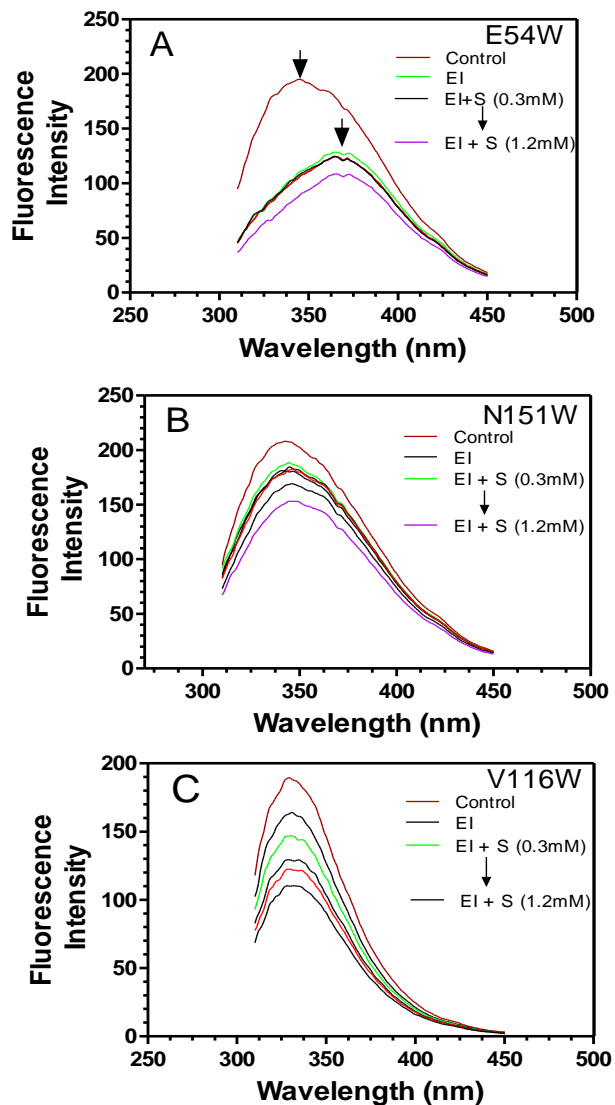


Figure 4.15: Compound 1 vs ATP competitive assays with 10 μ M E54W (panel A), N151W (panel B), and V116W (panel C). 10 μ M Compound 1 was preincubated with proteins for 20 min after which ATP (0.3 – 1.2 mM) was added to the binary complex. All reactions were run at room temperature in 100 mM Tris, pH 7.6, 50 mM KCl, 5 mM MgCl₂. Spectra are representative of triplicate experiments.

The impartation of intrinsic fluorescence also allows for the evaluation of fluorescent ligands. This is possible if the protein/donor and fluorescent ligand form a RET pair. An example of such a pair is Trp and mantATP (2'-/3'-O-(N'-Methylanthraniloyl) adenosine-5'-O-triphosphate) (**Figure 4.16**). RET-based interactions can be utilized to monitor the binding of other ligands. This donor-acceptor pair (Trp and mantATP), being chemically different, constitutes a hetero transfer pair (300). Here, the tryptophans (W54, W151, or W116) serve as donors and mantATP as the acceptor.

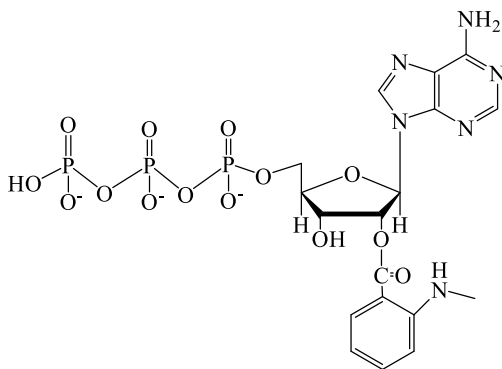


Figure 4.16: Structure of mantATP

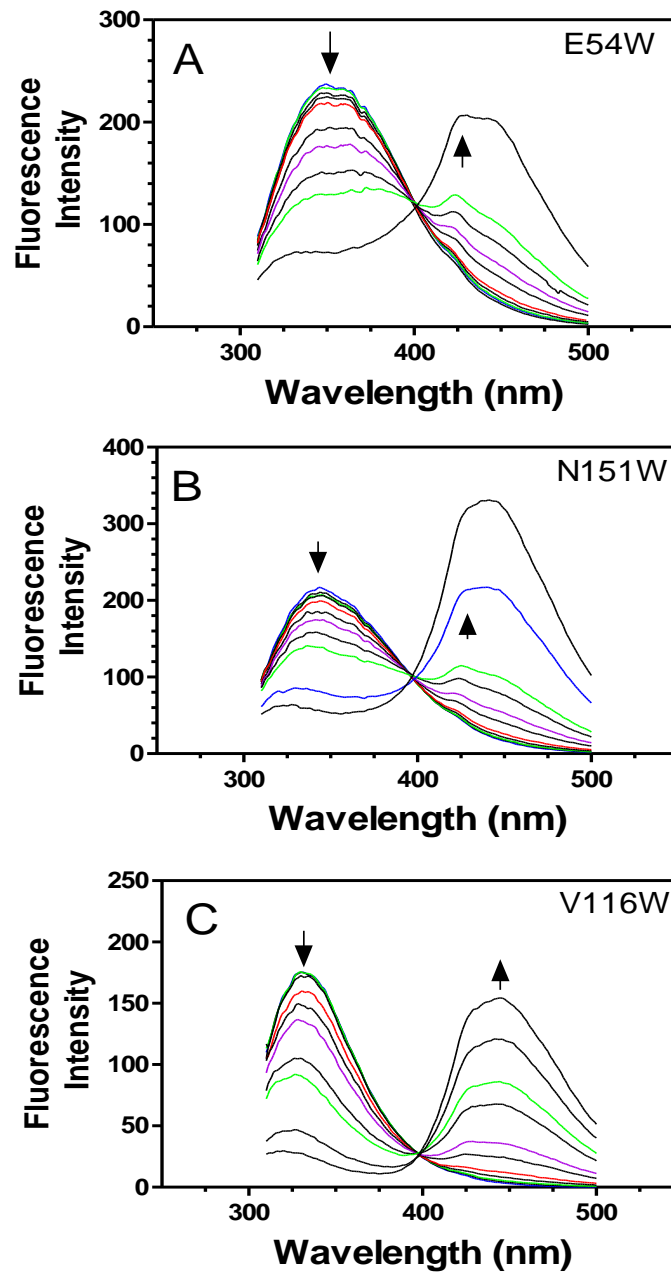


Figure 4.17: MantATP-dependent resonance energy transfer with 10 μ M W54 (A), W151 (B), and W116 (C) in 100 mM Tris-HCl 50 mM KCl, 5 mM MgCl₂, pH 7.6 in a black round bottom 96 well microtitre plates. MantATP concentrations used were 0 – 0.2 mM. Samples were excited at 290 nm. Spectra are representative of triplicate experiments.

All three variants showed differential responses to mantATP binding (**Figure 4.17**). Across the variants, the quenching of tryptophan fluorescence is accompanied by a subsequent fluorescence emission from the acceptor, with emission maxima around 425 nm. The line-shape of Trp emission spectra in all three proteins was different, indicative of different molecular transitions occurring in the different fluorophores as a result of the location and interaction with mantATP.

In addition to the differential Trp emission spectra, each variant also possessed a unique mantATP emission signature. It is also noteworthy that the resulting resonance energy transfer efficiencies across all variants showed similar responses to mantATP (**Figure 4.18**). However, E54W asymptotically approaches an upper limit in transfer efficiency of about 0.7. In contrast, RET efficiency remains essentially linear for N151W and V116W across the range of mantATP concentrations evaluated.

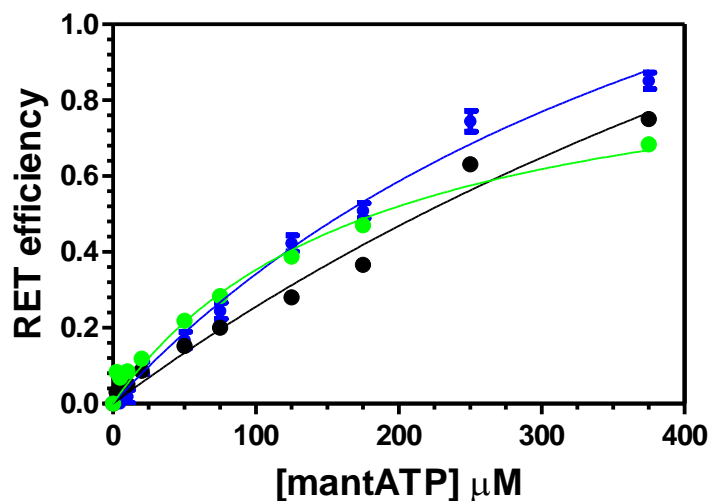


Figure 4.18: Resonance energy transfer efficiencies between mantATP and E54W (●), N151W (●) and V116W (●).

In order to determine possible interactions or the possibility of a competition between mantATP and Compound 1, we evaluated the effect of Compound 1 on the RET response of mantATP. Enzyme-Compound 1 complexes were preformed by incubating each variant with 10 μ M Compound 1. The titration of the equilibrated binary (EI) complex with mantATP produced additional quenching after the formation of the ternary complex (**Figure 4.19**). Only E54W showed a red shift to the free enzyme. No shifts were observed with N151W and V116W. There was no change in apparent K_D s for mantATP with and without Compound 1 across all three variants (data not shown). Suggesting mantATP and Compound 1 do not compete.

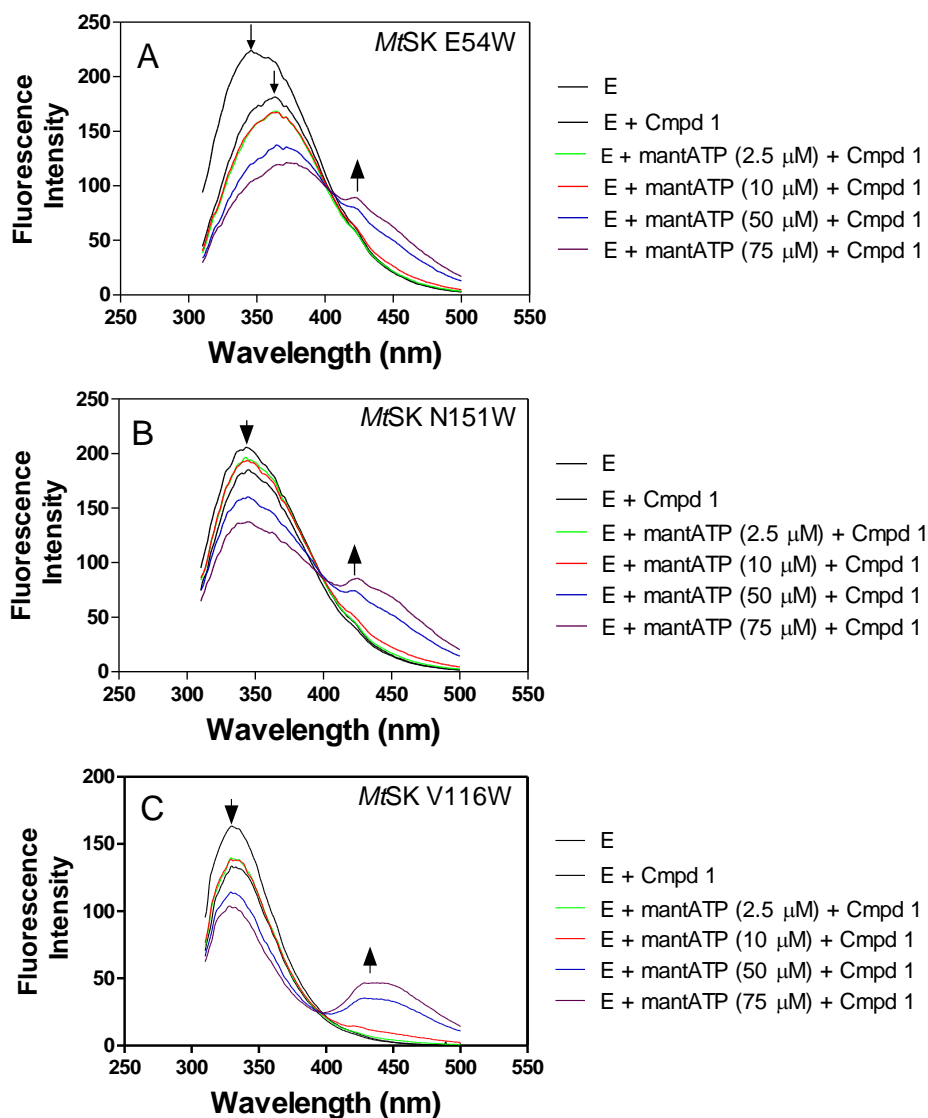


Figure 4.19: Compound 1 vs mantATP competitive assays with 10 μM E54W (panel A), N151W (panel B), and V116W (panel C). Samples were preincubated with 10 μM Compound 1 for 20 min after which mantATP was added to the EI complex, before excitation at 290 nm. All reactions were run at room temperature in 100 mM Tris, pH 7.6, 50 mM KCl, 5 mM MgCl_2 . Spectra are representative of triplicate experiments.

4.6 Discussion and Conclusions

We report here an application of targeted intrinsic fluorescence approach on *MtSK*. Wild-type *MtSK* is devoid of tryptophan. Intrinsic fluorescence was imparted via site-directed mutagenesis on key regions of the protein, substituting nonconserved residues or residues in positions which bear a Trp in shikimate kinases from other organisms. These factors were to increase the chances of a larger, aromatic group to be accommodated by *MtSK*. The target sites for substitution include E54 on the shikimate binding domain, N151 on the adenine binding domain and V116 on the lid domain. The substitution at these positions has the potential to report on binding events on the respective domains in which the fluorophores are located.

Together with the wild-type *MtSK*, all variants upon expression showed N-terminal methionine modification (400–403), a common post-translational modification in *E. coli* and in specifically in proteins with a small amino acid in the subsequent position (403), in the case of *MtSK*, an alanine. This results in two protein populations; one with and one without the N-terminal methionine. All three variants possessed comparable catalytic efficiency to the wild-type, making them suitable candidates for evaluating and reporting binding events on *MtSK*. In contrast to the wild-type which bears no Trp, all variants show characteristic emission spectra, though with differing emission maxima to that of free Trp. Again, indicating that these can report differentially on ligand binding to the enzymes.

Large conformational changes as a result of ATP binding (84,91,93) to the enzyme increase the proximity between the different domains thus increasing the potential of energy transfer. The closure of the lid domain and the inward movement of the adenine and shikimate binding domains decreases the distance between quencher and fluorophore resulting in

fluorescence from regions of the enzyme typically further away for the adenine binding domain. This, however, could make potential applications in ATP sensing systems and also serve as the basis of the development of resonance energy transfer pairs to monitor interdomain interactions and interactions with other ligands.

The structural and electronic predisposition of shikimate may account for its inability to act as an effective quencher. But, the occurrence of conformational shifts in kinases cannot be overstated. The moderate change in V116W fluorescence suggests a possible substrate-induced conformational change. Previous reports (70,98,404–409) implicate the lid domain in interactions with ligands and also how lid closure is essential for catalysis. The conformational flexibility and sensitivity of V116W support previously stated applications as a sensor.

Comparing overall or ‘global’ rotational (motion of shikimate kinase) and ‘local’ probe (tryptophan) motion, the latter comprises any mobility of the tryptophanyl residue far exceeding rotational movements of the entire enzyme. ‘Local’ motions in shikimate kinase would include domain motions or movements in shikimate (W54), nucleotide (W151) or lid (W116) domains. A stark contrast to other systems using noncovalent probes like NADH and porphyrins is the reduction in probe mobility resulting from higher binding energies and multiple interactions. Contradistinctively, movement in covalent probes like tyrosines and tryptophans are typically limited by the enzymes’ structure (410). Consistent with higher anisotropy values observed in proteins with flexible tags (411), the changes in anisotropy in V116W variant support evidence from crystallography that the lid domain is conformationally flexible (93,318,388). This is supported by the lack of assignable electron density to the residues of the lid domain of the free enzyme (388). Further, it supports our initial hypothesis that moderate changes in V116W

fluorescence when shikimate is titrated against the variant is as a result of substrate-induced conformational changes.

These variants could serve as potential mechanistic tools in evaluating the 'on' and 'off' rate constants of ligands and also probe binding event using kinetic techniques like stopped-flow fluorimetry or transient anisotropy. In shikimate kinase, the lid closure and substrate binding occur as separate events (93). Our data show that in the binary complexes of shikimate kinase, there exist conformational changes in the shikimate/ATP and lid domains. Substantial conformational changes occur in the lid domain both in the binary or ternary complex. The unique properties of these variants make them suitable for investigating inhibitor mechanism of action.

As previously stated, intrinsic fluorescence can be applied or used in developing RET-based systems to investigate interactions between ligands. All three variants showed different fluorescent spectral characteristics with the mantATP. Each protein had a unique spectral signature indicative of the environment of the fluorophore. This may seem counter-intuitive to the Franck-Codon principle stating that molecular transitions from equilibrium excited state to Franck-Codon ground state is not a unique transition but a combination of substates of vibrations and rotations of the electronic ground state. This implies fluorescence spectrum will show some general features (similar to absorbance) like peak broadening, asymmetry and possibly reveal vibrational information via the appearance of peaks and shoulders (300). However, though this holds true, these three variants show unique spectral features, representative of the environment or location of the fluorophore. They do not conform or obey the Franck-Codon principle even though it is essentially the same fluorophore. N151W and E54W show more peak broadening in

the tryptophanyl emission spectra in contrast to a rather narrow peak observed in V116W. This difference hints on the differences in their vibrational relaxation mechanisms, with a broad spectrum suggestion a transfer of vibrational energy to W151 and W54 vibrational modes while the narrow spectrum of W116 might be as a result of intramolecular energy distribution (412). the asymmetric distribution (413) or small development of shoulders in E54W and N151W spectra could be an indication of a likely similar orientation of the fluorophores to the mant group or an unresolved vibronic structure (414). It could also be suggested that N151W spectrum follows a Lorentzian distribution, indicating an uncertainty broadening resulting from short emission lifetimes (414).

The development of tools to accelerate initial screening processes and to replace more cumbersome and time-consuming tradition methods is quintessential. Thus, this panel of variants developed shows that intrinsic fluorescence can serve as a promising tool to probe and evaluate enzyme and inhibitor mechanism of action in fewer steps in contrast to traditional screening procedures. Together with traditional and fluorimetric methods, Compound 1 has shown preferential binding at or near the shikimate binding arm of *MtSK* with little or no interference with ATP binding. This panel of variants could also be used for screening ATP competitive inhibitors in the initial stages of drug screening, curbing valuable time spent on evaluating rather toxic compounds to host metabolism. Together, these variants show potential towards the development of high throughput based assays for drug development and screening.

Chapter 5

Summary

Tb is not a relic of the 19th century. It is still a persistent public health problem, and strikingly, it is one of the top ten causes of death, alongside diabetes and cardiovascular diseases (120). This bacterium has evolved in many ways to evade the immune system and antibiotics, resulting in resistance to first-line (i.e., MDR strains) and second-line (i.e., XDR strains) antitubercular agents. Unfortunately, the number of FDA-approved drugs against this prolific pathogen has been at a near stand-still with only one approved in the last five decades (12,316,317,325). The emergence and expanding prevalence of MDR and XDR strains coupled with lack of novel treatment options have created a profound need for new antitubercular agents.

Due to the absence of a mammalian analogue, the shikimate pathway and its enzymes represent a promising and target-rich setting for the discovery of the antitubercular drugs that are so desperately needed. Shikimate kinase (*MtSK* in *M. tuberculosis*) catalyzes the fifth step of this pathway. Based on its structural similarity to enzymes like adenylate kinase, it is classified as a nucleoside monophosphate kinase. It follows a random sequential mechanism (389) with ATP and shikimate as substrates. Substrate binding results in large conformational changes in the ATP-binding, shikimate-binding, and lid domains (93).

Targeting enzymes in pathways with no mammalian counterparts offers a greater advantage in the identification of drug candidates with minimal cross-reactivity with host

systems. *MtSK* fits in this category and is an excellent target for the development of new antibacterials. Still, simply targeting *MtSK* without elucidating the mechanisms of action of identified inhibitors and potential drug candidates overlooks a likely route to the unintended development of cross-reacting agents. With *MtSK* and most other enzymes of the shikimate pathway, one substrate is entirely absent from human metabolism (e.g., shikimate, dehydroquinone, etc.), but the other is nothing short of ubiquitous (e.g., ATP, NADH, etc.). Thus, to minimize the potential for cross-reactivity, it is essential that inhibition mechanisms avoid targeting the aspects of catalysis that depend on the ubiquitous substrate. Specifically, successful drug development is far more likely to emerge from leads that address shikimate- rather than ATP-dependent aspects of *MtSK* catalysis; inhibitors that mimic ATP interaction with *MtSK* are more likely to collaterally interfere with host kinases instead of mainly targeting the pathogen. This is critical since, as previously discussed, the nucleotide binding arm of kinases possesses high structural similarity. Inhibitors that compete with ATP binding would potentially have severe adverse effects, cross-reacting with closely related host kinases like adenylate kinase, gluconate kinase or pantothenate kinase and may even extend to more distantly related protein kinases. Thus, inhibitors targeting the shikimate-binding arm would be most effective due to the non-ubiquitous nature of this substrate. This, together with the urgent need for new anti-tubercular agents requires new methods of rapid screening of inhibitors against *MtSK* and evaluating their mode of action.

The data presented in this dissertation highlights the essentiality of detailed mechanistic investigation of *MtSK* inhibitors and couples it with the need for new approaches that would accelerate preliminary drug discovery stages and screen out ATP-based inhibition mechanisms. A substantial benefit is realized in minimizing the time, labor, and cost that accrue with the

pursuit of dead ends. We present here the first report on mass spectrometric characterization of marine sponge metabolites (manzamine alkaloids and ilimaquinone). This report elucidates the detailed mechanism of action of these classes of compounds. It showed that the manzamines followed a mixed-type, slow onset inhibition with 6-cyclohexamidemanzamine being the only tight binder with superior inhibitory properties. We also present a detailed kinetic profile of the non-specific, irreversible inhibitor, ilimaquinone. This report highlights and cautions on the subsequent use of ilimaquinone as a drug candidate. Presented here is an intrinsic fluorescence approach for both screening and mechanistic investigation of inhibitors. This approach is not only limited to evaluating inhibitors but can be used to investigate enzyme mechanisms. Strategic fluorescence impartation offers the advantage of time, material and cost over traditional mechanistic methods.

Research findings

The manzamine alkaloids (manzamine A, 8-hydroxymanzamine A, manzamine E, manzamine F, 6-deoxymanzamine X, and 6-cyclohexamidomanzamine A) were all identified as inhibitors of *MtSK*. All were reversible, but in each case, slow-onset or time-dependent inhibition was observed. These compounds were discovered to conform to a two-step mechanism with initial formation of an EI complex followed by slow isomerization to a higher affinity EI* complex. Steady-state kinetic evaluation by LC-MS revealed initial EI complex formation conformed to mixed-noncompetitive model of inhibition with respect to both *MtSK* substrates, shikimate, and ATP. With all six manzamines, slow binding inhibition was observed, but only 6-cyclohexamidomanzamine formed a tightly bound EI* complex was also observed. 6-cyclohexamidomanzamine A stood out as a superior inhibitor with inhibition constants for all

enzyme forms around 4 – 60 fold lower than those of the other manzamines. Taking into account the rate constants for the transition of EI to EI* and back, a K_I^* value of 60 nM was estimated for 6-cyclohexamidomanzamine A.

Docking studies performed with 6-cyclohexamidomanzamine A showed two poses that differed in the positioning of the pyridoindole-cyclohexamide moiety within the *MtSK* structure. Pose 1 was most favorable, and showed the 6-cyclohexamide ring extending deep into the shikimate binding pocket and stabilized through a series of non-polar interactions with surrounding residues. In pose 2 the pyridoindole-hexamido moiety was bound close to the surface with the cyclohexamide group overlapping with ADP. Together with steady-state kinetic data, this provides one possible explanation for the observed two-step binding mechanism, and how the inhibitor changes conformation to achieve a more effective pose (pose 1) which represents the EI*. This potency and uniqueness of 6-cyclohexamidomanzamine are attributed to pose 1, as it overlays with the unique shikimate-binding site, competing with shikimate. This property offers a remarkable advantage of this inhibitor over the others and would potentially minimize cross-reactivity with host systems as it forms a tightly-bound pose when competing with shikimate. The change in orientation of the pyridoindole-cyclohexamide moiety from a region closer to the surface to a deeper site may induce conformational changes in *MtSK* structure over time. The cyclohexamide group of 6-cyclohexamidomanzamine provides a possible explanation for its superior inhibitor activity, as it extends into the shikimate binding arm of *MtSK*, inhibiting the binding of shikimate. Its ability to switch conformations to a tightly bound complex with the cyclohexamide group buried in the unique shikimate-binding arm makes it an ideal candidate for the development of novel anti *MtSK* agents with minimal cross-reactivity to

host systems. The structure and mechanism of this class of compounds indicate that they may be used as scaffolds for the development of novel anti tubercular agents.

The research described in this dissertation also elucidates the mechanism of *MtSK* inhibition by ilimaquinone (IQ), a marine-based sponge metabolite. IQ-dependent inhibition contrasts starkly with the manzamines, first, in that it inhibits *MtSK* through covalent modification and is, therefore, irreversible. More importantly, IQ targets several residues of the enzyme's P-loop. Not only is this structure part of the ATP binding cleft, it is also a nearly universal structure among kinases, particularly among *MtSK*'s closest relatives, the NMP kinases which are widely distributed in human metabolism. IQ-dependent *MtSK* inactivation followed an apparent second-order rate constant of about $60 \text{ M}^{-1}\text{s}^{-1}$. Together with time-dependent and jump dilution experiments, intact protein mass spectrometry also showed an increase in protein molecular mass corresponding to the addition of 1 and 2 equivalents of IQ. Tandem MS-MS analyses showed several modifications, primarily serines and threonines with evidence of lysine and tyrosine modifications as well. Prominent modification sites were, as mentioned above, P-loop residues (Lys15, Ser 16, and Thr 17) along with Ser 44, Ser 77, Thr 111. Given the substantial number of *MtSK* residues modified following incubation with IQ, the PAINS behavior of IQ was evaluated by reacting the inhibitor with other enzymes PK, LDH, and *MtKatG*. Interestingly, LDH was also modified by IQ, showing a mass difference of 326 Da corresponding to the addition of +1 IQ. Also, at 10 and 100-fold lower IQ concentrations, modifications were also observed, though less prominent as at $100 \mu\text{M}$ IQ. *MtKatG* and PK were unaffected by the inhibitor.

The striking differences in the mechanisms of inhibition by 6-cyclohexamidemanzamine and ilimaquinone clearly illustrate the importance of elucidating inhibitor mechanism of action as opposed to a simple screening for inhibition by IC_{50} analysis. Its promiscuity and propensity for modifying structures universal among kinases (e.g., P-loop residues) ultimately makes ilimaquinone an undesirable candidate for drug development. In contrast, 6-cyclohexamido manzamine A appears to exploit the shikimate binding pocket, and this interaction points to strategies whereby the molecule may be modified to more effectively capitalize on this binding mode. The downside to these extensive characterizations of *MtSK* inhibition mechanism is their time- and resource-intensive nature. Drug discovery and development using promising targets like *MtSK* would be greatly aided by rapid procedures to make these same kinds of mechanistic determinations.

A rapid approach to drug screening and mechanistic evaluation of inhibitors was designed by imparting intrinsic fluorescence on key regions *MtSK*, to increase throughput for identifying inhibition mechanisms likely to be advantageous for further drug development and excluding those likely to result in dead ends. All the variants generated (E54W, L119W, L120W, V116W, N151W, L10W) showed masses (LC-MS analyses) consistent with the intended substitution and each showed characteristic tryptophan emission spectra absent from the wild-type enzyme. Of the variants generated, three (E54W, V116W, and N151W) were catalytically active and showed kinetic parameters similar to the wild-type enzyme. Importantly, each variant covered an important region of the protein in the context of catalytic events. Accordingly, these variants showed differential sensitivities to substrate binding and were able to probe conformational changes within the protein upon substrate binding.

This panel of Trp-bearing *MtSK* variants was used to evaluate so-called Compound 1, a molecule previously characterized as a noncompetitive inhibitor of shikimate kinase. All three variants showed a hyperbolic decrease in fluorescence intensity, with K_{DS} around $[E]_T$. E54W was most sensitive to the inhibitor. Supporting traditional inhibition studies, fluorescence studies indicated that the inhibitor binds in the vicinity of W54. This was also corroborated by competition experiments and the occurrence of a 15 nm red shift only in E54W.

It is essential for this panel of variants to discriminate ATP-competitive inhibitors and also evaluate the mechanism of fluorescent inhibitors. We utilized a fluorescent ATP analogue, mantATP as a competitive inhibitor to ATP and to also represent a fluorescent natural product. Competition experiments of mantATP vs Compound 1 showed no displacement of the inhibitor from the enzyme. This was evident from lack of gain of fluorescence in the ternary complex (E-I-mantATP). However, consistent with previous observations, only the E54W-I, and the E54W-I-mantATP complex showed red shifts. These, indicate that mantATP and Compound 1 do not compete for the same binding site and support previous observations that Compound 1 binds near W54.

This panel of variants has shown great potential towards applications on improving throughput in drug screening and mechanistic investigation. It is now possible to use these variants to investigate binding events with no naturally occurring tryptophanyl fluorophore using techniques like stopped-flow fluorimetry. We determined a similar mode of action of Compound 1, as previously determined (399) using these variants within a short time period and fewer materials than regular traditional techniques. These variants can also be used to screen against ATP competitive inhibitors which pose a greater risk for cross-reactivity and often lead to dead

ends. This transition from traditional methods of evaluating inhibition would enhance throughput and ultimately improve the drug discovery timeline. This is the first report of this approach on *MtSK* inhibitor screens and could be applied to other kinases; all with the potential of not only screening but also provide a cost-effective mechanistic evaluation of natural, synthetic or semisynthetic products.

Future studies and perspectives

Moving forward, fluorescently active variants could be used to determine the rate constants of substrates and inhibitors using stopped-flow fluorimetry. This would provide more mechanistic information, be it the occurrence of single or multiple binding steps or the preferential binding of substrates or inhibitors to the free enzyme or to one or more conformational states. Stopped-flow fluorimetry could also be applied to evaluate competition between substrates and inhibitors using a double mixing approach. Again, this is not only limited to *MtSK* but has potential applications to all kinases and enzymes out of the kinase fold.

Also, though intrinsic fluorescence reported here makes use of natural occurring tryptophan, the lifetime and quantum yield of Trp are very low. These could be enhanced by the use of unnatural amino acids or their derivatives thereof like coumarin-cysteine, acridonylalanine, cyano-tryptophan (288,415–417) etc. In addition, site-directed spin labeling studies can be performed using methanethiosulfonate, N-(1-oxyl-2,2,6,6-tetramethyl-4-piperidiny) maleimide, iodoacetamide (418–423) etc., to observe changes in radical signals and possibly trapping one or more conformational states of the enzyme at different time points.

In a broader scheme, the impartation of intrinsic fluorescence on *MtSK* could also be applied to the different enzymes of the shikimate pathway, which are all potential targets for

antibacterials and most are bisubstrate enzymes e.g. shikimate dehydrogenase, dehydroquinate synthase. Impartation of intrinsic fluorescence could be used to evaluate potential protein-protein interactions of enzymes in the shikimate pathway. The unique fluorescence signal generated from the interaction of two proteins would provide more information on the uniqueness of the pathway and its enzymes and its possible role in evolution. With the high structural similarity and ubiquity of kinases, this technique can be used to evaluate the effect of different anticancer agents targeting kinases. The nucleotide binding domain of most kinases is very similar. This would accelerate screening against nucleotide competitive inhibitors and reduce off-target toxicity.

Appendix 1

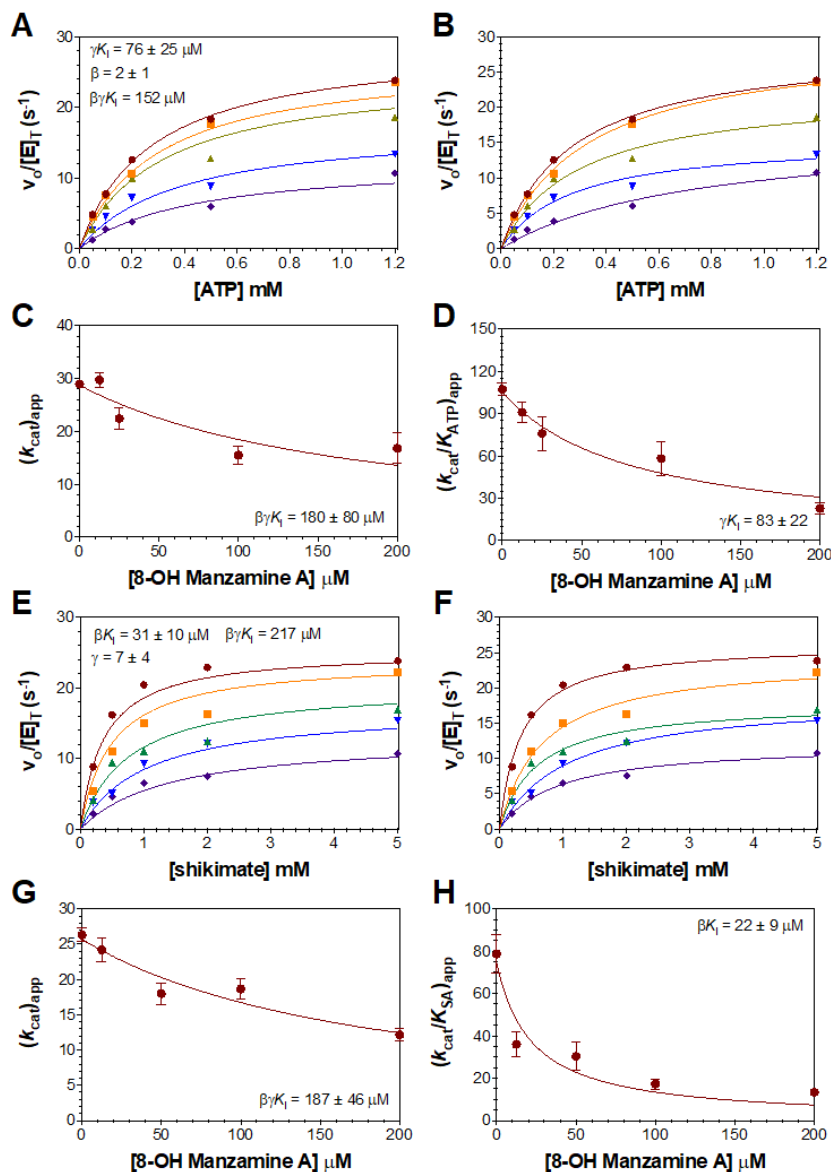


Figure 2.1. Non-linear least-squares analyses of rapid reversible inhibition by 8-hydroxymanzamine A (2). Data acquired varying [ATP] at fixed [SA] (and *vice versa*) were either fit to a global mixed-noncompetitive mechanism of inhibition or as individual Michaelis-Menten curves. Concentrations of **2** evaluated were 0 (●), 12.5 (■), 25 (▲)/50 (△), 100 (▼), and 200 (◆) μM .

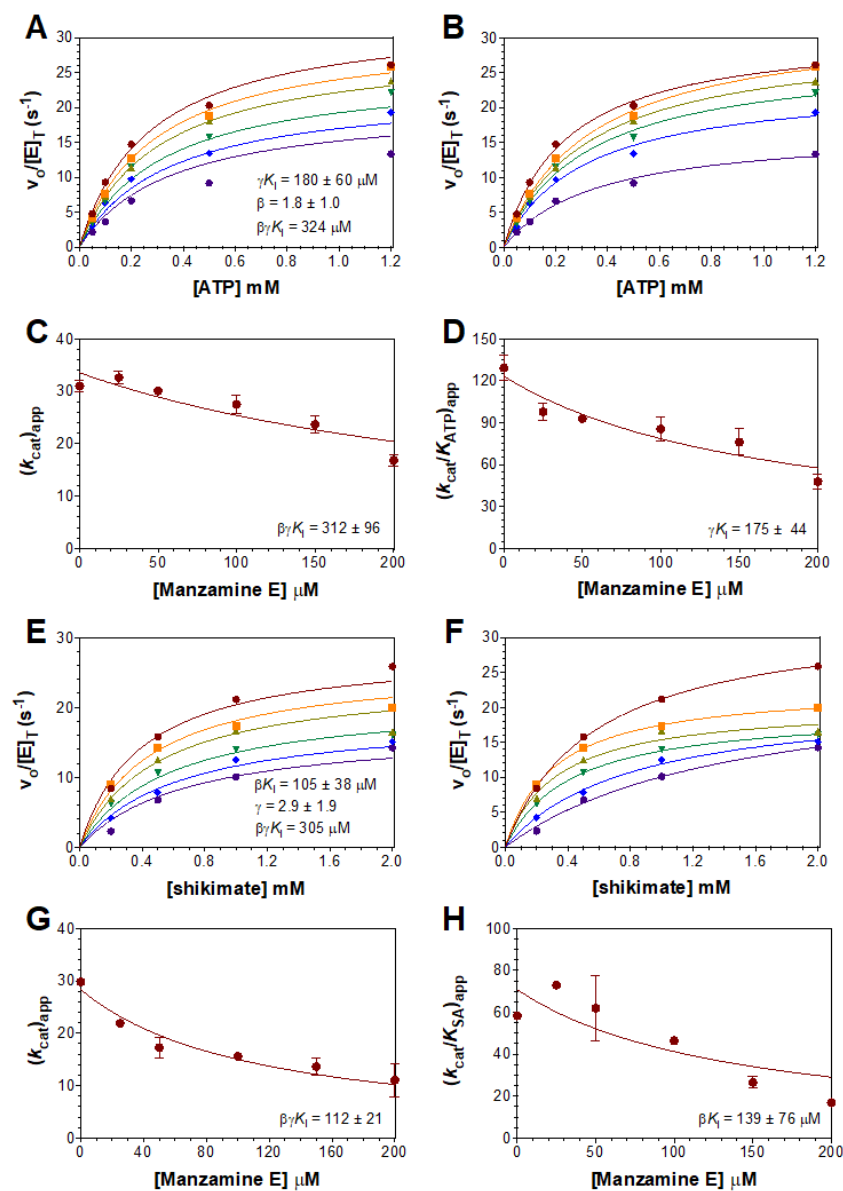


Figure 2.2. Non-linear least-squares analyses of rapid reversible inhibition by manzamine E (3). Data acquired varying [ATP] at fixed [SA] (and *vice versa*) were either fit to a global mixed-noncompetitive mechanism of inhibition or as individual Michaelis-Menten curves. Concentrations of **3** evaluated were 0 (●), 25 (■), 50 (▲), 100 (▼), 150 (◆), and 200 (●) μM .

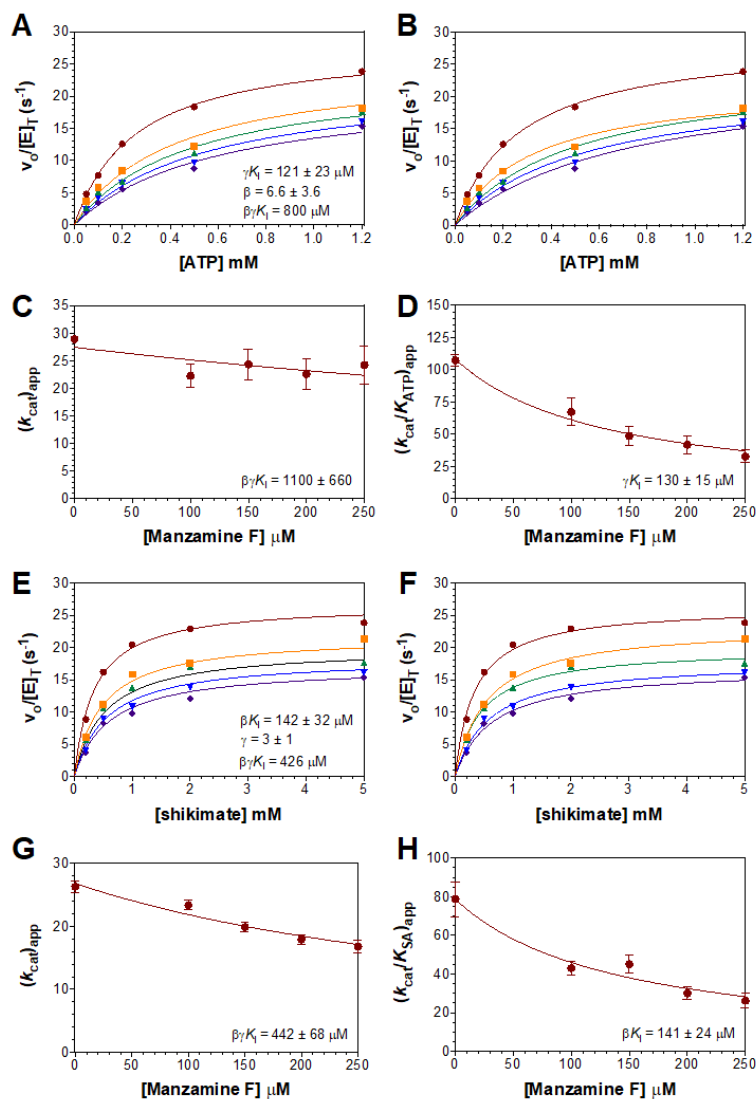


Figure 2.3. Non-linear least-squares analyses of rapid reversible inhibition by manzamine F (4). Data acquired varying [ATP] at fixed [SA] (and *vice versa*) were either fit to a global mixed-noncompetitive mechanism of inhibition or as individual Michaelis-Menten curves. Concentrations of 4 evaluated were 0 (\bullet), 100 (\blacksquare), 150 (\blacktriangle), 200 (\blacktriangledown), and 250 (\blacklozenge) μM .

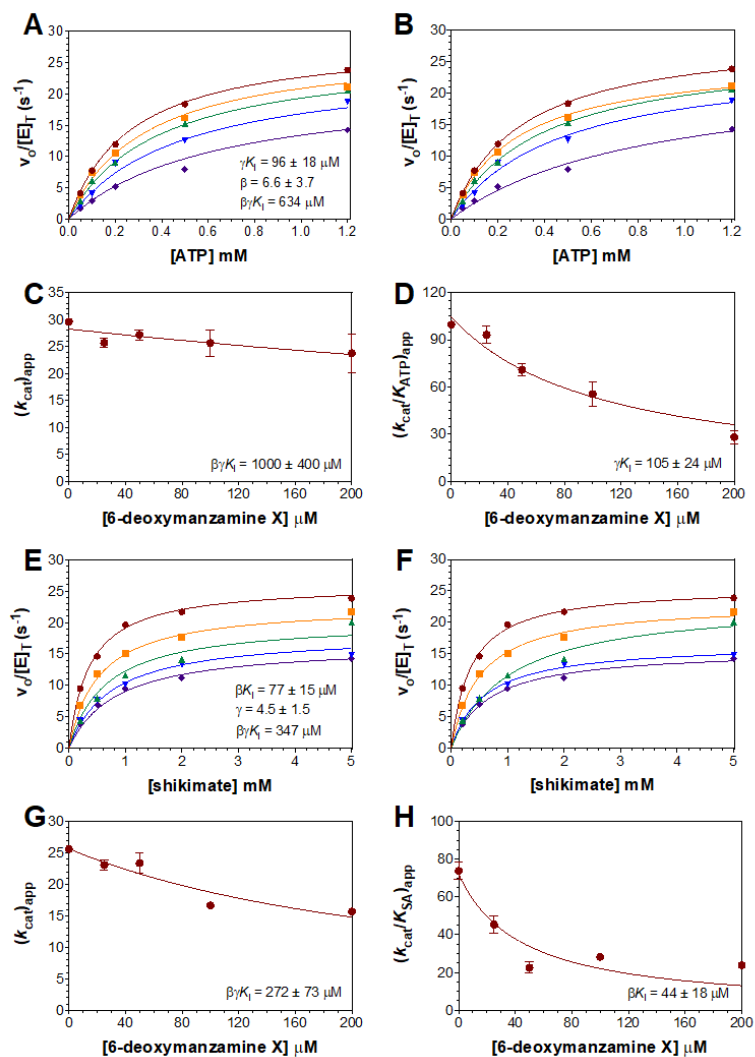


Figure 2.4: Non-linear least-squares analyses of rapid reversible inhibition by deoxymanzamine X (5). Data acquired varying [ATP] at fixed [SA] (and *vice versa*) were either fit to a global mixed-noncompetitive mechanism of inhibition or as individual Michaelis-Menten curves. Concentrations of 5 evaluated were 0 (●), 25 (■), 50 (▲), 100 (▼), and 200 (◆) μM.

Appendix 2

```

[M.tuberculosis]-----MAPKAV 6
[M.abscessus]-----MSPKAV 6
[E.coliSK]-----MAEKRNI 8
[E.coliF11] MGDLPSCGTRNSIEIIFSLTLAISYEVSVHVLRRSLSEAGLSLTNSLSSTKMAEKRNI 60
P32953-----MAEKRNI 8
P32953-----MTQTI 6
[E.faecium]-----MASIL 5
[Y.pestisKIM10+SK1]-----MAEKRNI 8
[Y.pestisKIM10+SK2]-----MTQTI 6
[S.enterica]-----MAEKRNI 8
[B.multivoransCF2]-----MAQARQGS--RFASKLRHTPARL-KQRKPLQARDPHANVF 37
[R.ornithinolytica2-156-04_s1_C1SK1]-----MAEKRNI 8
[R.ornithinolytica2-156-04_s1_C1SK2]-----MTLPI 6
[D.chrysanthemisK]-----MAEKRNI 8
[C.abortusS26/3]-----MNI 4
[P.atrosepticumSCRI1043]-----MTHPI 6
[H.pyloriSK]-----MQHLV 5
[K.pneumoniaSK]-----MAEKRNI 8
[S.aureusSK]-----MNHDKSPII 9
[A.baumanniiSK]-----MKAIEIGGA-LPSKAFETLPNIY 22
↓
[M.tuberculosis] LVALPGSGKSTIGRRLLAKALGVGLLDVVAIEQRTGR---SIADIFATDGEQEFRRIE 62
[M.abscessus] LVGLPGSGKSTIGRRLLAKALGVNVYDIDTGIETEAGR---TIAQIFANDGEPEFRRIE 62
[E.coliSK] LVGPMGAGKSTIGRQLAQQLNMEFYDSDQIEKRTGA---DVGWVFDLEEGEGRDRE 64
[E.coliF11] LVGPMGAGKSTIGRQLAQQLNMEFYDSDQIEKRTGA---DVGWVFDLEEGEGRDRE 116
P32953 LVGPMGAGKSTIGRQLAQQLNMEFFDSDQIEERTGA---DVGWVFDVEEGEGRDRE 64
P32953 MVGARGAGKTTIGKALAQAALGYRFVDTDLFMQOTSQM---TVAEVVESEGWDGFRLES 62
[E.faecium] LIGFMGAGKTTIGKGLAQRLLQKEYVDLDTKIEEHIQL---STAEYFHYGKSFRRVES 61
[Y.pestisKIM10+SK1] LVGPMGAGKSTIGRQLAQQLNMEFFDSDQIEERTGA---DVGWVFDVEEGEGRDRE 64
[Y.pestisKIM10+SK2] MVGARGAGKTTIGKALAQAALGYRFVDTDLFMQOTSQM---TVAEVVESEGWDGFRLES 62
[S.enterica] LVGPMGAGKSTIGRQLAQQLNMEFYDSDQIEKRTGA---DVGWVFDVEGEDGFRNRE 64
[B.multivoransCF2] FVGLMGAGKTTGRAVARRLDRTFFDSDHEIEARTGA---RIPVIFELEGEAGFRDRE 93
[R.ornithinolytica2-156-04_s1_C1SK1] LVGPMGAGKSTIGRQLAQQLNMEFYDSDQIEKRTGA---DVGWVFDVEGEDGFRDRE 64
[R.ornithinolytica2-156-04_s1_C1SK2] LIGPRGCGKTTIGHALARARHYQFTDIDHALQEREQR---TVATIVEQEGLWARFRELES 62
[D.chrysanthemisK] LVGPMGAGKSTIGRQLAQQLNMEFFDSDQIEERTGA---DVGWVFDVEEGEGRDRE 64
[C.abortusS26/3] LCGLPTVGKTLFGKALAKYLSVFFFDVDDLIVSNYGNKLYPSACEIFQAIGEQEFTKLEI 64
[P.atrosepticumSCRI1043] MVGARGCGKTTVGHQLAQAALGYDFVDTDLFMQOTTNM---TVADVVAQEGWHGFRQRES 62
[H.pyloriSK] LIGFMGSGKSSLAQELGLALKLEVLDIDMIISERVGL---SVREIFEELGEDNFRMFEX 61
[K.pneumoniaSK] LVGPMGAGKSTIGRQLAQQLNMEFYDSDQIEKRTGA---DVGWVFDVEEGEGRDRE 64
[S.aureusSK] LIGFMGTGKSTIGKYVAEQNLSFIDIDSYIEEKYKL---TIPEIFSKHGEQYFRLEF 65
[A.baumanniiSK] LVGPMGAGKTTVGRHLAELGREFLDSDHEIERKRTGA---TIPWIFEKEGEVGFRTRET 78
: . * : . : . * * : . * * *

```

```

[M.tuberculosis          DVVRAA-LADHDGVLSLGGGAVTSPGVRAALAGH-TVVYLEISAAGVRRRTGGNT---VR 117
[M.abscessus            SVIRRA-LDQQDGVVSLGGGAVLTPGVREALAGH-TVVYLEISAAGIRRTGGSV---VR 117
[E.coliSK]              KVINEL-TEKQGIIVLATGGGVSRSRETRNRLSARGVVVYLETTIEKQLARTQRDK---KR 120
[E.coliF11              KVINEL-TEKQGIIVLATGGGVSRSRETRNRLSARGVVVYLETTIEKQLARTQRDK---KR 172
P32953                  KVINEL-TEKQGIIVLATGGGVSRSRETRNRLSARGVVVYLETTIEKQLARTQRDK---KR 120
P32953                  MALQAV--TAPKVIIVATGGGAVLSSENRAFMRDHGRVIVLRASA AVLAKRLAE DPEEAQR 120
[E.faecium              DILRLK--SNEDKVIATGGGIVQSAENRFLKQIPIVLYLEAEADCLVDRIQQDQETS-IR 118
[Y.pestisKIM10+SK1]    KVINEL-TEKQGIIVLATGGGVSRSRETRNRLSARGVVVYLETTIEKQLARTQRDK---KR 120
[Y.pestisKIM10+SK2]    MALQAV--TAPKVIIVATGGGAVLSSENRAFMRDHGRVIVLRASA AVLAKRLAE DPEEAQR 120
[S.enterica             KVINEL-TEKQGIIVLATGGGVSRSRETRNRLSARGVVVYLETTIEKQLARTQRDK---KR 120
[B.multivoransCF2      QMIAEL-TQRENIVLATGGGAVLRAENRACLKNGIVVYLRANPHDLWLRTRKDK---NR 149
[R.ornithinolytica2-156-04_s1_C1SK1] KIINEL-TEKQGIIVLATGGGVSRSRETRNRLSARGVVVYLETTIEKQLARTQRDK---KR 120
[R.ornithinolytica2-156-04_s1_C1SK2] EALKAA--ARPEIVVATGGGII LAEANRQFMRENGVIVLQVPSALIERLEAYFKTEQR 120
[D.chrysanthemisSK]    KVINEL-TEKQGIIVLATGGGVSRSRETRNRLSARGVVVYLETTIEKQLARTQRDK---KR 120
[C.abortusS26/3        AALRSF--CLDHSVVALGGGTIMHQEACDIKHRGTIVLVSLPMAQIRERLRKRL---F 119
[P.atrosepticumSCRI1043] LALQQV--ASNRCIVATGGGMVLAENRRFMHDKGIVIVLHADAE LLAQRLEENPQDNQR 120
[H.pyloriSK]           NLIDELKTIKTIPTHISTGGGIVMHDN---LKLGLTTFVLRKMFELIKRMLNQRERE-KR 116
[K.pneumoniaSK]        KIINEL-TEKQGIIVLATGGGVSRSRETRNRLSARGVVVYLETTIEKQLARTQRDK---KR 120
[S.aureusSK]           TQLQEC--INTADIIATGGGII ESEEA FNFLKNGKNIWLDNCNIDIIYSRINDPF---HR 120
[A.baumanniiSK]        VVINEL-TSRKALVIVATGGGAI TQAPNREFLKQRGIVVYVLYTPVELQLQRTYRK---NR 134
:                       :      :  * * * :      :      :      :      :      :      :      :
:                       :      :      :      :      :      :      :      :      :

[M.tuberculosis          PLLAGPDRAEK-YRALMAKRAPLYRRVATMRVDTNRRRN-----GAVVRHILSR LQ 167
[M.abscessus            PLLAGPDRAEK-YHALMSQRVPLYQEVATIKVNTDRRN-----GAVVRMIVSRLE 167
[E.coliSK]              PLLHVETPPREVLEALANERNPLYEEIADVTIRTDQSA-----KVVANQI IHMLE 171
[E.coliF11              PLLHVETPPREVLEALANERNPLYEEIADVTIRTDQSA-----KVVANQI IHMLE 223
P32953                  PLLQVDEPPREVLEALAKERNPLYEEIADVTIRTDQSA-----KVVANQI IHMLE 171
P32953                  PSLTGKPIVEE-MLDVLASREALYQDVAAHVLDGT-QT-----SLVVEQILQMLT 169
[E.faecium              PLLALGKT-REE-IKALLAQRLSWYEEASATHRIMTNTQT-----EKIIDTIIERIK 167
[Y.pestisKIM10+SK1]    PLLQVDEPPREVLEALAKERNPLYEEIADVTIRTDQSA-----KVVANQI IHMLE 171
[Y.pestisKIM10+SK2]    PSLTGKPIVEE-ILDVLASREALYQDVAAHVLDGT-QT-----SLVVEQILQMLT 169
[S.enterica             PLLQVETPPREVLEALANERNPLYEEIADVTIRTDQSA-----KVVANQI IHMLE 171
[B.multivoransCF2      PLLQVDEPPREVLEALAKERNPLYEEIADVTIRTDQSA-----KVVANQI IHMLE 199
[R.ornithinolytica2-156-04_s1_C1SK1] PLLQVETPPREVLEALADERNPLYEEIADVTIRTDQSA-----KVVANQI IHMLE 171
[R.ornithinolytica2-156-04_s1_C1SK2] PTLTGKPIVDE-VGEVLAQREALYRATAHHIIDAT-AT-----DDVVGHI LALQ 169
[D.chrysanthemisSK]    PLLQVETPPREVLEALAKERNPLYEEIADVTIRTDQSA-----KVVANQI IHMLE 171
[C.abortusS26/3        ERL---KRAPN-MEILIQQRIERMQRICDYHFPDDEVNILDERSLFSACESFTLLNQ-- 173
[P.atrosepticumSCRI1043] PTLTGRPIAEE-MADVLAAREALYRGAHHVIDAS-QT-----DAIVSVVSLKAR 169
[H.pyloriSK]           PLLNDLT---Q-AKELFEKQALYERKNAFFIIDARG-GL-----NNSLKVQLQFIA 162
[K.pneumoniaSK]        PLLQVDEPPREVLEALADERNPLYEEIADVTIRTDQSA-----KVVANQI IHMLE 171
[S.aureusSK]           PNANIKT-IRK-LNDLYCSRILRYNEIAFRKFDSHLLS-----SEIYYELNLIK 169
[A.baumanniiSK]        PLLQVENPEQK-LRDLKIKIRDPLYREVAHYTITETQGA-----RDLAQKILQLIL 184
:                       :      :      :      :      :      :      :      :      :
:                       :      :      :      :      :      :      :      :      :

[M.tuberculosis          VPSPEAAT----- 176
[M.abscessus            NPEGNTGSASSRRRRPRRRPRRRSAGAAAAATQTNTSGTETKERADND 216
[E.coliSK]              SN----- 173
[E.coliF11              SN----- 225
P32953                  SN----- 173
P32953                  GEMVK----- 174
[E.faecium              SI----- 169
[Y.pestisKIM10+SK1]    SN----- 173
[Y.pestisKIM10+SK2]    GEMVK----- 174
[S.enterica             SN----- 173
[B.multivoransCF2      LAGVVAKPLQA----- 210
[R.ornithinolytica2-156-04_s1_C1SK1] SN----- 173
[R.ornithinolytica2-156-04_s1_C1SK2] NVFAPQEAQCVEAARE----- 185
[D.chrysanthemisSK]    SN----- 173
[C.abortusS26/3        ----- 173
[P.atrosepticumSCRI1043] LSAA----- 173
[H.pyloriSK]           ----- 173
[K.pneumoniaSK]        SN----- 173
[S.aureusSK]           ASDQY----- 174
[A.baumanniiSK]        SNKLK----- 189

```

Figure 4.1: Sequence alignment for some shikimate kinases. Regions highlighted represent the shikimate-binding domain (green), the lid domain (yellow) and the nucleotide binding domain (red).

References

1. Orgeur M, Brosch R. Evolution of virulence in the Mycobacterium tuberculosis complex. Vol. 41, *Current Opinion in Microbiology*. 2018. p. 68–75.
2. Prevention C for DC and. CDC | TB | Data and Statistics [Internet]. [cited 2018 Feb 8]. Available from: <https://www.cdc.gov/tb/statistics/default.htm>
3. Dallenga T, Schaible UE. Neutrophils in tuberculosis – first line of defence or booster of disease and targets for host directed therapy? *Pathog Dis*. 2016 Feb 22;74(3):ftw012.
4. Amulic B, Cazalet C, Hayes GL, Metzler KD, Zychlinsky A. Neutrophil Function: From Mechanisms to Disease. *Annu Rev Immunol*. 2012 Apr 23;30(1):459–89.
5. Guirado E, Schlesinger LS, Kaplan G. Macrophages in tuberculosis: friend or foe. *Semin Immunopathol*. 2013 Sep;35(5):563–83.
6. Weiss G, Schaible UE. Macrophage defense mechanisms against intracellular bacteria. *Immunol Rev*. 2015 Mar;264(1):182–203.
7. Prevention C for DC and. CDC | TB | Basic TB Facts | Latent TB Infection and TB Disease [Internet]. [cited 2018 Feb 8]. Available from: <https://www.cdc.gov/tb/topic/basics/tbinfectiondisease.htm>
8. Ker, B, Ortmann, J, Migliori, G. B, Sotgiu, G, Muetterlein, R, Centis, R, Hoffmann, H, Kirsten, D, Schaberg, T, Ruesch-gerdes, S, & Lange, C. Multidrug- and extensively drug-resistant tuberculosis, Germany. *Emerging Infectious Diseases* (2008). , 14(11) 1700-6. No Title.
9. Almeida Da Silva P. E & PJC. Molecular basis and mechanisms of drug resistance in Mycobacterium tuberculosis: classical and new drugs. *J Antimicrob Chemother*. 2011;66(7):1417–30.
10. Espinal M a., Laszlo A, Simonsen L, Boulahbal F, Kim SJ, Reniero A, et al. Global Trends in Resistance to Antituberculosis Drugs. *N Engl J Med*. 2001;344(17):1294–303.
11. CDC. Fact Sheets | Drug-Resistant TB | Extensively Drug-Resistant Tuberculosis (XDR TB) | TB | CDC [Internet]. CDC Website. 2016 [cited 2018 May 10]. Available from: <https://www.cdc.gov/tb/publications/factsheets/drtb/xdrtb.htm>
12. Prevention C for DC and. CDC | TB | Fact Sheets | Treatment of Multidrug-Resistant

- Tuberculosis: Bedaquiline [Internet]. [cited 2018 Feb 8]. Available from: <https://www.cdc.gov/tb/publications/factsheets/treatment/bedaquiline.htm>
13. Knowles JR. Enzyme-Catalyzed Phosphoryl Transfer Reactions. *Annu Rev Biochem.* 1980 Jun;49(1):877–919.
 14. Westheimer F. Why nature chose phosphates. *Science* (80-). 1987 Mar 6;235(4793):1173–8.
 15. Cleland WW, Hengge AC. Enzymatic mechanisms of phosphate and sulfate transfer. Vol. 106, *Chemical Reviews.* 2006. p. 3252–78.
 16. Lassila JK, Zalatan JG, Herschlag D. Biological Phosphoryl-Transfer Reactions: Understanding Mechanism and Catalysis. *Annu Rev Biochem.* 2011 Jul 7;80(1):669–702.
 17. Allen KN, Dunaway-Mariano D. Phosphoryl group transfer: Evolution of a catalytic scaffold. Vol. 29, *Trends in Biochemical Sciences.* 2004. p. 495–503.
 18. Hengge AC. Mechanistic studies on enzyme-catalyzed phosphoryl transfer. Vol. 40, *Advances in Physical Organic Chemistry.* 2005. p. 49–108.
 19. Sträter N, Lipscomb WN, Klabunde T, Krebs B. Two-Metal Ion Catalysis in Enzymatic Acyl- and Phosphoryl-Transfer Reactions. *Angew Chemie Int Ed English.* 1996 Oct 1;35(18):2024–55.
 20. Prado V, Lence E, Vallejo JA, Beceiro A, Thompson P, Hawkins AR, et al. Study of the Phosphoryl-Transfer Mechanism of Shikimate Kinase by NMR Spectroscopy. *Chem - A Eur J.* 2016;22(8):2758–68.
 21. Shchemelinin I, Šefc L, Nečas E. Protein kinases, their function and implication in cancer and other diseases. *Folia Biol (Praha).* 2006;52(3):81–101.
 22. García-Aranda M, Redondo M. Protein Kinase Targets in Breast Cancer. *Int J Mol Sci.* 2017 Nov 27;18(12):2543.
 23. Cheetham GMT. Novel protein kinases and molecular mechanisms of autoinhibition. Vol. 14, *Current Opinion in Structural Biology.* 2004. p. 700–5.
 24. Kondapalli L, Soltani K, Lacouture ME. The promise of molecular targeted therapies: Protein kinase inhibitors in the treatment of cutaneous malignancies. Vol. 53, *Journal of the American Academy of Dermatology.* 2005. p. 291–302.
 25. Knighton DR, Zheng JH, Ten Eyck LF, Ashford VA, Xuong NH, Taylor SS, et al. Crystal structure of the catalytic subunit of cyclic adenosine monophosphate-dependent protein kinase. *Science.* 1991;253(5018):407–14.
 26. Huse M, Kuriyan J. The conformational plasticity of protein kinases. Vol. 109, *Cell.* 2002.

p. 275–82.

27. Nolen B, Taylor S, Ghosh G. Regulation of protein kinases: Controlling activity through activation segment conformation. Vol. 15, *Molecular Cell*. 2004. p. 661–75.
28. Eswaran J, Bernad A, Ligos JM, Guinea B, Debreczeni JÉ, Sobott F, et al. Structure of the Human Protein Kinase MPSK1 Reveals an Atypical Activation Loop Architecture. *Structure*. 2008;16(1):115–24.
29. Eswaran J, Patnaik D, Filippakopoulos P, Wang F, Stein RL, Murray JW, et al. Structure and functional characterization of the atypical human kinase haspin. *Proc Natl Acad Sci U S A*. 2009;106(48):20198–203.
30. Zheng J, Trafny EA, Knighton DR, Xuong N, Taylor SS, Ten Eyck LF, et al. 2.2 Å refined crystal structure of the catalytic subunit of cAMP-dependent protein kinase complexed with MnATP and a peptide inhibitor. *Acta Crystallogr Sect D Biol Crystallogr*. 1993 May 1;49(3):362–5.
31. Endicott JA, Noble MEM, Johnson LN. The Structural Basis for Control of Eukaryotic Protein Kinases. *Annu Rev Biochem*. 2012;81(1):587–613.
32. Bossemeyer D, Engh RA, Kinzel V, Ponstingl H, Huber R. Phosphotransferase and substrate binding mechanism of the cAMP-dependent protein kinase catalytic subunit from porcine heart as deduced from the 2.0 Å structure of the complex with Mn²⁺ adenylyl imidodiphosphate and inhibitor peptide PKI(5-24). *EMBO J*. 1993;12:849–59.
33. Thorsell AG, Uppenberg J, Hogbom M, Ogg D, Arrowsmith C, Berglund H, et al. Structure of Human Phosphatidylinositol-4-phosphate 5-kinase, type II, gamma. *TO BE Publ*.
34. Herzberg O, Chen CC, Liu S, Tempczyk A, Howard A, Wei M, et al. Pyruvate site of pyruvate phosphate dikinase: crystal structure of the enzyme-phosphonopyruvate complex, and mutant analysis. *Biochemistry*. 2002;41:780–7.
35. Hartmann MD, Bourenkov GP, Oberschall A, Strizhov N BH. 2IYZ: Shikimate Kinase From Mycobacterium Tuberculosis In Complex With Shikimate-3-Phosphate And Adp - NCBI structure. *J Mol Biol*. 2006;364:411–23.
36. Tari LW, Matte A, Pugazhenti U, Goldie H, Delbaere LT. Snapshot of an enzyme reaction intermediate in the structure of the ATP-Mg²⁺-oxalate ternary complex of *Escherichia coli* PEP carboxykinase. *NatStructMolBiol*. 1996;3:355–63.
37. Roychowdhury A, Mukherjee S, Dutta D, Das AK. Structure based functional analysis of Staphylococcal Phosphoglycerate kinase. *TO BE Publ*.
38. Robin AY, Cobessi D, Curien G, Robert-Genthon M, Ferrer J-L, Dumas R. A new mode of dimerization of allosteric enzymes with ACT domains revealed by the crystal structure

- of the aspartate kinase from Cyanobacteria. *JMolBiol.* 2010;399:283–93.
39. Riley-Lovingshimer MR, Ronning DR, Sacchettini JC, Reinhart GD. Reversible Ligand-Induced Dissociation of a Tryptophan-Shift Mutant of Phosphofructokinase from *Bacillus stearothermophilus*. *Biochemistry.* 2002;41:12967–74.
 40. Petit P, Antoine M, Ferry G, Boutin JA, Lagarde A, Gluais L, et al. The active conformation of human glucokinase is not altered by allosteric activators. *Acta Crystallogr, Sect D.* 2011;67:929–35.
 41. R.HARINARAYANA, K.NARAYANA JS. Theoretical Model - 1LG3: THEORETICAL STRUCTURE OF HUMAN-CYCLIN DEPENDENT KINASE 7 TITLE 2 (CDK7) [Internet]. [cited 2018 May 11]. Available from: <https://www.rcsb.org/structure/removed/1lg3>
 42. Schwarzenbacher R, McMullan D, Krishna SS, Xu Q, Miller MD, Canaves JM, et al. Crystal structure of a glycerate kinase (TM1585) from *Thermotoga maritima* at 2.70 Å resolution reveals a new fold. *Proteins.* 2006;65:243–8.
 43. Strub M-P, Hoh F, Sanchez J-F, Strub JM, Bock A, Aumelas A, et al. Selenomethionine and Selenocysteine Double Labeling Strategy for Crystallographic Phasing. *Structure.* 2003;11:1359–67.
 44. Blaszczyk J, Li Y, Shi G, Yan H, Ji X. Dynamic Roles of Arginine Residues 82 and 92 of *Escherichia coli* 6-Hydroxymethyl-7,8-dihydropterin Pyrophosphokinase: Crystallographic Studies. *Biochemistry.* 2003;42:1573–80.
 45. Gattis JL, Ruben E, Fenley MO, Ellington WR, Chapman MS. The active site cysteine of arginine kinase: structural and functional analysis of partially active mutants. *Biochemistry.* 2004;43:8680–9.
 46. Cai Y, Su M, Ahmad A, Hu X, Sang J, Kong L, et al. Conformational dynamics of the essential sensor histidine kinase WalK. *Acta Crystallogr D Struct Biol.* 2017;73:793–803.
 47. Nishimasu H, Fushinobu S, Shoun H, Wakagi T. Crystal structures of an ATP-dependent hexokinase with broad substrate specificity from the hyperthermophilic archaeon *Sulfolobus tokodaii*. *JBiolChem.* 2007;282:9923–31.
 48. Rigden DJ, Phillips SE, Michels PA, Fothergill-Gilmore LA. The structure of pyruvate kinase from *Leishmania mexicana* reveals details of the allosteric transition and unusual effector specificity. *JMolBiol.* 1999;291:615–35.
 49. Thoden JB, Holden HM. Molecular Structure of Galactokinase. *JBiolChem.* 2003;278:33305–11.
 50. Abendroth J, Dranow DM, Lorimer DD, Edwards TE. Structure of thiamine-monophosphate kinase from *Acinetobacter baumannii* in complex with AMPPNP. TO BE

Publ.

51. Karthikeyan S, Zhou Q, Mseeh F, Grishin NV, Osterman AL, Zhang H. Crystal Structure of Human Riboflavin Kinase Reveals a Beta Barrel Fold and a Novel Active Site Arch. Structure. 2003;11:265–73.
52. Siebold C, Arnold I, Garcia-Alles LF, Baumann U, Erni B. Crystal Structure of the Citrobacter Freundii Dihydroxyacetone Kinase Reveals an Eight-Stranded Alpha-Helical Barrel ATP-Binding Domain. JBiolChem. 2003;278:48236.
53. Parnell AE, Mordhorst S, Kemper F, Giurrandino M, Prince JP, Schwarzer NJ, et al. Substrate recognition and mechanism revealed by ligand-bound polyphosphate kinase 2 structures. Proc Natl Acad Sci USA. 2018;115:3350–5.
54. Gandini R, Reichenbach T, Tan TC, Divne C. Structural basis for dolichylphosphate mannose biosynthesis. Nat Commun. 2017;8:120–120.
55. Grishin N V. Phosphatidylinositol phosphate kinase: A link between protein kinase and glutathione synthase folds. J Mol Biol. 1999;291(2):239–47.
56. Rossmann MG, Moras D, Olsen KW. Chemical and biological evolution of a nucleotide-binding protein. Nature. 1974;250(5463):194–9.
57. Cheek S, Zhang H, Grishin N V. Sequence and structure classification of kinases. J Mol Biol. 2002 Jul 19;320(4):855–81.
58. Bork P, Sander C, Valencia A. An ATPase domain common to prokaryotic cell cycle proteins, sugar kinases, actin, and hsp70 heat shock proteins. Proc Natl Acad Sci U S A. 1992 Aug 15;89(16):7290–4.
59. Aleshin AE, Kirby C, Liu X, Bourenkov GP, Bartunik HD, Fromm HJ, et al. Crystal structures of mutant monomeric hexokinase I reveal multiple ADP binding sites and conformational changes relevant to allosteric regulation. J Mol Biol. 2000;296(4):1001–15.
60. Arora K, Arora K, Pedersen L, Pedersen L. Glucose Phosphorylation. J Biol Chem. 1991;265(11):6481–8.
61. Larsen TM, Benning MM, Rayment I, Reed GH. Structure of the {Bis}({Mg} Mg^{2+})–{ATP}–{Oxalate} {Complex} of the {Rabbit} {Muscle} {Pyruvate} {Kinase} at 2.1 Å {Resolution}: {ATP} {Binding} over a {Barrel} Mg^{2+} Mg^{2+} . Biochemistry. 1998;37(18):6247–55.
62. Li C, Kappock TJ, Stubbe JA, Weaver TM, Ealick SE. X-ray crystal structure of aminoimidazole ribonucleotide synthetase (PurM), from the Escherichia coli purine biosynthetic pathway at 2.5 Å resolution. Structure. 1999 Sep;7(9):1155–66.

63. Mueller EJ, Oh S, Kavalerchik E, Kappock TJ, Meyer E, Li C, et al. Investigation of the ATP binding site of Escherichia coli aminoimidazole ribonucleotide synthetase using affinity labeling and site-directed mutagenesis. *Biochemistry*. 1999 Aug;38(31):9831–9.
64. Reichard P. Interactions Between Deoxyribonucleotide And DNA Synthesis. *Annu Rev Biochem*. 1988;57(1):349–74.
65. Van Rompay AR, Johansson M, Karlsson A. Phosphorylation of nucleosides and nucleoside analogs by mammalian nucleoside monophosphate kinases. *Pharmacol Ther*. 2000;87(2–3):189–98.
66. Johansson, N.G., Eriksson S. structure-activity relationships for phosphorylation of nucleoside analogs to monophosphates by nucleosides kinases. Vol. 43, *Acta Biochimica Polonica*. 1996. p. 143–60.
67. Van Rompay AR, Johansson M, Karlsson A. Identification of a novel human adenylate kinase. cDNA cloning, expression analysis, chromosome localization and characterization of the recombinant protein. *Eur J Biochem*. 1999 Apr;261(2):509–17.
68. Schneider B, Xu YW, Sellam O, Sarfati R, Janin J, Veron M, et al. Pre-steady state of reaction of nucleoside diphosphate kinase with anti- HIV nucleotides. *J Biol Chem*. 1998 May 8;273(19):11491–7.
69. Scheffzek K, Kliche W, Wiesmüller L, Reinstein J. Crystal structure of the complex of UMP/CMP kinase from Dictyostelium discoideum and the bisubstrate inhibitor P1-(5'-adenosyl) P5-(5'-uridylyl) pentaphosphate (UP5A) and Mg²⁺ at 2.2 Å: Implications for water-mediated specificity. *Biochemistry*. 1996 Jan 30;35(30):9716–27.
70. Gu Y, Reshetnikova L, Li Y, Wu Y, Yan H, Singh S, et al. Crystal structure of shikimate kinase from Mycobacterium tuberculosis reveals the dynamic role of the LID domain in catalysis. *J Mol Biol*. 2002 Jun 7;319(3):779–89.
71. Vonrhein C, Schlauderer GJ, Schulz GE. Movie of the structural changes during a catalytic cycle of nucleoside monophosphate kinases. *Structure*. 1995;3(5):483–90.
72. Panayiotou C, Solaroli N, Johansson M, Karlsson A. Evidence of an intact N-terminal translocation sequence of human mitochondrial adenylate kinase 4. *Int J Biochem Cell Biol*. 2010;42(1):62–9.
73. Dzeja PP, Vitkevicius KT, Redfield MM, Burnett JC, Terzic A. Adenylate Kinase Catalyzed Phosphotransfer in the Myocardium : Increased Contribution in Heart Failure. *Circ Res*. 1999;84(10):1137–43.
74. Bunkoczi G, Filippakopoulos P, Jansson A, Longman E, von Delft F, Edwards A, et al. Structure of Adenylate Kinase 1 in Complex with P1, P4-Di(Adenosine)Tetraphosphate. *TO BE Publ*.

75. Snow C, Qi G, Hayward S. Essential dynamics sampling study of adenylate kinase: Comparison to citrate synthase and implication for the hinge and shear mechanisms of domain motions. *Proteins Struct Funct Genet.* 2007 Feb 13;67(2):325–37.
76. Whitford PC, Gosavi S, Onuchic JN. Conformational transitions in adenylate kinase: Allosteric communication reduces misligation. *J Biol Chem.* 2008 Jan 25;283(4):2042–8.
77. Panayiotou C, Solaroli N, Karlsson A. The many isoforms of human adenylate kinases. *Int J Biochem Cell Biol.* 2014;49(1):75–83.
78. Panayiotou C, Solaroli N, Xu Y, Johansson M, Karlsson A. The characterization of human adenylate kinases 7 and 8 demonstrates differences in kinetic parameters and structural organization among the family of adenylate kinase isoenzymes. *Biochem J.* 2011 Feb 1;433(3):527–34.
79. Panayiotou C, Solaroli N, Xu Y, Johansson M, Karlsson A. The characterization of human adenylate kinases 7 and 8 demonstrates differences in kinetic parameters and structural organization among the family of adenylate kinase isoenzymes. *Biochem J.* 2011;433(3):527–34.
80. Amiri M, Conserva F, Panayiotou C, Karlsson A, Solaroli N. The human adenylate kinase 9 is a nucleoside mono- and diphosphate kinase. *Int J Biochem Cell Biol.* 2013;45(5):925–31.
81. Bucurenci N, Sakamoto H, Briozzo P, Palibroda N, Serina L, Sarfati RS, et al. CMP kinase from *Escherichia coli* is structurally related to other nucleoside monophosphate kinases. *J Biol Chem.* 1996 Feb 2;271(5):2856–62.
82. Gille C, Föhling M, Weyand B, Wieland T, Gille A. Alignment-Annotator web server: Rendering and annotating sequence alignments. *Nucleic Acids Res.* 2014 Jul 1;42(W1):W3–6.
83. Sekulic N, Shuvalova L, Spangenberg O, Konrad M, Lavie A. Structural characterization of the closed conformation of mouse guanylate kinase. *JBiolChem.* 2002;277:30236–43.
84. Pereira JH, De Oliveira JS, Canduri F, Dias MVB, Palma MS, Basso LA, et al. Structure of shikimate kinase from *Mycobacterium tuberculosis* reveals the binding of shikimic acid. *Acta Crystallogr Sect D Biol Crystallogr.* 2004 Dec 1;60(12 II):2310–9.
85. Briozzo P, Golinelli-Pimpaneau B, Gilles AM, Gaucher JF, Burlacu-Miron S, Sakamoto H, et al. Structures of *Escherichia coli* CMP kinase alone and in complex with CDP: a new fold of the nucleoside monophosphate binding domain and insights into cytosine nucleotide specificity. *Structure.* 1998;6:1517–27.
86. Blanco B, Prado V, Lence E, Otero JM, Garcia-Doval C, van Raaij MJ, et al. *Mycobacterium tuberculosis* Shikimate Kinase Inhibitors: Design and Simulation Studies of the Catalytic Turnover. *J Am Chem Soc.* 2013;135(33):12366–76.

87. Faim LM, Dias MVB, Vasconcelos IG, Basso LA, Santos DS, Azevedo WF, et al. Crystal Structure for shikimate kinase from *Mycobacterium tuberculosis* in complex with AMP-PNP. TO BE Publ.
88. Dias MVB, Faím LM, Vasconcelos IB, De Oliveira JS, Basso LA, Santos DS, et al. Effects of the magnesium and chloride ions and shikimate on the structure of shikimate kinase from *Mycobacterium tuberculosis*. *Acta Crystallogr Sect F Struct Biol Cryst Commun.* 2007 Jan 1;63(1):1–6.
89. Gan J, Gu Y, Li Y, Yan H, Ji X. Crystal structure of *Mycobacterium tuberculosis* shikimate kinase in complex with shikimic acid and an ATP analogue. *Biochemistry.* 2006;45(28):8539–45.
90. Pereira JH, De Oliveira JS, Canduri F, Dias MVB, Palma MS, Basso LA, et al. Structure of shikimate kinase from *Mycobacterium tuberculosis* reveals the binding of shikimic acid. *Acta Crystallogr Sect D Biol Crystallogr.* 2004;60(12 II):2310–9.
91. Dhaliwal B, Nichols CE, Ren J, Lockyer M, Charles I, Hawkins AR, et al. Crystallographic studies of shikimate binding and induced conformational changes in *Mycobacterium tuberculosis* shikimate kinase. *FEBS Lett.* 2004;574(1–3):49–54.
92. Gu Y, Reshetnikova L, Li Y, Wu Y, Yan H, Singh S, et al. Crystal structure of shikimate kinase from *Mycobacterium tuberculosis* reveals the dynamic role of the LID domain in catalysis. *J Mol Biol.* 2002;319(3):779–89.
93. Krell T, Maclean J, Boam DJ, Cooper A, Resmini M, Brocklehurst K, et al. Biochemical and X-ray crystallographic studies on shikimate kinase: The important structural role of the P-loop lysine. *Protein Sci.* 2001 Jun;10(6):1137–49.
94. Walker JE, Saraste M, Runswick M, Gay NJ. Distantly related sequences in the alpha- and beta-subunits of ATP synthase, myosin, kinases and other ATP-requiring enzymes and a common nucleotide binding fold. *EMBO J.* 1982;1(8):945–51.
95. Blagden, S., de Bono J. Drugging cell cycle kinases in cancer therapy. *Curr Drug Targets.* 2005;6:325–35.
96. Hartmann MD, Bourenkov GP, Oberschall A, Strizhov N, Bartunik HD. Mechanism of Phosphoryl Transfer Catalyzed by Shikimate Kinase from *Mycobacterium tuberculosis*. *J Mol Biol.* 2006;364(3):411–23.
97. Blanco B, Prado V, Lence E, Otero JM, Garcia-Doval C, Van Raaij MJ, et al. *Mycobacterium tuberculosis* shikimate kinase inhibitors: Design and simulation studies of the catalytic turnover. *J Am Chem Soc.* 2013;135(33):12366–76.
98. Dias MVB, Faím LM, Vasconcelos IB, De Oliveira JS, Basso LA, Santos DS, et al. Effects of the magnesium and chloride ions and shikimate on the structure of shikimate kinase from *Mycobacterium tuberculosis*. *Acta Crystallogr Sect F Struct Biol Cryst*

- Commun. 2007;63(1):1–6.
99. Coracini JD, de Azevedo WF. Shikimate kinase, a protein target for drug design. *Curr Med Chem*. 2014;21(5):592–604.
 100. Sprinsonj B, Public S. The biosynthesis from of shirimic. *Reactions*.
 101. Hawkes TR, Lewis T, Coggins JR, Mousedale DM, Lowe DJ TR 1990. . Chorismate synthase, presteady-state kinetics of phosphate release from 5-enolpyruvylshikimate 3phosphate. *Biochem J*. 1990;265:899–902.
 102. Balasubramanian S, Abel IC CJ. Observation of an isotope effect in the chorismate synthase reaction. *J Am Chem Soc*. 1990;(112):8581–83.
 103. Schönbrunn E, Eschenburg S, Shuttleworth WA, Schloss J V, Amrhein N, Evans JN, et al. Interaction of the herbicide glyphosate with its target enzyme 5-enolpyruvylshikimate 3-phosphate synthase in atomic detail. *Proc Natl Acad Sci U S A*. 2001;98(4):1376–80.
 104. Funke T, Han H, Healy-Fried ML, Fischer M, Schonbrunn E. Molecular basis for the herbicide resistance of Roundup Ready crops. *Proc Natl Acad Sci*. 2006;103(35):13010–5.
 105. Roberts F, Roberts CW, Johnson JJ, Kyle DE, Krell T, Coggins JR, et al. Evidence for the shikimate pathway in apicomplexan parasites. *Nature*. 1998;393(6687):801–5.
 106. Davies GM, Barrett-Bee KJ, Jude DA, Lehan M, Nichols WW, Pinder PE, et al. (6S)-6-Fluoroshikimic acid, an antibacterial agent acting on the aromatic biosynthetic pathway. Vol. 38, *Antimicrobial Agents and Chemotherapy*. American Society for Microbiology; 1994. p. 403–6.
 107. Dewick PM. The shikimate pathway: aromatic amino acids and phenylpropanoids. Vol. 0471496405, *Medicinal Natural Products*. 2009. 121-166 p.
 108. Herrmann KM. The Shikimate Pathway as an Entry to Aromatic Secondary Metabolism. *Plant Physiol*. 1995;107(1):7–12.
 109. Herrmann KM, Weaver LM. THE SHIKIMATE PATHWAY. *Annu Rev Plant Physiol Plant Mol Biol*. 1999;50(1):473–503.
 110. Weaver LM, Herrmann KM. Dynamics of the shikimate pathway in plants. Vol. 2, *Trends in Plant Science*. 1997. p. 346–51.
 111. Tzin V, Galili G. New Insights into the shikimate and aromatic amino acids biosynthesis pathways in plants. *Mol Plant*. 2010;3(6):956–72.
 112. Cragg GM, Newman DJ. Natural Product Drug Discovery in the Next Millennium. *Pharm Biol*. 2001 Jan 10;39(sup1):8–17.

113. Cragg GM, Newman DJ, Snader KM. Natural products in drug discovery and development. *J Nat Prod.* 1997;60(1):52–60.
114. Heinrich M. Ethnopharmacology and drug discovery. In: Reedijk ed. J, editor. *Elsevier Reference Module in Chemistry, Molecular Sciences and Chemical Engineering.* Elsevier, Waltham, MA.; 2013. p. 1–24.
115. Heinrich M, Gibbons S. Ethnopharmacology in drug discovery: an analysis of its role and potential contribution. *J Pharm Pharmacol.* 2001;53(4):425–32.
116. Schmitt EK, Moore CM, Krastel P, Petersen F. Natural products as catalysts for innovation: A pharmaceutical industry perspective. Vol. 15, *Current Opinion in Chemical Biology.* 2011. p. 497–504.
117. Dixon N, Wong LS, Geerlings TH, Micklefield J. Cellular targets of natural products. *Nat Prod Rep.* 2007 Dec;24(6):1288.
118. Bode HB, Müller R. The impact of bacterial genomics on natural product research. Vol. 44, *Angewandte Chemie - International Edition.* 2005. p. 6828–46.
119. Hertweck C. The biosynthetic logic of polyketide diversity. Vol. 48, *Angewandte Chemie - International Edition.* 2009. p. 4688–716.
120. WHO | The top 10 causes of death [Internet]. World Health Organization. World Health Organization; 2017 [cited 2018 Apr 6]. Available from: <http://www.who.int/mediacentre/factsheets/fs310/en/>
121. Duggar B. Aureomycin: a product of the continuing search for new antibiotics. *Annals of the New York Academy of Science.* Ann N Y Acad Sci. 1948 Nov 30;51(Art. 2):177–81.
122. Broschard RW, Dornbush AC, Gordon S, Hutchings BL, Kohler AR, Krupka G, et al. Aureomycin, a New Antibiotic. *Science* (80-). 1949 Feb 25;109(2826):199–200.
123. Conover LH, Moreland WT, English AR, Stephens CR, Pilgrim FJ. Terramycin. Xi. Tetracycline. *J Am Chem Soc.* 1953;75(18):4622–3.
124. Conover LH, Butler K, Johnston JD, Korst JJ, Woodward RB. The Total Synthesis of 6-Demethyl-6-Deoxytetracycline. *J Am Chem Soc.* 1962;84(16):3222–4.
125. Korst JJ, Johnston JD, Butler K, Bianco EJ, Conover LH, Woodward RB. The Total Synthesis of dl-6-Demethyl-6-deoxytetracycline. *J Am Chem Soc.* 1968;90(2):439–57.
126. K. C. Nicolaou and J. S. Chen. *Classics in Total Synthesis III.* Wiley-VCH, editor. Weinheim; 2011. 345-375 p.
127. Grossman TH, Starosta AL, Fyfe C, O'Brien W, Rothstein DM, Mikolajka A, et al. Target- and resistance-based mechanistic studies with TP-434, a novel fluorocycline

- antibiotic. *Antimicrob Agents Chemother.* 2012;56(5):2559–64.
128. Boucher HW, Talbot GH, Bradley JS, Edwards JE, Gilbert D, Rice LB, et al. Bad Bugs, No Drugs: No ESKAPE! An Update from the Infectious Diseases Society of America. *Clin Infect Dis.* 2009;48(1):1–12.
 129. Merlino J, Leroi M, Bradbury R, Veal D, Harbour C. New chromogenic identification and detection of *Staphylococcus aureus* and methicillin-resistant *S. aureus*. *J Clin Microbiol.* 2000;38(6):2378–80.
 130. Uttley AH, Collins CH, Naidoo J, George RC. Vancomycin-resistant enterococci. *Lancet.* 1988;1(8575–6):57–8.
 131. May J, Shannon K, King A, French G. Glycopeptide tolerance in *Staphylococcus aureus*. *J Antimicrob Chemother.* 1998 Aug;42(2):189–97.
 132. Ziglam HM, Finch RG. Limitations of presently available glycopeptides in the treatment of Gram-positive infection. *Clin Microbiol Infect.* 2001;7(SUPPL. 4):53–65.
 133. Centers for Disease Control and Prevention. *Staphylococcus aureus* resistant to vancomycin. *MMWR Morb Mortal Wkly Rep.* 2002;51(26):565–7.
 134. Chang S, Sievert DM, Hageman JC, Boulton ML, Tenover FC, Downes FP, et al. Infection with Vancomycin-Resistant *Staphylococcus aureus* Containing the *vanA* Resistance Gene. *N Engl J Med.* 2003 Apr 3;348(14):1342–7.
 135. Weigel LM, Clewell DB, Gill SR, Clark NC, McDougal LK, Flannagan SE, et al. Genetic Analysis of a High-Level Vancomycin-Resistant Isolate of *Staphylococcus aureus*. *Science* (80-). 2003 Nov 28;302(5650):1569–71.
 136. Bugg TDH, Wright GD, Walsh CT, Dutka-Malen S, Arthur M, Courvalin P. Molecular Basis for Vancomycin Resistance in *Enterococcus faecium* BM4147: Biosynthesis of a Depsipeptide Peptidoglycan Precursor by Vancomycin Resistance Proteins VanH and VanA. *Biochemistry.* 1991 Oct;30(43):10408–15.
 137. Crowley BM, Boger DL. Total synthesis and evaluation of [Ψ [CH₂NH]Tpg 4]vancomycin aglycon: Reengineering vancomycin for dual D-Ala-D-Ala and D-Ala-D-Lac binding. *J Am Chem Soc.* 2006;128(9):2885–92.
 138. Xie J, Pierce JG, James RC, Okano A, Boger DL. A redesigned vancomycin engineered for dual d-Ala-d-Ala and d-Ala-d-Lac binding exhibits potent antimicrobial activity against vancomycin-resistant bacteria. *J Am Chem Soc.* 2011;133(35):13946–9.
 139. Xie J, Okano A, Pierce JG, James RC, Stamm S, Crane CM, et al. Total synthesis of [ψ [C(=S)NH]Tpg 4]vancomycin aglycon, [ψ [C(=NH)NH]Tpg 4]vancomycin aglycon, and related key compounds: Reengineering vancomycin for dual D-Ala-D-Ala and D-Ala-D-Lac binding. *J Am Chem Soc.* 2012;134(2):1284–97.

140. Newman DJ, Cragg GM. Natural Products as Sources of New Drugs over the 30 Years. *J Nat Prod.* 2012;75(3):311–35.
141. Pettit GR, Kamano Y, Herald CL, Tuinman AA, Boettner FE, Kizu H, et al. The Isolation and Structure of a Remarkable Marine Animal Antineoplastic Constituent: Dolastatin 10. *J Am Chem Soc.* 1987;109(22):6883–5.
142. Warsame M, Olumese P, Mendis K. Role of medicines in malaria control and elimination. Vol. 71, *Drug Development Research.* 2010. p. 4–11.
143. Schmid G, Hofheinz W. Total Synthesis of Qinghaosu. *Journal of the American Chemical Society.* 1983 Feb;105(3):624–5.
144. Zhou WS, Xu XX. Total Synthesis of the Antimalarial Sesquiterpene Peroxide Qinghaosu and Yingzhaosu A. *Acc Chem Res.* 1994 Jul;27(7):211–6.
145. Yadav, J. S.; Thirupathaiah, B.; Srihari, P. A concise stereoselective total synthesis of (+)-artemisinin. *Tetrahedron.* 2010;66(11):2005–9.
146. Hao HD, Li Y, Han WB, Wu Y. A hydrogen peroxide based access to qinghaosu (artemisinin). *Org Lett.* 2011 Aug 19;13(16):4212–5.
147. O'Neill PM, Posner GH. A medicinal chemistry perspective on artemisinin and related endoperoxides. Vol. 47, *Journal of Medicinal Chemistry.* 2004. p. 2945–64.
148. N. Burrows J, Chibale K, N.C. Wells T. The State of the Art in Anti-Malarial Drug Discovery and Development. *Curr Top Med Chem.* 2011;11(10):1226–54.
149. World Health Organization. Guidelines for the treatment of malaria, 2nd edition. Who. 2010;197p.
150. Newman DJ, Cragg GM, Battershill CN. Therapeutic agents from the sea: Biodiversity, chemo-evolutionary insight and advances to the end of Darwin's 200th year. Vol. 39, *Diving and Hyperbaric Medicine.* 2009. p. 216–25.
151. Thomas X. Chemotherapy of acute leukemia in adults. *Expert Opin Pharmacother.* 2009;10(2):221–37.
152. Absalon MJ, Smith FO. Treatment strategies for pediatric acute myeloid leukemia. *Expert Opin Pharmacother.* 2009 Jan 16;10(1):57–79.
153. Wisher D. Martindale: The Complete Drug Reference. 37th ed. *J Med Libr Assoc.* 2012;100(1):75–6.
154. Olivera BM. -Conotoxin MVIIA : From Marine Snail Venom to Analgesic Drug. *Drugs from Sea.* 2000;74–85.

155. Miljanich GP. Ziconotide: neuronal calcium channel blocker for treating severe chronic pain. *Curr Med Chem*. 2004;11:3029–40.
156. McGivern JG. Rev N-type T-type Ca(II) calcium channel for pain [Prialt gabapentin nociception]. *Drug Disc Today*. 2006;11:245.
157. Staats PS, Yearwood T, Charapata SG, Presley RW, Wallace MS, Byas-Smith M, et al. Intrathecal ziconotide in the treatment of refractory pain in patients with cancer or AIDS: a randomized controlled trial. Pretreatment of patients with atrial fibrillation who undergo electrical cardioversion. *JAMA*. 2004;291(1):63–70.
158. Rauck RL, Wallace MS, Burton AW, Kapural L, North JM. Intrathecal ziconotide for neuropathic pain: A review. Vol. 9, *Pain Practice*. 2009. p. 327–37.
159. Rinehart KL, Holt TG, Fregeau NL, Stroh JG, Keifer PA, Sun F, et al. Ecteinascidins 729, 743, 745, 759A, 759B, and 770: Potent Antitumor Agents from the Caribbean Tunicate *Ecteinascidia turbinata*. *J Org Chem*. 1990;55(15):4512–5.
160. Wright AE, Forleo DA, Gunawardana GP, Gunasekera SP, Koehn FE, McConnell OJ. Antitumor Tetrahydroisoquinoline Alkaloids from the Colonial Ascidian *Ecteinascidia turbinata*. *J Org Chem*. 1990;55(15):4508–12.
161. Verweij J. Soft tissue sarcoma trials: One size no longer fits all. *Journal of Clinical Oncology*. 2009;27(19):3085–7.
162. Yap TA, Carden CP, Kaye SB. Beyond chemotherapy: Targeted therapies in ovarian cancer. Vol. 9, *Nature Reviews Cancer*. 2009. p. 167–81.
163. Zewail-Foote M, Hurley LH. Differential rates of reversibility of ecteinascidin 743-DNA covalent adducts from different sequences lead to migration to favored bonding sites. *J Am Chem Soc*. 2001;123(27):6485–95.
164. Takebayashi Y, Pourquier P, Zimonjic DB, Nakayama K, Emmert S, Ueda T, et al. Antiproliferative activity of ecteinascidin 743 is dependent upon transcription-coupled nucleotide-excision repair. *Nat Med*. 2001;7(8):961–6.
165. Soares DG, Escargueil AE, Poindessous V, Sarasin A, de Gramont A, Bonatto D, et al. Replication and homologous recombination repair regulate DNA double-strand break formation by the antitumor alkylator ecteinascidin 743. *Proc Natl Acad Sci U S A*. 2007;104(32):13062–7.
166. Herrero AB, Martín-Castellanos C, Marco E, Gago F, Moreno S. Cross-talk between nucleotide excision and homologous recombination DNA repair pathways in the mechanism of action of antitumor trabectedin. *Cancer Res*. 2006;66(16):8155–62.
167. Jackson KL, Henderson JA, Phillips AJ. The halichondrins and E7389. *Chem Rev*. 2009;109(7):3044–79.

168. Fodstad O, Breistol K, Pettit GR, Shoemaker RH, Boyd MR. Comparative antitumor activities of halichondrins and vinblastine against human tumor xenografts. *J Exp Ther Oncol.* 1996;1(2):119–25.
169. Towle MJ, Salvato KA, Budrow J, Wels BF, Kuznetsov G, Aalfs KK, et al. In vitro and in vivo anticancer activities of synthetic macrocyclic ketone analogues of halichondrin B. *Cancer Res.* 2001;61(3):1013–21.
170. Yu, M.J., Kishi, Y., and Littlefield B. Discovery of E7389, a fully synthetic macrocyclic ketone analog of halichondrin B. In: Cragg, G.M., Kingston, D.G.I. and Newman, D.J. eds, editor. *In Anticancer Agents from Natural Products.* Boca Raton, Fl., CRC Press, Taylor and Francis Group; 2005. p. 241–65.
171. Jordan MA. The primary antimitotic mechanism of action of the synthetic halichondrin E7389 is suppression of microtubule growth. *Mol Cancer Ther.* 2005;4(7):1086–95.
172. Okouneva T, Azarenko O, Wilson L, Littlefield BA, Jordan MA. Inhibition of centromere dynamics by eribulin (E7389) during mitotic metaphase. *Mol Cancer Ther.* 2008;7(7):2003–11.
173. Kuznetsov G, Towle MJ, Cheng H, Kawamura T, TenDyke K, Liu D, et al. Induction of morphological and biochemical apoptosis following prolonged mitotic blockage by halichondrin B macrocyclic ketone analog E7389. *Cancer Res.* 2004;64(16):5760–6.
174. Kem WR. Hydroxy Metabolites of the Alzheimer's Drug Candidate 3-[(2,4-Dimethoxy)Benzylidene]-Anabaseine Dihydrochloride (GTS-21): Their Molecular Properties, Interactions with Brain Nicotinic Receptors, and Brain Penetration. *Mol Pharmacol.* 2004 Jan 1;65(1):56–67.
175. Buckingham SD, Jones AK, Brown LA, Sattelle DB. Nicotinic Acetylcholine Receptor Signalling: Roles in Alzheimer's Disease and Amyloid Neuroprotection. *Pharmacol Rev.* 2009 Mar 6;61(1):39–61.
176. Thinschmidt JS, Frazier CJ, King MA, Meyer EM, Papke RL. Septal innervation regulates the function of $\alpha 7$ nicotinic receptors in CA1 hippocampal interneurons. *Exp Neurol.* 2005 Oct;195(2):342–52.
177. Shimohama S. Nicotinic Receptor-Mediated Neuroprotection in Neurodegenerative Disease Models. *Biol Pharm Bull.* 2009;32(3):332–6.
178. Pavlov VA, Ochani M, Yang L-H, Gallowitsch-Puerta M, Ochani K, Lin X, et al. Selective $\alpha 7$ -nicotinic acetylcholine receptor agonist GTS-21 improves survival in murine endotoxemia and severe sepsis*. *Crit Care Med.* 2007;35(4):1139–44.
179. Rosas-Ballina M, Goldstein RS, Gallowitsch-Puerta M, Yang L, Valdés-Ferrer SI, Patel NB, et al. The selective $\alpha 7$ agonist GTS-21 attenuates cytokine production in human whole blood and human monocytes activated by ligands for TLR2, TLR3, TLR4, TLR9,

- and RAGE. *Mol Med*. 2009;15(7–8):195–202.
180. Kitagawa H, Takenouchi T, Azuma R, Wesnes KA, Kramer WG, Clody DE, et al. Safety, pharmacokinetics, and effects on cognitive function of multiple doses of GTS-21 in healthy, male volunteers. *Neuropsychopharmacology*. 2003;28(3):542–51.
 181. Olincy A, Harris JG, Johnson LL, Pender V, Kongs S, Allensworth D, et al. Proof-of-concept trial of an $\alpha 7$ nicotinic agonist in schizophrenia. *Arch Gen Psychiatry*. 2006;63(6):630–8.
 182. Freedman R, Olincy A, Buchanan RW, Harris JG, Gold JM, Johnson L, et al. Initial phase 2 trial of a nicotinic agonist in schizophrenia. *Am J Psychiatry*. 2008;165(8):1040–7.
 183. Talpir R, Benayahu Y, Kashman Y, Pannell L, Schleyer M. Hemiasterlin and geodiamolide TA; two new cytotoxic peptides from the marine sponge *Hemiasterella minor* (Kirkpatrick). *Tetrahedron Lett*. 1994;35(25):4453–6.
 184. Kuznetsov G, TenDyke K, Towle MJ, Cheng H, Liu J, Marsh JP, et al. Tubulin-based antimetabolic mechanism of E7974, a novel analogue of the marine sponge natural product hemiasterlin. *Mol Cancer Ther*. 2009;8(10):2852–60.
 185. Kuznetsov G, TenDyke K, Towle MJ, Cheng H, Liu J, Marsh JP, et al. Tubulin-based antimetabolic mechanism of E7974, a novel analogue of the marine sponge natural product hemiasterlin. *Mol Cancer Ther*. 2009 Oct 1;8(10):2852–60.
 186. Madajewicz, S; Zojwalla, NJ; Lucarelli, AG; Hentschel, P; Giardelli, J; Schuck, EL; Krivelevich, I; Wong, BY; Vogelzang, NJ; Sharma S. A phase I trial of E7974 administered on days 1 and 15 of a 28-day cycle in patients with solid malignancies. *J Clin Oncol*. 2007;25:2550.
 187. Alan F. Structure and mechanism in protein science, a guide to enzyme catalysis and protein folding. *LavoisierFr*. 1999;7(1):2011.
 188. Prusakiewicz JJ, Duggan KC, Rouzer CA, Marnett LJ. Differential sensitivity and mechanism of inhibition of COX-2 oxygenation of arachidonic acid and 2-arachidonoylglycerol by ibuprofen and mefenamic acid. *Biochemistry*. 2009 Aug 11;48(31):7353–5.
 189. Cho H, Tai HH. Inhibition of NAD⁺-dependent 15-hydroxyprostaglandin dehydrogenase (15-PGDH) by cyclooxygenase inhibitors and chemopreventive agents. *Prostaglandins Leukot Essent Fat Acids*. 2002 Dec;67(6):461–5.
 190. Copeland RA. Evaluation of Enzyme Inhibitors in Drug Discovery: A Guide for Medicinal Chemists and Pharmacologists: Second Edition. *Evaluation of Enzyme Inhibitors in Drug Discovery: A Guide for Medicinal Chemists and Pharmacologists: Second Edition*. 2013. 1-538 p.

191. Morris SK, Lindsley JE. Yeast topoisomerase II is inhibited by etoposide after hydrolyzing the first ATP and before releasing the second ADP. *J Biol Chem.* 1999;274(43):30690–6.
192. Hande KR. Etoposide: Four decades of development of a topoisomerase II inhibitor. Vol. 34, *European Journal of Cancer.* 1998. p. 1514–21.
193. Williams JW, Morrison JF. The Kinetics of Reversible Tight-Binding Inhibition. *Methods Enzymol.* 1979;63(C):437–67.
194. Murphy DJ. Determination of accurate K_i values for tight-binding enzyme inhibitors: An in silico study of experimental error and assay design. *Anal Biochem.* 2004 Apr 1;327(1):61–7.
195. Silverman RB. *The organic chemistry of enzyme-catalyzed reactions.* Academic Press; 2002. 717 p.
196. McGovern SL, Helfand BT, Feng B, Shoichet BK. A specific mechanism of nonspecific inhibition. *J Med Chem.* 2003;46(20):4265–72.
197. McGovern SL, Caselli E, Grigorieff N, Shoichet BK. A common mechanism underlying promiscuous inhibitors from virtual and high-throughput screening. *J Med Chem.* 2002;45(8):1712–22.
198. Feng BY, Simeonov A, Jadhav A, Babaoglu K, Inglese J, Shoichet BK, et al. A high-throughput screen for aggregation-based inhibition in a large compound library. *J Med Chem.* 2007;50(10):2385–90.
199. Alturki MS, Fuanta NR, Jarrard MA, Hobrath J V, Goodwin DC, Rants'o TA, et al. A multifaceted approach to identify non-specific enzyme inhibition: Application to *Mycobacterium tuberculosis* shikimate kinase. *Bioorg Med Chem Lett.* 2018 Feb 15;28(4):802–8.
200. Baell JB, Holloway GA. New substructure filters for removal of pan assay interference compounds (PAINS) from screening libraries and for their exclusion in bioassays. *J Med Chem.* 2010 Apr 8;53(7):2719–40.
201. Loughrey BT, Williams ML, Carruthers TJ, Parsons PG, Healy PC. Synthesis, structure, and selective cytotoxicity of organometallic Cp *RuII O-alkyl-N-phenylcarbamate sandwich complexes. *Aust J Chem.* 2010 Jan 10;63(2):245–51.
202. Baell J, Walters MA. *Chemistry: Chemical con artists foil drug discovery.* Vol. 513, *Nature.* 2014. p. 481–3.
203. Baell JB. Feeling Nature's PAINS: Natural Products, Natural Product Drugs, and Pan Assay Interference Compounds (PAINS). Vol. 79, *Journal of Natural Products.* 2016. p. 616–28.

204. Bisson J, McAlpine JB, Friesen JB, Chen SN, Graham J, Pauli GF. Can Invalid Bioactives Undermine Natural Product-Based Drug Discovery? Vol. 59, *Journal of Medicinal Chemistry*. 2016. p. 1671–90.
205. Baell JB, Ferrins L, Falk H, Nikolakopoulos G. PAINS: Relevance to tool compound discovery and fragment-based screening. *Aust J Chem*. 2013;66(12):1483–94.
206. Kilchmann F, Marcaida MJ, Kotak S, Schick T, Boss SD, Awale M, et al. Discovery of a Selective Aurora A Kinase Inhibitor by Virtual Screening. *J Med Chem*. 2016;59(15):7188–211.
207. Laplante SR, Carson R, Gillard J, Aubry N, Coulombe R, Bordeleau S, et al. Compound aggregation in drug discovery: Implementing a practical NMR assay for medicinal chemists. *J Med Chem*. 2013;56(12):5142–50.
208. Chai CL, Mátyus P. One size does not fit all: Challenging some dogmas and taboos in drug discovery. *Future Med Chem*. 2016 Jan;8(1):29–38.
209. Senger MR, Fraga CAM, Dantas RF, Silva FP. Filtering promiscuous compounds in early drug discovery: Is it a good idea? *Drug Discov Today*. 2016;21(6):868–72.
210. Capuzzi SJ, Muratov EN, Tropsha A. Phantom PAINS: Problems with the Utility of Alerts for P an- A ssay in terference Compound S. *J Chem Inf Model*. 2017;57(3):417–27.
211. Lagorce D, Sperandio O, Baell JB, Miteva MA, Villoutreix BO. FAF-Drugs3: A web server for compound property calculation and chemical library design. *Nucleic Acids Res*. 2015;43(W1):W200–7.
212. Canny SA, Cruz Y, Southern MR, Griffin PR. PubChem promiscuity: A web resource for gathering compound promiscuity data from PubChem. *Bioinformatics*. 2012 Jan 1;28(1):140–1.
213. Dahlin JL, Walters MA. How to Triage PAINS-Full Research. *Assay Drug Dev Technol*. 2016 Apr;14(3):168–74.
214. Cohen P. Protein kinases--the major drug targets of the twenty-first century? *Nat Rev Drug Discov*. 2002;1(April):309–15.
215. Traxler P, Furet P. Strategies toward the Design of Novel and Selective Protein Tyrosine Kinase Inhibitors. *Pharmacol Ther*. 1999;82(2–3):195–206.
216. Zhang J, Yang PL, Gray NS. Targeting cancer with small molecule kinase inhibitors. *Nat Rev Cancer*. 2009;9(1):28–39.
217. Manley PW, Cowan-Jacob SW, Mestan J. Advances in the structural biology, design and clinical development of Bcr-Abl kinase inhibitors for the treatment of chronic myeloid leukaemia. *Biochim Biophys Acta*. 2005;1754:3–13.

218. Wan PTC, Garnett MJ, Roe SM, Lee S, Niculescu-Duvaz D, Good VM, et al. Mechanism of activation of the RAF-ERK signaling pathway by oncogenic mutations of B-RAF. *Cell*. 2004;116(6):855–67.
219. Knight ZA, Gonzalez B, Feldman ME, Zunder ER, Goldenberg DD, Williams O, et al. A Pharmacological Map of the PI3-K Family Defines a Role for p110 α in Insulin Signaling. *Cell*. 2006;125(4):733–47.
220. Ohren JF, Chen H, Pavlovsky A, Whitehead C, Zhang E, Kuffa P, et al. Structures of human MAP kinase kinase 1 (MEK1) and MEK2 describe novel noncompetitive kinase inhibition. *Nat Struct Mol Biol*. 2004;11(12):1192–7.
221. Cohen MS, Zhang C, Shokat KM, Taunton J. Biochemistry: Structural bioinformatics-based design of selective, irreversible kinase inhibitors. *Science* (80-). 2005;308(5726):1318–21.
222. Kwak EL, Sordella R, Bell DW, Godin-Heymann N, Okimoto RA, Brannigan BW, et al. Irreversible inhibitors of the EGF receptor may circumvent acquired resistance to gefitinib. *Proc Natl Acad Sci*. 2005;102(21):7665–70.
223. Fry DW, Kraker AJ, McMichael A, Ambroso LA, Nelson JM, Leopold WR, et al. A specific inhibitor of the epidermal growth factor receptor tyrosine kinase. *Sci* . 1994;265(5175):1093–5.
224. Schirmer A, Kennedy J, Murli S, Reid R, Santi D V. Targeted covalent inactivation of protein kinases by resorcylic acid lactone polyketides. *Proc Natl Acad Sci U S A*. 2006;103(11):4234–9.
225. Mehra R, Rajput VS, Gupta M, Chib R, Kumar A, Wazir P, et al. Benzothiazole Derivative as a Novel Mycobacterium tuberculosis Shikimate Kinase Inhibitor: Identification and Elucidation of Its Allosteric Mode of Inhibition. *J Chem Inf Model*. 2016 May 23;56(5):930–40.
226. Abunada N, Hassaneen H, Kandile N, Miqdad O. Synthesis and Biological Activity of Some New Pyrazoline and Pyrrolo[3,4-c]pyrazole-4,6-dione Derivatives: Reaction of Nitrilimines with Some Dipolarophiles. *Molecules*. 2008 Apr 29;13(4):1011–24.
227. Castagnolo D, Manetti F, Radi M, Bechi B, Pagano M, De Logu A, et al. Synthesis, biological evaluation, and SAR study of novel pyrazole analogues as inhibitors of Mycobacterium tuberculosis: Part 2. Synthesis of rigid pyrazolones. *Bioorg Med Chem*. 2009 Aug 1;17(15):5716–21.
228. Balachandra Shankar Bandodkar, Stefan Schmitt. Pyrazoline derivatives for the treatment of tuberculosis. US Patent App. 12/063,740, 2010.
229. Gordon S, Simithy J, Goodwin DC, Calderón AI. Selective mycobacterium tuberculosis shikimate kinase inhibitors as potential antibacterials. *Perspect Medicin Chem*. 2015;7:9–

- 20.
230. Mulabagal V, Calderón AI. Development of an ultrafiltration-liquid chromatography/mass spectrometry (UF-LC/MS) based ligand-binding assay and an LC/MS based functional assay for mycobacterium tuberculosis shikimate kinase. *Anal Chem.* 2010;82(9):3616–21.
231. McGaw LJ, Jäger AK, van Staden J, Eloff JN. Isolation of β -asarone, an antibacterial and anthelmintic compound, from *Acorus calamus* in South Africa. *South African J Bot.* 2002 Feb 1;68(1):31–5.
232. Obonyo M, Zhang L, Thamphiwatana S, Pornpattananankul D, Fu V, Zhang L. Antibacterial Activities of Liposomal Linolenic Acids against Antibiotic-Resistant *Helicobacter pylori*. *Mol Pharm.* 2012 Sep 4;9(9):2677–85.
233. Leu G-Z, Lin T-Y, Hsu JT. Anti-HCV activities of selective polyunsaturated fatty acids. *Biochem Biophys Res Commun.* 2004 May 21;318(1):275–80.
234. Raynor L, Mitchell A, Walker R, Walker R, Walker K. Antifungal Activities of Four Fatty Acids against Plant Pathogenic Fungi. *Mycopathologia.* 2004 Jan;157(1):87–90.
235. Masoko P, Mabusa IH, Howard RL. Isolation of alpha-linolenic acid from *Sutherlandia frutescens* and its inhibition of Mycobacterium tuberculosis' shikimate kinase enzyme. *BMC Complement Altern Med.* 2016;16(1).
236. Segura-Cabrera A, Rodríguez-Pérez MA. Structure-based prediction of Mycobacterium tuberculosis shikimate kinase inhibitors by high-throughput virtual screening. *Bioorganic Med Chem Lett.* 2008;18(11):3152–7.
237. Blanco B, Prado V, Lence E, Otero JM, Garcia-Doval C, van Raaij MJ, et al. Mycobacterium tuberculosis Shikimate Kinase Inhibitors: Design and Simulation Studies of the Catalytic Turnover. *J Am Chem Soc.* 2013 Aug 21;135(33):12366–76.
238. Rajput VS, Mehra R, Kumar S, Nargotra A, Singh PP, Khan IA. Screening of antitubercular compound library identifies novel shikimate kinase inhibitors of Mycobacterium tuberculosis. *Appl Microbiol Biotechnol.* 2016 Jun 18;100(12):5415–26.
239. Cuatrecasas P. Drug discovery in jeopardy. Vol. 116, *Journal of Clinical Investigation.* 2006. p. 2837–42.
240. Kelleher NL. Peer Reviewed: Top-Down Proteomics. *Anal Chem.* 2004;76(11):196 A-203 A.
241. Chait BT. Mass spectrometry: Bottom-up or top-down? Vol. 314, *Science.* 2006. p. 65–6.
242. Smith LM, Kelleher NL. Proteoform: A single term describing protein complexity. Vol. 10, *Nature Methods.* 2013. p. 186–7.

243. Siuti N, Roth MJ, Mizzen CA, Kelleher NL, Pesavento JJ. Gene-specific characterization of human histone H2B by electron capture dissociation. *J Proteome Res.* 2006;5(2):233–9.
244. Li M, Jiang L, Kelleher NL. Global histone profiling by LC-FTMS after inhibition and knockdown of deacetylases in human cells. *J Chromatogr B Anal Technol Biomed Life Sci.* 2009;877(30):3885–92.
245. Resemann A, Wunderlich D, Rothbauer U, Warscheid B, Leonhardt H, Fuchser J, et al. Top-down de novo protein sequencing of a 13.6 kDa camelid single heavy chain antibody by matrix-assisted laser desorption ionization-time-of-flight/ time-of-flight mass spectrometry. *Anal Chem.* 2010;82(8):3283–92.
246. Zhang J, Guy MJ, Norman HS, Chen YC, Xu Q, Dong X, et al. Top-down quantitative proteomics identified phosphorylation of cardiac troponin i as a candidate biomarker for chronic heart failure. *J Proteome Res.* 2011;10(9):4054–65.
247. Barrera NP, Isaacson SC, Zhou M, Bavro VN, Welch A, Schaedler TA, et al. Mass spectrometry of membrane transporters reveals subunit stoichiometry and interactions. *Nat Methods.* 2009;6(8):585–7.
248. Eralles J, Gontero B, Whitelegge J, Halgand F. Mapping of a copper-binding site on the small CP12 chloroplastic protein of *Chlamydomonas reinhardtii* using top-down mass spectrometry and site-directed mutagenesis. *Biochem J.* 2009;419(1):75–82, 4 p following 82.
249. Catherman AD, Skinner OS, Kelleher NL. Top Down proteomics: Facts and perspectives. Vol. 445, *Biochemical and Biophysical Research Communications.* 2014. p. 683–93.
250. Taylor GK, Kim Y Bin, Forbes AJ, Meng F, McCarthy R, Kelleher NL. Web and database software for identification of intact proteins using “top down” mass spectrometry. *Anal Chem.* 2003;75(16):4081–6.
251. Zamdborg L, LeDuc RD, Glowacz KJ, Kim Y Bin, Viswanathan V, Spaulding IT, et al. ProSight PTM 2.0: Improved protein identification and characterization for top down mass spectrometry. *Nucleic Acids Res.* 2007;35(SUPPL.2).
252. Horn DM, Zubarev RA, McLafferty FW. Automated de novo sequencing of proteins by tandem high-resolution mass spectrometry. *Proc Natl Acad Sci.* 2000;97(19):10313–7.
253. Tran JC, Zamdborg L, Ahlf DR, Lee JE, Catherman AD, Durbin KR, et al. Mapping intact protein isoforms in discovery mode using top-down proteomics. *Nature.* 2011;480(7376):254–8.
254. Karabacak NM, Li L, Tiwari A, Hayward LJ, Hong P, Easterling ML, et al. Sensitive and Specific Identification of Wild Type and Variant Proteins from 8 to 669 kDa Using Top-down Mass Spectrometry. *Mol Cell Proteomics.* 2009;8(4):846–56.

255. Tsai YS, Scherl A, Shaw JL, MacKay CL, Shaffer SA, Langridge-Smith PRR, et al. Precursor Ion Independent Algorithm for Top-Down Shotgun Proteomics. *J Am Soc Mass Spectrom.* 2009;20(11):2154–66.
256. Perkins D, Pappin D, Creasy D, Cottrell J. Probability-based protein identification by searching sequence databases using mass spectrometry data. *Electrophoresis.* 1999;20:3551–67.
257. Eng JK, McCormack ALL, Yates III JR, Yates JR. An approach to correlate tandem mass spectral data of peptides with amino acid sequences in a protein database. *J Am Soc Mass Spectrom.* 1994;5(11):976–989.
258. Mann M, Wilm M. Error-Tolerant Identification of Peptides in Sequence Databases by Peptide Sequence Tags. *Anal Chem.* 1994 Dec 15;66(24):4390–9.
259. Hunt DF, Yates JR, Shabanowitz J, Winston S, Hauer CR. Protein sequencing by tandem mass spectrometry. *Proc Natl Acad Sci.* 1986;83(17):6233–7.
260. Yates JR, Eng JK, McCormack AL, Schieltz D. Method to Correlate Tandem Mass Spectra of Modified Peptides to Amino Acid Sequences in the Protein Database. *Anal Chem.* 1995 Apr 15;67(8):1426–36.
261. McCormack AL, Schieltz DM, Goode B, Yang S, Barnes G, Drubin D, et al. Direct Analysis and Identification of Proteins in Mixtures by LC/MS/MS and Database Searching at the Low-Femtomole Level. *Anal Chem.* 1997 Feb 15;69(4):767–76.
262. RG Cooks, G Chen CW. Quadrupole mass filters and quadrupole ion traps. In: *Selected Topics in Mass Spectrometry in the Biomolecular Sciences.* Kluwer Academic Publishers; 1997. p. 213–38.
263. Schwartz JC, Senko MW, Syka JEP. A two-dimensional quadrupole ion trap mass spectrometer. *J Am Soc Mass Spectrom.* 2002;13(6):659–69.
264. Chernushevich I V., Loboda A V., Thomson BA. An introduction to quadrupole-time-of-flight mass spectrometry. *J Mass Spectrom.* 2001;36(8):849–65.
265. Hu Q, Noll RJ, Li H, Makarov A, Hardman M, Cooks RG. The Orbitrap: A new mass spectrometer. Vol. 40, *Journal of Mass Spectrometry.* 2005. p. 430–43.
266. Bogdanov B, Smith RD. Proteomics by fticr mass spectrometry: TOP down and bottom up. Vol. 24, *Mass Spectrometry Reviews.* 2005. p. 168–200.
267. Geddes CD, Lakowicz JR, Rosenfeld MY. *Methods and Applications of Fluorescence.* J Fluoresc. 2002;12(2):119.
268. Gardecki JA, Maroncelli M. Set of secondary emission standards for calibration of the spectral responsivity in emission spectroscopy. *Appl Spectrosc.* 1998;52(9):1179–89.

269. Ghisaidoobe ABT, Chung SJ. Intrinsic tryptophan fluorescence in the detection and analysis of proteins: a focus on Förster resonance energy transfer techniques. *Int J Mol Sci*. 2014 Dec 5;15(12):22518–38.
270. Royer CA. Probing Protein Folding and Conformational Transitions with Fluorescence. *Chem Rev*. 2006 May;106(5):1769–84.
271. Phys DZ-AC, 2009 undefined. Hydration dynamics and coupled water-protein fluctuations probed by intrinsic tryptophan. books.google.com.
272. Callis PR. Binding phenomena and fluorescence quenching. II: Photophysics of aromatic residues and dependence of fluorescence spectra on protein conformation. *J Mol Struct*. 2014 Dec 5;1077:22–9.
273. Eftink MR. Fluorescence techniques for studying protein structure. *Methods Biochem Anal*. 1991;35:127–205.
274. Steiner RF, Kirby EP. The interaction of the ground and excited states of indole derivatives with electron scavengers. *J Phys Chem*. 1969 Dec;73(12):4130–5.
275. Adams PD, Chen Y, Ma K, Zagorski MG, Sönnichsen FD, McLaughlin ML, et al. Intramolecular quenching of tryptophan fluorescence by the peptide bond in cyclic hexapeptides. *J Am Chem Soc*. 2002 Aug 7;124(31):9278–86.
276. Chen Y, Liu B, Yu HT, Barkley MD. The peptide bond quenches indole fluorescence. *J Am Chem Soc*. 1996;118(39):9271–8.
277. Swaminathan R, Krishnamoorthy G, Periasamy N. Similarity of fluorescence lifetime distributions for single tryptophan proteins in the random coil state. *Biophys J*. 1994 Nov;67(5):2013–23.
278. Gudgin E, Lopez-Delgado R, Ware WR. The tryptophan fluorescence lifetime puzzle. A study of decay times in aqueous solution as a function of pH and buffer composition. *Can J Chem*. 1981 Apr;59(7):1037–44.
279. Albani JR. Origin of Tryptophan Fluorescence Lifetimes Part 1. Fluorescence Lifetimes Origin of Tryptophan Free in Solution. *J Fluoresc*. 2014 Jan 4;24(1):93–104.
280. Cohen BE, McAnaney TB, Park ES, Jan YN, Boxer SG, Jan LY. Probing protein electrostatics with a synthetic fluorescent amino acid. *Science* (80-). 2002 May 31;296(5573):1700–3.
281. Smirnov A V., English DS, Rich RL, Lane J, Teyton L, Schwabacher AW, et al. Photophysics and Biological Applications of 7-Azaindole and Its Analogs. *J Phys Chem B*. 1997;101(15):2758–69.
282. Lepthien S, Hoesl MG, Merkel L, Budisa N. Azatryptophans endow proteins with intrinsic

- blue fluorescence. *Proc Natl Acad Sci U S A*. 2008 Oct 21;105(42):16095–100.
283. Moroz YS, Binder W, Nygren P, Caputo GA, Korendovych I V. Painting proteins blue: β -(1-azulenyl)-l-alanine as a probe for studying protein–protein interactions. *Chem Commun*. 2013 Dec 11;49(5):490–2.
284. Goodman HM, Olson M V., Hall BD, Tsien RY, Chin JW, Schultz PG. Nucleotide sequence of a mutant eukaryotic gene: the yeast tyrosine-inserting ochre suppressor SUP4-o. *Proc Natl Acad Sci*. 1977 Dec 1;74(12):5453–7.
285. Chatterjee A, Guo J, Lee HS, Schultz PG. A genetically encoded fluorescent probe in mammalian cells. *J Am Chem Soc*. 2013 Aug 28;135(34):12540–3.
286. Hamada H, Kameshima N, Szymańska A, Wegner K, Łankiewicz L, Shinohara H, et al. Position-specific incorporation of a highly photodurable and blue-laser excitable fluorescent amino acid into proteins for fluorescence sensing. *Bioorganic Med Chem*. 2005 May 16;13(10):3379–84.
287. Talukder P, Chen S, Liu CT, Baldwin EA, Benkovic SJ, Hecht SM. Tryptophan-based fluorophores for studying protein conformational changes. *Bioorg Med Chem*. 2014 Nov 1;22(21):5924–34.
288. Talukder P, Chen S, Roy B, Yakovchuk P, Spiering MM, Alam MP, et al. Cyanotryptophans as Novel Fluorescent Probes for Studying Protein Conformational Changes and DNA-Protein Interaction. *Biochemistry*. 2015 Dec 29;54(51):7457–69.
289. Hilaire MR, Ahmed IA, Lin C-W, Jo H, DeGrado WF, Gai F. Blue fluorescent amino acid for biological spectroscopy and microscopy. *Proc Natl Acad Sci U S A*. 2017 Jun 6;114(23):6005–9.
290. Padayachee ER, Whiteley CG. Etiology of Alzheimer’s disease: Kinetic, thermodynamic and fluorimetric analyses of interactions of pseudo A β -peptides with neuronal nitric oxide synthase. *Neuropeptides*. 2013 Oct;47(5):321–7.
291. Yang X, Hu X, Xu B, Wang X, Qin J, He C, et al. Fluorometric Titration Approach for Calibration of Quantity of Binding Site of Purified Monoclonal Antibody Recognizing Epitope/Hapten Nonfluorescent at 340 nm. *Anal Chem*. 2014 Jun 17;86(12):5667–72.
292. Guo X, Li X, Jiang Y, Yi L, Wu Q, Chang H, et al. A spectroscopic study on the interaction between p-nitrophenol and bovine serum albumin. *J Lumin*. 2014 May 1;149:353–60.
293. Xu C, Gu J, Ma X, Dong T, Meng X. Investigation on the interaction of pyrene with bovine serum albumin using spectroscopic methods. *Spectrochim Acta Part A Mol Biomol Spectrosc*. 2014 May 5;125:391–5.
294. Chen Y-W, Lee C-H, Huang Y-T, Pan Y-J, Lin S-M, Lo Y-Y, et al. Functional and

- fluorescence analyses of tryptophan residues in H⁺-pyrophosphatase of *Clostridium tetani*. *J Bioenerg Biomembr*. 2014 Apr 12;46(2):127–34.
295. Gasymov OK, Abduragimov AR, Glasgow BJ. Tryptophan Rotamer Distribution Revealed for the α -Helix in Tear Lipocalin by Site-Directed Tryptophan Fluorescence. *J Phys Chem B*. 2012 Nov 15;116(45):13381–8.
 296. Halder UC, Chakraborty J, Das N, Bose S. Tryptophan dynamics in the exploration of micro-conformational changes of refolded β -lactoglobulin after thermal exposure: A steady state and time-resolved fluorescence approach. *J Photochem Photobiol B Biol*. 2012 Apr 2;109:50–7.
 297. Chen Y, Liu B, Yu HT, Barkley MD. The peptide bond quenches indole fluorescence. *J Am Chem Soc*. 1996 Mar 12;118(39):9271–8.
 298. Li J, Henry E, Wang L, Delelis O, Wang H, Simon F, et al. Comparative Study of the Fatty Acid Binding Process of a New FABP from *Cherax quadricarinatus* by Fluorescence Intensity, Lifetime and Anisotropy. Uversky VN, editor. *PLoS One*. 2012 Dec 21;7(12):e51079.
 299. Giuliano KA, Post PL, Hahn KM, Taylor DL. Fluorescent protein biosensors: measurement of molecular dynamics in living cells. *Annu Rev Biophys Biomol Struct*. 1995;24:405–34.
 300. Clegg RM. Fluorescence resonance energy transfer. *Curr Opin Biotechnol*. 1995;6(1):103–10.
 301. Lakowicz JR. Principles of fluorescence spectroscopy, 3rd Edition. Principles of Fluorescence Spectroscopy. 2006. 1-954 p.
 302. Stryer L. Fluorescence Energy Transfer as a Spectroscopic Ruler. *Annu Rev Biochem*. 1978 Jun;47(1):819–46.
 303. Hemmilä I, Dakubu S, Mikkala VM, Siitari H, Lövgren T. Europium as a label in time-resolved immunofluorometric assays. *Anal Biochem*. 1984 Mar;137(2):335–43.
 304. Mathis G. Rare earth cryptates and homogeneous fluoroimmunoassays with human sera. *Clin Chem*. 1993;39(9):1953–9.
 305. Karvinen, J., Hurskainen, P., Gopalakrishnan, S., Burns, D., Warrior, U., and Hemmila I. Homogeneous time resolved fluorescence quenching assay (LANCE) for caspase 3. *J Biomol Screen*. 2002;7:223–31.
 306. Cisbio. HTRF® Technology [Internet]. Vol. 4, journal of biomolecular screening. 2017 [cited 2018 Feb 9]. p. 6. Available from: <http://journals.sagepub.com/doi/pdf/10.1177/108705719900400605>

307. Turconi, S., Bingham, R.P., Haupts, U., Pope AJ. Developments in fluorescence lifetime-based analysis for ultra-HTS. *Drug Discov Today*. 2001;6:27–39.
308. Eggeling C, Brand L, Ullmann D, Jäger S. Highly sensitive fluorescence detection technology currently available for HTS. Vol. 8, *Drug Discovery Today*. 2003. p. 632–41.
309. Hovius R, Vallotton P, Wohland T, Vogel H. Fluorescence techniques: shedding light on ligand-receptor interactions. Vol. 21, *Trends in Pharmacological Sciences*. 2000. p. 266–73.
310. Clegg RM, Schneider PC. Fluorescence Lifetime-Resolved Imaging Microscopy: A General Description of Lifetime-Resolved Imaging Measurements. In: *Fluorescence Microscopy and Fluorescent Probes*. Boston, MA: Springer US; 1996. p. 15–33.
311. Weber G. Resolution of the fluorescence lifetimes in a heterogeneous system by phase and modulation measurements. *J Phys Chem*. 1981 Apr;85(8):949–53.
312. Wild UP, Holzwarth AR, Good HP. Measurement and analysis of fluorescence decay curves. *Rev Sci Instrum*. 1977 Dec 26;48(12):1621–7.
313. Wahl M, Gmbh P. Time-Correlated Single Photon Counting. 2009;288.
314. WHO | Global tuberculosis report 2016. WHO.
315. Matteelli A, Carvalho AC, Dooley KE, Kritski A. TMC207: the first compound of a new class of potent anti-tuberculosis drugs. *Future Microbiol*. 2010 Jun;5(6):849–58.
316. Haagsma AC, Abdillahi-Ibrahim R, Wagner MJ, Krab K, Vergauwen K, Guillemont J, et al. Selectivity of TMC207 towards Mycobacterial ATP synthase compared with that towards the eukaryotic homologue. *Antimicrob Agents Chemother*. 2009 Mar;53(3):1290–2.
317. Mahajan R. Bedaquiline: First FDA-approved tuberculosis drug in 40 years. *Int J Appl Basic Med Res*. 2013;3(1):1–2.
318. Chahine EB, Karaoui LR, Mansour H. Bedaquiline: a novel diarylquinoline for multidrug-resistant tuberculosis. *Ann Pharmacother*. 2014 Jan;48(1):107–15.
319. Pereira JH, Vasconcelos IB, Oliveira JS, Caceres RA, de Azevedo Jr. WF, Basso LA, et al. Shikimate kinase: A potential target for development of novel antitubercular agents. *Curr Drug Targets*. 2007;8(3):459–68.
320. Parish T, Stoker NG. The common aromatic amino acid biosynthesis pathway is essential in *Mycobacterium tuberculosis*. *Microbiology*. 2002;148(10):3069–77.
321. Dias MVB, Faím LM, Vasconcelos IB, de Oliveira JS, Basso LA, Santos DS, et al. Effects of the magnesium and chloride ions and shikimate on the structure of shikimate kinase

- from *Mycobacterium tuberculosis*. *Acta Crystallogr Sect F Struct Biol Cryst Commun*. 2006 Dec;63(Pt 1):1–6.
322. Bentley R. The shikimate pathway--a metabolic tree with many branches. *Crit Rev Biochem Mol Biol*. 1990;25(5):307–84.
 323. Palomino JC, Ramos DF, da Silva PA. New anti-tuberculosis drugs: strategies, sources and new molecules. *Curr Med Chem*. 2009;16(15):1898–904.
 324. Maitra A, Bates S, Kolvekar T, Devarajan P V., Guzman JD, Bhakta S. Repurposing-a ray of hope in tackling extensively drug resistance in tuberculosis. *Int J Infect Dis IJID Off Publ Int Soc Infect Dis*. 2015 Mar;32:50–5.
 325. Palomino JC, Martin A. Is repositioning of drugs a viable alternative in the treatment of tuberculosis? *J Antimicrob Chemother*. 2013 Feb;68(2):275–83.
 326. Mdluli K, Kaneko T, Upton A. The tuberculosis drug discovery and development pipeline and emerging drug targets. *Cold Spring Harb Perspect Med*. 2015 Jan;5(6).
 327. Dover LG, Coxon GD. Current Status and Research Strategies in Tuberculosis Drug Development. *J Med Chem*. 2011 Sep;54(18):6157–65.
 328. Butera JA. Phenotypic screening as a strategic component of drug discovery programs targeting novel antiparasitic and antimycobacterial agents: an editorial. *J Med Chem*. 2013 Oct;56(20):7715–8.
 329. Ji H-F, Li X-J, Zhang H-Y. Natural products and drug discovery. Can thousands of years of ancient medical knowledge lead us to new and powerful drug combinations in the fight against cancer and dementia? *EMBO Rep*. 2009 Mar;10(3):194–200.
 330. Nguta JM, Appiah-Opong R, Nyarko AK, Yeboah-Manu D, Addo PGA. Medicinal plants used to treat TB in Ghana. *Int J Mycobacteriology*. 2015 Jun;4(2):116–23.
 331. Butler MS, Newman DJ. Mother Nature's gifts to diseases of man: the impact of natural products on anti-infective, anticholesteremics and anticancer drug discovery. *Prog Drug Res*. 2008;65:1, 3–44.
 332. El Sayed KA, Bartyzel P, Shen X, Perry TL, Zjawiony JK, Hamann MT. Marine Natural Products as Antituberculosis Agents. *Tetrahedron*. 2000 Feb;56(7):949–53.
 333. Ang KKH, Holmes MJ, Higa T, Hamann MT, Kara UAK. In Vivo Antimalarial Activity of the Beta-Carboline Alkaloid Manzamine A. *Antimicrob Agents Chemother*. 2000 Jan;44(6):1645–9.
 334. Yousaf M, El Sayed KA, Rao K V, Lim CW, Hu JF, Kelly M, et al. 12,34-Oxamanzamines, novel biocatalytic and natural products from manzamine producing Indo-Pacific sponges. *Tetrahedron*. 2002 Sep;58(37):7397–402.

335. Rao K V., Santarsiero BD, Mesecar AD, Schinazi RF, Tekwani BL, Hamann MT. New manzamine alkaloids with activity against infectious and tropical parasitic diseases from an Indonesian sponge. *J Nat Prod.* 2003 Jun;66(6):823–8.
336. Rao K V., Kasanah N, Wahyuono S, Tekwani BL, Schinazi RF, Hamann MT. Three New Manzamine Alkaloids from a Common Indonesian Sponge and Their Activity against Infectious and Tropical Parasitic Diseases. *J Nat Prod.* 2004 Aug;67(8):1314–8.
337. Sakai R, Higa T, Jefford CW, Bernardinelli G. Manzamine A, a novel antitumor alkaloid from a sponge. *J Am Chem Soc.* 1986 Oct;108(20):6404–5.
338. Edrada RA, Proksch P, Wray V, Witte L, Müller WEG, Van Soest RWM. Four New Bioactive Manzamine-Type Alkaloids from the Philippine Marine Sponge *Xestospongia ashmorica*. *J Nat Prod.* 1996 Jan;59(11):1056–60.
339. Peng J, Kudrimoti S, Prasanna S, Odde S, Doerksen RJ, Pennaka HK, et al. Structure-activity relationship and mechanism of action studies of manzamine analogues for the control of neuroinflammation and cerebral infections. *J Med Chem.* 2010 Jan;53(1):61–76.
340. Rao K V., Donia MS, Peng J, Garcia-Palomero E, Alonso D, Martinez A, et al. Manzamine B and E and ircinal A related alkaloids from an Indonesian *Acanthostrongylophora* sponge and their activity against infectious, tropical parasitic, and Alzheimer's diseases. *J Nat Prod.* 2006 Jul;69(7):1034–40.
341. Waters AL, Hill RT, Place AR, Hamann MT. The expanding role of marine microbes in pharmaceutical development. *Curr Opin Biotechnol.* 2010 Dec;21(6):780–6.
342. Wahba AE, Peng J, Kudrimoti S, Tekwani BL, Hamann MT. Structure–activity relationship studies of manzamine A: Amidation of positions 6 and 8 of the β -carboline moiety. *Bioorg Med Chem.* 2009 Nov;17(22):7775–82.
343. Simithy J, Gill G, Wang Y, Goodwin DC, Calderón AI. Development of an ESI-LC-MS-based assay for kinetic evaluation of mycobacterium tuberculosis shikimate kinase activity and inhibition. *Anal Chem.* 2015;87(4):2129–36.
344. Copeland a. R. *Enzymes: A Practical Introduction to Structure, Mechanism, and Data Analysis.* Zhurnal Eksperimental'noi i Teoreticheskoi Fiziki. John Wiley & Sons; 2000. 76-79 p.
345. Rosado LA, Vasconcelos IB, Palma MS, Frappier V, Najmanovich RJ, Santos DS, et al. The Mode of Action of Recombinant Mycobacterium tuberculosis Shikimate Kinase: Kinetics and Thermodynamics Analyses. Agarwal PK, editor. *PLoS One.* 2013 May 6;8(5):e61918.
346. Copeland RA. Evaluation of enzyme inhibitors in drug discovery. A guide for medicinal chemists and pharmacologists. *Methods Biochem Anal.* 2005;46:1–265.

347. Stein RL. Tight-Binding, Slow-Binding, and Irreversible Inhibition. In: Kinetics of Enzyme Action. John Wiley & Sons, Inc.; 2011. p. 115–40.
348. Callan OH, So O-Y, Swinney DC. The Kinetic Factors That Determine the Affinity and Selectivity for Slow Binding Inhibition of Human Prostaglandin H Synthase 1 and 2 by Indomethacin and Flurbiprofen. *J Biol Chem.* 1996 Feb;271(7):3548–54.
349. Baici A, Gyger-Marazzi M. The slow, tight-binding inhibition of cathepsin B by leupeptin. A hysteric effect. *Eur J Biochem.* 1982 Dec;129(1):33–41.
350. Peng J, Rao K V., Choo Y-M, Hamann MT. Manzamine Alkaloids. In: Fattorusso E, Taglialatela-Scafati O, editors. *Modern Alkaloids.* Wiley-VCH Verlag GmbH & Co. KGaA; 2007. p. 189–232.
351. Hamann M, Alonso D, Martín-Aparicio E, Fuertes A, Pérez-Puerto MJ, Castro A, et al. Glycogen synthase kinase-3 (GSK-3) inhibitory activity and structure-activity relationship (SAR) studies of the manzamine alkaloids. Potential for Alzheimer’s disease. *J Nat Prod.* 2007 Sep;70(9):1397–405.
352. Ibrahim MA, Shilabin AG, Prasanna S, Jacob M, Khan SI, Doerksen RJ, et al. 2-N-Methyl modifications and SAR studies of manzamine A. *Bioorg Med Chem.* 2008 Jul;16(14):6702–6.
353. Schaffer BAJ, Bertram L, Miller BL, Mullin K, Weintraub S, Johnson N, et al. Association of GSK3B with Alzheimer disease and frontotemporal dementia. *Arch Neurol.* 2008 Oct;65(10):1368–74.
354. Chan MMP, Cheung BKW, Li JCB, Chan LLY, Lau ASY. A role for glycogen synthase kinase-3 in antagonizing mycobacterial immune evasion by negatively regulating IL-10 induction. *J Leukoc Biol.* 2009 Aug;86(2):283–91.
355. Redford PS, Murray PJ, O’Garra A. The role of IL-10 in immune regulation during *M. tuberculosis* infection. *Mucosal Immunol.* 2011 May;4(3):261–70.
356. Cyktor JC, Turner J. Interleukin-10 and Immunity against Prokaryotic and Eukaryotic Intracellular Pathogens ∇ . *Infect Immun.* 2011 Aug;79(8):2964–73.
357. Copeland RA, Pompliano DL, Meek TD. Drug–target residence time and its implications for lead optimization. *Nat Rev Drug Discov.* 2006 Sep;5(9):730–9.
358. Copeland RA. Conformational adaptation in drug-target interactions and residence time. *Future Med Chem.* 2011 Sep;3(12):1491–501.
359. Welsch ME, Snyder SA, Stockwell BR. Privileged scaffolds for library design and drug discovery. Vol. 14, *Current Opinion in Chemical Biology.* 2010. p. 347–61.
360. Catalán LE, Maturana EB, Marín KC, Olivares MO, Altamirano HC, Fritis MC, et al.

- Synthesis and antitumor activity of diterpenylhydroquinone derivatives of natural ent-labdanes. *Molecules*. 2010 Sep 17;15(9):6502–11.
361. Luibrand RT, Erdman TR, Vollmer JJ, Scheuer PJ, Finer J, Clardy J. Ilimaquinone, a sesquiterpenoid quinone from a marine sponge. *Tetrahedron*. 1979 Jan 1;35(5):609–12.
 362. Kim BG, Chun TG, Lee HY, Snapper ML. A new structural class of S-adenosylhomocysteine hydrolase inhibitors. *Bioorganic Med Chem*. 2009 Sep 15;17(18):6707–14.
 363. Popov AM, Stekhova SI, Utkina NK, Rebachuk NM. Antimicrobial and cytotoxic activity of sesquiterpenequinones and brominated diphenyl esters isolated from marine sponges. *Pharm Chem J*. 1999;33(2):71–3.
 364. Fattorusso E, Tagliatela-Scafati O. Marine antimalarials. Vol. 7, *Marine Drugs*. 2009. p. 130–52.
 365. Tziveleka L-A, Vagias C, Roussis V. Natural products with anti-HIV activity from marine organisms. *Curr Top Med Chem*. 2003 Sep 1;3(13):1512–35.
 366. Veit B, Yucel JK, Malhotra V. Microtubule independent vesiculation of Golgi membranes and the reassembly of vesicles into Golgi stacks. *J Cell Biol*. 1993;122(6):1197–206.
 367. Takizawa PA, Yucel JK, Veit B, Faulkner DJ, Deerinck T, Soto G, et al. Complete vesiculation of Golgi membranes and inhibition of protein transport by a novel sea sponge metabolite, ilimaquinone. *Cell*. 1993 Jun 18;73(6):1079–90.
 368. Jamora C, Takizawa PA, Zaarour RF, Denesvre C, Faulkner DJ, Malhotra V. Regulation of Golgi Structure through Heterotrimeric G Proteins vesicles requires two distinct cytosolic factors: a mono-meric G protein called ARF (for ADP-ribosylating factor) and a complex of proteins collectively known as coat- Reconstitution of IQ-M. *Cell*. 1997;91:617–26.
 369. Sonoda H, Okada T, Jahangeer S, Nakamura SI. Requirement of phospholipase D for ilimaquinone-induced Golgi membrane fragmentation. *J Biol Chem*. 2007;282(47):34085–92.
 370. Ratovitski EA. Tumor Protein (TP)-p53 Members as Regulators of Autophagy in Tumor Cells upon Marine Drug Exposure. *Mar Drugs*. 2016 Aug;14(8).
 371. Lee HY, Chung KJ, Hwang IH, Gwak J, Park S, Ju BG, et al. Activation of p53 with ilimaquinone and ethylsmenoquinone, marine sponge metabolites, induces apoptosis and autophagy in colon cancer cells. *Mar Drugs*. 2015 Jan;13(1):543–57.
 372. Lee HY, Chung KJ, Hwang IH, Gwak J, Park S, Ju BG, et al. Activation of p53 with ilimaquinone and ethylsmenoquinone, marine sponge metabolites, induces apoptosis and autophagy in colon cancer cells. *Mar Drugs*. 2015;13(1):543–57.

373. Lu P-H, Chueh S-C, Kung F-L, Pan S-L, Shen Y-C, Guh J-H. Ilimaquinone, a marine sponge metabolite, displays anticancer activity via GADD153-mediated pathway. *Eur J Pharmacol.* 2007 Feb;556(1):45–54.
374. Du L, Zhou Y-D, Nagle DG. Inducers of hypoxic response: marine sesquiterpene quinones activate HIF-1. *J Nat Prod.* 2013 Jun;76(6):1175–81.
375. Oda T, Wang W, Ukai K, Nakazawa T, Mochizuki M. A sesquiterpene quinone, 5-Epi-smenospongine, promotes TNF- α production in LPS-stimulated RAW 264.7 cells. *Mar Drugs.* 2007;5(4):151–6.
376. Radeke HS, Digits CA, Casaubon RL, Snapper ML. Interactions of (-)-ilimaquinone with methylation enzymes: implications for vesicular-mediated secretion. *Chem Biol.* 1999 Sep;6(9):639–47.
377. Bentley R, Haslam E. The shikimate pathway - A metabolic tree with many branches. *Crit Rev Biochem Mol Biol.* 1990;25(5):307–84.
378. Simithy J, Gill G, Wang Y, Goodwin DC, Calderón AI. Development of an ESI-LC-MS-based assay for kinetic evaluation of mycobacterium tuberculosis shikimate kinase activity and inhibition. *Anal Chem.* 2015;87(4):2129–36.
379. Ndontsa EN, Moore RL, Goodwin DC. Stimulation of KatG catalase activity by peroxidatic electron donors. *Arch Biochem Biophys.* 2012 Sep;525(2):215–22.
380. Nelson DP, Kiesow LA. Enthalpy of decomposition of hydrogen peroxide by catalase at 25 degrees C (with molar extinction coefficients of H₂O₂ solutions in the UV). *Anal Biochem.* 1972 Oct;49(2):474–8.
381. Singh J, Petter RC, Baillie TA, Whitty A. The resurgence of covalent drugs. Vol. 10, *Nature Reviews Drug Discovery.* Nature Publishing Group; 2011. p. 307–17.
382. Garuti L, Roberti M, Bottegoni G. Irreversible protein kinase inhibitors. *Curr Med Chem.* 2011;18(20):2981–94.
383. Bentley R, Haslam E. The shikimate pathway - A metabolic tree with many branches. *Crit Rev Biochem Mol Biol.* 1990 Jan 26;25(5):307–84.
384. Roberts F, Roberts CW, Johnson JJ, Kyle DE, Krell T, Coggins JR, et al. Evidence for the shikimate pathway in apicomplexan parasites [published erratum appears in *Nature* 1998 Sep 17;395(6699):801]]. *Nature.* 1998;393(6687):801–5.
385. Mir R, Jallu S, Singh TP. The shikimate pathway: Review of amino acid sequence, function and three-dimensional structures of the enzymes. Vol. 41, *Critical Reviews in Microbiology.* Informa Healthcare; 2015. p. 172–89.
386. Campbell SA, Richards TA, Mui EJ, Samuel BU, Coggins JR, McLeod R, et al. A

- complete shikimate pathway in *Toxoplasma gondii*: An ancient eukaryotic innovation. *Int J Parasitol.* 2004;34(1):5–13.
387. Ridley RG. Planting new targets for antiparasitic drugs. Vol. 4, *Nature Medicine.* 1998. p. 894–5.
388. Coggins JR. The Shikimate Pathway as a Target for Herbicides. A. Dodge (Ed.), editor. *Herbic Plant Metab.* 1989;38:97–112.
389. Gan J, Gu Y, Li Y, Yan H, Ji X. Crystal structure of *Mycobacterium tuberculosis* shikimate kinase in complex with shikimic acid and an ATP analogue. *Biochemistry.* 2006 Jul 18;45(28):8539–45.
390. Rosado LA, Vasconcelos IB, Palma MS, Frappier V, Najmanovich RJ, Santos DS, et al. The Mode of Action of Recombinant *Mycobacterium tuberculosis* Shikimate Kinase: Kinetics and Thermodynamics Analyses. Agarwal PK, editor. *PLoS One.* 2013 May 6;8(5):e61918.
391. Blondin C, Serina L, Wiesmüller L, Gilles AM, Barzu O. Improved Spectrophotometric Assay of Nucleoside Monophosphate Kinase Activity Using the Pyruvate Kinase/Lactate Dehydrogenase Coupling System. *Anal Biochem.* 1994 Jul 1;220(1):219–21.
392. Jäger S, Brand L, Eggeling C. New fluorescence techniques for high-throughput drug discovery. *Curr Pharm Biotechnol.* 2003;4(6):463–76.
393. Bose S. Use of steady-state and time-resolved fluorescence spectroscopy as a tool to investigate photophysics of biologically and environmentally relevant systems. Thesis. 2010;
394. Grossman TH, Starosta AL, Fyfe C, O'Brien W, Rothstein DM, Mikolajka A, et al. Target- and resistance-based mechanistic studies with TP-434, a novel fluorocycline antibiotic. *Antimicrob Agents Chemother.* 2012 May;56(5):2559–64.
395. Giuliano KA, Taylor DL. Fluorescent-protein biosensors: New tools for drug discovery. *Trends Biotechnol.* 1998;16(3):135–40.
396. Mutagenesis S. Site-directed Mutagenesis.
397. Varnado CL, Hertwig KM, Thomas R, Roberts JK, Goodwin DC. Properties of a novel periplasmic catalase-peroxidase from *Escherichia coli* O157:H7. *Arch Biochem Biophys.* 2004;421(1):166–74.
398. Fang X, Cao Z, Beck T, Tan W. Molecular aptamer for real-time oncoprotein platelet-derived growth factor monitoring by fluorescence anisotropy. *Anal Chem.* 2001;73(23):5752–7.
399. Li Q, Du H-N, Hu H-Y. Study of protein-protein interactions by fluorescence of

- tryptophan analogs: Application to immunoglobulin G binding domain of streptococcal protein G. *Biopolymers*. 2003 Jan 1;72(2):116–22.
400. Han C, Zhang J, Chen L, Chen K, Shen X, Jiang H. Discovery of *Helicobacter pylori* shikimate kinase inhibitors: Bioassay and molecular modeling. *Bioorganic Med Chem*. 2007;15(2):656–62.
 401. Giglione C, Boularot A, Meinnel T. Protein N-terminal methionine excision. *C Cell Mol Life Sci*. 2004;61:1455–74.
 402. Bonissone S, Gupta N, Romine M, Bradshaw RA, Pevzner PA. N-terminal protein processing: a comparative proteogenomic analysis. *Mol Cell Proteomics*. 2013 Jan;12(1):14–28.
 403. Frottin F, Martinez A, Peynot P, Mitra S, Holz RC, Giglione C, et al. The proteomics of N-terminal methionine cleavage. *Mol Cell Proteomics*. 2006 Dec 1;5(12):2336–49.
 404. Hirel P-H, Schmitter J-M, Dessen P, Fayat G, Blanquet S. Extent of N-terminal methionine excision from *Escherichia coli* proteins is governed by the side-chain length of the penultimate amino acid. *Biochemistry*. 1989;86:8247–51.
 405. Hutter MC, Helms V. Phosphoryl transfer by a concerted reaction mechanism in UMP/CMP-kinase. *Protein Sci*. 2000 Nov;9(11):2225–31.
 406. Sutton KA, Breen J, MacDonald U, Beanan JM, Olson R, Russo TA, et al. Structure of shikimate kinase, an in vivo essential metabolic enzyme in the nosocomial pathogen *Acinetobacter baumannii*, in complex with shikimate. *Acta Crystallogr Sect D Biol Crystallogr*. 2015 Aug 1;71(8):1736–44.
 407. Blanco B, Prado V, Lence E, Otero JM, Garcia-Doval C, Van Raaij MJ, et al. *Mycobacterium tuberculosis* shikimate kinase inhibitors: Design and simulation studies of the catalytic turnover. *J Am Chem Soc*. 2013 Aug 21;135(33):12366–76.
 408. Prado V, Lence E, Maneiro M, Vázquez-Ucha JC, Beceiro A, Thompson P, et al. Targeting the Motion of Shikimate Kinase: Development of Competitive Inhibitors that Stabilize an Inactive Open Conformation of the Enzyme. *J Med Chem*. 2016 Jun 9;59(11):5471–87.
 409. Whitford PC, Gosavi S, Onuchic JN. Conformational transitions in adenylate kinase: Allosteric communication reduces misligation. *J Biol Chem*. 2008;283(4):2042–8.
 410. Cheng WC, Chen YF, Wang HJ, Hsu KC, Lin SC, Chen TJ, et al. Structures of *Helicobacter pylori* shikimate kinase reveal a selective inhibitor-induced-fit mechanism. Boneca IG, editor. *PLoS One*. 2012 Mar 16;7(3):e33481.
 411. Weber G. Polarization of the fluorescence of macromolecules. I. Theory and experimental method. *Biochem J*. 1952;51(2):145–55.

412. Mattheyses AL, Kampmann M, Atkinson CE, Simon SM. Fluorescence Anisotropy Reveals Order and Disorder of Protein Domains in the Nuclear Pore Complex. *Biophysj.* 2010;99:1706–17.
413. Plakhotnik T, Nonn T, Palm V. Saturation spectroscopy of vibronic transitions in single molecules. *Chem Phys Lett.* 2002 Mar 9;357(5–6):397–402.
414. Siano DB, Metzler DE. Band shapes of the electronic spectra of complex molecules. *J Chem Phys.* 1969 Sep 5;51(5):1856–61.
415. Gurchiek JK, Bao H, Domínguez-Martín MA, McGovern SE, Marquardt CE, Roscioli JD, et al. Fluorescence and Excited State Conformational Dynamics of the Orange Carotenoid Protein. *J Phys Chem B.* 2018;acs.jpcc.7b09435.
416. Wang J, Xie J, Schultz PG. A genetically encoded fluorescent amino acid. *J Am Chem Soc.* 2006 Dec 1;128(27):8738–9.
417. Ferrie JJ, Ieda N, Haney CM, Walters CR, Sungwienwong I, Yoon J, et al. Multicolor protein FRET with tryptophan, selective coumarin-cysteine labeling, and genetic acridonylalanine encoding. *Chem Commun.* 2017 Oct 5;53(80):11072–5.
418. Yan H, Tsai MD. Nucleoside monophosphate kinases: structure, mechanism, and substrate specificity. Vol. 73, *Advances in enzymology and related areas of molecular biology.* 1999. 103-34, x p.
419. Stone TJ, Buckman T, Nordio PL, McConnell HM. Spin-labeled biomolecules. *Proc Natl Acad Sci.* 1965;54(4):1010–7.
420. Cornish VW, Benson DR, Altenbach CA, Hideg K, Hubbell WL, Schultz PG. Site-specific incorporation of biophysical probes into proteins. *Proc Natl Acad Sci U S A.* 1994 Apr 12;91(8):2910–4.
421. Klare JP, Steinhoff HJ. Spin labeling EPR. Vol. 102, *Photosynthesis Research.* 2009. p. 377–90.
422. Steinhoff H-J. Multi-Frequency EPR Spectroscopy Studies of the Structure and Conformational Changes of Site- Directed Spin Labelled Membrane Proteins. *Supramol Struct Funct* 8. 2005;6–9.
423. Sahu ID, Lorigan GA. Site-Directed Spin Labeling EPR for Studying Membrane Proteins. Vol. 2018, *BioMed Research International.* Hindawi; 2018. p. 1–13.
424. Sahu ID, McCarrick RM, Lorigan GA. Use of electron paramagnetic resonance to solve biochemical problems. *Biochemistry.* 2013 Sep 3;52(35):5967–84.